DISSERTATION

SOURCES, SINKS, AND TRENDS OF OZONE PRECURSORS AND THEIR IMPACT ON OZONE IN NORTHERN COLORADO

Submitted by

Andrew Joseph Abeleira

Department of Chemistry

In partial fulfillment of the requirements

For the Degree of Doctor of Philosophy

Colorado State University

Fort Collins, Colorado

Fall 2017

Doctoral Committee:

Advisor: Delphine K. Farmer

Charles Henry
Emily Fischer
Debbie Crans

ABSTRACT

SOURCES, SINKS, AND TRENDS OF OZONE PRECURSORS AND THEIR IMPACT ON OZONE IN NORTHERN COLORADO

Ozone is a structurally simple molecule that plays immensely important roles in Earth's atmosphere. In the troposphere, ozone is vital in maintaining the oxidative capacity of the lower atmosphere. However, unlike the chemical structure, the formation and lifecycle of ozone in the troposphere is anything but simple. The role of ozone in severe air pollution episodes, and the negative human and ecosystem health impacts of ozone were first established in the United States during the "smog" pollution episodes of the early 1950s in the Los Angeles basin. Since then, understanding the formation and impacts of ozone has been an air quality research priority in the United States. The primary source of tropospheric ozone is the photochemically initiated oxidation of anthropogenic or biogenic volatile organic compounds in the presence of nitrogen oxides. The production of ozone relies on the interplay between two catalytic cycles that share initiation and termination reactions. The linkage of the ozone catalytic cycles, via those initiation and termination reactions, leads to the non-linear nature of the chemical production of ozone.

The urbanization of the United States in the 1950s-1970s led to increased frequency of severe ozone events in urban areas from increased ozone precursor emissions – specifically emissions of NO and NO_2 from automobiles and coal-fired electricity generating power plants. These high ozone events, coupled with results from ozone epidemiologic, exposure, and toxicology studies, prompted the U.S. Congress to establish the Clean Air Act of 1970. The Clean Air Act authorized the U.S. Environmental Protection Agency to establish the National Air Quality

Standards for six criteria air pollutants – including ozone. The goal of this new standard was to systematically reduce ambient ozone concentrations by targeting major ozone precursor emission sources.

Near 50 years later high ozone events are still occurring in densely populated urban and suburban regions in the United States. Herein, an in-depth study of the sources and sinks of ozone precursors, and the impact of precursor reductions on long-term ozone trends in Northern Colorado is presented. Chapter 1 of this dissertation provides relevant historical context regarding ozone in the United States, pertinent tropospheric ozone chemistry for urban and suburban regions, ozone precursor trends in the United States, and other important processes that affect regional and global ozone. Chapter 2 examines long-term (15 year) trends in ozone and ozone precursors in Northern Colorado with a focus on day of week ozone and NO_2 trends that suggest Northern Colorado is transitioning from a NO_x-saturated to peak ozone production region. Additionally, the impact of severe drought on the ozone/temperature relationship is addressed. Chapter 3 details the seasonal sources of a suite of volatile organic compounds measured during two 8-week periods in spring and summer 2015 at a ground site in Northern Colorado, and demonstrates the impact of drought on the local isoprene and reactive carbon budget. The reduction in isoprene emissions during drought is tied back to the suppression of the ozone/temperature relationship in the region. In the fourth chapter, the sources and sinks of alkyl nitrates, a key ozone precursor sink, are investigated using a simple sequential production-destruction reaction model. The final chapter highlights the need for long-term ozone and ozone precursor monitoring in Northern Colorado as population, energy demands, and ozone precursor emissions change.

ACKNOWLEDGEMENTS

I would like to thank my friends (those near and far) and family for the continued support and reassurance during the last 5 years. Finishing my Ph.D in the midst of recovering from a serious traumatic accident has granted me a new perspective on perseverance in the face of the unknown. Without my friends guiding me through that unknown I do not think I would have succeeded. I would like to thank my advisor, Dr. Delphine Farmer, for allowing me to build, and fail, and build again. A special thanks to Delphine for being patient with me while I put my broken body back together. Without her guidance, support, and occasional forceful prodding I would not have made it this far. I would like to thank the current and previous members of the Farmer group with whom I have shared laughs, tough times, and good times. I would like to thank the organizers and principal investigators of the Front Range Air Pollution and Photochemistry Experiment (FRAPPE) and the Shale Oil and Natural Gas Nexus (SONGNEX) field campaigns for providing the opportunity and support to work on the projects that became the focus of my research.

DEDICATION

This work is dedicated to those in pain that struggle to see the light in their lives…

'Do not go gentle into that good night,

Old Age should burn and rave at the close of day;

Rage, rage against the dying of the light.'

-Dylan Thomas

TABLE OF CONTENTS

CHAPTER 1 – AN OVERVIEW OF URBAN AND SUBURBAN TROPOSPHERIC OZONE

1.1 History of ozone research in the United States.

Tropospheric ozone (O_3) is a well-known, multifarious atmospheric compound that is both a product of the oxidation of volatile organic compounds (VOCs) and a VOC oxidant itself. Despite early identification by German chemist C.F. Schönbein in 1843 [*Monks et al.*, 2015], the formation and impact of O_3 in the United States was not rigorously investigated until the end of the 1940s and beginning of the 1950s. During a period of rapid expansion in both population and local industry, the Los Angeles basin began experiencing severe air quality issues.[*Haagen-Smit et al.*, 1952] The term 'smog' was created as a contraction of the words 'smoke' and 'fog' to describe the thick, soupy quality of air in Los Angeles. Severe smog events in Los Angeles decreased visibility and caused crop damage, mild to severe eye irritation, and rubber deterioration in city infrastructure and automobile tires.[*Haagen-Smit*, 1952; *Haagen-Smit et al.*, 1952] Arie Haagen-Smit, a bio-organic chemist at the California Institute of Technology, noted that the Los Angeles smog exhibited a different smell than the sulfurous coal-derived smog in Europe and southeastern United States.[*Haagen-Smit*, 1952] Haagen-Smit observed that the Los Angeles smog had a "bleach-like" smell similar to the oxygenated hydrocarbons, *e.g.* organic peroxides, commonly used in natural synthesis laboratories.[*Haagen-Smit*, 1952] Drawing on his synthetic chemistry background, Haagen-Smit theorized that the oxygenated hydrocarbons were the result of O_3 oxidation of hydrocarbon emissions from Los Angeles' growing petroleum industry.

During this time, experts in the rubber industry knew that exposure to O_3 caused visible surface cracking with rubber products.[*Crabtree et al.*, 1946] The duration of time required for visible surface cracking of a standardized rubber depended on the ambient O_3 concentration. This

phenomenon allowed for the development of a quantitative O_3 sensor. With this sensor, O_3 concentrations in excess of 200 ppbv were measured during a severe winter smog episode in February of 1951 (Fig. 1.1).[*Haagen-Smit et al.*, 1952]

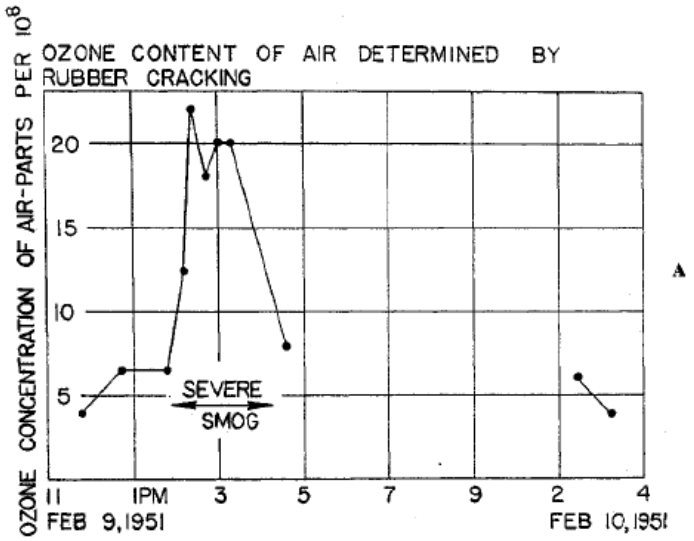

Figure 1.1 Ambient O_3 concentrations determined with the rubber cracking technique in Los Angeles on 9 February, 1951.[*Haagen-Smit et al.*, 1952]

However, the formation mechanism to explain the high O_3 concentrations during smog episodes remained unknown. At the same time, a separate group of investigators at the Earhart Plant Research Laboratories at the California Institute of Technology were attempting to identify the cause of damage to local vegetable crops after severe smog episodes. Haagen-Smit joined the group of plant researchers, and conducted a series of plant chamber fumigation experiments. The group found that fumigation of plants with artificially generated O_3, hydrocarbons from gasoline distillates, and NO_2 replicated the smog plant damage.[*Haagen-Smit et al.*, 1952] Additional fumigation experiments with NO_2 and hydrocarbon mixtures showed that when the mixtures were irradiated with sunlight, O_3 was formed and the plants exhibited similar damage to the fumigation experiments with artificially produced O_3.[*Haagen-Smit et al.*, 1952] These initial discoveries

prompted further experiments investigating O_3 formation from NO_2 and hydrocarbons, and led to the publication of the seminal paper "Ozone Formation in Photochemical Oxidation of Organic Substances".[*Haagen-Smit et al.*, 1953] These experiments showed that the amount of O_3 formed could not be explained by the stoichiometry of the initial amounts of NO_2 and hydrocarbons, and a catalytic formation process was proposed. *Haagen-Smit et al.* [1953] proposed that a catalytic reaction system involving peroxide radicals, the hydroperxoyl radical (HO_2), atomic oxygen from NO_2, and O_2 was responsible for producing O_3.

Through the 1960s, many laboratory photochemistry experiments were conducted with mixtures of hydrocarbon, NO, and NO_2 that yielded key information regarding the consumption of the starting chemicals and production of secondary chemicals.[*Leighton*, 1961] Figure 1.2 summarizes one such experiment in which a mixture of isobutene and NO, with trace amounts of NO_2, was irradiated. Early modeling work by Hiriam Levy and Paul Crutzen identified the key reactions involved in the photochemical production of O_3 in the troposphere.[*Crutzen*, 1973a; *Crutzen*, 1973b; *Levy*, 1971; 1972; 1973] Key insights included: **(1)** hydroxyl radicals (OH) initiate oxidation of methane (CH_4) as a source of formaldehyde and CO, and **(2)** HO_2 are converted by NO to reform OH.[*Crutzen*, 1973b; *Levy*, 1971; 1972; 1973] Building upon the photochemical processes outlined in those modeling studies, *Chameides et al.* [1973] found that photochemical production of O_3 from CH_4 could explain the seasonal and altitudinal variations in O_3 without the need for invoking transport of O_3-rich air masses from the stratosphere. At the time, stratosphere-troposphere exchange of O_3 was thought to be the dominant source of tropospheric O_3. Following decades of intense focus on tropospheric O_3, the dominance of lower tropospheric O_3 production from both natural and anthropogenic sources was established.[*Monks et al.*, 2015]

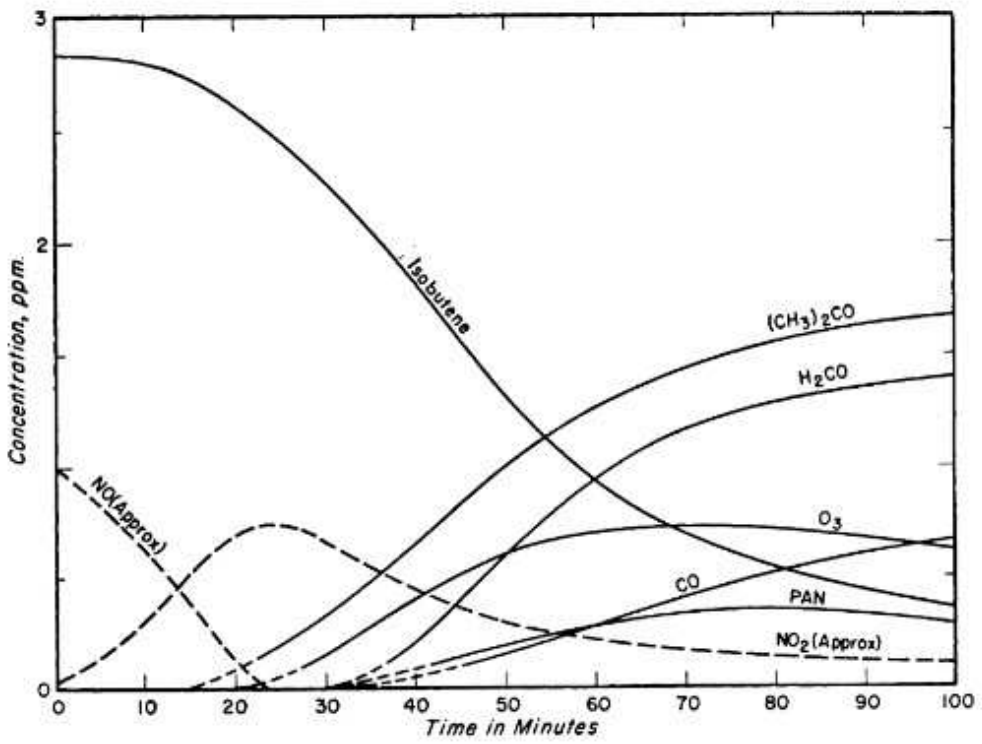

Figure 1.2. Measurement of changes in concentration of isobutene, NO, and secondary products from the irradiation of a mixture of isobutene and NO.[*Leighton*, 1961]

1.2 Elevated O_3 has negative impacts on human and ecosystem health

The oxidative capacity of O_3 induces inflammation of the respiratory tract even from short-term inhalation, which decreases lung function, and exacerbates chronic respiratory conditions such as asthma.[*Anderson et al.*, 2004; *Bell et al.*, 2004; *Brunekreef et al.*, 1995; *Ross et al.*, 2012; *Thurston et al.*, 1999] Exposure to high O_3 levels is linked to increased hospital admissions and emergency room visits [*Anderson et al.*, 2004; *Yang et al.*, 2003], and can disproportionately affect at-risk populations including children [*Gauderman et al.*, 2002; *Gilliland et al.*, 2001] and the elderly [*Yang et al.*, 2003]. Population densities are shifting globally with half of the global population living in urban areas in 2007, and future projections of 2/3 of the global population living in urban areas by 2050.[*Montgomery*, 2008; *Zhu et al.*, 2012] Major urban centers are areas

with high energy consumption from human and industrial activities, which results in concentrated emissions of O_3 precursors and high O_3 production rates in surrounding areas.[*Marr et al.*, 2002] Mortality rates from O_3 are projected to increase with increasing O_3 from further urbanization and a changing climate.[*Ebi et al.*, 2008; *West et al.*, 2007]

Plants exchange gases with the atmosphere, including CO_2, O_2, and water vapor, during photosynthesis through pores in surface tissues called stomata.[*Fowler et al.*, 2009; *Matyssek et al.*, 2003] During stomata exchange, pollutants such as O_3, are also taken up in plant tissues. After stomatal uptake into plant tissue, O_3 reacts with the plant tissue to produce reactive oxidants that interfere with physiological processes including further gas exchange of the leaves and photosynthetic performance.[*Fowler et al.*, 2009; *Matyssek et al.*, 2003] Stomatal uptake is controlled by stomatal conductance (*i.e.* diffusion of O_3 through the stomata), and varies according to plant species, seasonal changes in leaf area, and meteorological conditions.[*Fowler et al.*, 2001; *Fowler et al.*, 2009; *Hardacre et al.*, 2015; *Wesely et al.*, 2000] Non-stomatal uptake occurs by reactions between O_3 and external plant surfaces. O_3 rapidly oxidizes plant material, thus stomatal and non-stomatal uptake by plants is a permanent O_3 sink. Short and long-term exposure to high O_3 reduces leaf area and causes visible injury from necrotic lesions on staple food crops including wheat, soybean, and rice and common tree species.[*Hayes et al.*, 2007; *Matyssek et al.*, 2003; *Mills et al.*, 2007; *Mills et al.*, 2011] Societal and ecological impacts of O_3 induced plant damage include a reduction in agricultural yields and food security [*Ashmore*, 2005; *Avnery et al.*, 2011; *Tai et al.*, 2014] and reduced ecological diversity [*Ashmore*, 2005; *Davison et al.*, 1998]. *Avnery et al.* [2011] estimate a global soybean, maize, and wheat crop loss of \$11 – 18 billion (79 – 121 metric tons) from O_3 in 2000 and a projection of \$12-21 billion in 2030.

1.3 Tropospheric ozone chemistry.

The formation of tropospheric O_3 depends on the photolysis of NO_2 to produce NO and $O(^3P)$ (R1), and the association of $O(^3P)$ with O_2 (R2).

$$NO_2 \cdot + h\nu \rightarrow NO \cdot + O(^3P) \quad \text{(R1)}$$

$$O(^3P) + O_2 + M \rightarrow O_3 + M \quad \text{(R2)}$$

O_3 and NO react rapidly (R3, $k_3 = 2.0 \times 10^{-12}$ cm^3 $molecule^{-1}$ s^{-1} at 298 K), and NO is an important O_3 reservoir in urban areas with high NO concentrations.

$$O_3 + NO \cdot \rightarrow NO_2 \cdot + O_2 \quad \text{(R3)}$$

Reactions 1-3 represent a null O_3 formation cycle (NO_x photochemical cycle) that quickly reaches a pseudo-steady-state in which the production and consumption of $O(^3P)$ is virtually instantaneous and the rate of O_3 production equals the rate of destruction. The net production of O_3 relies on oxidation chemistry initiated by the hydroxyl radical (OH). The photolysis of O_3 (R4) is the dominant source of OH (R5), which is the major daytime oxidant in the troposphere.[*Monks*, 2005]

$$O_3 + h\nu(\lambda < 320\ nm) \rightarrow O(^1D) + O_2 \quad \text{(R4)}$$

$$O(^1D) + H_2O \rightarrow OH \cdot + OH \cdot \quad \text{(R5)}$$

OH is responsible for the daytime removal of a majority of global volatile organic compound (VOC) emissions via oxidation [*Atkinson*, 1990; *Atkinson et al.*, 2003], and initiates the HO_x ($HO_x \equiv OH + HO_2 + RO_2$) catalytic cycle (R6). The following reactions are described for an alkane (RH), and are grouped into chain initiation (R6), chain propagation that leads to net O_3 production (R7-10), and chain termination reactions (R11-14).

The oxidation of alkanes proceeds by proton abstraction from RH by OH to form H_2O and an alkyl radical R (R6). The fraction of protons abstracted at a particular carbon atom is denoted as α-$_{RH}$.

$$RH + OH\cdot \xrightarrow[\alpha_{RH}]{} R\cdot + H_2O \quad \text{(R6)}$$

Due to the high abundance of O_2 in the troposphere and a rate constant for R+O_2 of $\geq 1x10^{-12}$ cm^3 $molecule^{-1}$ s^{-1} at room temperature and atmospheric pressure, R7 between R and O_2 to form a peroxy radical (RO_2) occurs instantaneously relative to the other reactions in the HO_x cycle.

$$R\cdot + O_2 + M \rightarrow RO_2\cdot \quad \text{(R7)}$$

RO_2 reacts with NO to either oxidize NO to NO_2 (R8a), producing an alkoxy radical (RO), or form an organic nitrate ($RONO_2$) (R8b). The formation of $RONO_2$ terminates the chain and is discussed below with the chain termination reactions. The fraction of RO_2+NO reactions that forms an $RONO_2$ is denoted as α-$_{RONO2}$.

$$RO_2\cdot + NO\cdot \xrightarrow[1-\alpha_{RONO2}]{} RO\cdot + NO_2\cdot \quad \text{(R8a)}$$

$$RO_2\cdot + NO\cdot \xrightarrow[\alpha_{RONO2}]{} RONO_2 \quad \text{(R8b)}$$

NO_2 from R8 can then undergo photolysis, and eventually produce O_3 (R1-2). RO from R8 propagates the O_3 production chain by reacting with O_2 to produce a carbonyl and a hydroperoxyl radical (HO_2) (R9).

$$RO\cdot + O_2 \rightarrow RCHO + HO_2\cdot \quad \text{(R9)}$$

Similar to RO_2, HO_2 oxidizes NO to yield a second NO_2, but also recycles OH to continue the O_3 production cycle (R10).

$$HO_2\cdot + NO\cdot \rightarrow NO_2\cdot + OH\cdot \quad \text{(R10)}$$

The propensity for chain termination reactions to occur depends on the relative abundances of VOC and NO_x [*Sillman*, 1995; 1999; *Sillman et al.*, 2002; *Sillman et al.*, 1990; *Thornton*, 2002]. Reactions between OH and NO_2 to form HNO_3 (R11) occur in high NO_x environments (NO_x-saturated) typical of urban areas with NO_x > 2 ppbv [*Sillman*, 1999; *Sillman et al.*, 1997; *Sillman et al.*, 1990].

$$OH\cdot + NO_2\cdot \rightarrow HNO_3 \quad \text{(R11)}$$

HNO_3 is highly soluble in water and is efficiently removed by rainfall – *i.e.* wet deposition .[*Zhang et al.*, 2012] In rural environments, with NO_x < 0.25 ppbv (NO_x-limited or VOC-saturated), chain termination is dominated by HO_x self-reactions to form peroxides (R12-14).[*Kleinman et al.*, 1994; *McKeen et al.*, 1991; *Sillman et al.*, 1990]

$$RO_2\cdot + HO_2\cdot \rightarrow ROOH + O_2 \quad \text{(R12)}$$

$$HO_2\cdot + HO_2\cdot \rightarrow H_2O_2 + O_2 \quad \text{(R13)}$$

$$RO_2\cdot + R'O_2\cdot \rightarrow ROOR' + O_2 \quad \text{(R14)}$$

The suppression of O_3 production from NO_x-limited and NO_x-saturated termination reactions is apparent in Figure 1.3a. O_3 production, denoted as $P(O_3)$, was modeled with E1, where R_{VOC} is the VOC reactivity of an air mass (E2), and $[OH_{calc}]$ is the OH concentration in the system from a constant R_{VOC} and varying NO_x calculated with E3 [*Farmer et al.*, 2011]. VOC reactivity is calculated as the summation of the product of individual VOC concentrations and the VOC+OH rate coefficient (E2).

$$P(O_3) = 2 \times R_{VOC} \times [OH_{calc}] \quad \text{(E1)}$$

$$R_{VOC} = \sum_i \ k_{OH+VOC}[VOC_i] \quad \text{(E2)}$$

$$OH_{calc} = \frac{-b \pm \sqrt{b^2-4ac}}{2a} \quad \text{(E3)}$$

The loss of HO_2 and RO_2 via HO_x self-reactions and RO_2+NO is calculated with E3a for different NO concentrations and a constant R_{VOC}. In E3a, $k_{HO2+HO2}$, $k_{RO2+HO2}$, and $k_{RO2+RO2}$ are the HO_x self-reaction rate coefficients, and k_{NO+RO2} is the rate coefficient of NO oxidation by the ethane derived $C_2H_5O_2$ peroxy radical. Values of $2.74x10^{-12}$, $8x10^{-12}$, $6.8x10^{-12}$, and $9.1x10^{-12}$ cm^3 $molecule^{-1}$ s^{-1} are used for $k_{HO2+HO2}$, $k_{RO2+HO2}$, $k_{RO2+RO2}$, and k_{NO+RO2} respectively.[*Farmer et al.*, 2011; *Sander et al.*, 2015; *Saunders et al.*, 2003]

$$a = 2\left(k_{HO_2+HO_2} + k_{RO_2+HO_2} + k_{RO_2+RO_2}\right) \times \left(\frac{R_{VOC}}{(1-\beta) \times k_{NO+RO_2} \times [NO]}\right)^2 \quad \text{(E3a)}$$

The loss of OH and NO_2 via the OH+NO_2 chain termination reaction is calculated with E3b as NO and NO_2 increases. The value of $3.6x10^{-11}$ cm^3 $molecule^{-1}$ s^{-1} is used for k_{OH+NO2}.[*Saunders et al.*, 2003]

$$b = \ k_{OH+NO_2} \ \times \ [NO_2] + \frac{\beta \times k_{NO+RO_2} \times R_{VOC}}{(1-\beta)k_{NO+RO_2}} \quad \text{(E3b)}$$

P_{HOx} is the production rate of OH, RO_2, and HO_2, and can be calculated with E4, assuming the HO_x family is in steady state.

$$c = \ -P_{HO_x} \quad \text{(E3c)}$$

$$P_{HO_x} = L_{HO_x} = \ k_{OH+NO_2}[OH][NO_2] + \beta k_{NO+RO_2}[NO][RO_2] +$$

$$2(k_{HO_2+HO_2}[HO_2][HO_2] + k_{RO_2+RO_2}[RO_2][RO_2] + k_{RO_2+HO_2}[RO_2][HO_2]) \quad \text{(E4)}$$

At low NO concentrations (NO < 0.1 ppbv), $P(O_3)$ is suppressed (NO_x-limited) due to the

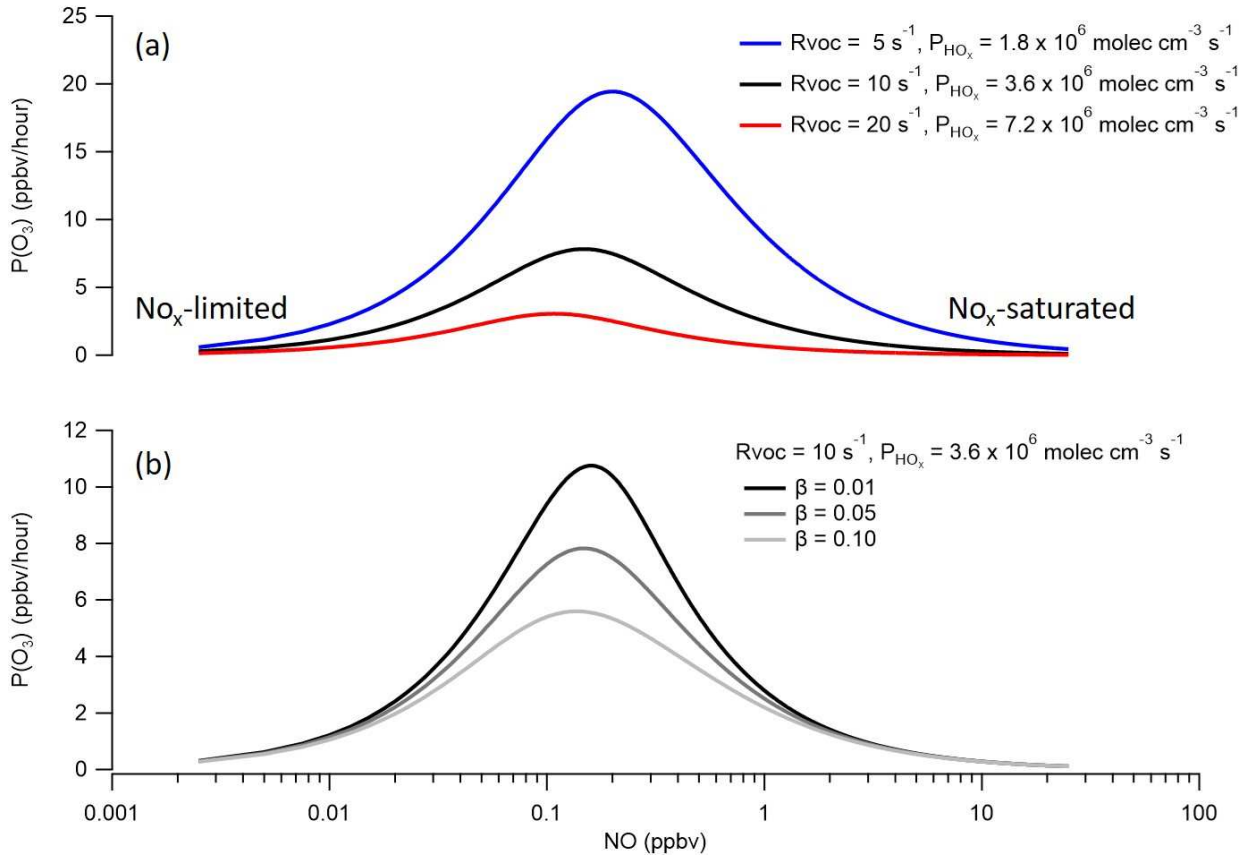

Figure 1.3. $P(O_3)$ as a function of NO concentrations calculated with E1-E3. In (a) VOC reactivity and HO_x production were increased by a factor of 2 and 4. In (b) the $RONO_2$ branching ratio (β) was increased from 0.01 to 0.10 while VOC reactivity and HO_x production were held constant.

formation of peroxides from HO_x self-reactions (R12-14). As NO increases (NO = 0.1 – 0.5 ppbv), it competes with the HO_x self-reactions, and is oxidized to NO_2 by RO_2 or HO_2 (R8a, R10), which goes on to produce O_3 (R1-3). As NO increases further (NO > 0.6 ppbv), NO_2 also increases and reacts with OH to form HNO_3 (R11, NO_x-saturated). R_{VOC} and P_{HOx} values in Figure 1.3a are representative of a polluted urban region with high O_3.[*Farmer et al.*, 2011] At either end of the NO concentration regimes, $P(O_3)$ and ambient O_3 are suppressed. Urban areas and surrounding suburban areas often have gradients of NO and VOC concentrations outside of city centers, where O_3 concentrations are typically highest.[*Ebben et al.*, 2017; *Marr et al.*, 2002; *Murphy et al.*, 2007; *Pusede et al.*, 2012] These regions that are at or near peak $P(O_3)$ can effectively reduce O_3 by reducing NO_x, VOCs, or both.

Chain termination also occurs via R8b, via $RONO_2$ formation. The formation of $RONO_2$ is typically the minor pathway during R8. The branching ratio of $RONO_2$ production is denoted as β, and is the product of α-$_{RH}$ and α-$_{RONO2}$. The branching ratio increases with increasing carbon number and pressure, and decreasing temperature [*Atkinson et al.*, 1982; *Butkovskaya et al.*, 2010a; 2012; *Butkovskaya et al.*, 2010b; *Butkovskaya et al.*, 2015; *Roberts*, 1990]. For alkanes, branching ratios increase from 0.001 [*Flocke et al.*, 1991] for CH_3O_2 + NO to 0.42 [*Saunders et al.*, 2003] for $CH_3(CH_2)O_2$ + NO. The branching ratio used in E3-E4 depends on the distribution of VOCs and VOC concentrations in an air mass, but is typically in the range of 0.02 – 0.08 for ambient air mixtures [*Perring et al.*, 2013]. In Figure 1.3b, the branching ratio increases from 0.01 to 0.10, which decreases peak $P(O_3)$ from 10.7 ppbv/hr to 5.6 ppbv/hr. The suppression of $P(O_3)$ by increased $RONO_2$ formation highlights the importance of understanding the production of $RONO_2$.[*Farmer et al.*, 2011]

1.4 Important processes that affect regional ozone

O_3 production modeled with E1-E3 in Fig. 1.3 is not a complete representation of the different parameters that impact O_3 in a region, but provides a useful framework to think about the photochemical production of O_3 in different environments. The concentration of ambient tropospheric O_3 is affected by more than just photochemical production from local anthropogenic precursor emissions. Ozone concentrations at a given location also depends on photochemical destruction, atmospheric transport of O_3 and O_3 precursors from anthropogenic and biogenic sources, exchange of O_3 rich air masses from the stratosphere, and losses to surfaces by dry deposition.[*Monks et al.*, 2015]

1.4.1 Dry deposition

Dry deposition is the loss of compounds to Earth's surface through physical processes including stomatal uptake and chemical reactions between those compounds and surfaces.[*Fowler et al.*, 2009; *Val Martin et al.*, 2014] Dry deposition processes are estimated to remove 25% of total tropospheric O_3.[*Lelieveld et al.*, 2000] Dry deposition of O_3 is dominated by vegetative uptake at Earth's surface.[*Val Martin et al.*, 2014; *Wesely et al.*, 2000] The rate of O_3 deposition (deposition velocity, V_d) is typically in the range of 0.6 – 1.0 cm s^{-1} to vegetation, and results in a deposition lifetime of about one day with a daily average 1 km boundary layer height.[*Fowler et al.*, 2001] However, due to the reactivity of O_3, dry deposition to other surfaces such as common building materials and cement is non-negligible and on the order of 0.008 – 0.064 cm s^{-1}.[*Grøntoft*, 2004; *Lin et al.*, 2015] The link between dry deposition, the characteristics of surface cover (oceans vs cities vs forests vs snow and ice), and meteorological conditions highlights the complexities in understanding the global impact of O_3 dry deposition. Understanding global O_3 trends relies on understanding the relationships between the myriad of different surfaces globally, how different

meteorological conditions affect uptake parameters such as stomatal conductance (*i.e.* diffusion of O_3 through the stomata), and understanding the feedback mechanisms caused by plant damage from O_3 uptake.[*Hardacre et al.*, 2015]

1.4.2 Regional transport of O_3 and anthropogenic precursors

Transport of O_3 and anthropogenic precursors occurs at different spatial scales including from city/urban centers to downwind receptor sites, regional transport, and intercontinental transport.[*Cooper et al.*, 2012; *Fujita et al.*, 2003; *Jacob et al.*, 1999; *Jaffe et al.*, 1999; *Jaffe et al.*, 2003; *Marr et al.*, 2002; *Murphy et al.*, 2007; *Pusede et al.*, 2012] High concentrations of VOCs and NO_x are typically emitted in urban areas with high traffic density, close proximity to electricity generating power plants, or large industrial sectors such as oil and gas refineries.[*Fujita et al.*, 2003; *Gilman et al.*, 2009; *Pusede et al.*, 2012; *Trainer et al.*, 1995; *Warneke et al.*, 2012] Urban centers often have lower ambient O_3 due to high NO_x levels, which suppresses O_3 production and titrates O_3. Polluted urban air masses are transported out of the source region which decreases NO_x concentrations and promotes more favorable O_3 production conditions and less O_3 titration.[*Marr et al.*, 2002; *Murphy et al.*, 2007; *Pusede et al.*, 2012; *Trainer et al.*, 1995]

1.4.3 Long-range transport of anthropogenic ozone precursors

Considerable effort has been put into understanding the impact of the long-range transport of anthropogenic O_3 precursors on O_3 levels in downwind regions, specifically from East Asia to Western United States.[*Cooper et al.*, 2010; *Jacob et al.*, 1999; *Parrish et al.*, 2004; *Pfister et al.*, 2011; *Sudo et al.*, 2007; *Weiss-Penzias et al.*, 2006] *Fiore et al.* [2003] found that anthropogenic emissions originating outside of the U.S. contributed 4-7 ppbv of afternoon summer O_3 over the United States. East Asia has been found to be the most important source region affecting the global

tropospheric O_3 burden due to high emissions of precursors, high surface radiation at lower latitudes, and efficient vertical transportation mechanisms.[*Bey et al.*, 2001; *Stohl et al.*, 2002; *Sudo et al.*, 2007; *Wild et al.*, 2001] Transportation of pollution from East Asia particularly impacts the higher elevation areas in the western United States.[*Brown-Steiner et al.*, 2011] *Cooper et al.* [2012] note that baseline O_3 (defined as the 5th percentile of measured O_3 values) increased at rural sites in the western U.S. from 1990 – 2010. *Jaffe et al.* [2003] reports a 10 ppbv increase in O_3 at an elevated rural site in California in air arriving from the Eastern Pacific from 1984 to 2002, and attributed the increase to increasing emissions of NO_x in Asia during that period.

1.4.4 Wildfires and biomass burning emissions

Wildfires and biomass burning emit substantial amounts of VOCs and NO_x.[e.g. *Akagi et al.*, 2011; *Andreae et al.*, 2001; *Burling et al.*, 2010] The number and intensity of wildfires and biomass burning episodes exhibit inter-annual variability due to the dependence on drought, meteorology, and human activities including politically and economically driven large-scale land clearing.[*Duncan et al.*, 2003] Global wildfires are estimated to produce 170 Tg of O_3 per year, or 3.5% of all global tropospheric O_3 production.[*Jaffe et al.*, 2008] However, large uncertainties exist in the impact of wildfire emissions on O_3 production including the magnitude of precursor emissions from different fuel sources, the effect of aerosol and particle emissions on downwind chemistry and radiation, atmospheric dynamics that affect local and downwind meteorological patterns, and the impact of long-range transport of fire emissions.[*Jaffe et al.*, 2012; *Monks et al.*, 2015] Large boreal wildfires are linked to convection episodes capable of injecting O_3 precursors and particulate matter into the upper troposphere where the emissions are distributed from long-range transport processes.[*Freitas et al.*, 2007; *Martin et al.*, 2010; *Monks et al.*, 2015] The impacts from the long-range transport of biomass emissions are highly variable, but can lead to increased

O_3 thousands of kilometers away from the burning location.[*Cook et al.*, 2007; *Real et al.*, 2007] Specifically the western United States is impacted by wildfire emissions with background O_3 concentrations in the western United States positively correlated with burn area.[*Jaffe et al.*, 2008] Recently, elevated O_3 in Northern Colorado has been linked to the transport of wildfire emissions from the Pacific Northwest.[*Lindas et al.*, 2017]

1.4.5 Stratosphere-troposphere exchange

Stratosphere-troposphere exchange from stratospheric intrusions draws O_3-rich air down from the stratosphere to the upper troposphere or close to Earth's surface if the intrusion is strong enough.[*Davies et al.*, 1994] Tropospheric O_3 levels respond to seasonal changes in O_3 transport from the stratosphere with a maximum contribution during spring at mid-latitude sites.[*Langford et al.*, 2009; *Lin et al.*, 2012; *Yates et al.*, 2013] Short episodic stratospheric intrusions have increased average surface O_3 over the western U.S> by 20-40 ppbv for short durations.[*Lin et al.*, 2012] However, the net global stratosphere-troposphere exchange O_3 burden is estimated at 550 ± 140 Tg yr^{-1} while global chemical production contributes an estimated 5000 Tg yr^{-1} of O_3.[*McLinden et al.*, 2000; *Stevenson et al.*, 2006; *Young et al.*, 2013]

1.5 Ozone and precursor trends in the United States.

The reduction of O_3 precursor emissions in the United States led to the reduction of O_3 levels in most, but not all regions of the country.[*Cooper et al.*, 2012; *EPA*, 2017; *Lefohn et al.*, 2010; *Simon et al.*, 2015] Specifically the intermountain west region including Northern Colorado exhibits increasing O_3 trends from 1990-2010 and 2000-2015.[*Abeleira et al.*, 2017; *Cooper et al.*, 2012] O_3 was identified as one of six criteria pollutants by the 1970 Clean Air Act in the United States due to the negative impacts of O_3 on human and ecosystem health. The Clean Air Act gives

the U.S. Environmental Protection Agency (EPA) the power to set a National Ambient Air Quality Standard (NAAQS) for O_3. In 2015, the EPA set the O_3 NAAQS to 70 ppbv.[*EPA*, 2015] A geographic region is out of O_3 attainment when a qualified EPA monitoring site exceeds 70 ppbv for the 4th highest maximum daily 8-hour average concentration (MDA-8), averaged over 3 years.[*EPA*, 2015] The MDA-8 metric has been adopted by the EPA to minimize the impact of inter-annual variability in O_3 levels not attributable to significant differences in precursor emissions.[*EPA*, 2015] Despite the known impacts of dry deposition, long-range O_3 precursor transport, wildfire/biomass burning emissions, and stratosphere-troposphere exchange on O_3 concentrations, the main target for reducing O_3 in the United States is the reduction of NO_x and VOC emissions from sources within the United States.

The EPA reports a 31% decrease in the aggregated nationwide annual MDA-8 from 100 ppbv in 1980 to 69 ppbv in 2016 based on ambient O_3 measurements from 206 sites across the United States.[*EPA*, 2017] The nationwide reduction in O_3 is attributed to a significant NO_x reduction in 22 eastern states – *i.e.* a 71% reduction in NO_x emissions between 1990 and 2005 in response to EPA regulations.[*EPA*, 2006] However, the national average does not capture regional trends in O_3. Ozone MDA-8 reductions between 2000 and 2015 varied in the U.S. with the largest reduction (25%) in the southeast states, followed by 16% in the northeast, 10% in the southwest, 4-10% on the west coast, and 1% in the intermountain west/northern Rockies.[*EPA*, 2016] This discrepancy is likely due to NO_x reductions not occurring uniformly across the country as the Western U.S. was not mandated by the EPA to reduce NO_x emission.[*Simon et al.*, 2015]

Since 2008, a region encompassing 8 counties in Northern Colorado has violated the O_3 National Ambient Air Quality Standard. The region is designated as a non-attainment zone, which has prompted the development of regional VOC and NO_x emission reduction plans.[*CDPHE*,

2008; 2014; 2016] Northern Colorado is a mixture of urban, suburban, and rural areas with an increasing population and substantial oil and natural gas extraction activities.[*EIA*, 2016a; b; 2017; *U.S.-Census*, 2016] The VOC and NO_x reduction plans designed by the Colorado Department of Public Health and Environment aim to reduce NO_x and VOC emissions from automobiles and electricity generating power plants, and VOC emissions from oil and gas operations.[*CDPHE*, 2008; 2014; 2016] However, this has so far led to increased O_3 levels in the Denver metropolitan region. VOC and NO_x emissions from mobile sources have decreased in major U.S. urban centers between 1990 and 2007, which has led to a decreasing VOC/NO_x ratio in urban centers.[*McDonald et al.*, 2013] Changes in VOC/NO_x in urban centers affects $P(O_3)$ and ambient O_3 levels within urban areas, and also at downwind suburban regions (Figure 1.3a).[*Murphy et al.*, 2007; *Pusede et al.*, 2012] The deviation of Northern Colorado O_3 trends from trends in much of the rest of the country prompted the analyses detailed in the following chapters.

1.6 Overview of chapters 2, 3, and 4

Ozone and NO_2 trends from 2000 – 2015 are investigated from monitoring sites in Northern Colorado in chapter 2. The two Denver sites exhibit significant increases in high O_3, median O_3, and baseline O_3 over the 15-year period with statistically significant decreases in NO_2. Sites throughout the rest of Northern Colorado exhibit no statistically significant changes in O_3 during the same period. A day of week analysis of O_3 and NO_2 at the two sites in Denver suggests that the Denver metropolitan region is transitioning from a NO_x-saturated O_3 production regime to peak production. NO_x emission reductions have been successful in the region, but further reduction is needed to reduce O_3. The O_3-temperature relationship in Northern Colorado is lower than other regions in the U.S., and the relationship is suppressed in years with severe drought. In chapter 3, the sources of VOCs in Northern Colorado are determined using Positive Matrix Factorization for

measurements campaigns in the spring and summer of 2015 at a site in Northern Colorado. Oil and natural gas related VOCs account for 40-60% of VOC reactivity at the site in both spring and summer, but during summer afternoons isoprene accounts for up to 49% of the VOC reactivity. The magnitude of isoprene concentrations in summer 2015 was 2-3x greater than values reported in summer 2012 at the same site. The NFRMA was impacted by a severe drought during summer 2012. Decreased isoprene emissions during drought years in the NFRMA explains the suppression of the O_3-temperature relationship in chapter 2 as isoprene emissions increase with increasing temperature outside of severe drought episodes. Lastly, in chapter 4 seasonal sources and sinks of C_1-C_5 alkyl nitrates at a site in Northern Colorado are investigated. Mixing ratios of C_1-C_2 alkyl nitrates are similar to rural and remote sites around the globe despite precursor mixing ratios being 10-30x greater in Northern Colorado. Diel variability of C_3-C_5 alkyl nitrates is greater during summer though mean mixing ratios between seasons are similar, which highlights the importance of the balance between photochemical production and sinks of alkyl nitrates in Northern Colorado. Winter and spring dry deposition velocities are calculated for C_1-C_5 alkyl nitrates with a range of 0.15 – 0.34 cm s^{-1}. Dry deposition is found to be an important winter and spring alkyl nitrate sink, especially for methyl nitrate.

CHAPTER 1 REFERENCES

Abeleira, A. A., and D. K. Farmer (2017), Summer ozone in the Northern Front Range Metropolitan Area: Weekend-weekday effects, temperature dependences and the impact of drought, *Atmos. Chem. Phys. Discuss.*, *2017*, 1-21, doi:10.5194/acp-2017-160.

Akagi, S., et al. (2011), Emission factors for open and domestic biomass burning for use in atmospheric models, *Atmospheric Chemistry and Physics*, *11*(9), 4039-4072.

Anderson, H. R., et al. (2004), Meta-analysis of time-series studies and panel studies of particulate matter (PM) and ozone (O3): report of a WHO task group.

Andreae, M. O., and P. Merlet (2001), Emission of trace gases and aerosols from biomass burning, *Global biogeochemical cycles*, *15*(4), 955-966.

Ashmore, M. R. (2005), Assessing the future global impacts of ozone on vegetation, *Plant, Cell & Environment*, *28*(8), 949-964, doi:10.1111/j.1365-3040.2005.01341.x.

Atkinson, R. (1990), Gas-phase tropospheric chemistry of organic compounds: a review, *Atmospheric Environment. Part A. General Topics*, *24*(1), 1-41.

Atkinson, R., and J. Arey (2003), Atmospheric Degradation of Volatile Organic Compounds, *Chemical Reviews*, *103*(12), 4605-4638, doi:10.1021/cr0206420.

Atkinson, R., et al. (1982), Alkyl nitrate formation from the nitrogen oxide (NOx)-air photooxidations of C2-C8 n-alkanes, *The Journal of Physical Chemistry*, *86*(23), 4563-4569.

Avnery, S., D. L. Mauzerall, J. Liu, and L. W. Horowitz (2011), Global crop yield reductions due to surface ozone exposure: 2. Year 2030 potential crop production losses and economic damage under two scenarios of O3 pollution, *Atmospheric Environment*, *45*(13), 2297-2309, doi:http://dx.doi.org/10.1016/j.atmosenv.2011.01.002.

Bell, M. L., et al. (2004), Ozone and short-term mortality in 95 US urban communities, 1987-2000, *Jama*, *292*(19), 2372-2378.

Bey, I., D. J. Jacob, J. Logan, and R. M. Yantosca (2001), Asian chemical outflow to the Pacific in spring: Origins, pathways, and budgets, *Journal of Geophysical Research: Atmospheres*, *106*(D19), 23097-23113.

Brown-Steiner, B., and P. Hess (2011), Asian influence on surface ozone in the United States: A comparison of chemistry, seasonality, and transport mechanisms, *Journal of Geophysical Research: Atmospheres*, *116*(D17), n/a-n/a, doi:10.1029/2011JD015846.

Brunekreef, B., D. W. Dockery, and M. Krzyzanowski (1995), Epidemiologic studies on short-term effects of low levels of major ambient air pollution components, *Environmental health perspectives*, *103*(Suppl 2), 3.

Burling, I., et al. (2010), Laboratory measurements of trace gas emissions from biomass burning of fuel types from the southeastern and southwestern United States, *Atmospheric Chemistry and Physics*, *10*(22), 11115-11130.

Butkovskaya, N., A. Kukui, and G. Le Bras (2010a), Pressure and Temperature Dependence of Ethyl Nitrate Formation in the C2H5O2 + NO Reaction, *The Journal of Physical Chemistry A*, *114*(2), 956-964, doi:10.1021/jp910003a.

Butkovskaya, N., A. Kukui, and G. Le Bras (2012), Pressure and Temperature Dependence of Methyl Nitrate Formation in the CH3O2 + NO Reaction, *The Journal of Physical Chemistry A*, *116*(24), 5972-5980, doi:10.1021/jp210710d.

Butkovskaya, N. I., A. Kukui, and G. Le Bras (2010b), Pressure Dependence of Iso-Propyl Nitrate Formation in the i-C3H7O2+ NO Reaction, *Zeitschrift für Physikalische Chemie*, *224*(7-8), 1025-1038.
Butkovskaya, N. I., et al. (2015), Pressure Dependence of Butyl Nitrate Formation in the Reaction of Butylperoxy Radicals with Nitrogen Oxide, *The Journal of Physical Chemistry A*, *119*(19), 4408-4417, doi:10.1021/jp509427x.
CDPHE (2008), Denver Metro Area & North Front Range Ozone Action Plan., edited, Colorado Air Quality Control Commission, Denver, CO.
CDPHE (2014), Control of Ozone Via Ozone Precursors and Control of Hydocarbons Via Oil and Gas Emissions., edited, Colorado Air Quality Control Commission, Denver, CO.
CDPHE (2016), Moderate area ozone SIP for the Denver Metro and North Front Range nonattaiment area., edited, Denver, CO.
Chameides, W., and J. C. Walker (1973), A photochemical theory of tropospheric ozone, *Journal of Geophysical Research*, *78*(36), 8751-8760.
Cook, P. A., et al. (2007), Forest fire plumes over the North Atlantic: p-TOMCAT model simulations with aircraft and satellite measurements from the ITOP/ICARTT Campaign, *Journal of Geophysical Research: Atmospheres*, *112*(D10).
Cooper, O., et al. (2010), Increasing springtime ozone mixing ratios in the free troposphere over western North America, *Nature*, *463*(7279), 344-348.
Cooper, O. R., et al. (2012), Long-term ozone trends at rural ozone monitoring sites across the United States, 1990–2010, *Journal of Geophysical Research: Atmospheres*, *117*(D22).
Crabtree, J., and A. Kemp (1946), Weathering of Soft Vulcanized Rubber, *Industrial & Engineering Chemistry*, *38*(3), 278-296.
Crutzen, P. (1973a), A discussion of the chemistry of some minor constituents in the stratosphere and troposphere, *Pure and Applied Geophysics*, *106*(1), 1385-1399.
Crutzen, P. J. (1973b), Gas-phase nitrogen and methane chemistry in the atmosphere, in *Physics and Chemistry of Upper Atmosphere*, edited, pp. 110-124, Springer.
Davies, T. D., and E. Schuepbach (1994), Episodes of high ozone concentrations at the earth's surface resulting from transport down from the upper troposphere/lower stratosphere: a review and case studies, *Atmospheric Environment*, *28*(1), 53-68, doi:https://doi.org/10.1016/1352-2310(94)90022-1.
Davison, A. W., and J. D. Barnes (1998), Effects of ozone on wild plants, *New Phytologist*, *139*(1), 135-151, doi:undefined.
Duncan, B. N., et al. (2003), Interannual and seasonal variability of biomass burning emissions constrained by satellite observations, *Journal of Geophysical Research: Atmospheres*, *108*(D2).
Ebben, C. J., et al. (2017), Evolution of NOx in the Denver Urban Plume during the Front Range Air Pollution and Photochemistry Experiment, *Atmos. Chem. Phys. Discuss.*, *2017*, 1-13, doi:10.5194/acp-2017-671.
Ebi, K. L., and G. McGregor (2008), Climate Change, Tropospheric Ozone and Particulate Matter, and Health Impacts, *Environmental Health Perspectives*, *116*(11), 1449-1455, doi:10.1289/ehp.11463.
EIA (2016a), Natural Gas Gross Withdrawals and Production, edited.
EIA (2016b), Number of Producing Gas Wells, edited.
EIA (2017), Number and capacity of petroleum refineries, in *Petroleum & Other Liquids*, edited.

EPA (2006), NOx budget trading program 2005 program compliance and environmental results, edited by O. o. A. a. Radiation, EPA, Washington, DC.
EPA (2015), National Ambient Air Quality Standards for Ozone, edited.
EPA (2016), Ozone Trends, edited.
EPA (2017), Ozone Trends, edited.
Farmer, D., et al. (2011), Impact of organic nitrates on urban ozone production, *Atmospheric Chemistry and Physics*, *11*(9), 4085-4094.
Fiore, A. M., D. J. Jacob, R. Mathur, and R. V. Martin (2003), Application of empirical orthogonal functions to evaluate ozone simulations with regional and global models, *Journal of Geophysical Research: Atmospheres*, *108*(D14), n/a-n/a, doi:10.1029/2002JD003151.
Flocke, F., A. Volz-Thomas, and D. Kley (1991), Measurements of alkyl nitrates in rural and polluted air masses, *Atmospheric Environment. Part A. General Topics*, *25*(9), 1951-1960.
Fowler, D., et al. (2001), Measurements of Ozone Deposition to Vegetation Quantifying the Flux, the Stomatal and Non-Stomatal Components, *Water, Air, and Soil Pollution*, *130*(1), 63-74, doi:10.1023/A:1012243317471.
Fowler, D., et al. (2009), Atmospheric composition change: Ecosystems–Atmosphere interactions, *Atmospheric Environment*, *43*(33), 5193-5267, doi:http://dx.doi.org/10.1016/j.atmosenv.2009.07.068.
Freitas, S. R., et al. (2007), Including the sub-grid scale plume rise of vegetation fires in low resolution atmospheric transport models, *Atmospheric Chemistry and Physics*, *7*(13), 3385-3398.
Fujita, E. M., et al. (2003), Evolution of the magnitude and spatial extent of the weekend ozone effect in California's South Coast Air Basin, 1981–2000, *Journal of the Air & Waste Management Association*, *53*(7), 802-815.
Gauderman, W. J., et al. (2002), Association between air pollution and lung function growth in southern California children: results from a second cohort, *American journal of respiratory and critical care medicine*, *166*(1), 76-84.
Gilliland, F. D., et al. (2001), The effects of ambient air pollution on school absenteeism due to respiratory illnesses, *Epidemiology*, *12*(1), 43-54.
Gilman, J. B., et al. (2009), Measurements of volatile organic compounds during the 2006 TexAQS/GoMACCS campaign: Industrial influences, regional characteristics, and diurnal dependencies of the OH reactivity, *Journal of Geophysical Research*, *114*, doi:10.1029/2008jd011525.
Grøntoft, T. (2004), Measurements and modelling of the ozone deposition velocity to concrete tiles, including the effect of diffusion, *Atmospheric Environment*, *38*(1), 49-58, doi:http://dx.doi.org/10.1016/j.atmosenv.2003.09.044.
Haagen-Smit, A. (1952), Chemistry and physiology of Los Angeles smog, *Industrial & Engineering Chemistry*, *44*(6), 1342-1346.
Haagen-Smit, A., et al. (1952), Investigation on injury to plants from air pollution in the Los Angeles area, *Plant Physiology*, *27*(1), 18.
Haagen-Smit, A. J., C. Bradley, and M. M. Fox (1953), Ozone formation in photochemical oxidation of organic substances, *Industrial & Engineering Chemistry*, *45*(9), 2086-2089.

Hardacre, C., O. Wild, and L. Emberson (2015), An evaluation of ozone dry deposition in global scale chemistry climate models, *Atmos. Chem. Phys.*, *15*(11), 6419-6436, doi:10.5194/acp-15-6419-2015.

Hayes, F., M. L. M. Jones, G. Mills, and M. Ashmore (2007), Meta-analysis of the relative sensitivity of semi-natural vegetation species to ozone, *Environmental Pollution*, *146*(3), 754-762, doi:http://dx.doi.org/10.1016/j.envpol.2006.06.011.

Jacob, D. J., J. A. Logan, and P. P. Murti (1999), Effect of rising Asian emissions on surface ozone in the United States, *Geophysical Research Letters*, *26*(14), 2175-2178.

Jaffe, D., et al. (1999), Transport of Asian air pollution to North America, *Geophysical Research Letters*, *26*(6), 711-714.

Jaffe, D., et al. (2008), Influence of fires on O3 concentrations in the western US, *Environmental science & technology*, *42*(16), 5885-5891.

Jaffe, D., et al. (2003), Increasing background ozone during spring on the west coast of North America, *Geophysical Research Letters*, *30*(12).

Jaffe, D. A., and N. L. Wigder (2012), Ozone production from wildfires: A critical review, *Atmospheric Environment*, *51*, 1-10.

Kleinman, L., et al. (1994), Ozone formation at a rural site in the southeastern United States, *Journal of Geophysical Research: Atmospheres*, *99*(D2), 3469-3482.

Langford, A. O., K. C. Aikin, C. S. Eubank, and E. J. Williams (2009), Stratospheric contribution to high surface ozone in Colorado during springtime, *Geophysical Research Letters*, *36*(12), n/a-n/a, doi:10.1029/2009GL038367.

Lefohn, A. S., D. Shadwick, and S. J. Oltmans (2010), Characterizing changes in surface ozone levels in metropolitan and rural areas in the United States for 1980–2008 and 1994–2008, *Atmospheric Environment*, *44*(39), 5199-5210.

Leighton, P. (1961), *Photochemistry of air pollution*, Academic Press, New York.

Lelieveld, J., and F. J. Dentener (2000), What controls tropospheric ozone?, *Journal of Geophysical Research: Atmospheres*, *105*(D3), 3531-3551, doi:10.1029/1999JD901011.

Levy, H. (1971), Normal atmosphere: Large radical and formaldehyde concentrations predicted, *Science*, *173*(3992), 141-143.

Levy, H. (1972), Photochemistry of the lower troposphere, *Planetary and Space Science*, *20*(6), 919-935.

Levy, H. (1973), Photochemistry of minor constituents in the troposphere, *Planetary and Space Science*, *21*(4), 575-591.

Lin, C.-C., and S.-C. Hsu (2015), Deposition velocities and impact of physical properties on ozone removal for building materials, *Atmospheric Environment*, *101*, 194-199, doi:http://dx.doi.org/10.1016/j.atmosenv.2014.11.029.

Lin, M., et al. (2012), Springtime high surface ozone events over the western United States: Quantifying the role of stratospheric intrusions, *Journal of Geophysical Research: Atmospheres*, *117*(D21), n/a-n/a, doi:10.1029/2012JD018151.

Lindas, J., et al. (2017), The impact of aged wildfire smoke on atmospheric composition and ozone in the Colorado Front Range in summer 2015, *Atmospheric Chemistry and Physics*, *in preparation*.

Marr, L. C., and R. A. Harley (2002), Modeling the Effect of Weekday− Weekend Differences in Motor Vehicle Emissions on Photochemical Air Pollution in Central California, *Environmental science & technology*, *36*(19), 4099-4106.

Martin, M. V., et al. (2010), Smoke injection heights from fires in North America: analysis of 5 years of satellite observations, *Atmos. Chem. Phys*, *10*(4), 1491-1510.
Matyssek, R., and H. Sandermann Jr (2003), Impact of ozone on trees: an ecophysiological perspective, in *Progress in botany*, edited, pp. 349-404, Springer.
McDonald, B. C., D. R. Gentner, A. H. Goldstein, and R. A. Harley (2013), Long-term trends in motor vehicle emissions in US urban areas, *Environmental science & technology*, *47*(17), 10022-10031.
McKeen, S., E. Y. Hsie, and S. Liu (1991), A study of the dependence of rural ozone on ozone precursors in the eastern United States, *Journal of Geophysical Research: Atmospheres*, *96*(D8), 15377-15394.
McLinden, C. A., et al. (2000), Stratospheric ozone in 3-D models: A simple chemistry and the cross-tropopause flux, *Journal of Geophysical Research: Atmospheres*, *105*(D11), 14653-14665, doi:10.1029/2000JD900124.
Mills, G., et al. (2007), A synthesis of AOT40-based response functions and critical levels of ozone for agricultural and horticultural crops, *Atmospheric Environment*, *41*(12), 2630-2643, doi:http://dx.doi.org/10.1016/j.atmosenv.2006.11.016.
Mills, G., et al. (2011), Evidence of widespread effects of ozone on crops and (semi-) natural vegetation in Europe (1990–2006) in relation to AOT40-and flux-based risk maps, *Global Change Biology*, *17*(1), 592-613.
Monks, P. S. (2005), Gas-phase radical chemistry in the troposphere, *Chemical Society Reviews*, *34*(5), 376-395.
Monks, P. S., et al. (2015), Tropospheric ozone and its precursors from the urban to the global scale from air quality to short-lived climate forcer, *Atmospheric Chemistry and Physics*, *15*(15), 8889-8973.
Montgomery, M. R. (2008), The urban transformation of the developing world, *science*, *319*(5864), 761-764.
Murphy, J. G., et al. (2007), The weekend effect within and downwind of Sacramento–Part 1: Observations of ozone, nitrogen oxides, and VOC reactivity, *Atmospheric Chemistry and Physics*, *7*(20), 5327-5339.
Parrish, D., et al. (2004), Changes in the photochemical environment of the temperate North Pacific troposphere in response to increased Asian emissions, *Journal of Geophysical Research: Atmospheres*, *109*(D23).
Perring, A., S. Pusede, and R. Cohen (2013), An observational perspective on the atmospheric impacts of alkyl and multifunctional nitrates on ozone and secondary organic aerosol, *Chemical reviews*, *113*(8), 5848-5870.
Pfister, G., et al. (2011), Characterizing summertime chemical boundary conditions for airmasses entering the US West Coast, *Atmospheric Chemistry and Physics*, *11*(4), 1769-1790.
Pusede, S. E., and R. C. Cohen (2012), On the observed response of ozone to NO_x and VOC reactivity reductions in San Joaquin Valley California 1995–present, *Atmospheric Chemistry and Physics*, *12*(18), 8323-8339, doi:10.5194/acp-12-8323-2012.
Real, E., et al. (2007), Processes influencing ozone levels in Alaskan forest fire plumes during long-range transport over the North Atlantic, *Journal of Geophysical Research: Atmospheres*, *112*(D10), n/a-n/a, doi:10.1029/2006JD007576.
Roberts, J. M. (1990), The atmospheric chemistry of organic nitrates, *Atmospheric Environment. Part A. General Topics*, *24*(2), 243-287.

Ross, K., J. F. Chmiel, and T. Ferkol (2012), The impact of the Clean Air Act, *The Journal of pediatrics*, *161*(5), 781-786, doi:10.1016/j.jpeds.2012.06.064.
Sander, S. P., et al. (2015), Chemical kinetics and photochemical data for use in atmospheric studies evaluation number 18.
Saunders, S. M., M. E. Jenkin, R. Derwent, and M. Pilling (2003), Protocol for the development of the Master Chemical Mechanism, MCM v3 (Part A): tropospheric degradation of non-aromatic volatile organic compounds, *Atmospheric Chemistry and Physics*, *3*(1), 161-180.
Sillman, S. (1995), The use of NO y, H2O2, and HNO3 as indicators for ozone-NO x-hydrocarbon sensitivity in urban locations, *Journal of Geophysical Research: Atmospheres*, *100*(D7), 14175-14188.
Sillman, S. (1999), The relation between ozone, NO x and hydrocarbons in urban and polluted rural environments, *Atmospheric Environment*, *33*(12), 1821-1845.
Sillman, S., and D. He (2002), Some theoretical results concerning O3-NOx-VOC chemistry and NOx-VOC indicators, *Journal of Geophysical Research: Atmospheres*, *107*(D22).
Sillman, S., D. He, C. Cardelino, and R. E. Imhoff (1997), The use of photochemical indicators to evaluate ozone-NOx-hydrocarbon sensitivity: Case studies from Atlanta, New York, and Los Angeles, *Journal of the Air & Waste Management Association*, *47*(10), 1030-1040.
Sillman, S., J. A. Logan, and S. C. Wofsy (1990), The sensitivity of ozone to nitrogen oxides and hydrocarbons in regional ozone episodes, *Journal of Geophysical Research: Atmospheres*, *95*(D2), 1837-1851.
Simon, H., et al. (2015), Ozone Trends Across the United States over a Period of Decreasing NOx and VOC Emissions, *Environmental Science & Technology*, *49*(1), 186-195, doi:10.1021/es504514z.
Stevenson, D. S., et al. (2006), Multimodel ensemble simulations of present-day and near-future tropospheric ozone, *Journal of Geophysical Research: Atmospheres*, *111*(D8), n/a-n/a, doi:10.1029/2005JD006338.
Stohl, A., et al. (2002), On the pathways and timescales of intercontinental air pollution transport, *Journal of Geophysical Research: Atmospheres*, *107*(D23).
Sudo, K., and H. Akimoto (2007), Global source attribution of tropospheric ozone: Long-range transport from various source regions, *Journal of Geophysical Research: Atmospheres*, *112*(D12), n/a-n/a, doi:10.1029/2006JD007992.
Tai, A. P., M. V. Martin, and C. L. Heald (2014), Threat to future global food security from climate change and ozone air pollution, *Nature Climate Change*, *4*(9), 817.
Thornton, J. A. (2002), Ozone production rates as a function of NOxabundances and HOxproduction rates in the Nashville urban plume, *Journal of Geophysical Research*, *107*(D12), doi:10.1029/2001jd000932.
Thurston, G. D., and K. Ito (1999), Epidemiological studies of ozone exposure effects, *Air pollution and health*, *1*, 485-509.
Trainer, M., et al. (1995), Regional ozone and urban plumes in the southeastern United States: Birmingham, a case study, *Journal of Geophysical Research: Atmospheres*, *100*(D9), 18823-18834.
U.S.-Census (2016), Quick Facts - Colorado, edited.
Val Martin, M., C. L. Heald, and S. R. Arnold (2014), Coupling dry deposition to vegetation phenology in the Community Earth System Model: Implications for the simulation of

surface O3, *Geophysical Research Letters*, *41*(8), 2988-2996, doi:10.1002/2014GL059651.
Warneke, C., et al. (2012), Multiyear trends in volatile organic compounds in Los Angeles, California: Five decades of decreasing emissions, *Journal of Geophysical Research: Atmospheres*, *117*(D21).
Weiss-Penzias, P., et al. (2006), Observations of Asian air pollution in the free troposphere at Mount Bachelor Observatory during the spring of 2004, *Journal of Geophysical Research: Atmospheres*, *111*(D10).
Wesely, M. L., and B. B. Hicks (2000), A review of the current status of knowledge on dry deposition, *Atmospheric Environment*, *34*(12), 2261-2282, doi:http://dx.doi.org/10.1016/S1352-2310(99)00467-7.
West, J. J., S. Szopa, and D. A. Hauglustaine (2007), Human mortality effects of future concentrations of tropospheric ozone, *Comptes Rendus Geoscience*, *339*(11), 775-783, doi:http://dx.doi.org/10.1016/j.crte.2007.08.005.
Wild, O., and H. Akimoto (2001), Intercontinental transport of ozone and its precursors in a three-dimensional global CTM, *Journal of Geophysical Research: Atmospheres*, *106*(D21), 27729-27744.
Yang, Q., et al. (2003), Association between ozone and respiratory admissions among children and the elderly in Vancouver, Canada, *Inhalation toxicology*, *15*(13), 1297-1308.
Yates, E. L., et al. (2013), Airborne observations and modeling of springtime stratosphere-to-troposphere transport over California, *Atmos. Chem. Phys.*, *13*(24), 12481-12494, doi:10.5194/acp-13-12481-2013.
Young, P. J., et al. (2013), Pre-industrial to end 21st century projections of tropospheric ozone from the Atmospheric Chemistry and Climate Model Intercomparison Project (ACCMIP), *Atmos. Chem. Phys.*, *13*(4), 2063-2090, doi:10.5194/acp-13-2063-2013.
Zhang, L., et al. (2012), Nitrogen deposition to the United States: distribution, sources, and processes, *Atmos. Chem. Phys.*, *12*(10), 4539-4554, doi:10.5194/acp-12-4539-2012.
Zhu, T., et al. (2012), Impacts of megacities on air pollution and climate, *WMO, Geneva*.

CHAPTER 2 – SUMMER OZONE IN THE NORTHERN FRONT RANGE METROPOLITAN AREA: WEEKEND-WEEKDAY EFFECTS, TEMPERTURE DEPENDENCES AND THE IMPACT OF DROUGHT[1]

2.1. Introduction

Tropospheric ozone (O_3) is detrimental to human health, impacting asthma attacks, cardiovascular disease, missed school days, and premature deaths. Based on these impacts, the Environmental Protection Agency (EPA) projects that reducing the O_3 standard to the new 70 ppb_v 8-hour average will result in health benefits of $6.4-13 billion/yr [*EPA*, 2014]. O_3 also damages plants, reducing agricultural yields [*Tai et al.*, 2014]. Using crop yields and ambient O_3 concentrations for 2000, *Avnery et al.* [2011] estimate the loss of $11-18 billion/yr worldwide as a result of the reduction of staple worldwide crops (soybean, maize, and wheat) from O_3 damage. During summer months, the Northern Front Range Metropolitan Area (NFRMA) of Colorado consistently violated the pre-2016 U.S. EPA National Ambient Air Quality Standard (NAAQS) of 75 ppb_v fourth-highest daily maximum 8-hour average (MDA8) ambient O_3 concentration, despite proposed reductions in anthropogenic emissions [*CDPHE*, 2014]. The NFRMA has been an O_3 non-attainment zone since 2008 [*CDPHE*, 2009], prompting the Colorado Air Pollution Control Division and the Regional Air Quality Council to develop the Colorado Ozone Action Plan in 2008 to target key O_3 precursors: volatile organic compounds (VOCs) and NO_x ($NO+NO_2$)[*CDPHE*, 2008]. Despite these control efforts, 2013 was the NFRMA's fourth year in a row to exceed the federal O_3 standard [*CDPHE*, 2016], and the eight NFRMA non-attainment counties, with their

[1] Abeleira, A. A., and D. K. Farmer (2017), Summer ozone in the Northern Front Range Metropolitan Area: Weekend-weekday effects, temperature dependences and the impact of drought, *Atmos. Chem. Phys. Discuss.*, *2017*, 1-21, doi:10.5194/acp-2017-160.

combined population >3.5 million, exceeded the MDA8 75 ppb_v O_3 standard 9-48 days between 2010 and 2012 [*AMA*, 2015]. However, Colorado must comply with the new 70 ppb_v MDA8 standard by 2018. In order to accurately design and implement O_3 reduction schemes, a thorough understanding of local O_3 trends and chemistry is required.

Ground-level or boundary layer O_3 depends on local production, transport, and meteorological parameters:

$$\frac{\partial[O_3]}{\partial t} = P(O_3) + \frac{w_e O_3 - u_d[O_3]}{H} - \nabla \times (v[O_3]) \quad \text{(E1)}$$

where $\partial[O_3]/\partial t$ represents the time rate of change of O_3 concentration, $P(O_3)$ is the instantaneous net photochemical O_3 production rate (production – loss), $w_e O_3 - u_d[O_3]/H$ represents the entrainment rate (w_e) of O_3 in and deposition rate (u_d) of O_3 out of the mixing layer height (H), and $\nabla \times (v[O_3])$ describes the advection of O_3 mixing layer height. Briefly, ground-level O_3 is driven by a catalytic chain that is initiated by RO_2 production from VOC oxidation (R1), and propagated by local NO_x emissions (R2,3).

$$RH + OH + O_2 \rightarrow RO_2 + HO_2 \quad \text{(R1)}$$

Chain propagation occurs through reactions between HO_2 or RO_2 radicals with NO to form NO_2 (R2a,b, R3), which is photolyzed (R4) and leads to net O_3 formation (R5). Reactions between NO and O_3 also produces NO_2 (R6), leading to a null cycle with no net O_3 production. Alkoxy (RO) radicals form carbonyl-containing compounds and HO_2 (R7).

$$RO_2 + NO \rightarrow RO + NO_2 \quad \text{(R2a)}$$

$$RO_2 + NO \rightarrow RONO_2 \quad \text{(R2b)}$$

$$HO_2 + NO \rightarrow NO_2 + OH \quad \text{(R3)}$$

$$NO_2 + h\nu \rightarrow NO + O(\,^3P) \quad \text{(R4)}$$

$$O(\,^3P) + O_2 \rightarrow O_3 \quad \text{(R5)}$$

$$NO + O_3 \rightarrow NO_2 + O_2 \quad \text{(R6)}$$

$$RO + O_2 \rightarrow R'CHO + HO_2 \quad \text{(R7)}$$

For every VOC that enters the cycle, approximately two NO_2 radicals are produced – but the resulting carbonyl-containing compounds and organic nitrates can be repeatedly oxidized or photolyzed, further propagating the $P(O_3)$ chain. Chain termination occurs through RO_2 and HO_2 self-reactions to form peroxides (dominant termination reactions in the "NO_x-limited regime"), OH and NO_2 reactions to form HNO_3 ("NO_x-saturated" or "VOC-limited" regime), or RO_2 and NO_x reactions to form organic nitrates ($RONO_2$) or peroxyacyl nitrates ($RC(O)O_2NO_2$). Formation of organic and peroxyacyl nitrates suppresses $P(O_3)$, but does not shift the cross-over point between NO_x-limited and NO_x-saturated $P(O_3)$ regimes [*Farmer et al.*, 2011]. This cross-over point of maximum, or peak, O_3 production is controlled by the chain termination reactions, and is sensitive to the HO_x production rate and thus VOC reactivity. Decreasing NO_x is an effective O_3 control strategy in a NO_x-limited system, but will increase O_3 in a NO_x-saturated system. Controls for NO_x-saturated systems often focus on reducing anthropogenic VOC reactivity, and/or suppressing NO_x emissions sufficiently that the system becomes NO_x-limited.

Trends in O_3 for 2000 – 2015 varied across the United States [*EPA*, 2016b]. Using the annual 4th maximum of daily 8-hour averages (MDA-8), the EPA reported a 17% decrease in the aggregated national average O_3. However, regional trends deviated substantially from the national average. For example, the EPA reported a 25% decrease in O_3 throughout the southeast, while the northeast shows a 16% decrease. Smaller decreases in O_3 occurred in the northern Rockies (1%),

the southwest (10%) and the west coast (4-10%). These O_3 reductions are concurrent with national reductions in O_3 precursors of 54% for NO_x, 21 % for VOCs, and 50% for CO [*EPA*, 2016a]. Due to the non-linear behavior of O_3 chemistry described above, reductions in O_3 precursors do not necessarily result in reductions of ambient O_3. *Cooper et al.* [2012] reported that 83%, 66%, and 20% of rural eastern U.S. sites exhibited statistically significant decreases in summer O_3 at the 95^{th}, 50^{th}, and 5^{th} percentiles (1990-2010). No increases in O_3 occurred at any sites, indicating that local emission reductions have been effective in those regions. In contrast, O_3 in the western US followed a very different trend: only 8% of western U.S. sites exhibited decreased O_3 at the 50^{th} percentile; the 5^{th} percentiles for O_3 at 33% of the sites actually increased. These increases were larger for the lower percentiles, indicating that while local emissions reductions may have been effective at some sites, increased background O_3 offset the improvement.

Lefohn et al. [2010] found that when comparing O_3 at the same sites for a longer period of 1980-2008 and shorter period of 1994-2008 that the predominant pattern was a change from a negative trend (decreasing O_3) during the longer period to no trend (stagnant O_3) in the shorter period, indicating that O_3 reductions had leveled off by the late 2000s. The leveling off could be a result of either slowed precursor emissions reductions, which is contrary to the EPA estimates, or, more likely, shifting O_3 chemistry regimes as precursor emissions are changing. *McDonald et al.* [2013] report decreased VOC, CO, and NO_x automobile emissions in major US urban centers, and decreasing VOC/NO_x trends from 1990 to 2007 with a turnaround and small increase after 2007. This will affect local O_3 chemistry within the city and at downwind receptor sites. *Lefohn et al.* [2010] reported that the distributions of high and low hourly O_3 values narrowed toward mid-level values in the 12 cities studied, consistent with a reduction in domestic O_3 precursors and possibly increased transport of O_3 precursors from east Asia. Modeling and measurement studies have also

reported increased baseline O_3 in the western U.S. due to the transport of O_3 precursors from east Asia [*Cooper et al.*, 2010; *Parrish et al.*, 2004; *Pfister et al.*, 2011; *Weiss-Penzias et al.*, 2006]. These studies questioned the effectiveness of local precursor emission reductions in controlling local O_3 in impacted regions.

The intermountain West is an intriguing environment with potentially increasing background O_3 [*Cooper et al.*, 2012]. The NFRMA is of particular interest due to the challenge in effective O_3 regulation, its growing population and the dominantly anthropogenic sources of O_3 precursors. VOCs have been well-studied in the region, with a particular focus on the Boulder Atmospheric Observatory (BAO) in Erie, CO [e.g. *Gilman et al.*, 2013; *McDuffie et al.*, 2016; *Pétron et al.*, 2012; *Swarthout et al.*, 2013; *Thompson et al.*, 2014]. VOC composition in the NFRMA was heavily influenced by oil and natural gas (ONG) sources, as well as traffic. In winter 2011, ~50% of VOC reactivity was attributed to ONG-related VOCs and ~10% to traffic [*Gilman et al.*, 2013; *Swarthout et al.*, 2013]. Recent studies have shown that ONG and traffic contributed up to 66% and 13% of the VOC reactivity respectively at BAO in mornings for both spring and summer 2015, but that biogenic isoprene was a large, temperature-dependent component of VOC reactivity in the summer, contributing up to 49% of calculated daytime VOC reactivity [*Abeleira et al.*, 2017]. We note that the anthropogenic VOCs were typically lower in 2015 than previous measurements, pointing to the complex roles of meteorology, transport and local emissions. In contrast, observed isoprene in summer 2012 was much lower than summer 2015, likely due to shifting drought conditions. While temperatures across the two summers were similar, 2012 was a widespread drought year in the region, and 2015 was not. Drought is typically associated with suppressed biogenic VOC emissions [*Brilli et al.*, 2007; *Fortunati et al.*, 2008; *Guenther*, 2006]. Local anthropogenic and biogenic sources are not the only VOC sources in the region: longer-

lived VOCs consistent with transport have also been observed (21-44% of afternoon reactivity in 2015), and smoke from both local and long-distance wildfires impacted air quality in the NFRMA in punctuated events. This smoke was sometimes, but not always, associated with elevated O_3 [*Lindas et al.*, 2017].

The impact of a changing climate on air quality is poorly understood due to the complex climate-chemistry interactions and numerous feedbacks [*Jacob et al.*, 2009; *Palut et al.*, 2007]. However, increasing temperature is expected to increase O_3 [*Bloomer et al.*, 2009; *Jacob et al.*, 2009; *Palut et al.*, 2007]. The O_3-temperature relationship is attributed to (1) temperature-dependent biogenic VOC emissions that provide a source of VOCs for OH oxidation leading to increased HO_x cycling [*Guenther*, 2006; *Guenther et al.*, 1996], (2) thermal decomposition of peroxyacetylnitrate (PAN) to HO_x and NO_x [*Fischer et al.*, 2014; *Singh et al.*, 1981], and (3) increased likelihood of favorable meteorological conditions for ozone formation (*i.e.* high insolation, stagnation, circulating wind patterns) [*Reddy et al.*, 2016; *Thompson et al.*, 2001]. In addition, increased temperatures and changing soil moisture could alter soil emissions of NO_x. Due to the non-linearity of $P(O_3)$ chemistry as a function of NO_x, the increased VOC and NO_x emissions associated with warming can either increase or decrease $P(O_3)$ depending on local NO_x levels (i.e. NO_x-limited vs. NO_x-saturated). Interactions between climate change and regional-scale meteorology are complex, and may also impact O_3. High and low O_3 in the U.S is coupled to a variety of meteorological parameters including planetary boundary layer (PBL) heights [*Reddy et al.*, 2016; *White et al.*, 2007], surface temperatures [*Bloomer et al.*, 2009], stratospheric intrusions [*Lin et al.*, 2015], soil-moisture and regional winds [*Davis et al.*, 2011; *Thompson et al.*, 2001]. PBL height is coupled to increased temperatures, reduced cloud cover, stronger insolation,

and lighter circulating wind patterns with higher 500 hPa heights correlating to higher average July O_3 in the NFRMA [*Reddy et al.*, 2016].

In this paper, we used temperature, O_3, and NO_2 data from 2000-2015 at multiple sites in the NFRMA to investigate why O_3 has not decreased in the region despite decreases in NO_x. We used a weekend-weekday analysis to elucidate the NO_x regime for $P(O_3)$ in Denver, and explored the temperature dependence of O_3 and the role of drought in influencing that relationship in the NFRMA.

2.2. Methods

2.2.1. Measurement sites

We used publicly available O_3, NO_2 and temperature data (https://aqs.epa.gov/aqsweb/documents/data_mart_welcome.html) from eight sites in the NFRMA (Fig. 2.1). The CAMP site is 1 mile east of the I-25 interstate highway in downtown Denver. O_3 data was available for 2005 – 2007 and 2012 – 2015, while NO_2 data was available for 2001 – 2007 and 2010 – 2015. Welby is roughly 8 miles northeast from the CAMP site, and is adjacent to a large lake and less than 1-mile west of the Rocky Mountain Arsenal open space. O_3 data was available for 2000 – 2009 and 2011 – 2015, while NO_2 data was available for 2001 – 2002, 2004 – 2005, 2007 – 2008, and 2010 – 2015. The Carriage site is <1 mile west of the I-25 interstate at the same latitude as the CAMP site. O_3 data was available for 2000 – 2012 for the Carriage site. The Fort Collins site is adjacent to Colorado State University near downtown Fort Collins. O_3 data was available for 2000 – 2015. The Greeley site was located on the southeast side of Greeley and <1 mile south of CO state highway 34. O_3 data was available for 2002 – 2015. The Rocky Flats site is in a rural area adjacent to the Rocky Flats Wildlife Refuge <15 miles south of Boulder. The I-25 site is adjacent to the I-25 interstate

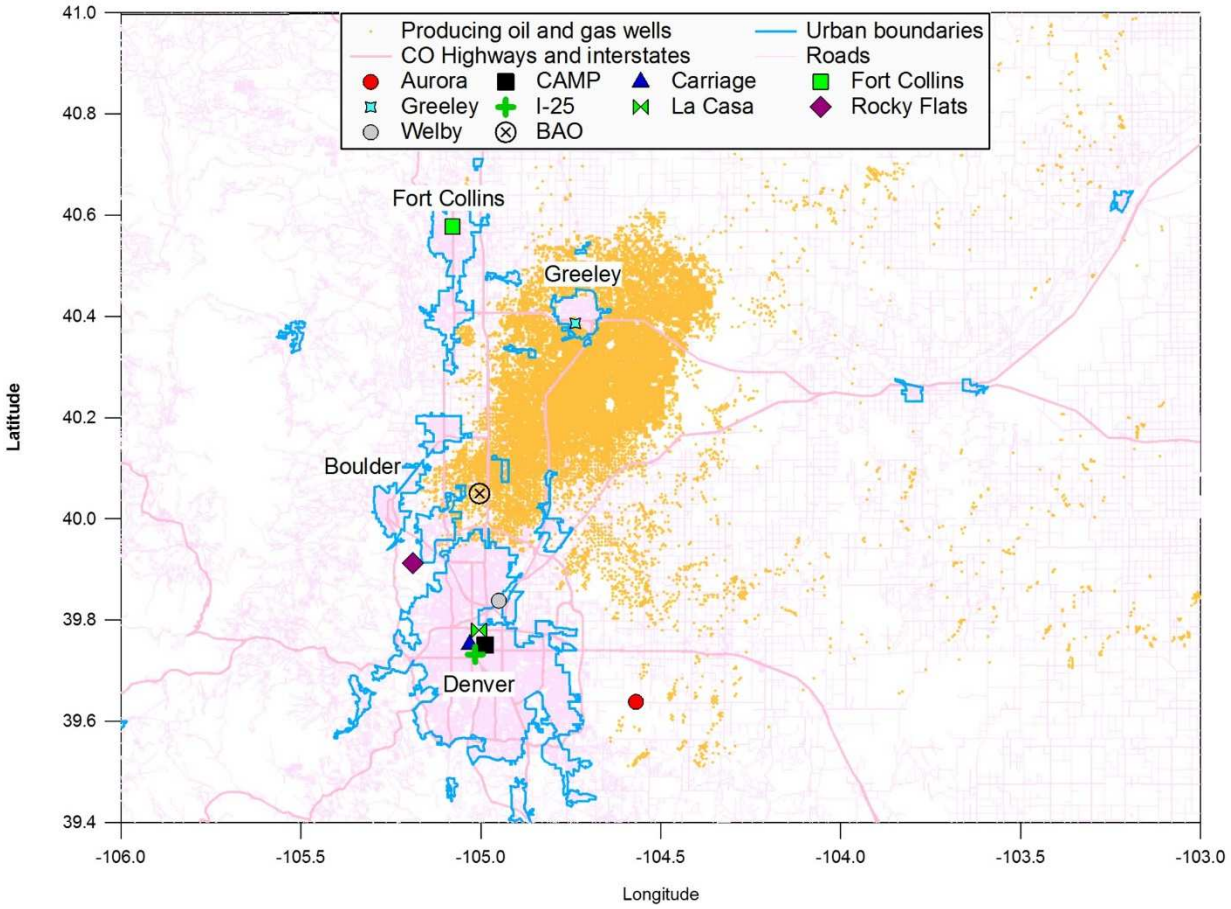

Figure 2.1. Site map for O_3 and NO_2 measurements in the NFRMA identified by shapes and colors. Producing oil and gas wells as of 2012 are identified on the map with gold dots. Urban areas are outlined with thick light-blue lines. Major interstates and state highways are identified by thick pink lines.

2-miles south of the Carriage and CAMP sites, and likely intercepts fresh NO_x emissions directly from the I-25 interstate. NO_2 data was available for 2015, but not O_3. The La Casa site is <1 mile west of the I-70 and I-25 interstate junction. O_3 and NO_2 data were available for 2015. Temperature data was available for all sites for all years.

2.2.2. Ozone and NO_2 data treatment

Ambient NO_2 concentrations were measured by chemiluminescence monitors equipped with molybdenum oxide converters. These monitors are used as the EPA Federal Reference Method for monitoring ambient NO_2 concentrations, and have a known interference from nitric acid and organic nitrates [*Dunlea et al.*, 2007]. The true ambient NO_2 mixing ratio is a component of the reported values. NO_2* will be used in this manuscript to refer to the EPA NO_2 measurements,

Table 2.1. Summary of Measurements sites used in this analysis. Note that NO_2^* refers to the NO_2 detected by the EPA reference method, and thus includes a fraction of NO_y species.

Site	Latitude	Longitude	Elevation (m)	Measurements
CAMP	39.7512	-104.988	1591	O_3 & NO_2^*
Welby	39.8382	-104.955	1554	O_3 & NO_2^*
Carriage	39.7518	-105.031	1619	O_3
Fort Collins	40.5775	-105.079	1523	O_3
Greeley	40.3864	-104.737	1476	O_3
Rocky Flats	39.9128	-105.189	1784	O_3
I-25	39.7321	-105.015	1586	NO_2^*
La Casa	39.7795	-105.005	1601	O_3 & NO_2^*

which includes the interference, and can be considered to be a proxy for total reactive nitrogen oxides (NO_y). While the absolute NO_2* concentration will be greater than NO_2 but less than NO_y, trends in NO_2* provided insight on trends in local NO_x emissions. The O_3 and NO_2* mixing ratios

are filtered to summer months (June 1 – August 31), and averaged to a daytime value (10:00 am – 4:00 pm local). A site was excluded for a given year when <50% of data is available for that summer.

2.2.3. Trend analysis

Following the analyses of *Cooper et al.* [2012], the statistical significance of the linear trends were tested with a standard F-test with the null hypothesis that there is no linear trend ($R^2 = 0$). The null hypothesis was rejected with a confidence level ≥ 95% if the probability (p) associated with the F-statistics was low ($p \leq 0.05$).

2.3. Results and Discussion

2.3.1. Long term trends in O_3 and NO_2* in the Northern Front Range Metropolitan Area

Contrary to most other places in the U.S., O_3 in the NFRMA was either stagnant or increasing between 2000 and 2015, despite substantial decreases in NO_x emissions. At most sites in the eastern U.S. and some on the west coast, O_3 was decreasing at all percentiles. In the NFRMA, however, five out of six monitoring sites exhibited no change or increasing O_3 at the 50th and 95th percentiles in the 2000 – 2015 period (Fig. 2.2).

The 5th percentile is often taken as background O_3, and studies have shown that background O_3 in the Western US has increased [*Cooper et al.*, 2010; *Parrish et al.*, 2004; *Pfister et al.*, 2011; *Weiss-Penzias et al.*, 2006]. However, only the CAMP and Welby sites in Denver exhibit significant increasing O_3 with trends of 1.3 ± 1.0 ppb_v/year and 1.1 ± 1.0 ppb_v/year respectively at the 5th percentile with significance determined by passing an F-Test (section 2.2.2). The CAMP and Welby sites also exhibit statistically significant increases at the 50th (CAMP: 1.2 ± 0.4, Welby:

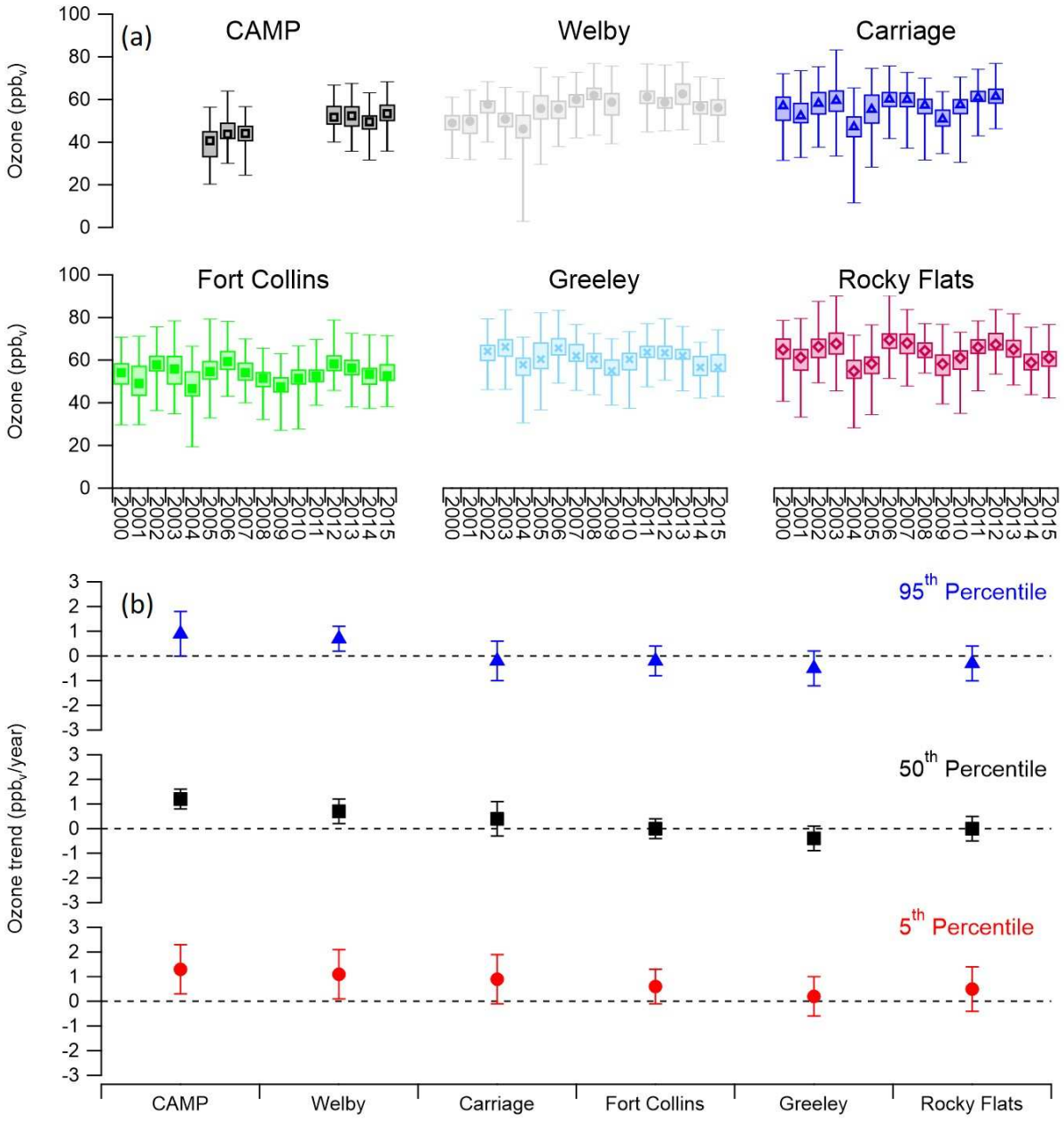

Figure 2.2. (a) Trends in summer (June 1 – August 31) daytime (10:00 am – 4:00 pm) O_3 for six sites in the NFRMA between 2000 and 2015. Whiskers correspond to 5th and 9th percentiles, box thresholds correspond to 33rd and 67th percentiles, and the marker corresponds to the 50th percentile. Percentiles were calculated from daily daytime averages of hourly O_3 measurements at each site. The number of days used for each year's statistics depended on available data (n = 64 – 92). (b) O_3 temporal trends were determined as the slope from annual trends (ppb_v O_3/year) from simple one-sided linear regression for the six NFRMA sites for the 95th (blue triangles), 50th (black squares), and 5th (red circles) percentiles. Error bars represent the 95% confidence interval around the ozone/year linear regression slope.

0.7 ± 0.5 ppb_v/year) and 95th (CAMP: 1.0 ± 0.9, Welby: 0.7 ± 0.5 ppb_v/year) percentiles. *Cooper et al.* [2012] reported that the Welby site exhibited no statistically significant increase in O_3 from 1990 – 2010, contrary to what we found for 2000 – 2015 at the 95th percentile, which could be a result of changing VOC and NO_2^* emissions in the 2010 - 2015 period.

The increasing O_3 trends in the NFRMA occurred despite reductions in NO_x. NO_2* at the CAMP site decreased significantly from 2000 at a rate of -1.0 ± 0.6 and -1.4 ± 0.6 ppb_v/yr for the 50th and 95th percentiles for CAMP (Fig. 2.3). Welby exhibited a non-significant decreasing NO_2* trend at the 95th percentile of -0.7 ± 0.8 ppb_v/yr (Fig. 2.3). The increased O_3 may be due to increased summer temperatures in Colorado, increased regional baseline O_3, or increased local P(O_3) from unknown emission sources [*Cooper et al.*, 2012]. VOC emissions steadily increased in Colorado from 2000 to 2012 per the EPA state average annual emissions trend (Fig. 2.4). To the best of our knowledge, the NFRMA does not have any long-term VOC datasets, but the EPA state average annual emissions trend for Colorado provided an estimate for yearly anthropogenic VOC (AVOC) emissions [*EPA*, 2016a]. All categories of AVOC emissions decreased slightly from 2000 – 2015, except for petroleum related VOCs which increased from 7.4 x 10^3 tons in 2000 to 2.6 x 10^5 tons in 2011 with a decrease to 1.5 x 10^5 tons in 2015 (Fig. 2.4). The US Energy Information Administration (EIA) report a 2-fold increase in active ONG wells from ~25,000 to ~40,000 from 2010 to 2012 (Fig. 4c) [*US-EIA*, 2017]. However, we note the state average annual emissions is only an estimate and does not include biogenic sources of VOCs, which can contribute substantially to VOC reactivity in the region, but vary substantially from year to year [*Abeleira et al.*, 2017].

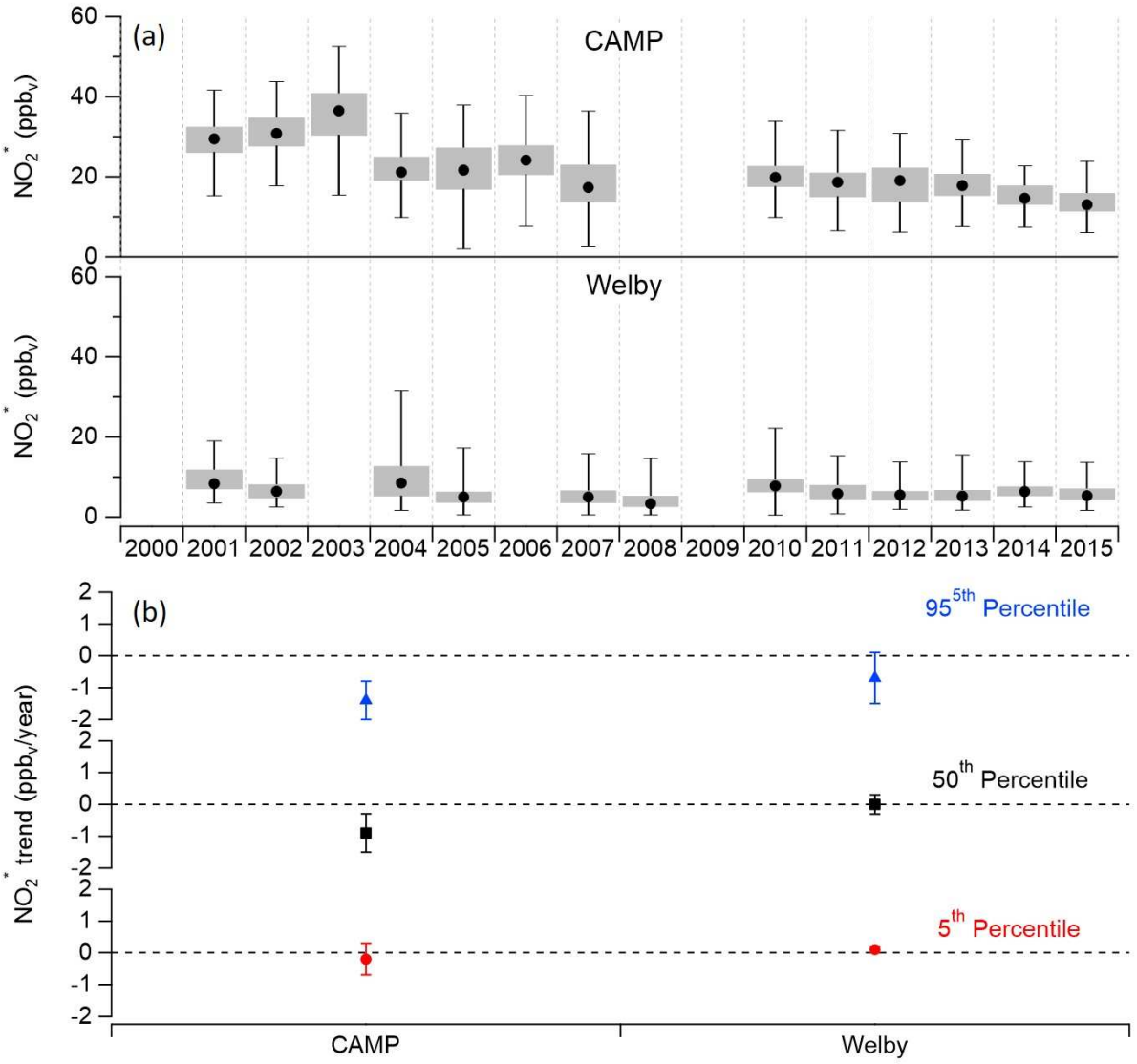

Figure 2.3. (a) Trends in summer (June 1 – August 31) daytime (10:00 am – 4:00 pm) NO_2* for the CAMP and Welby sites in Denver for all available data from 2000 – 2015. Whiskers correspond to 5th and 95th percentiles, box thresholds correspond to 33rd and 67th percentiles, and the black marker corresponds to the 50th percentile. (b) NO_2^* temporal trends were determined as the slope from annual trends (ppb_v NO_2/year) from simple one-sided linear regression for the six NFRMA sites for the 95th (blue triangles), 50th (black squares), and 5th (red circles) percentiles. Error bars represent the 95% confidence interval around the NO_2*/year linear regression slope.

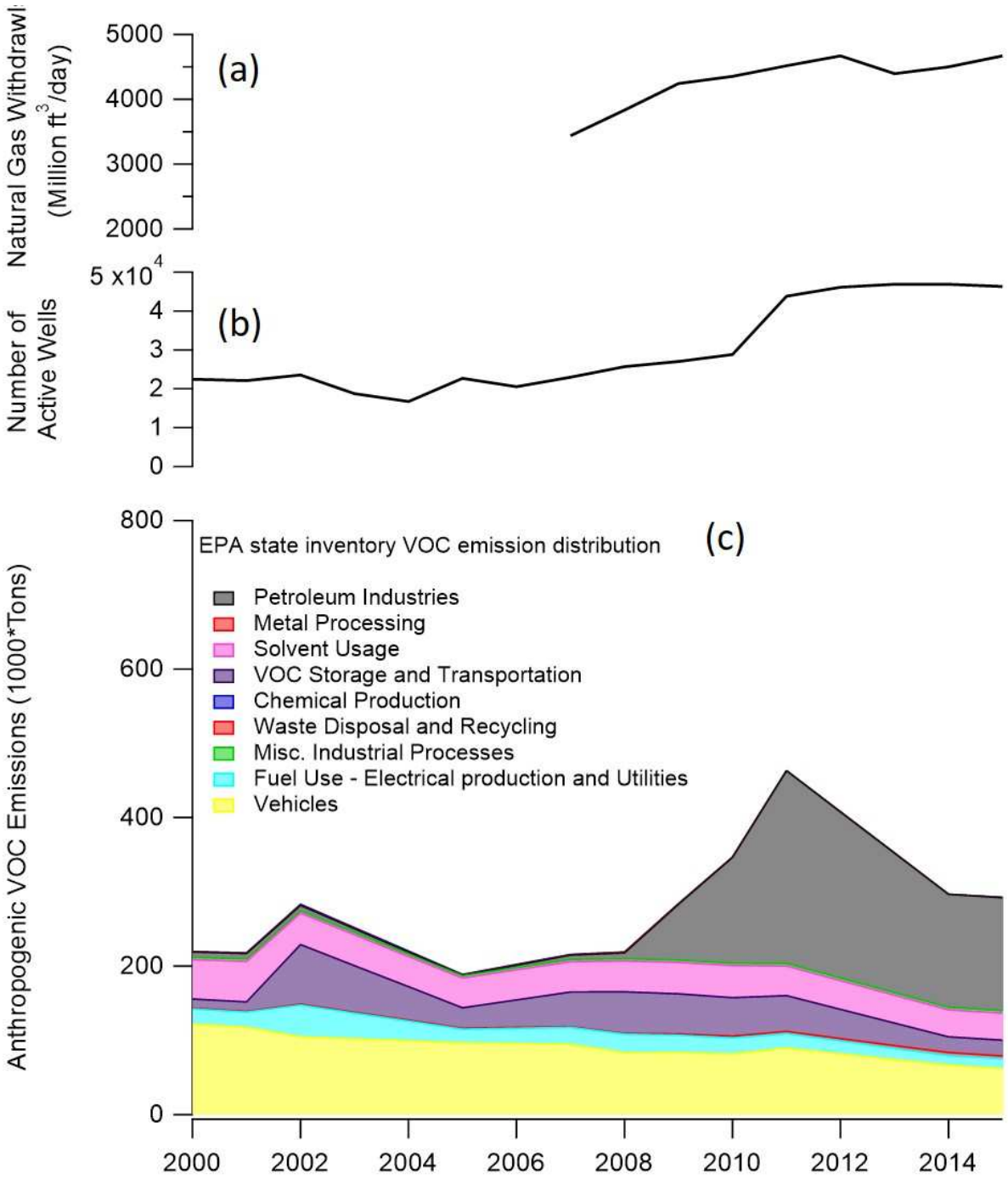

Figure 2.4. (a) Estimated yearly averaged natural gas withdrawals in Colorado [*US-EIA*, 2017], (b) Yearly average number of active ONG well operations [*US-EIA*, 2017]. (c) Anthropogenic VOC emission estimates from the EPA state average annual emissions trend for Colorado. Emission sources are separated by color, and are added to give the total VOC emission estimates for anthropogenic VOCs. Biogenic VOCs and VOCs from biomass burning (controlled fires and wildfires) are not included.

The increased O_3 is thus unsurprising for the 2000 – 2015 timeframe. The long-term reduction in NO_x with increasing VOC emissions concurrent with an increase in O_3 at both sites suggests that the downtown Denver sites were in a NO_x-saturated $P(O_3)$ regime, and as NO_2* decreases and VOC reactivity increases, $P(O_3)$ was increasing towards peak production.

2.3.2. Weekend-Weekday effect in Denver, CO

The 'weekend-weekday effect' describes how anthropogenic emissions of O_3 precursors can be statistically different on weekdays versus weekends, resulting in different secondary chemistry. This effect can be used to elucidate information about local chemical regimes [i.e. *CARB*, 2003; *Cleveland et al.*, 1974; *Fujita et al.*, 2003; *Heuss et al.*, 2003; *Murphy et al.*, 2007; *Pollack et al.*, 2012; *Warneke et al.*, 2013]. Traffic patterns in urban regions are different between weekends and weekdays from a decrease in heavy-duty truck traffic on weekends [*Marr et al.*, 2002].

VOCs are expected to be stable across the week, as major VOC sources do not vary by day-of-week. Despite this reduction in heavy-duty trucking traffic, O_3 can be higher on weekends than on weekdays if the system is in a NO_x-saturated regime because decreased NO_x increases $P(O_3)$, while decreased NO also reduces O_3 titration to NO_2 [*Fujita et al.*, 2003; *Heuss et al.*, 2003; *Marr et al.*, 2002; *Murphy et al.*, 2007; *Pollack et al.*, 2012; *Pusede et al.*, 2012]. Thus urban regions, which are often NO_x-saturated, tend to follow a day-of-week pattern in both NO_x and O_3 [*Fujita et al.*, 2003; *Heuss et al.*, 2003; *Pusede et al.*, 2012], while rural and semi-urban areas often experience no change in NO_x or O_3 from weekdays to weekends. Rural regions have a lower population density, less defined daily traffic patterns, and minimal or no commercial trucking [*Heuss et al.*, 2003]. The weekend-weekday effect typically relies on the assumption that the VOC reactivity and thus HO_x production is unchanged between the weekend and weekday. However,

this is not always the case, as decreased weekend NO_x reduces NO_x+OH reactions, and thereby increases weekend OH and increased O_3 [*Warneke et al.*, 2013]. Few studies of VOCs in the NFRMA exist, but our previous work found no significant difference in measured VOC reactivity at the BAO site between weekends and weekdays in summer 2015 [*Abeleira et al.*, 2017].

In the NFRMA, long-term (i.e. 10+ years) NO_2* datasets only existed at the CAMP and Welby sites. Two sites in Denver added NO_2* measurements in 2015, the I-25 and La Casa sites. The CAMP, I-25, and La Casa sites are all located within a 4-mile radius that straddles the I-25 motorway; are surrounded by a dense network of roads, businesses, and industrial operations; and experience high traffic density. Welby is located roughly 8-miles northeast from the three other sites, and borders a large lake and the Rocky Mountain Arsenal open space. Welby is thus more 'suburban' than the other sites. Median NO_2* at CAMP has decreased from 37 ppb_v in 2003 to 13 ppb_v in 2015. The median weekday I-25 and La Casa NO_2* mixing ratios in 2015 were similar to CAMP in 2007 (Fig. 2.5) indicating that although NO_2* emission reductions have been effective in the region, mixing ratios in Denver are very site specific

An observable weekend-weekday effect in NO_2* existed for all years at the CAMP site, and most years at the Welby site with intermittent years with that do not have a clear difference in weekday and weekend NO_2^*. NO_2* decreased by 20-50% from weekdays to weekends. Assuming that meteorology doesn't systematically change between weekends and weekdays, we consider the weekend-weekday effect in O_3 to be indicative of changes in $P(O_3)$ due to lower NO_x. Figure 2.6 follows the analysis of *Pusede et al.* [2012], presenting summer average weekday and weekend O_3 values for Welby and CAMP with the values tethered for each year. The values followed a curve similar to a modeled $P(O_3)$ curve, and indicates that reductions in NO_x emissions from 2000 to 2015 have placed O_3 production in the Denver region in a transitional phase from NO_x-saturated

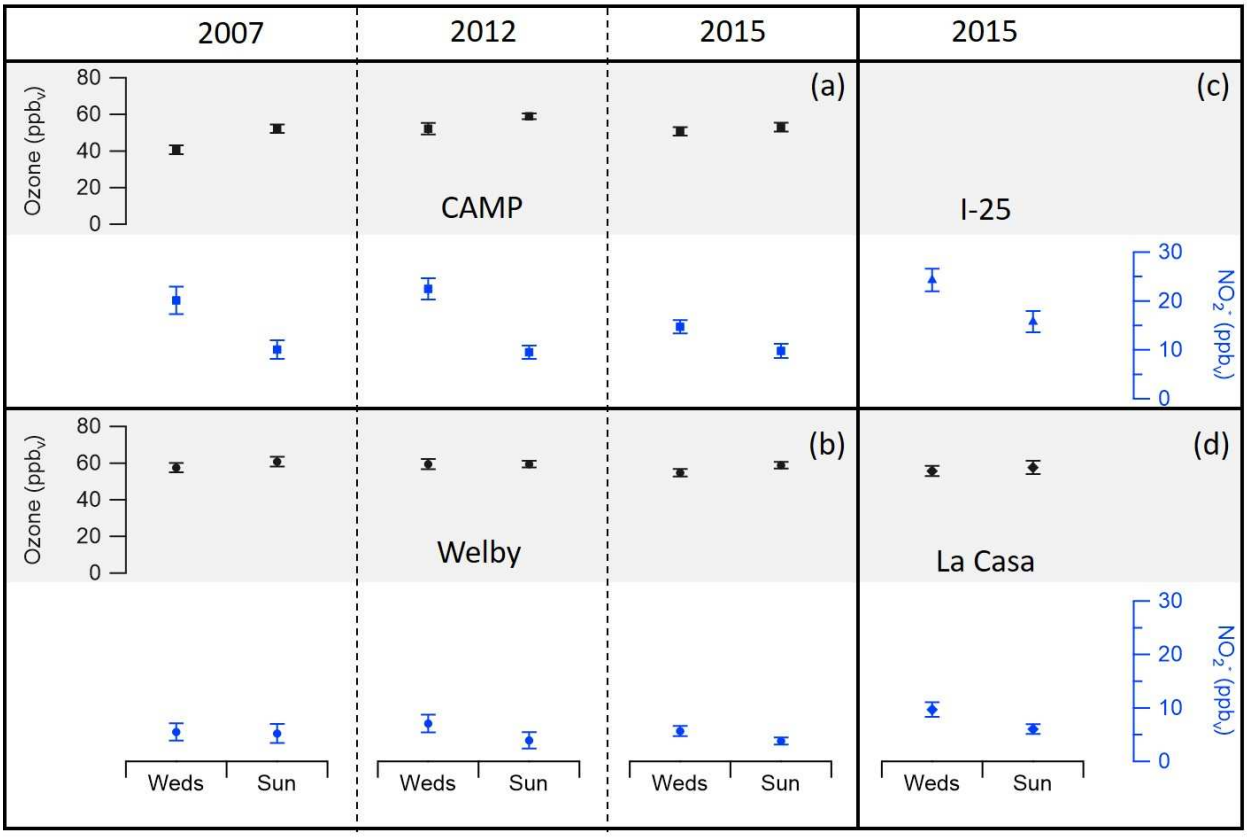

Figure 2.5. Weekend-Weekday analysis (Sunday vs Wednesday) for O_3 (black with shading) and NO_2* (blue) for the CAMP (a, squares), Welby (b, circles), and the La Casa (c, diamonds) sites in Denver. I-25 (d, triangles) is limited to NO_2^* due to data availability. All sites have plots for 2015, but only CAMP (a) and Welby (b) are additionally plotted for 2007 and 2012 due to data availability. Wednesday is representative of weekday NO_2^* and typically is not different than the average of Tuesday, Wednesday and Thursday at a 95% confidence for this dataset. Monday, Friday, and Saturday are considered carry-over or "mixed" days between weekdays and weekends and are ignored. Error bars represent a 95% confidence intervals around the summertime mean of Wednesday or Sunday O_3 or NO_2^*.

to peak $P(O_3)$. This analysis suggests that continued reductions of NO_x would shift the system to a NO_x-limited regime, in which changes in VOC reactivity due to shifting anthropogenic or biogenic emissions would have little effect on O_3.

The average change in O_3 (ΔO_3) and NO_2* (ΔNO_2*) from weekend to weekday is plotted as a function of year for the six available O_3 NFRMA sites and the two NO_2^* sites (Fig. 2.7a, 2.7b). A positive ΔO_3 reflects a higher O_3 concentration on the weekend than weekday, consistent with a NO_x-saturated system. A negative ΔO_3 is consistent with a NO_x-limited system in which O_3 decreases when NO_x decreases. The weekend-weekday effect exhibits a non-significant decreasing trend from 2000 to 2015 for yearly averages of the six sites. This is consistent with the decreased regional NO_x emissions, which would move the system from NO_x-saturated to peak $P(O_3)$ in the absence of large changes in VOC reactivity. The CAMP site was the exception, and consistently had a larger ΔO_3 than the other sites. This was consistent with the CAMP site's higher NO_2* relative to Welby and the 30-50% decrease in NO_2* from weekdays to weekend. Measured NO_2* decreased at both CAMP and Welby (Fig. 2.3b), but with larger decreases at the CAMP site. The ΔNO_2* at Welby remained stable with an average value of -1.7 ± 0.9 ppb_v, while ΔNO_2* at the CAMP exhibited a statistically significant decrease of 0.6 ± 0.4 ΔNO_2* ppb_v/yr . The decreasing ΔNO_2* at the CAMP site appears to be converging with the ΔNO_2* at the Welby site. It is unlikely that traffic patterns are assimilating between the two sites, and a more plausible explanation is that emission control technologies on heavy duty commercial fleet vehicles are reducing the impact on emissions of those specific vehicles, and are reducing the measurable ΔNO_2* [*Bishop et al.*, 2015]. The ΔO_3 decreased across the NFRMA outside of the highest traffic regions in Denver, again consistent with the hypothesis that the NFRMA $P(O_3)$ regime has transitioned from NO_x-saturated chemistry towards peak $P(O_3)$. Two sites, Greeley and Rocky Flats, show negative ΔO_3 values in

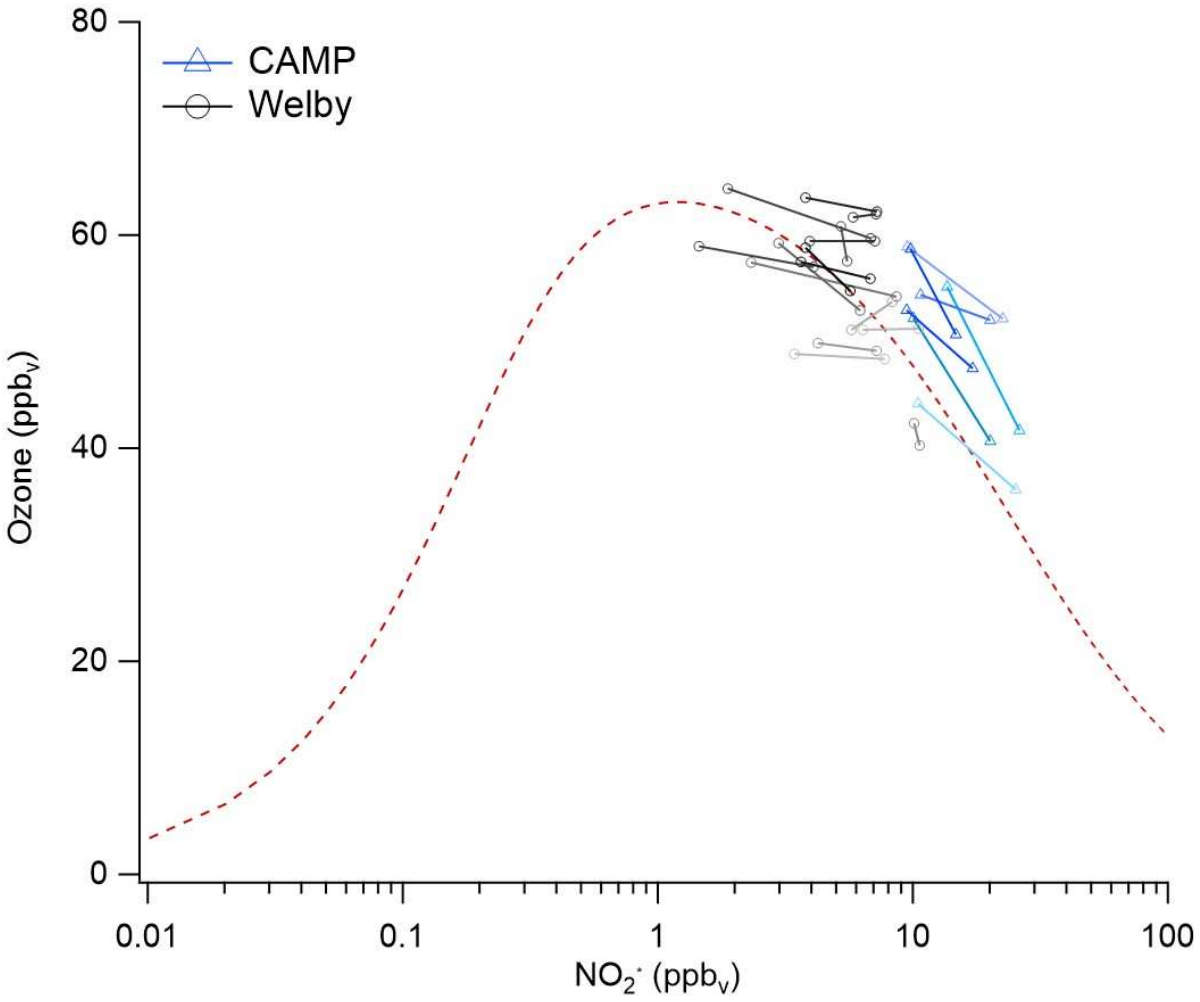

Figure 2.6. Weekday and weekend O_3 versus NO_2* for Welby (black) and CAMP (blue) sites. Tethered symbols correspond to average Wednesday values for weekdays, and average Sunday values for weekends for each year depending on data availability. The colour shading corresponds to year, with the lightest shade corresponding to the earliest year (2000 for Welby, 2005 for CAMP) and 2015 as the darkest shade. The 95% confidence intervals for each year are <5 ppb_v for O_3 and <2.5 ppb_v for NO_2*. The dashed blue line is a visual aid to guide the readers eye to the non-linear O_3 curve, and was generated from the simple analytic model described by *Farmer et al.* [2011].

recent years, suggesting that those sites have, at least in those specific years, transitioned to NO_x-limited chemistry. Collectively, this weekend-weekday analysis suggests that the region is NO_x-saturated, but transitioning to a NO_x-limited region. Increases in O_3 may thus be due to a combination of decreasing NO_x and increasing VOC emissions. While the lack of long-term VOC measurements prevents identification and quantification of those VOC sources, the state average annual emissions suggested that petroleum-related VOCs have increased. However, we note that large increases in VOC reactivity shift the transition point between NO_x-limited and NO_x-saturated regions to higher NO_x concentrations. The clear regional decrease in the weekend-weekday effect, as evidenced by the decreasing ΔO_3 trend, indicates that the region is transitioning, and that any increases in VOC reactivity have not been so large as to dramatically inhibit this effect.

2.3.3. The O_3-temperature penalty in the NFRMA

Increasing temperature can increase $P(O_3)$ by enhancing biogenic and evaporative VOC emissions, but has variable impacts on the weekend-weekday effect as a result of changing NO_x emissions [*Pusede et al.*, 2014]. We showed that while O_3 increased with temperature in the NFRMA, consistent with a NO_x-saturated regime, this relationship was variable year to year. Ambient O_3 was correlated with increasing temperature across the U.S. [*Bloomer et al.*, 2009; *Jacob et al.*, 2009; *Pusede et al.*, 2014]. While one study in the NFRMA from summer 2012 found that biogenic VOCs (*i.e.* isoprene) had a minor impact on VOC reactivity at the BAO site [*McDuffie et al.*, 2016], *Abeleira et al.* [2017] found that isoprene contributed up to 47% of VOC reactivity on average in the late afternoon in summer 2015. Studying the temperature dependence of O_3 allows us to investigate the extent to which biogenic VOCs influenced $P(O_3)$ in the NFRMA and the interannual variability of those temperature-dependent VOC sources, as well as the shift from a NO_x-saturated to NO_x-limited $P(O_3)$ regime. NO_x-saturated regimes should be sensitive to

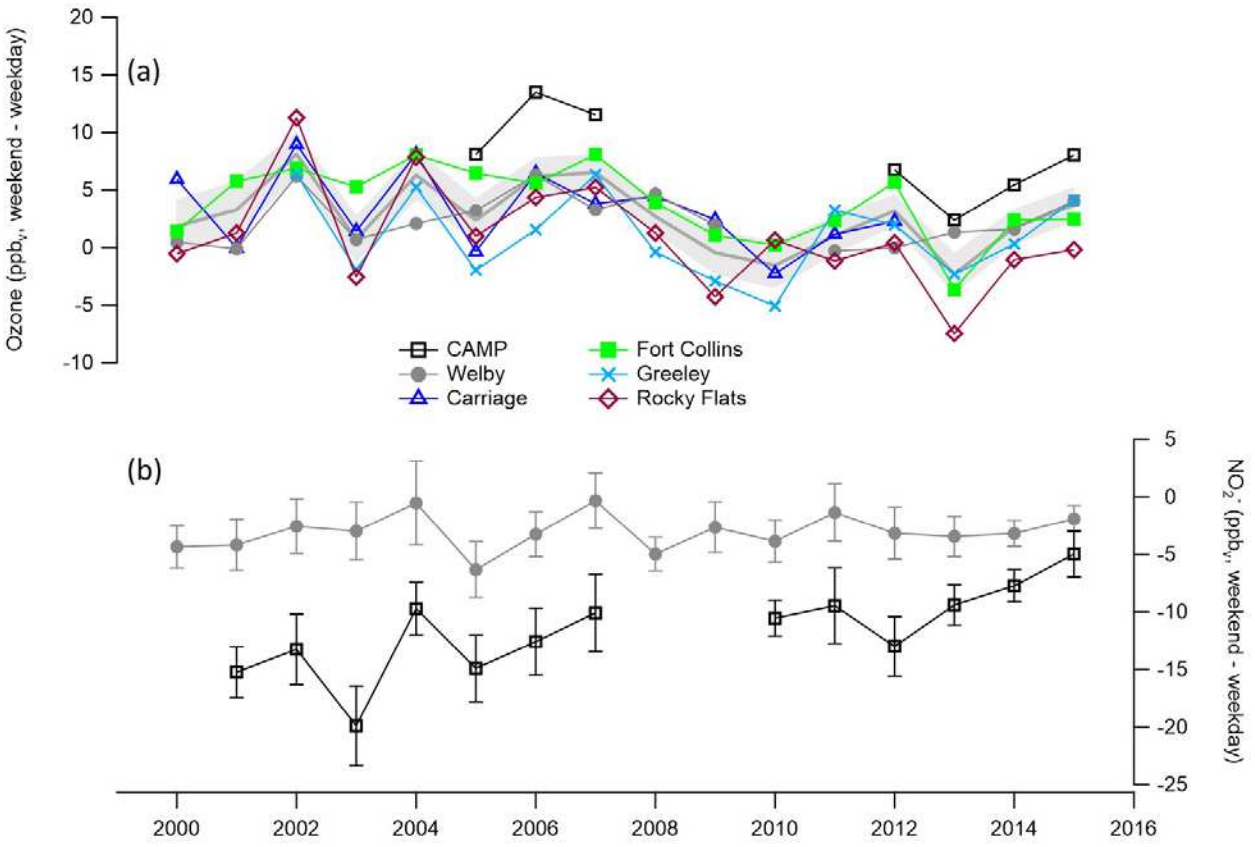

Figure 2.7. (a) The change in O_3 calculated as average weekend (Sunday) minus weekday (Wednesday) O_3 for the six NFRMA sites identified by color and marker. The solid grey line is the average of the sites. The inclusion of a site in the averaging for a given year was dependent on available data for that year. The light grey shading represents ± the 95% confidence interval of all Wednesday and Sunday hourly values for each year for sites with available data. (b) The change in NO_2* is calculated identically to O_3 in (a) for the CAMP and Welby sites, and the error bars represent the 95% confidence interval of the averages.

changes in VOC reactivity, while NO_x-limited systems should not. We note that while anthropogenic VOCs, such as solvents, may be temperature dependent and contribute to this trend, we only observed temperature trends in isoprene at the BAO site in 2015 – though we acknowledge that the observed VOC suite in that study was limited [*Abeleira et al.*, 2017].

O_3 in the NFRMA demonstrated a clear temperature dependence at all percentiles for all sites, but with slopes that vary by site and year (Fig. 2.8, Fig. 2.9). The NFRMA appears to be NO_x-saturated or near peak $P(O_3)$ for all years, consistent with temperature dependent biogenic emissions impacting ambient O_3. The variance in the O_3-temperature dependence was likely external to meteorological effects. High temperature and linked meteorological parameters such as high 500 hPa heights, and stagnant winds, or circulating wind patterns do indeed correlate with high O_3 events in Colorado [*Reddy et al.*, 2016], but those parameters should not affect the O_3-temperature relationship.

Figure 2.8a shows daytime, summer O_3 averaged in non-uniform temperature bins with bin size dictated by maintaining an equal number of data points in each temperature bin for CAMP, Fort Collins, and Rocky Flats for years in which data was available at all sites. For every temperature bin, O_3 was higher at Rocky Flats than at Fort Collins, and both were higher than at CAMP. The Rocky Flats site was the most rural of the chosen sites adjacent to the 4,000 acre Rocky Flats Wildlife Refuge, but was <15 miles from downtown Boulder. Rocky Flats likely had higher O_3 because it was downwind of both NO_x (Boulder, Denver) and VOC sources (forested regions in the neighboring foothills), had fewer nearby fresh NO_x sources and thus less $NO+O_3$ titration, and experienced enhanced $P(O_3)$ due to the region being near the cross-over point between NO_x-saturated and NO_x-limited chemical regimes (Fig. 2.6).

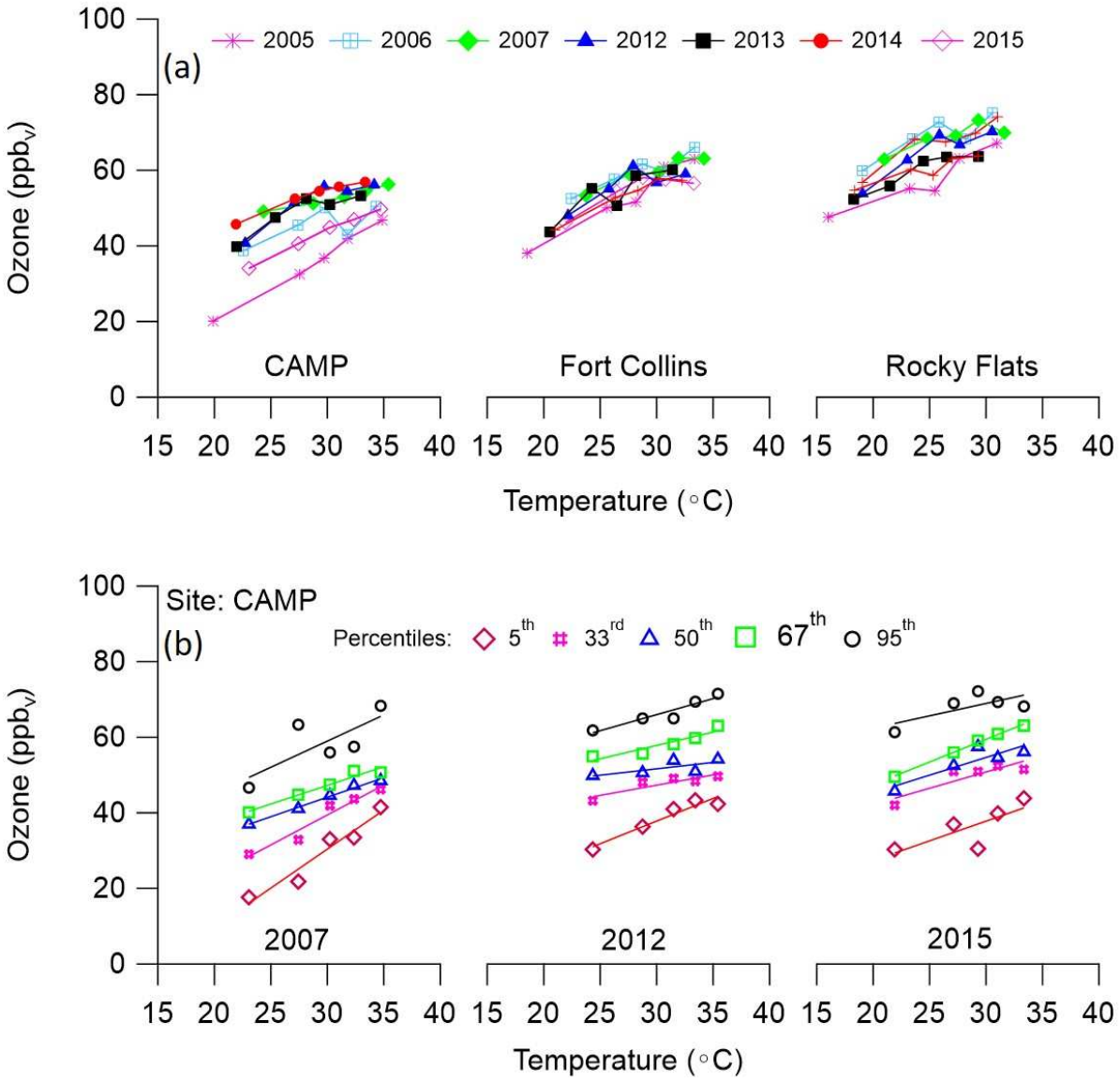

Figure 2.8. a) O_3 versus temperature for CAMP, Fort Collins, and Rocky Flats. Hourly O_3 is binned by hourly temperature with bins containing 51 - 110 points for O_3 and temperature depending on data availability at a site. The temperature bins typically contained 100 – 110 data points (>90% of temperature bins for all sites in all available years). Average O_3 of each bin is plotted versus the average temperature of each bin. Markers and colors represent yearly averages for each site. Error bars were left off for visual clarity, but the 95% confidence interval around the yearly bin averages are typically <8 ppb_v. Years were selected based on availability of overlapping data for multiple sites. b) One-sided linear regressions of equal point temperature bins for the 5th (red open diamond), 33rd (pink hash), 50th (green open triangle), 67th (blue open square), and 95th (black open circle) percentiles for the CAMP site for 2007 (left), 2012 (middle), and 2015 (right).

Bloomer et al. [2009] reported average O_3-temperature relationships of 2.2 – 2.4 ppb_v/°C for the Northeast, Southeast, and Great Lakes regions of the U.S. across all O_3 percentiles. In contrast, the Southwest region, including Colorado, had an average relationship of 1.4 ppb_v/°C [*Bloomer et al.*, 2009]. We find that O_3 was indeed correlated with temperature at all NFRMA sites, with relationships that ranged from 0.07 to 1.95 ppb_v/°C with an average of 1.0 ± 0.4 ppb_v/°C (Fig. 2.8) for all sites and years. Quantitatively, this temperature dependence was low relative to other U.S. sites, consistent with previous findings that biogenic VOCs contribute to, but do not dominate, VOC reactivity in the NFRMA [*Abeleira et al.*, 2017; *McDuffie et al.*, 2016]. However, the six NFRMA sites exhibited significant variability in the 5th, 50th, and 95th percentiles among the sites both within a given year and across years (Fig. 2.9). The 5th and 95th O_3 percentiles showed greater variability and larger uncertainties in the slopes than the 50th percentile. This indicated that baseline O_3 and high O_3 events in the region were less dependent on temperature. Baseline O_3 was likely tied to the transport of O_3 and O_3 precursors from the west coast [*Cooper et al.*, 2012], while the high O_3 events were likely tied to a combination of meteorological parameters, including 500 hPa heights and stagnation events [*Reddy et al.*, 2016], stratospheric intrusions [*Lin et al.*, 2015], and local, temperature independent VOC emissions. In contrast, the 50th percentile showed a clear temperature dependence at all sites in most years (Fig. 2.8, Fig. 2.9), indicating that mean O_3 was typically influenced by local temperature dependent, and likely biogenic, VOC emissions.

Unlike ambient O_3 and the weekend to weekday ΔO_3, we noted no clear long-term trend in the O_3-temperature relationship. The O_3-temperature relationships showed similar interannual patterns for the six sites at the 50th percentile (Fig. 2.9). Specifically, years 2008, and 2011-2012 have suppressed O_3-temperature slopes for the 50th percentile. *Reddy et al.* [2016] reported high 500 hPa heights and O_3 for 2002-2003, 2006, and 2012 while 2004 and 2009 had low 500 hPa

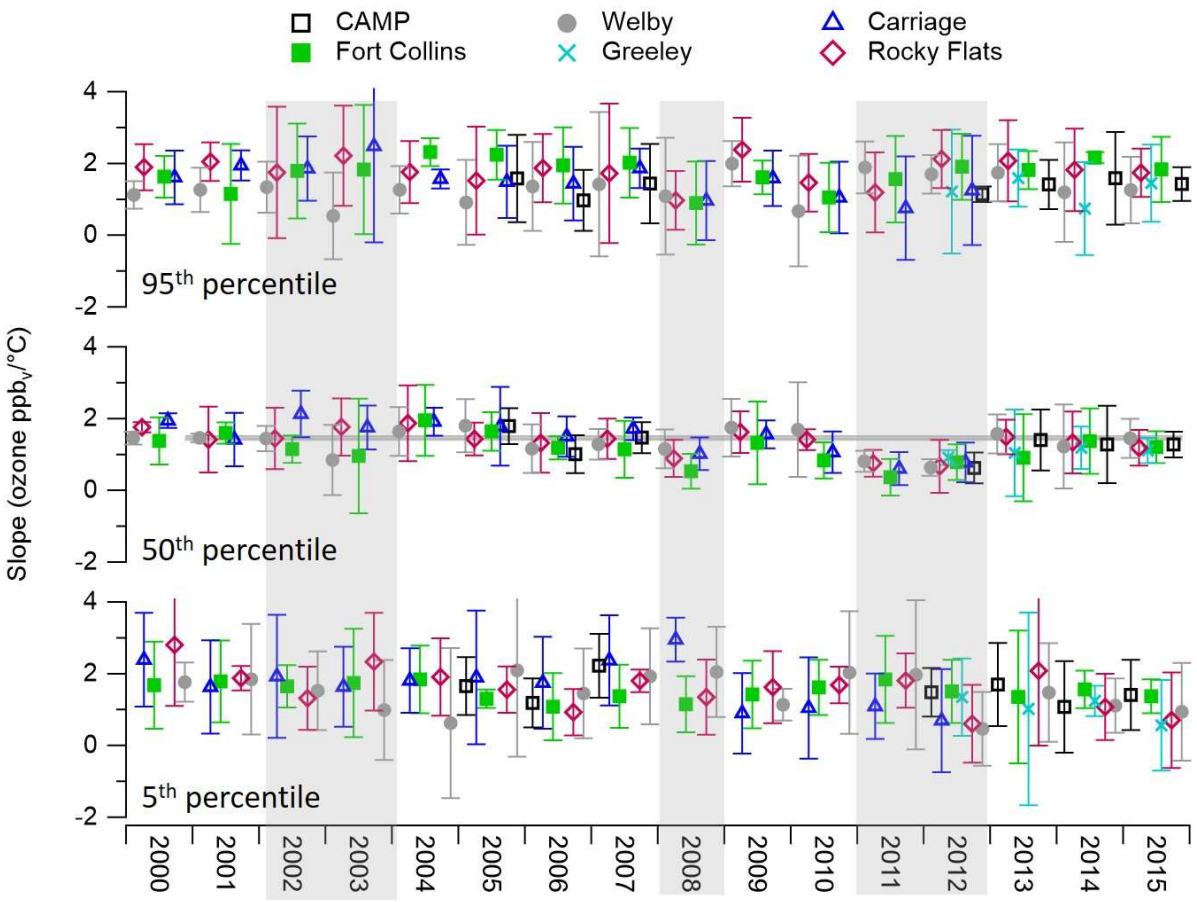

Figure 2.9. Slopes from one-sided linear regression of O_3 versus temperature (i.e. the temperature dependence of O_3). Hourly O_3 (10:00 am – 4:00 pm) is binned by hourly temperature with bins containing 51 - 110 points for O_3 and temperature depending on data availability at a site. The temperature bins typically contained 100 – 110 data points (>90% of temperature bins for all sites in all available years). The slopes of O_3 versus temperature for the 5th, 50th, and 95th percentiles for the O_3-tempetature bins are shown. Data are shown for CAMP (black squares), Welby (grey solid circles), Carriage (blue open triangles), Fort Collins (green solid squares), Greeley (teal X's), and Rocky Flats (magenta open diamonds). Shaded years correspond to Colorado summers with moderate to severe drought conditions. Error bars are ± 95% confidence interval of the slopes. Faint grey line across the 50th percentile is the average slope bounded by the 95% confidence interval for years excluding 2008, 2011, and 2012.

heights and low O_3, so those exceptional years cannot be explained solely by meteorology. However, those exceptional years (2008, and 2011-2012) did correspond to years in which Colorado was in moderate-severe drought with little soil moisture [*NOAA*, 2017]. Years 2002-2003 also exhibited moderate to severe drought conditions in Colorado, and some but not all sites exhibited suppressed O_3-temperature slopes.

Drought in the NFRMA is connected to changes in mountain-plains circulation and lower surface moisture, which reduces the surface latent heat flux and causes increased surface temperature. These increased surface temperatures lead to strong mountain-plains circulation, stagnant wind conditions, higher PBLs, and 500 hPa heights, all of which are known to correlate with high O_3 episodes [*Ek et al.*, 2004; *Reddy et al.*, 2016; *Zhou et al.*, 2013]. Drought is also connected to reduced isoprene emissions [*Brilli et al.*, 2007; *Fortunati et al.*, 2008; *Guenther*, 2006]. Consistent with this concept, *Abeleira et al.* [2017] noted that isoprene was 2-4 times higher at the Boulder Atmospheric Observatory site in summer 2015 (a non-drought year) than in summer 2012 (a drought year). Such a decrease in biogenic isoprene emissions should also suppress the O_3-temperature dependence in NO_x-saturated regimes, a trend that was observed in the NFRMA (Fig. 2.9).

The suppressed O_3-temperature relationship during drought years in the NFRMA demonstrated the importance of temperature dependent VOCs in driving $P(O_3)$ in the region, particularly at the mid-range 50th percentile – but not at the baseline 5th percentile. A standard t-test showed that the 50th and 95th percentile slopes (i.e. temperature dependence of average and high O_3 concentrations) are indeed different between the drought and non-drought years at the 95% confidence limit. If NO_x emissions continue to decrease, and the NFRMA continues its trend towards a NO_x-limited regime (Fig. 2.7), the O_3-temperature dependence should also decrease and

temperature-dependent VOCs will play a smaller role in driving O_3 production. However, this would require substantial decreases in NO_x for the heavy traffic region of Denver to become fully NO_x-limited, so temperature dependent VOCs will likely remain important in at least some regions of the NFRMA.

2.4. Conclusions

O_3 decreased across most of the country as anthropogenic NO_x and VOC emissions were reduced, with the exception of background O_3 in the west [*Cooper et al.*, 2012]. In contrast, five out of six sites in the NFRMA showed no change or increasing O_3 at the 50^{th} and 95^{th} percentiles between 2000 and 2015. While NO_x levels have been reduced at the CAMP and Welby sites in Denver, anthropogenic VOC emission estimates have increased as a result of increased petroleum related activities (Fig. 2.4). A weekend-weekday analysis demonstrated that most sites in the NFRMA were NO_x-saturated, but are transitioning to, and in two cases may already have reached, the peak $P(O_3)$ cross-over point between NO_x-saturated and NO_x-limited regimes. Some of the more rural NFRMA sites may already be in or near a NO_x-limited system. This transition suggests that increasing anthropogenic VOC emissions will have less of an effect on $P(O_3)$ in the region if NO_x reductions continue, though VOCs remain the limiting reagent for ozone production in most of the NFRMA sites in 2015. Thus, the combined factors of increasing anthropogenic VOC emissions and decreasing NO_x in a NO_x-saturated system are likely culprits for the increasing O_3 trends within the NFRMA over the past 15 years. Although the median NO_2* has decreased at the CAMP site from 37 ppb_v in 2003 to 13 ppb_v in 2015, the site remains on the steep transitional part of the $P(O_3)$ curve between NO_x-saturated and peak $P(O_3)$ chemistry (Fig. 2.6). Continued reductions in NO_x emissions alone could lead to increased O_3 in the downtown Denver area until the $P(O_3)$ chemistry passed the peak production region, although concurrent reductions in VOCs

could mitigate the increase in $P(O_3)$. As sources of VOCs and NO_x change in the NFRMA with increased population, growth in the oil and gas sector, and changing emissions regulations, continued analysis of O_3 and NO_x will be essential for understanding the shifting $P(O_3)$ regime. However, such analyses would benefit greatly from long-term NO_x measurements at additional sites in the NFRMA.

O_3 in the NFRMA exhibits temperature dependence at all sites, but with varying intensities for different years. The 5th and 95th O_3 percentiles demonstrated significant variability in temperature dependence for different sites in the same year and across the study period, indicating that high O_3 events and background O_3 have other important controlling factors such as transport of long-lived O_3 precursors from the west or meteorological parameters. Two time periods exhibit a clearly suppressed O_3-temperature dependence at the 50th percentile (2008 and 2011-2012), coinciding with moderate to extreme drought conditions in the NFRMA. These observations are consistent with the hypothesis that long-term drought stress reduces biogenic VOC emissions and suppresses the O_3-temperature dependency. However, we emphasize that this effect is most clearly observed at the 50th percentile, rather than the 5th or 95th percentiles, suggesting that biogenic VOCs have a greater influence on mean O_3 than on background or high O_3 events in the NFRMA. Climate change is predicted to increase temperatures and thus increase O_3 by 1 – 10 ppb_v on a national scale [*Jacob et al.*, 2009]. However, climate change models predict more extreme precipitation events in many areas, and estimates for Colorado and the intermountain west suggest that drought may become more common in the region [*IPCC*, 2014]. The work herein suggests that drought can temporarily suppress the O_3-temperature penalty in the NFRMA and perhaps other NO_x-saturated regions by reducing temperature dependent biogenic VOC emissions.

CHAPTER 2 REFERENCES

Abeleira, A., et al. (2017), Source Characterization of Volatile Organic Compounds in the Colorado Northern Front Range Metropolitan Area during Spring and Summer 2015, *Journal of Geophysical Research*, *In Press*.

AMA (2015), State of the Air 2015, edited by A. L. Association, Chicago, IL.

Avnery, S., D. L. Mauzerall, J. Liu, and L. W. Horowitz (2011), Global crop yield reductions due to surface ozone exposure: 1. Year 2000 crop production losses and economic damage, *Atmospheric Environment*, *45*(13), 2284-2296.

Bishop, G. A., et al. (2015), On-road Heavy-duty Vehicle Emissions Monitoring System, *Environmental Science & Technology*, *49*(3), 1639-1645, doi:10.1021/es505534e.

Bloomer, B. J., et al. (2009), Observed relationships of ozone air pollution with temperature and emissions, *Geophysical Research Letters*, *36*(9).

Brilli, F., et al. (2007), Response of isoprene emission and carbon metabolism to drought in white poplar (Populus alba) saplings, *New Phytologist*, *175*(2), 244-254.

CARB (2003), The Ozone Weekend Effect in California, *California Air Reasearch Board Planning and Technical Support Division*.

CDPHE (2008), Denver Metro Area & North Front Range Ozone Action Plan., edited, Denver, CO.

CDPHE (2009), For Recommended 8-Hour Ozone Designations, edited by C. D. o. P. H. a. Environment, CDPHE, Denver, Colorado.

CDPHE (2014), Control of Ozone Via Ozone Precursors and Control of Hydocarbons Via Oil and Gas Emissions., edited, Denver, CO.

CDPHE (2016), Moderate area ozone SIP for the Denver Metro and North Front Range nonattaiment area., edited, Denver, CO.

Cleveland, W. S., T. E. Graedel, B. Kleiner, and J. Warner (1974), Sunday and workday variations in photochemical air pollutants in New Jersey and New York, *Science*, *186*(4168), 1037-1038.

Cooper, O., et al. (2010), Increasing springtime ozone mixing ratios in the free troposphere over western North America, *Nature*, *463*(7279), 344-348.

Cooper, O. R., et al. (2012), Long-term ozone trends at rural ozone monitoring sites across the United States, 1990–2010, *Journal of Geophysical Research: Atmospheres*, *117*(D22).

Davis, J., W. Cox, A. Reff, and P. Dolwick (2011), A comparison of CMAQ-based and observation-based statistical models relating ozone to meteorological parameters, *Atmospheric environment*, *45*(20), 3481-3487.

Dunlea, E. J., et al. (2007), Evaluation of nitrogen dioxide chemiluminescence monitors in a polluted urban environment, *Atmos. Chem. Phys.*, *7*(10), 2691-2704, doi:10.5194/acp-7-2691-2007.

Ek, M., and A. Holtslag (2004), Influence of soil moisture on boundary layer cloud development, *Journal of hydrometeorology*, *5*(1), 86-99.

EPA (2014), National Ambient Air Quality Standards for Ozone; Propose Rule, edited by EPA.

EPA (2016a), Air Pollutants Emission Trends, edited.

EPA (2016b), Ozone Trends, edited.

Farmer, D., et al. (2011), Impact of organic nitrates on urban ozone production, *Atmospheric Chemistry and Physics*, *11*(9), 4085-4094.
Fischer, E. V., et al. (2014), Atmospheric peroxyacetyl nitrate (PAN): a global budget and source attribution, *Atmos. Chem. Phys.*, *14*(5), 2679-2698, doi:10.5194/acp-14-2679-2014.
Fortunati, A., et al. (2008), Isoprene emission is not temperature-dependent during and after severe drought-stress: a physiological and biochemical analysis, *The Plant Journal*, *55*(4), 687-697.
Fujita, E. M., et al. (2003), Evolution of the magnitude and spatial extent of the weekend ozone effect in California's South Coast Air Basin, 1981–2000, *Journal of the Air & Waste Management Association*, *53*(7), 802-815.
Gilman, J. B., B. M. Lerner, W. C. Kuster, and J. A. de Gouw (2013), Source signature of volatile organic compounds from oil and natural gas operations in northeastern Colorado, *Environ Sci Technol*, *47*(3), 1297-1305, doi:10.1021/es304119a.
Guenther, A. (2006), Estimates of global terrestrial isoprene emissions using MEGAN (Model of Emissions of Gases and Aerosols from Nature), *Atmospheric Chemistry and Physics*, *6*.
Guenther, A., et al. (1996), Estimates of regional natural volatile organic compound fluxes from enclosure and ambient measurements, *Journal of Geophysical Research: Atmospheres*, *101*(D1), 1345-1359.
Heuss, J. M., D. F. Kahlbaum, and G. T. Wolff (2003), Weekday/weekend ozone differences: what can we learn from them?, *Journal of the Air & Waste Management Association*, *53*(7), 772-788.
IPCC (2014), Climate Change 2014–Impacts, Adaptation and Vulnerability: Regional Aspects, edited by I. P. o. C. Change, Cambridge University Press.
Jacob, D. J., and D. A. Winner (2009), Effect of climate change on air quality, *Atmospheric environment*, *43*(1), 51-63.
Lefohn, A. S., D. Shadwick, and S. J. Oltmans (2010), Characterizing changes in surface ozone levels in metropolitan and rural areas in the United States for 1980–2008 and 1994–2008, *Atmospheric Environment*, *44*(39), 5199-5210.
Lin, M., et al. (2015), Climate variability modulates western US ozone air quality in spring via deep stratospheric intrusions, *Nature communications*, *6*.
Lindas, J., et al. (2017), The impact of aged wildfire smoke on atmospheric composition and ozone in the Colorado Front Range in summer 2015, *Atmospheric Chemistry and Physics*, *in preparation*.
Marr, L. C., and R. A. Harley (2002), Modeling the Effect of Weekday− Weekend Differences in Motor Vehicle Emissions on Photochemical Air Pollution in Central California, *Environmental science & technology*, *36*(19), 4099-4106.
McDonald, B. C., D. R. Gentner, A. H. Goldstein, and R. A. Harley (2013), Long-term trends in motor vehicle emissions in US urban areas, *Environmental science & technology*, *47*(17), 10022-10031.
McDuffie, E. E., et al. (2016), Influence of oil and gas emissions on summertime ozone in the Colorado Northern Front Range, *Journal of Geophysical Research: Atmospheres*, *121*(14), 8712-8729.
Murphy, J. G., et al. (2007), The weekend effect within and downwind of Sacramento–Part 1: Observations of ozone, nitrogen oxides, and VOC reactivity, *Atmospheric Chemistry and Physics*, *7*(20), 5327-5339.
NOAA (2017), North American Drought Monitor, edited, NOAA.

Palut, M. P. J., and O. F. Canziani (2007), Contribution of working group II to the fourth assessment report of the intergovernmental panel on climate change, edited, Cambridge University Press.
Parrish, D., et al. (2004), Changes in the photochemical environment of the temperate North Pacific troposphere in response to increased Asian emissions, *Journal of Geophysical Research: Atmospheres*, *109*(D23).
Pétron, G., et al. (2012), Hydrocarbon emissions characterization in the Colorado Front Range: A pilot study, *Journal of Geophysical Research: Atmospheres*, *117*(D4), n/a-n/a, doi:10.1029/2011jd016360.
Pfister, G., et al. (2011), Characterizing summertime chemical boundary conditions for airmasses entering the US West Coast, *Atmospheric Chemistry and Physics*, *11*(4), 1769-1790.
Pollack, I., et al. (2012), Airborne and ground-based observations of a weekend effect in ozone, precursors, and oxidation products in the California South Coast Air Basin, *Journal of Geophysical Research: Atmospheres*, *117*(D21).
Pusede, S., et al. (2014), On the temperature dependence of organic reactivity, nitrogen oxides, ozone production, and the impact of emission controls in San Joaquin Valley, California, *Atmospheric Chemistry and Physics*, *14*(7), 3373-3395.
Pusede, S. E., and R. C. Cohen (2012), On the observed response of ozone to NO_x and VOC reactivity reductions in San Joaquin Valley California 1995–present, *Atmospheric Chemistry and Physics*, *12*(18), 8323-8339, doi:10.5194/acp-12-8323-2012.
Reddy, P. J., and G. G. Pfister (2016), Meteorological factors contributing to the interannual variability of mid-summer surface ozone in Colorado, Utah, and other western US states, *Journal of Geophysical Research: Atmospheres*.
Singh, H. B., and P. L. Hanst (1981), Peroxyacetyl nitrate (PAN) in the unpolluted atmosphere: An important reservoir for nitrogen oxides, *Geophysical Research Letters*, *8*(8), 941-944.
Swarthout, R. F., et al. (2013), Volatile organic compound distributions during the NACHTT campaign at the Boulder Atmospheric Observatory: Influence of urban and natural gas sources, *Journal of Geophysical Research: Atmospheres*, *118*(18), 10,614-610,637, doi:10.1002/jgrd.50722.
Tai, A. P., M. V. Martin, and C. L. Heald (2014), Threat to future global food security from climate change and ozone air pollution, *Nature Climate Change*, *4*(9), 817-821.
Thompson, C. R., J. Hueber, and D. Helmig (2014), Influence of oil and gas emissions on ambient atmospheric non-methane hydrocarbons in residential areas of Northeastern Colorado, *Elementa: Science of the Anthropocene*, *2*, 000035, doi:10.12952/journal.elementa.000035.
Thompson, M. L., et al. (2001), A review of statistical methods for the meteorological adjustment of tropospheric ozone, *Atmospheric environment*, *35*(3), 617-630.
US-EIA (2017), Natural Gas - Data, edited by U. D. o. E.-E. I. Administration, Washington, DC.
Warneke, C., et al. (2013), Photochemical aging of volatile organic compounds in the Los Angeles basin: Weekday-weekend effect, *Journal of Geophysical Research: Atmospheres*, *118*(10), 5018-5028.
Weiss-Penzias, P., et al. (2006), Observations of Asian air pollution in the free troposphere at Mount Bachelor Observatory during the spring of 2004, *Journal of Geophysical Research: Atmospheres*, *111*(D10).

White, A., et al. (2007), Comparing the impact of meteorological variability on surface ozone during the NEAQS (2002) and ICARTT (2004) field campaigns, *Journal of Geophysical Research: Atmospheres*, *112*(D10).

Zhou, X., and B. Geerts (2013), The influence of soil moisture on the planetary boundary layer and on cumulus convection over an isolated mountain. Part I: observations, *Monthly Weather Review*, *141*(3), 1061-1078.

CHAPTER 3 – SOURCE CHARACTERIZATION OF VOLATILE ORGANIC COMPOUNDS IN THE COLORADO NORTHERN FRONT RANGE METROPOLITAN AREA DURING SPRING AND SUMMER 2015[2]

3.1. Introduction

On a global scale, biogenic emissions dominate the organic carbon budget, with anthropogenic emissions contributing <15% [*Goldstein*, 2007; *Kesselmeier et al.*, 1999]. Biogenic VOCs include isoprene and other terpenoids, as well as small oxygenated VOCs (OVOCs) and alkenes. Anthropogenic emission sources include oil and natural gas (ONG) operations (*i.e.* removal, refining, storage, and transport of oil or natural gas), gasoline storage and transportation, combustion (*i.e.* automobiles or biomass), chemical manufacturing, and solvent use [*Piccot et al.*, 1992]. However, the relative importance of anthropogenic and biogenic VOC emissions vary across regions with biogenic emissions dominating carbon mixing ratios in rural and forested regions [*Karl et al.*, 2003], and anthropogenic emissions dominating urban areas [*Baker et al.*, 2008; *Borbon et al.*, 2013; *Gilman et al.*, 2009]. Dense urban areas such as Los Angeles are dominated by automobile-related VOC emissions [*Borbon et al.*, 2013], while ONG producing regions experience large emissions of light alkanes associated with fossil fuel extraction and refinement [e.g. *Katzenstein et al.*, 2003].

Ground-level ozone (O_3) production occurs when volatile organic compounds (VOCs) are oxidized in the presence of NO_x ($NO + NO_2$) and sunlight. The propensity of a given VOC to

[2] Abeleira, A., I. Pollack, B. Sive, Y. Zhou, E. Fischer, and D. Farmer (2017), Source characterization of volatile organic compounds in the Colorado Northern Front Range Metropolitan Area during spring and summer 2015, *Journal of Geophysical Research: Atmospheres*, *122*(6), 3595-3613.

initiate the O_3 production cycle can be described by its reactivity with the OH radical, $R_{OH, X}$ (s^{-1}). While this parameter does not account for chain propagation or termination steps, the OH reactivity of a given species can provide insight into relative contributions of different hydrocarbons to the rate of O_3 production. The OH reactivity of a particular species is defined as the species mixing ratio in molecule cm^{-3} multiplied by its rate constant with OH,

$$R_{OH,X} = k_{OH+X}[X] \quad \text{(E1)}$$

The summed reactivity of all VOC species (VOC reactivity or $R_{OH, VOCs}$, s^{-1}) contributes to the total OH reactivity ($R_{OH, Total}$; s^{-1}), which includes reaction with inorganic species:

$$R_{OH,VOCs} = \sum_i (k_{OH+VOC_i}[VOC_i]) \quad \text{(E2)}$$

$$R_{OH,Total} = R_{OH,NO_x} + R_{OH,CH_4} + R_{OH,CO} + R_{OH,VOCs} \quad \text{(E3)}$$

These terms are typically calculated from an observed suite of VOCs. Atmospheric instrumentation quantitatively detects only a sub-set of VOCs. The calculated VOC and OH reactivity thus underestimates directly observed reactivity in urban, rural, and remote regions [e.g. *Chatani et al.*, 2009; *Di Carlo et al.*, 2004; *Dolgorouky et al.*, 2012; *Dusanter et al.*, 2009; *Edwards et al.*, 2013; *Hansen et al.*, 2014; *Whalley et al.*, 2016]. However, standard measurements of VOCs by gas chromatography or proton transfer reaction mass spectrometry still provide insight on the key reactivity sources at a given site.

Multiple short (<4 weeks) field campaigns have focused on understanding the primary sources contributing to VOCs in the Northern Front Range Metropolitan Area (NFRMA) of Colorado[*Brown et al.*, 2013; *Gilman et al.*, 2013; *McDuffie et al.*, 2016; *Pétron et al.*, 2012; *Swarthout et al.*, 2013; *Thompson et al.*, 2014]. This region has repeatedly exceeded the National Ambient Air Quality Standard for O_3 in the past decade, and is home to a large and rapidly growing

population (3.5+ million people in 2015). Repeated measurements of VOCs have been made at the Boulder Atmospheric Observatory (BAO) in Erie, CO (Fig. 3.1). These measurements showed that the region experiences higher mixing ratios of C_2-C_6 alkanes relative to other U.S. regions, with propane, butane isomers, and pentane isomers exceeding summer time average mixing ratios in 28 other U.S. cities[*Baker et al.*, 2008]. This strong alkane source signature was highly correlated with propane, a known marker for natural gas production [*Pétron et al.*, 2012]. *Gilman et al.* [2013] reported that the majority (73 - 96%) of measured C_2-C_6 alkanes, and approximately half (55 ± 18%) of the calculated VOC reactivity (*i.e.* derived from measured VOCs via equation E2; Average $R_{OH,VOC}$ = 3 ± 3 s^{-1}), can be attributed to oil and gas production. Simultaneous and nominally co-located measurements verified the ONG source of this C_2-C_5 alkane enhancement with wind direction and back trajectory analysis showing the largest enhancements came from the Wattenberg Field natural gas production region northeast of the sampling site [*Swarthout et al.*, 2013]. *Swarthout et al.*, [2013] found that C_2-C_8 alkanes accounted for 61% of VOC reactivity, moreover, the C_2-C_6 alkanes, which were attributed almost exclusively to ONG activities [*Gilman et al.*, 2013], accounted for 52% of VOC reactivity. Both studies also noted a second distinct VOC source related to urban combustion (*i.e.* tail-pipe emissions, or traffic sources). Enhanced tail-pipe related VOCs (aromatics, alkenes, and ethyne) were most often associated with air mass transport from the south and west, implying sources from Denver, Boulder, and Longmont [*Swarthout et al.*, 2013].

Using VOC and trace gas measurements from a summer 2012 campaign at the BAO site, *McDuffie et al.* [2016] reported an average calculated VOC reactivity of 2.4 ± 0.9 s^{-1}, of which alkanes contributed 56% and biogenic VOCs contributed 8%. Measurements from Erie, Longmont, Platteville (Wattenberg Natural Gas Field), downtown Denver, and Boulder County

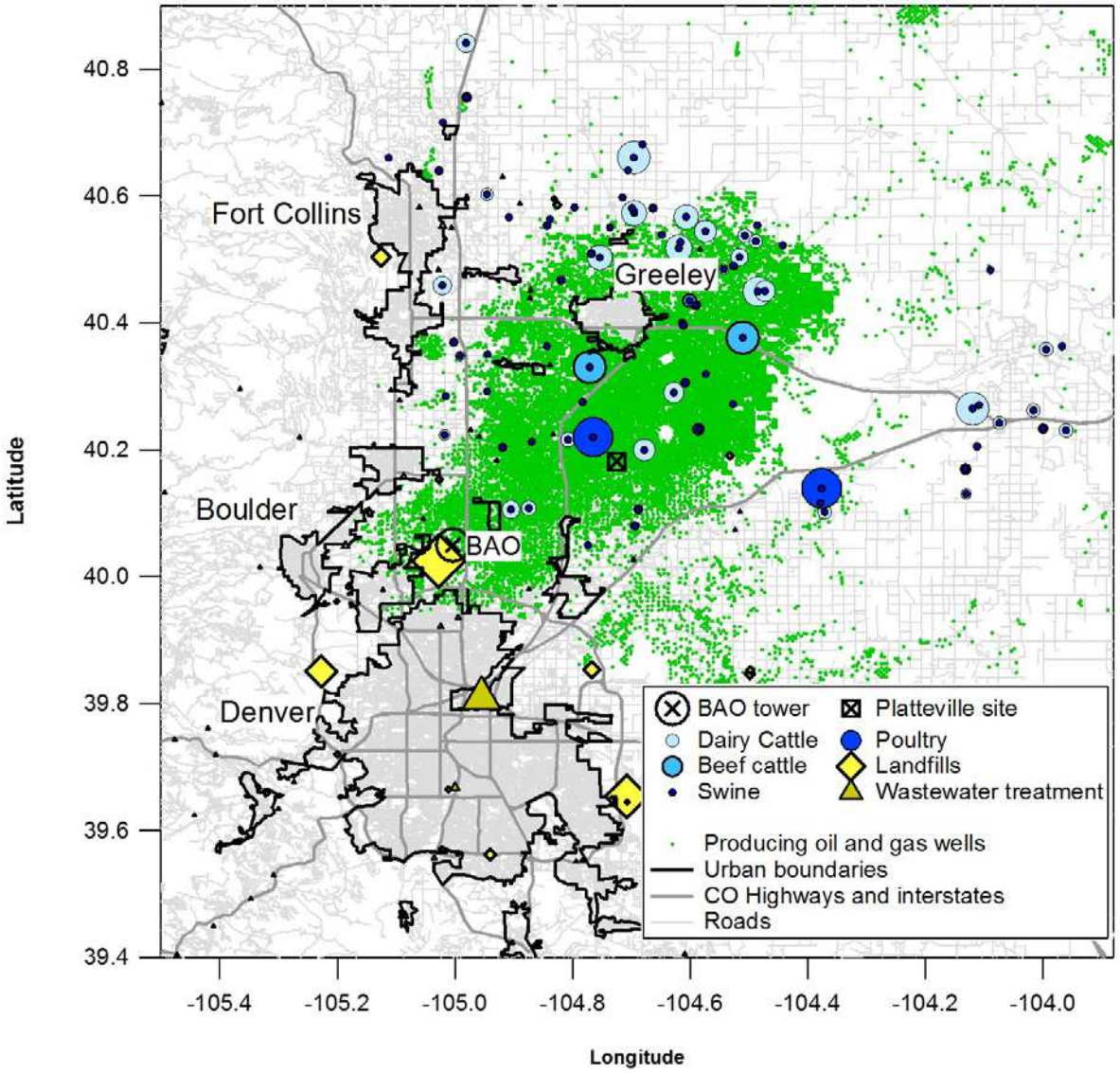

Figure 3.1. Major urban centers in the NFRMA include Fort Collins, Boulder, Denver, and Greeley (black outlines). The BAO site is at the SW corner of Weld County near the interface between rural and urban areas. Concentrated agriculture feed operations for beef cattle (light blue circle), poultry (dark blue circle), and dairy cattle (pale blue circle) are sized based on 2012 operation sizes. Swine operations (purple circles) are not sized. Landfills (yellow diamonds) are sized with operation size. Producing oil and gas wells as of 2012 are represented by green circles (no sizing).

showed higher C_2-C_5 alkane mixing ratios in residential neighborhoods near the densest drilling in the Wattenberg Natural Gas Field (Platteville) with reduced mixing ratios in areas further from drilling operations (*i.e.* Denver, Boulder County) [*Thompson et al.*, 2014]. Correlations of benzene and toluene with ONG tracers were higher in the Platteville area relative to Denver, where vehicular tail-pipe emissions dominate the benzene, toluene, and xylene (BTEX) sources [*Thompson et al.*, 2014]. Collectively, these studies suggest that ONG and traffic sources dominate VOC reactivity in the NFRMA.

Here, we describe VOC measurements collected during a lengthy campaign at the BAO site from spring and summer 2015. We evaluate seasonal variability and sources of VOCs at the BAO site using Positive Matrix Factorization (PMF), and consider the contribution of different sources to VOC reactivity.

3.2. Methods

3.2.1. Research Site

A suite of VOCs (Tables 3.1, A1.1) and reactive trace gases (Figs. A1.1-A1.3) were measured at the NOAA BAO site in Weld County. Spring measurements were made between 20 March and 17 May 2015; summer measurements were made between 5 July and 6 September 2015. The BAO site is semirural, surrounded by agricultural operations, but with growing sub-urban development in the town of Erie. Major urban centers are located 35 km to the south (Denver), 30 km to the west (Boulder), 65 km to the north (Fort Collins), and 65 km to the northeast (Greely) (Fig. 3.1). A major interstate highway (I-25) runs north to south 2 km to the east of the site. The site is in the Denver-Julesberg basin on the edge of the Wattenberg natural gas field, an area of active and extensive ONG exploration and production [*Pétron et al.*, 2014]. All instruments

were located in air-conditioned trailers at the site. Average temperatures at the site were 10 °C (range -2.5 - 27 °C) in the spring and 24 °C (range 14.5 - 36 °C) in the summer (10 m above ground level, a.g.l., Fig. A1.4).

3.2.2. Measurements

3.2.2.1. Volatile Organic Compounds

An automated 4-channel online gas chromatographic (GC) system was used for *in situ* VOC measurements. The GC system used 4 different separation columns and 4 detectors (3 flame ionization detectors (FID), 1 electron capture detector (ECD)) to measure 46 individual VOCs (Table 3.1, A1.1) including C_2-C_8 non-methane hydrocarbons (NHMCs), C_1-C_2 halocarbons, C_1-C_5 alkyl nitrates, and several OVOCs with hourly time-resolution [*Sive et al.*, 2005; *Zhou et al.*, 2008; *Zhou et al.*, 2005]. The version of the GC system deployed for this project used a cryogen-free concentration system for the online pre-concentration of ambient samples that was similar to *Sive et al.* [2005], but was equipped with a different cryogen-free cooler (Q-Drive, Model 2S102K). Ambient air was collected on 1 mm silica beads at -160°C for 5 minutes at a flow rate of 200 mL/min for a total sample volume of 1 L. Water was removed prior to sample trapping with a higher temperature cold trap. The GC columns used for this deployment included: (1) a CP-Al_2O_3/Na_2SO_4 PLOT column (50 m x 0.53 mm I.D. 10 µm film thickness; Varian, Inc.) connected to an FID for the C_2-C_6 hydrocarbons; (2) a VF-1ms column (60 m x 0.32 mm I.D. 1 µm film thickness, Agilent Technologies) connected to an FID for the C_{7+} hydrocarbons and aromatics; (3) a CP-PoraBond-Q column (25 m x 0.25 mm I.D. 3 µm film thickness, Agilent Technologies) coupled to an XTI-5 (30 m x 0.25 mm I.D. 0.25 µm film thickness, Restek) connected to an FID for the OVOCs; and (4) an OV-1701 column (60 m x 0.25 mm I.D. 1 µm film thickness, Ohio Valley Specialty) connected to an ECD for C_1-C_5 alkyl nitrates and C_1-C_2 halocarbons.

Table 3.1. Observed mixing ratios, VOC reactivity, OH rate coefficients and LODs for select VOCs at BAO in spring and summer 2015. Data for the complete suite of measured VOCs is in the supplemental materials (Table A1.1).

	Mean Mixing Ratio (ppbv)[a]		Mean $R_{OH,VOC}$ (s^{-1})[a]				
Compound	Spring	Summer	Spring	Summer	$k_{OH,VOC}$ [b]	Ref[c]	LOD (ppbv)
Ethane	16 (22)	23 (33)	0.07 (0.10)	0.1 (0.2)	0.25	a	0.008
Propane	9 (13)	8 (11)	0.2 (0.3)	0.2 (0.2)	1.09	a	0.01
i-Butane	1 (1)	2 (2)	0.04 (0.07)	0.07 (0.09)	2.1	a	0.007
n-Butane	2 (3)	4 (6)	0.1 (0.2)	0.2 (0.3	2.4	a	0.005
i-Pentane	1 (3)	3 (5)	0.1 (0.2)	0.2 (0.4)	3.6	a	0.003
n-Pentane	1 (2)	3 (5)	0.1 (0.2)	0.2 (0.4)	3.8	a	0.003
cyclopentane	0.1 (0.1)	0.7 (1.0)	0.01 (0.01	0.1 (0.1)	5.1	b	0.004
n-Hexane	0.2 (0.3)	0.4 (0.5)	0.02 (0.03)	0.04 (0.05)	5.2	a	0.004
Cyclohexane	0.2 (0.3)	0.2 (0.2	0.03 (0.04)	0.03 (0.03)	7	a	0.02
2,3-DMP	0.1 (0.1)	0.09 (0.09)	0.02 (0.02)	0.01 (0.01)	7	c	0.02
2-methylhexane	0.04 (0.05)	0.09 (0.09)	0.006 (0.008)	0.01 (0.01)	7	c	0.02
3-methylhexane	0.1 (0.2)	0.1 (0.1)	0.02 (0.03)	0.01 (0.02)	7	c	0.02
n-Heptane	0.1 (0.2)	0.1 (0.2)	0.02 (0.03)	0.02 (0.02)	6.76	a	0.01
MCH	0.2 (0.3)	0.2 (0.2)	0.05 (0.07)	0.04 (0.05)	9.6	a	0.02
2,2,4-TMP	0.05 (0.07)	0.06 (0.06)	0.004 (0.004)	0.004 (0.004	3.34	a	0.02
2,2,3-TMP	0.02 (0.03)	0.03 (0.04)	0.003 (0.005)	0.004 (0.006)	6.6	a	0.02
2-Methylheptane	0.07 (0.09)	0.04 (0.05)	0.01 (0.02)	0.008 (0.009)	9	c	0.02
3-Methylheptane	0.04 (0.05)	0.06 (0.07)	0.007 (0.010)	0.01 (0.01)	9	c	0.01
n-Octane	0.06 (0.08)	0.06 (0.07)	0.01 (0.01)	0.01 (0.01)	8.11	a	0.02
Ethene	0.04 (0.10)	0.3 (0.2)	0.01 (0.02)	0.05 (0.04)	8.5	a	0.003
Propene	0.01 (0.02)	0.05 (0.04)	0.005 (0.009)	0.03 (0.02)	26.3	a	0.01
cis-2-Butene	0.01 (0.01)	0.02 (0.03)	0.01 (0.02)	0.03 (0.04)	56.4	a	0.004
Isoprene		0.2 (0.3)		0.5 (0.5)	100	a	0.01
Benzene	0.2 (0.2)	0.2 (0.1)	0.006 (0.005)	0.004 (0.003)	1.22	a	0.03
Toluene	0.3 (0.3)	0.3 (0.2)	0.02 (0.02)	0.02 (0.02)	5.63	a	0.02
Ethylbenzene	0.03 (0.05)	0.04 (0.05)	0.005 (0.007)	0.005 (0.008)	7	a	0.01
ortho-Xylene	0.03 (0.04)	0.05 (0.05)	0.01 (0.01)	0.01 (0.01)	13.6	a	0.01
Ethyne	0.2 (0.1)	0.2 (0.2)	0.004 (0.003)	0.004 (0.003)	0.87	d	0.006
Acetaldehyde	1.2 (0.5)	1.9 (0.6)	0.3 (0.1)	0.4 (0.1)	15	a	0.08
Acetone	2.2 (0.7)	3 (1)	0.008 (0.002)	0.001 (0.004)	0.17	a	0.1
MEK	0.3 (0.2)	0.4 (0.3)	0.008 (0.004)	0.010 (0.006)	1.22	a	0.06

[a]Standard deviation of averages reported in parentheses

[b] $k_{OH,VOC}$: x 10^{-12} cm^3 $molec^{-1}$ s^{-1}.

[c]References for $k_{OH,VOC}$: (a) *Atkinson et al.* [2003] (b) *Rosen et al.* [2004], (c) *Farmer et al.* [2011], (d) *Atkinson et al.* [1986], (e) *Sander et al.* [2005], and (f) *Atkinson et al.* [2001].

The VOC manifold included a ¼" O.D. PFA line (flow rate 0.2 lpm) with a 1 µm Teflon filter at the inlet, which was located 6 m a.g.l. A whole air calibration standard (Cyl S; D. Blake, University of California, Irvine) with quantified levels of NHMCs, halocarbons, OVOCs, and alkyl nitrates was analyzed every 10th sampling run in the same manner as the ambient samples [*Sive et al.*, 2005] in order to monitor changes in detector sensitivity and measurement precision. Mixing ratios in the whole air standard were representative of rural air (*e.g.,* ~400 pptv for the C_2-C_{10} NMHCs), and were similar to the cleaner air masses encountered during the campaign. This whole air standard is part of a suite of standards used with this system, that includes ten high pressure cylinders, five 36-liter electropolished low-pressure pontoons (~350 psi), and three 34-liter electropolished high-pressure pontoons (~900 psi) containing whole air standards (D. Blake, UC-Irvine). Calibration checks were carried out routinely for the entire suite of standards; the upper limit of the absolute accuracy of the calibrated standard is ±1–10% for the VOCs reported here.

Additional analyses were carried out in order to verify and validate the mixing ratios of the whole air working standard. Both pre- and post-campaign, the working standard was analyzed on the CSU canister analytical system against one of the high pressure pontoons (HPP C), one of the low pressure pontoons (Pont S) and one of the high pressure cylinders (CCR24) in order to ensure the standard integrity and accuracy of the mixing ratios [e.g. *Russo et al.*, 2010b; *Sive et al.*, 2005; *Swarthout*, 2014; *Swarthout et al.*, 2013; *Zhou et al.*, 2005]. The post-campaign analyses included cross-referencing to two additional standards. An additional low pressure pontoon (PTX, D. Blake, UCI) was analyzed against the same group of standards in order to confirm consistent and comparable mixing ratios for the target gases, including the alkyl nitrates. Dilutions of a certified 1 ppmv Linde Gas NMHC multi-component high pressure synthetic standard were analyzed against the group of standards to further verify the calibration standards. Multipoint calibrations

using primary standards evaluated the detector response and linearity over the observed mixing ratio ranges for all classes of compounds.

The measurement precision of all species were determined from replicate analysis of the whole air standard prior to deployment, and were 0.6% – 10% for all VOCs. Limits of detection (LODs, Table 1) were calculated as the mixing ratio required to generate a peak with a signal-to-noise ratio of 3 from replicate whole air standard analyses, where noise is defined as the standard deviation of chromatogram baseline adjacent to peaks. The LODs ranged from 2 – 23 pptv for NMHCs, <1 pptv – 6 pptv for C_1-C_2 halocarbons, 0.2 – 0.5 pptv for alkyl nitrates, and 60 – 100 pptv for OVOCs. Mixing ratios were calculated from adjacent points in the time-series of response factors to account for variations in system sensitivity throughout the campaigns, and are summarized in Table 1. The spring dataset includes 1341 individual hourly samples of the full VOC suite (Table 1) minus isoprene, which was <LOD during the entire spring campaign. The summer dataset includes 1054 individual hourly samples of the full VOC suite (including isoprene).

3.2.2.2. Other Trace Gases

Peroxyacetyl nitrate (PAN) was measured with the custom-built NCAR GC-ECD [*Flocke et al.*, 2005]. Throughout the measurement period, the LOD for PAN was 2 pptv and measurement precision was 16%. PAN was sampled through a ¼" O.D. PFA line (flow rate ~7 LPM) with a 1 µm Teflon filter at the inlet, located 6 m a.g.l. The total sampling line length was ~10 m from the inlet filter to the detector. PAN was produced for calibrations by photolyzing an abundance of acetone (20 ppmv) in the presence of a precisely controlled flow of NO (1 ppmv), and diluted with zero-air. Point calibrations were performed every four hours. NO and NO_2 were measured by chemiluminescence (Teledyne model 200EU). A blue light converter (395 nm LED-based

photolytic converter; Air Quality Designs, Inc.) was placed at the inlet tip (6 m a.g.l.) to selectively convert ambient NO_2 to NO, and routinely provided >90% conversion efficiency. The LED was switched on and off for alternating 1-minute samples of NO or NO+NO_2. The NO_2 mixing ratio was determined by subtracting the ambient NO measurement from the NO detected after photolytic conversion of NO_2 to NO. CO and CH_4 were measured with a commercial Cavity Ring-Down Spectrometer (Picarro 6401). The instrument precision during the campaign was 6 and 12% for CH_4 and CO respectively. O_3 was measured with a 2B O_3 monitor (Model 202) with a precision of 1 ppbv over a range of 0-100 ppmv when calibrated with the 2B O_3 Source (Model 306).

3.2.2.3. Data Treatment

All trace gas measurements were aligned with the hourly VOC measurements by averaging the measurement values that fell within ± 2 minutes of the VOC timestamps to encompass the 5 minute VOC sampling window. Eighteen days were significantly impacted by smoke transported from wildfires in the western U.S. as indicated by elevated CO [*Lindaas et al.*, 2017]. These data were excluded for the analysis herein, resulting in 512 time points (24 July 2015 – 14 August 2015) of overlapping VOC and trace gas data for a 'smoke-free' summer campaign data set.

3.2.3. Positive Matrix Factorization (PMF)

Source apportionment techniques are statistical analysis approaches used to separate ambient mixing ratios of multiple species into factors that co-vary simultaneously, thus representing direct sources of species, chemical processes affecting those species, or transport processes [e.g. *Guha et al.*, 2015; *Lanz et al.*, 2007; *Lee et al.*, 1999; *Paatero*, 2000; *Paatero et al.*, 1994; *Song et al.*, 2006; *Ulbrich et al.*, 2009; *Watson et al.*, 2001]. Positive Matrix Factorization (PMF) is an algorithm for solving a source-receptor model that assumes that species in a measured

dataset adhere to a mass-balance for a number of source profiles with varying contributions to each species over the duration of the dataset [*Hopke*, 2000; *Paatero*, 2000; *Paatero et al.*, 1994; *Ulbrich et al.*, 2009]. PMF has been widely used as a source apportionment technique for aerosols [e.g. *Lanz et al.*, 2007; *Lee et al.*, 1999; *Song et al.*, 2006; *Ulbrich et al.*, 2009] and VOCs [e.g. *Bon et al.*, 2011; *Guha et al.*, 2015; *Yuan et al.*, 2012].

For a PMF analysis, data are arranged in a $m \times n$ 2-dimensional matrix (X). In Equation E4, X_{ij} represents an element of the matrix X that will be fit, where the matrix columns *(j)* are individual VOC species, and the rows *(i)* are measured VOC mixing ratios. A second matrix containing the errors for each data point is also required for the PMF algorithm to weight the importance of any data point based on the uncertainty reported in that data point. Errors for each VOC data point are defined below (section 3.2.3.1).

$$X_{ij} = \sum_p g_{ip} f_{pj} + e_{ij} \quad \text{(E4)}$$

The PMF algorithm solves the model with positively-constrained factor values *(p)*; each factor has a single time-series and factor contribution profile for each VOC included in the input matrix. Moreover, in Equation E4, g_{ip} represents an element of the factor time-series matrix *(G)*, in which columns are individual factor time-series; f_{pj} represents an element of the factor profile matrix *(F)*, in which rows are the individual factor profiles; e_{ij} represents an element of the residuals matrix (E) for data points not fully fit by the selected number of factors.

The PMF algorithm uses a least-squares method to iteratively fit values of the G and F matrices to minimize a quality of fit parameter Q, defined in equation E5 as

$$Q = \sum_{i=1}^{m} \sum_{j=1}^{n} \left(\frac{e_{ij}}{\sigma_{ij}} \right)^2 \quad \text{(E5)}$$

where σ_{ij} is an element of the $m \times n$ matrix of estimated errors of the points in the data matrix. In Equation E4, Q is the sum of the squares of the scaled residuals, where the scaling factor is the given error value of the data point being fit. A theoretical value of Q, or "*Q Expected*" (Q_{exp}), is equal to the degrees of freedom of the fitted data:

$$Q_{exp} = mn - p(m + n) \quad \text{(E6)}$$

If the estimation of errors in the input error matrix accurately describes the true error in the measurements, then Q_{exp} should approximate Q, and Q/Q_{exp} should approach 1 with the appropriate number of factors.

The PMF user must select the appropriate number of factors that best explains the variability in the dataset without including so many factors that spurious 'factor splitting' occurs [*Ulbrich et al.*, 2009]. This is accomplished by using the Q/Q_{exp} value as a metric for the "goodness" of fit, and by evaluating how well each species is reconstructed by the chosen number of factors. Factor splitting occurs when too many factors are included, and real, physically-relevant factors (sources) are separated into multiple unrealistic factors (sources). *A priori* information regarding the number of factors/sources and the identity of those factors/sources is not required for PMF analysis, but prior knowledge of potential sources provides the user with real physical constraints upon which to base the factor number selection.

Here, we applied PMF to the spring and summer datasets to investigate VOC sources and chemical processes in the NFRMA (bilinear model solved with the PMF2 algorithm in robust-mode; PMF output was evaluated using the PMF Evaluation Tool [*Ulbrich et al.*, 2009]). The ratio of Q/Q_{exp} and FPEAK are two parameters commonly included in the PMF literature to describe the factor solutions [*Hopke*, 2000; *Paatero*, 2000; *Paatero et al.*, 1994; *Ulbrich et al.*, 2009]. For the

spring VOC dataset, we selected a five factor solution with $Q/Q_{exp} = 2.51$ at FPEAK = 1. For the summer dataset, we selected a six factor solution with $Q/Q_{exp} = 5.87$ at FPEAK = 1. Exploration and investigation of Q/Qexp and FPEAK are described in the Supplemental Information. The additional summer factor was required to accurately explain the summer isoprene mixing ratios, which had a unique diel cycle relative to other VOCs, but contributes substantially to OH reactivity (see Section 3.3.4). We evaluate the two seasonal solutions, and compare VOC sources in spring versus summer. Solutions with more than five factors for the spring solution (or six for the summer) yielded uninterpretable factors, likely the result of the splitting of physically meaningful factors into multiple meaningless factors.[*Bon et al.*, 2011; *Lee et al.*, 1999; *Ulbrich et al.*, 2009].

3.2.3.1. PMF Data Preparation

We applied the PMF analysis separately for the VOC data for spring and summer, and interpreted the resulting factors with other trace gas measurements. Missing time points for each VOC species are due to unclear or indiscernible chromatograms, and were thus deemed to be below the LOD. The statistics for ethene and propene are provided in Table 1 for summer but not spring because the summer chromatographs contained reliable peaks for those two compounds while the spring measurement did not. However, in order to be able to directly compare spring and summer PMF factors, we left them out of the PMF analysis. Such points were replaced with the relevant LOD divided by three, and the error associated with that point was assigned a value equal to the LOD in order to reduce the weight of that point in the PMF algorithm. Each species time-series was scaled to obtain a campaign median value for each species of 1. This scaling provides a consistent range of values to represent species that typically vary over orders of magnitude, and improves the visualization of the PMF output plots in order to improve the ease in interpretation. This does not affect the interpretation of the PMF results because the PMF algorithm explores co-

variability among species in the input matrix, which is independent of the actual magnitude of each species. The error matrices were generated using the relative standard deviation (RSD) of the whole air standard time-series instead of the reported replicate measurement precision. This approach to errors yielded satisfactory Q/Q_{exp} values and better species reconstructions than other methods, yet represents physical uncertainty in the VOC measurements. Variations on scaling methods, error estimation, and missing data handling exist, but are similar to the procedures used herein [*Bon et al.*, 2011; *Guha et al.*, 2015; *Hopke*, 2000; *Williams et al.*, 2010; *Yuan et al.*, 2012].

We estimated the uncertainty for each factor time-series (Figs. A1.5-A1.6) and factor profiles (Figs. 3.2a,b) using 1000 bootstrapping runs for each season [*Ulbrich et al.*, 2009]. Bootstrap datasets are constructed from randomly sampled blocks of observations of varying length from the original dataset matrix for the user specified number of factors. The PMF output of the sampled blocks are averaged with the standard deviations providing an error estimate for the chosen PMF solution [*EPA*, 2014].

3.3. Results and Discussion

3.3.1 VOC Mixing Ratios: Seasonality and Context

Similar to previous studies in the NFRMA [*Gilman et al.*, 2013; *Pétron et al.*, 2012; *Swarthout et al.*, 2013; *Thompson et al.*, 2014], the values presented in Table 1 indicate that we observed higher mixing ratios of C_2-C_6 alkanes relative to 28 cities and urban areas in the U.S. [*Baker et al.*, 2008]. For example, typical urban U.S. sites show summer daytime propane mixing ratios of 0.29 - 3.51 ppbv, with Los Angeles exhibiting propane mixing ratios up to 6.05 ppbv [*Baker et al.*, 2008]. In contrast, the summer NFRMA average mixing ratio of propane was 8 ppbv. However, these mixing ratios are generally lower than observed in the Marcellus Shale natural gas

producing region of Southwest Pennsylvania, where propane averaged 13 ppbv at a site close to a cluster of unconventional natural gas wells [*Swarthout et al.*, 2015]. Propane is not the only elevated light alkane in the NFRMA: average daytime summer n-butane and n-pentane mixing ratios in this study were 2 and 1 ppbv, respectively. These observations are consistent with a strong contribution of ONG activities to the VOCs in air masses impacting the BAO site relative to urban areas in the U.S, but with lower mixing ratios of ONG-linked hydrocarbons than reported by for the Marcellus shale sites adjacent to wells [*Swarthout et al.*, 2015].

Most of the average VOC mixing ratios exhibited marked changes between the spring and summer campaigns (Table 3.1). VOCs in urban regions often reach a maxima during winter months resulting from decreased photochemistry and shallower, more stable boundary layers [*Russo et al.*, 2010b]. However, at the BAO site, average mixing ratios of C_4-C_6 alkanes were typically higher in the summer than in the spring; butane doubled between the seasons, while pentane mixing ratios increased by a factor of three. These observations are similar to previous studies in New England [*Russo et al.*, 2010b] and San Paulo, Brazil [*Dominutti et al.*, 2016], which attributed the seasonality to enhanced evaporative emissions with increased temperature. The other notable exception to the pattern of higher VOC mixing ratios in the spring versus summer was isoprene, which was below the detection limit in the spring but observable in the summer, consistent with isoprene's known temperature- and light-dependent biogenic source.

Repeated measurements of VOCs have been made at BAO; however, the short nature of the campaigns and differences in measurement time periods limits our ability to make quantitative comparisons between past data and the 2015 datasets. Changes in ambient VOC mixing ratios could be due to a number of factors including changes in local emissions from regulatory action, well number or production, background VOC abundances [e.g. *Helmig et al.*, 2016], traffic

patterns, local industrial practices, synoptic scale transport, and local meteorology. Average 2015 spring C_2-C_5 alkane and ethyne mixing ratios from this study were lower than those reported by *Swarthout et al.* [2013] and *Gilman et al.* [2013] for the previous (18 Feb 2011 – 14 Mar 2011) NACHTT campaign at BAO. Benzene and toluene mixing ratios were similar in spring 2015 to measurements from the NACHTT 2011 campaign. Some species were also lower in summer 2015 (8 week average) relative to summer 2012 (14 day average) [*McDuffie et al.*, 2016]. For example, propane and n-butane were higher in summer 2012 (14 and 6 ppbv averages, respectively) [*McDuffie et al.*, 2016] than summer 2015 (8 and 4 ppbv). However, this trend was not universal across the hydrocarbons: i-pentane and n-pentane were higher in summer 2015 (3 ppbv for both) than summer 2012 (2 ppbv for both) [*McDuffie et al.*, 2016]. Direct comparison of average mixing ratios between the two campaigns is currently qualitative at best, and a more comprehensive comparative analysis is beyond the scope of this paper.

3.3.2 PMF Factors

The PMF analysis discussed here describes the VOC sources in the NFRMA (Fig. 3.2), as observed at the BAO site in spring and summer 2015. Five factors were identified for the spring VOC dataset, which are described as the following: (1) ONG-Long Lived, (2) ONG-Short Lived, (3) Traffic, (4) Background, and (5) Secondary. A sixth factor was identified for the summer VOC dataset, (6) Biogenics (Fig. 3.2). PMF assumes no loss or production processes occur between the emission point and measurement location, but in reality that is not the case. These factors are not complete representations of sources, and are limited in that they do not capture the loss of highly reactive species, dry deposition processes, or gas-particle partitioning, but nonetheless the groupings in these factors provide useful information regarding local emissions. CO, NO_x, and CH_4 were left out of the PMF analysis in order to be used as emission tracers to aid in

characterizing the PMF output. That is, if all the trace gas data is incorporated in the PMF analysis, there is no remaining tracers with which to independently identify or validate factors.

Two factors were consistent with ONG-related hydrocarbons, one dominated by higher-reactivity alkanes ('ONG-Short Lived'), and one dominated by lower-reactivity species ('ONG-Long Lived'). The ONG-Long Lived factor accounted for 36 - 100% of the observed C_2-C_6 alkane mixing ratios, and is similar to percentages attributed to unconventional natural gas operations in the Marcellus Shale producing region of Pennsylvania [*Swarthout et al.*, 2015]. Previous studies have attributed the elevated C_2-C_6 alkane mixing ratios in the NFRMA to regional ONG operations [*Gilman et al.*, 2013; *Pétron et al.*, 2012; *Swarthout et al.*, 2013; *Thompson et al.*, 2014]. The ONG-Long Lived factor was the sole source of propane, reconstructing 100% of the measured propane mixing ratios for both spring and summer (r^2 of 0.96 for both seasons). ONG activity is thought to be the dominant source of propane in the NFRMA [*Gilman et al.*, 2013; *Swarthout et al.*, 2013], which is consistent with this factor assignment and it is unlikely that other anthropogenic sources would contribute such high mixing ratios of propane in this region. The propane-to-ethyne emission ratio normalized to volume of fuel consumed in vehicle exhaust is typically <0.1 [*Fraser et al.*, 1998], in contrast to the observed propane-to-ethyne ratios of 45 and 40 for spring and summer, respectively. While emission ratios normalized to fuel consumption will not be identical to the observed ratio, the comparison supports the conclusion that combustion was not the dominant source of propane.

The ONG-Short Lived factor was dominated by larger C_7 and C_8 alkanes (*e.g.* 2-methylhexane, 2-methylheptane, n-octane). These alkanes are known ONG emissions; for example flashing from oil and condensate tanks emits VOCs enriched in C_7 and larger alkanes [*Berger et al.*, 1981; *Warneke et al.*, 2014]. While this ONG-Short Lived factor does not contain

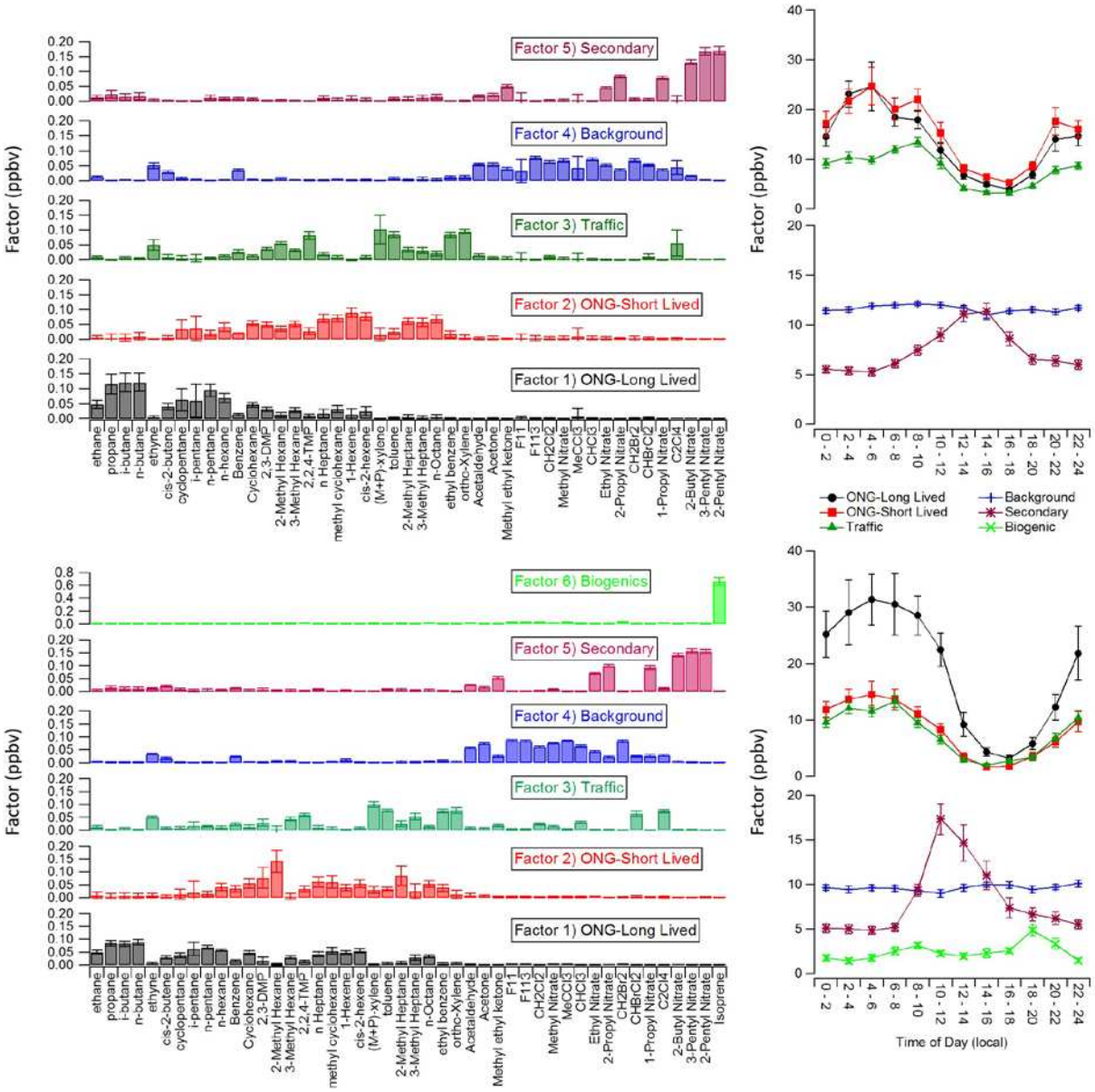

Figure 3.2. PMF VOC factor profiles for (a) spring and (b) summer were generated from 1,000 bootstrapping PMF runs. The y-axis for each factor profile is the fractional contribution that each species makes to each factor; error bars represent one standard deviation from the mean of the bootstrapping runs. The PMF algorithm generates an hourly time-series of each factor (Figure S5-S6). Diel cycles (ppbv) were calculated from those time-series for 2-hour time-bins in (c,d) spring and (e,f) summer. Error bars represent the standard error of the mean (spring n = 90 – 130, summer n = 37 – 48) for each time bin average. Isoprene was measured only in the warmer summer months (average of 0.200 ppbv), dominating a sixth Biogenic PMF factor in the summer. Abbreviated compound names: 2,3-DMP = 2,3-dimethylpentane; 2,2,4-TMP = 2,2,4-trimethylpentane.

the propane expected in an ONG source, the ONG-Long Lived and ONG-Short Lived factors share temporal characteristics indicative of a common source, with high correlation coefficients between ONG-Long Lived and ONG-Short Lived factors (r^2 = 0.62 and 0.63 for spring and summer, respectively; Fig. A1.7). However, the factors are distinguished by their photochemical lifetimes. The C_2-C_5 alkanes that dominate the ONG-Long Lived factor have rate constants with OH on the order of (0.25 – 4) x 10^{-12} cm^3 $molec^{-1}$ s^1, while the C_7-C_8 alkanes that dominate the ONG-Short Lived factor have faster rate constants with OH of (7 – 10) x 10^{-12} cm^3 $molec^{-1}$ s^{-1} (Table 3.1). These faster rate constants cause the larger alkanes to be removed 2-40 times faster than their smaller counterparts, and thus to have shorter atmospheric lifetimes than the C_2-C_5 alkanes. This is consistent with *Yuan et al.* [2012], which showed "chemical splitting" of a single source resulted in multiple factors separated by photochemical lifetime. Further evidence for chemical splitting of the ONG factors lies in i-pentane/n-pentane ratios. The individual factors have different pentane isomer ratios that do not represent typical ONG VOC composition, but summing the two ONG factors results in i-pentane/n-pentane ratios of 0.82 and 0.99 for spring and summer, respectively. These ratios are consistent with the i-pentane/n-pentane ratio range of natural gas from NFRMA sources (1.11 for Weld County natural gas [*Swarthout et al.*, 2013] and 0.86 for Wattenberg basin raw natural gas; [*Gilman et al.*, 2013]). The Traffic PMF factor has an i-pentane/n-pentane ratio <1.0, much lower than the ratios typical of combustion emissions (*e.g.* 2.45, for traffic dominated VOCs in the Los Angeles tunnel study [*Fraser et al.*, 1998]). This discrepancy may be the result of co-location of vehicle and ONG emissions that are not separated by the PMF algorithm and cause larger residuals for the pentane isomers resulting in poorer factor separation.

Figure 3.3 highlights the potential impact of these sources on the ambient VOC mixture. The ONG factors dominated the ambient pentane isomer levels at BAO in 2015 accounting for 58 - 63% of pentane isomers in spring and summer. The observed spring 2015 i-pentane/n-pentane ratio (1.17) was slightly higher than previous observations at BAO and other NFRMA measurements. NACHTT 2011 (winter/spring) measurements yielded i-pentane/n-pentane ratios of 0.89 [*Gilman et al.*, 2013] and 1.0 [*Swarthout et al.*, 2013]. The increased ratio could be due to one or a combination of changing background VOC mixing ratios, decreasing ONG VOC emissions as a result of regulation [*CDPHE*, 2014], changes in oil and gas production in the NFRMA [*EIA*, 2016a; b; c], increased traffic emissions from increased NFRMA population (14% increase in Denver county population between 2010 and 2015 [*U.S.-Census*, 2016]), or differences in meteorology and circulation that would draw air masses from areas in the NFRMA with different emissions (*e.g.* downtown Denver versus northeast NFRMA). Figure 3.3 contrasts the observed i-pentane/n-pentane ratios with other sites. The ratios in the NFRMA outside of downtown Denver were still lower than those observed in Pasadena (2.41) or Houston (1.39, [*Gilman et al.*, 2009]), suggesting that the relative contribution of ONG and traffic to pentane in the NFRMA was still more weighted towards ONG than for other U.S. cities.

The third PMF factor (Traffic) described traffic-related VOCs, and was dominated by ethyne, aromatic species (*i.e.* toluene, o-xylene, m+p-xylenes), and larger alkanes (*i.e.* 2-methyl heptane and 2,2,4-trimethyl pentane), consistent with tail-pipe or gasoline evaporative emissions [*Fraser et al.*, 1998; *Gentner et al.*, 2009; *Gentner et al.*, 2013]. Two well-known markers for combustion engine emissions are NO_x [*Baudic et al.*, 2016; *Pierson et al.*, 1990] and CO [*Baudic et al.*, 2016; *Fraser et al.*, 1998; *Pierson et al.*, 1990]. Correlations between both of these markers and the PMF Traffic factor are stronger in the spring (r^2 of 0.61) than in the summer (r^2 of 0.37-

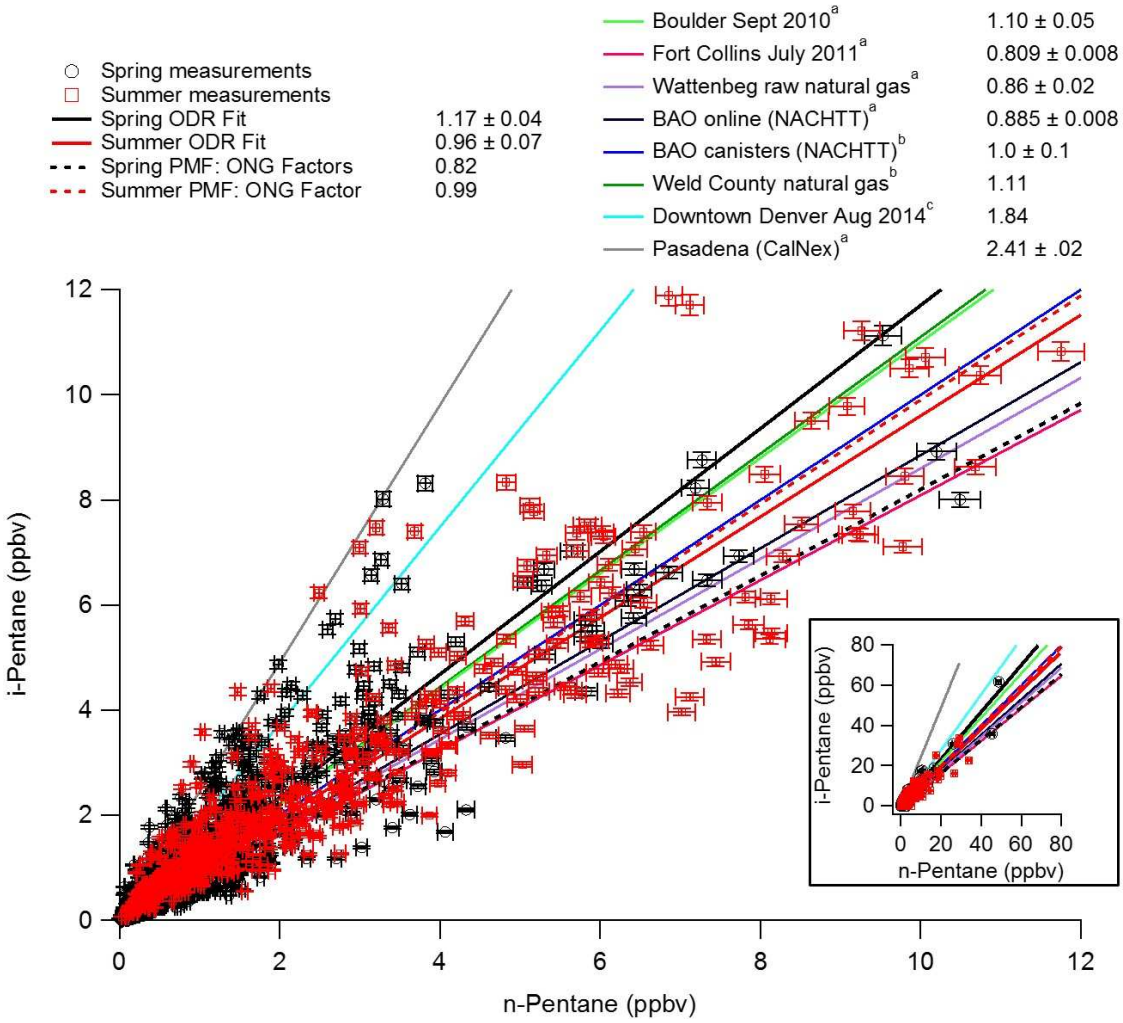

Figure 3.3. The ratio of i-pentane to n-pentane is used as a tracer for the relative influence of oil and natural gas production versus traffic sources. Black circles (red squares) are hourly spring (summer) measurements of i-pentane and n-pentane from the 2015 campaign. Error bars represent the uncertainty in each measurement. The solid black (red) line is the slope for spring (summer) data from an orthogonal distance regression (ODR). The dashed red and black lines represent the i-pentane/n-pentane ratios generated from the summed short+long lived ONG PMF factor profiles. The remaining solid lines are i-pentane/n-pentane ratios from previous NFRMA studies (Boulder 2010, Fort Collins 2011, BAO 2011, downtown Denver 2014), raw natural gas samples from the Wattenberg natural gas field and Weld County Natural gas in NFRMA, and the CalNex 2010 campaign in Pasadena, CA. Citations: (a) *Gilman et al.* [2013], (b) *Swarthout et al.* [2013], and (c) B. Sive, unpublished data.

0.38). These relatively weak summer correlations may be a result of differences in photochemical lifetimes: NO_x is short-lived, with a typical lifetime of 10 hours for an [OH] of 1 x 10^6 molec cm^{-3}, in contrast to the 77-day lifetime of CO. The key traffic VOCs have lifetimes on the order of 13 days (ethyne), 20 hours (o-xylene) and 49 hours (toluene). Thus, in the summer, we expect stronger photochemistry and weaker correlations between NO_x, CO and the Traffic VOCs. To this end, we find that NO_x and CO have a correlation coefficient of 0.73 in spring and 0.51 in summer (Fig. A1.8).

The fourth PMF factor, Background, was comprised of longer-lived VOCs with average lifetimes up to 116 days with respect to oxidation by OH under typical summertime conditions (1 x 10^6 molec cm^{-3} [OH]), and shorter-lived acetaldehyde and cis-2-butene. This factor also included two chlorofluorcarbons (CFC-11, CFC-113) with atmospheric lifetimes of 54 and 109 years respectively [*Rigby et al.*, 2013]. This factor represents observed species with local, regional and/or global sources. Because of their long lifetimes, these background VOCs show little diel variability (Figure A1.9). This factor is dominated by halocarbons, which are typically emitted from industrial sources including degreasing agents and dry cleaning solvents (C_2Cl_4) [*Simpson et al.*, 2004], paint stripping (CH_2Cl_2)[*McCulloch et al.*, 1996], drinking water and wastewater treatment ($CHCl_3$) [*McCulloch*, 2003], and phased out refrigerants and propellants (CFC-11, CFC-113) [*Martinerie et al.*, 2009].

These halocarbons are ubiquitous in the atmosphere and contribute to the destruction of stratospheric ozone [*Martinerie et al.*, 2009; *Seinfeld*, 2016]. Ethyne and benzene, with summertime lifetimes of approximately 46 and 9 days respectively, are also present in the Background factor. Acetone and acetaldehyde have very different lifetimes, 68 days and 19 hours respectively against OH oxidation, but both had average mixing ratios >1 ppbv (acetone) and >2

ppbv (acetaldehyde) throughout the day for spring and summer indicating significant background mixing ratios that were captured by the PMF analysis (Fig.A1.11).

The diel profile of the fifth factor, Secondary (Figs. 3.2d,f), had a pronounced afternoon rise (12:00 – 4:00 pm) consistent with photochemically-driven production on timescales similar to the photochemical production of PAN. PAN, a tracer for secondary or multi-generational chemistry [*Altshuller*, 1993], is well correlated with the Secondary factor (r^2 of 0.62 and 0.59 for spring and summer). The main contributors to this Secondary factor are short-chain alkyl nitrates and oxidized hydrocarbons including acetone, acetaldehyde and MEK. In urban areas, small-chain monofunctional alkyl nitrates, acetaldehyde, and PAN are dominantly produced by oxidation of primary anthropogenic emissions [e.g. *Flocke et al.*, 1998; *Russo et al.*, 2010a; *Seinfeld*, 2016; *Sommariva et al.*, 2011], while acetone and MEK have primary and secondary anthropogenic sources [*Fischer et al.*, 2012; *Yañez-Serrano et al.*, 2016].

Of the three measured OVOCs, MEK is the single largest OVOC contributor to the Secondary factor, although the correlation between MEK and the Secondary factor suggests that the Secondary source accounts for 38% of the MEK mixing ratios. This is more than double the percentage reported by *De Gouw et al.* [2005] for secondary anthropogenic production of MEK in New England urban areas. Furthermore, *Sommariva et al.* [2011] modeled the major photochemical production pathways for OVOCs, including MEK, in New England using VOC data from the 2002 New England Air Quality Study [*De Gouw et al.*, 2005; *Goldan et al.*, 2004], and found n-butane to be the dominant source of MEK (20-30%). The MEK yield from n-butane oxidation is on the order of 80% [*Singh et al.*, 2004]. n-Butane is higher in the NFRMA (summer average = 2 ppbv) relative to New York (0.760 ppbv) and Boston (0.190 ppbv) [*Baker et al.*, 2008], indicating that photochemical oxidation of n-butane is likely a major source of MEK in the

NFRMA. This implies that ONG activities in the region influence both primary VOC mixing ratios and the atmospheric oxidation chemistry in the region. Acetaldehyde is only weakly correlated with the Secondary factor, and this factor makes a small contribution to acetaldehyde (<9%) in the spring. In summer, the secondary factor explains 34% of the observed acetaldehyde mixing ratios.

PMF inherently groups compounds for which the timescale of production and loss are similar [*Yuan et al.*, 2012]. This causes VOCs that are photochemically produced or removed on different (slower or faster) timescales than the identified factors to be excluded. The Secondary factor is dominated by 2-butyl nitrate, 2-pentyl nitrate, and 3-pentyl nitrate with smaller contributions from ethyl nitrate and propyl nitrates. Alkyl nitrates are formed from the reaction of an alkyl peroxy radical (RO_2) with NO [*Roberts*, 1990]. Hydrogen atom abstraction from a parent alkane by OH is typically the rate limiting step in RO_2 formation [*Seinfeld*, 2016], and we can compare rate constants (k_{OH+VOC}) of those parent alkanes with the formation pathway of OVOCs and PAN. n-Butyl nitrate is formed almost exclusively from the oxidation of n-butane, and the pentyl nitrates from i-pentane and n-pentane; rate constants with OH for these parent hydrocarbons are (2.36 – 3.9) x 10^{-12} cm^3 $molec^{-1}$ s^1 [*Sommariva et al.*, 2008]. As described above, the oxidation of n-butane is also a primary pathway for MEK production [*Singh et al.*, 2004], demonstrating that timescales for secondary formation of MEK and C_4-C_5 nitrates are similar. Timescales for loss by OH reaction with MEK and C_4-C_5 alkyl nitrates are also similar: both are primarily removed by OH (τ_{OH} = 7 – 13.5 days for the alkyl nitrates; τ_{OH} = 5.4 days for MEK) [*Chew et al.*, 1996; *Simpson et al.*, 2006; *Yañez-Serrano et al.*, 2016]. While the photochemical sources of acetone and acetaldehyde are dominated by OH oxidation of propane and ethane, respectively, the lifetimes of these two compounds are quite different (0.8 days for acetaldehyde; 14 days for acetone, [*Fischer et al.*, 2014]). *Sommariva et al.* [2011] found that acetone and acetaldehyde are predominately

formed from OH oxidation of propane and ethane in urban airsheds in New England. Considering the elevated mixing ratios of ethane and propane in the NFRMA versus values reported by [*Baker et al.*, 2008] for those New England urban areas, this conclusion is likely also true for the NFRMA. This discrepancy may explain the relatively low correlations of the two OVOCs with the Secondary factor.

While isoprene was below the LOD in the spring, an additional PMF factor was identified in the summer that was almost exclusively comprised of isoprene (Fig. 3.2f). Isoprene is the globally dominant biogenic VOC [*Fuentes et al.*, 2000; *Kesselmeier et al.*, 1999] with a light- and temperature-dependent emission rate. Isoprene is emitted from many broadleaf plants, including spruce, sycamore, poplar, oak and multiple crops [*Guenther*, 2006; *Guenther et al.*, 1994]. The diel profile and temperature dependence (Fig. A1.10) is consistent with an exclusively biogenic source of isoprene in the NFRMA. Isoprene is suppressed in the mid-afternoon during the sunlight maxima, likely due to a combination of removal by reaction with OH ($k_{OH,isoprene}$ = 1 x 10^{-10} cm^3 $molec^{-1}$ s^{-1}), and an expanding afternoon boundary layer.

While monoterpenes are emitted by the pine trees that dominate the Rocky Mountains, and can be measured by the GC system described herein (LODs of 1 - 2 pptv), none were observed above the LOD in this 2015 campaign. We hypothesize that the lack of observed monoterpenes was due to their rapid oxidation by O_3 and OH before airmasses reached BAO. We note that substantial urban development has occurred in the Front Range in the last 3 decades, often accompanied by planting of urban trees. Several common native species, including aspen, oak, and spruce, are moderate to major isoprene emitters [*Guenther et al.*, 1994], and common isoprene-emitting urban trees in the NFRMA include oaks, poplars, and willows [*Guenther et al.*, 1994; *McHale et al.*, 2009].

3.3.3. PMF Reconstructions of Measured VOCs

The PMF factors and their time-series were used to reconstruct the mixing ratio of each VOC (Fig. 3.4, Table A1.2). The difference between the 'reconstructed' and 'observed' VOC mixing ratios can be attributed to the residual – *i.e.*, components that are not captured by the PMF solution. The lack of a suitable reconstruction for some species (*i.e.* OVOCs) indicates that the sources were not fully captured by PMF, potentially due to the lack of co-variability in the dataset or to the difficulty in capturing chemical processes that occur on multiple timescales. The C_2-C_8 alkanes, with the exceptions of ethane, the pentane isomers, and n-octane, were well captured by both spring and summer PMF solutions. The PMF reconstruction captured >80% of the mass as defined by the slope of reconstruction versus observation, and >80% of the variance, as defined by the correlation coefficients (Table A1.2). Benzene and toluene were also well reconstructed. The ONG factors accounted for 74% and 71% of measured benzene for spring and summer respectively, indicating that traffic is a minor source of benzene in the NFRMA. Toluene was more evenly split between ONG and Traffic factors, with 30% from ONG factors and 38% from Traffic in spring and 41% from ONG factors and 48% from Traffic in the summer. Acetone, acetaldehyde and MEK were associated with the background and secondary factors, but contained large residual components that were not captured by the PMF solution (<55 % of the mass and variance), suggesting that secondary sources operated on timescales that were quite different from the bulk of the secondary factor, or that primary emissions (*e.g.* solvent use) were not captured by the PMF solution. Similar to the oxygenated organic compounds, the halogenated organic species were poorly reconstructed (<58% of the mass), consistent with either local primary emission sources or incomplete capture of the background.

3.3.4. Organic Carbon Mass and VOC Reactivity

Figure 3.5 and A1.12 summarize the relative contributions from NO_x, CH_4, CO and VOCs on the total calculated OH reactivity (Figs. 3.5a,b). The average calculated total OH reactivity was 2.7 and 4.0 s^{-1} in the spring and summer, respectively, with NO_x dominating in the morning (44%, 1.8 s^{-1} in the spring; 36%, 2.1 s^{-1} in the summer). However, observed VOCs dominated the afternoon total calculated OH reactivity (0.7 - 1.1s^{-1} in the spring; 1.3 - 2.4 s^{-1} in the summer). VOCs contributed more OH reactivity in the summer (50 - 64%) than in the spring (35 – 48%), resulting from the relative enhancement of biogenics and the evaporative emission of anthropogenic hydrocarbons (Section 3.3.2.). VOCs are a major OH sink in both spring and summer, and provide carbon reactivity to initiate the HO_x catalytic cycle from which O_3 is produced. To better understand how different sources affect gas phase organic carbon and VOC reactivity, we investigated the contribution of each PMF factor to total calculated VOC reactivity and total observed organic carbon (Figs. 3.5c-3.5f). Total observed organic carbon (excluding methane) averaged 100 and 150 ppbC in the spring and summer, respectively, while total observed VOC reactivity (excluding methane) averaged 1.2 and 2.4 s^{-1}. The PMF factors reconstructed >84% of the total observed organic carbon mixing ratio and observed VOC reactivity, accounting for >93% of the variance. The total observed organic carbon mixing ratio was dominated by the ONG factors, which collectively accounted for 43 - 72% of ppbC in the spring, and 39 - 76% of ppbC in the summer. The ONG factors also accounted for the bulk of the morning VOC reactivity in the spring (52 - 66% of the VOC reactivity), with additional contributions from the background/long-lived factor in the late afternoon (4 - 6 PM). In contrast, the summer VOC reactivity was dominated by the ONG factors only in the morning (46 - 58% of the reactivity). Despite accounting for <6% of the observed organic carbon mixing ratio during the day, the

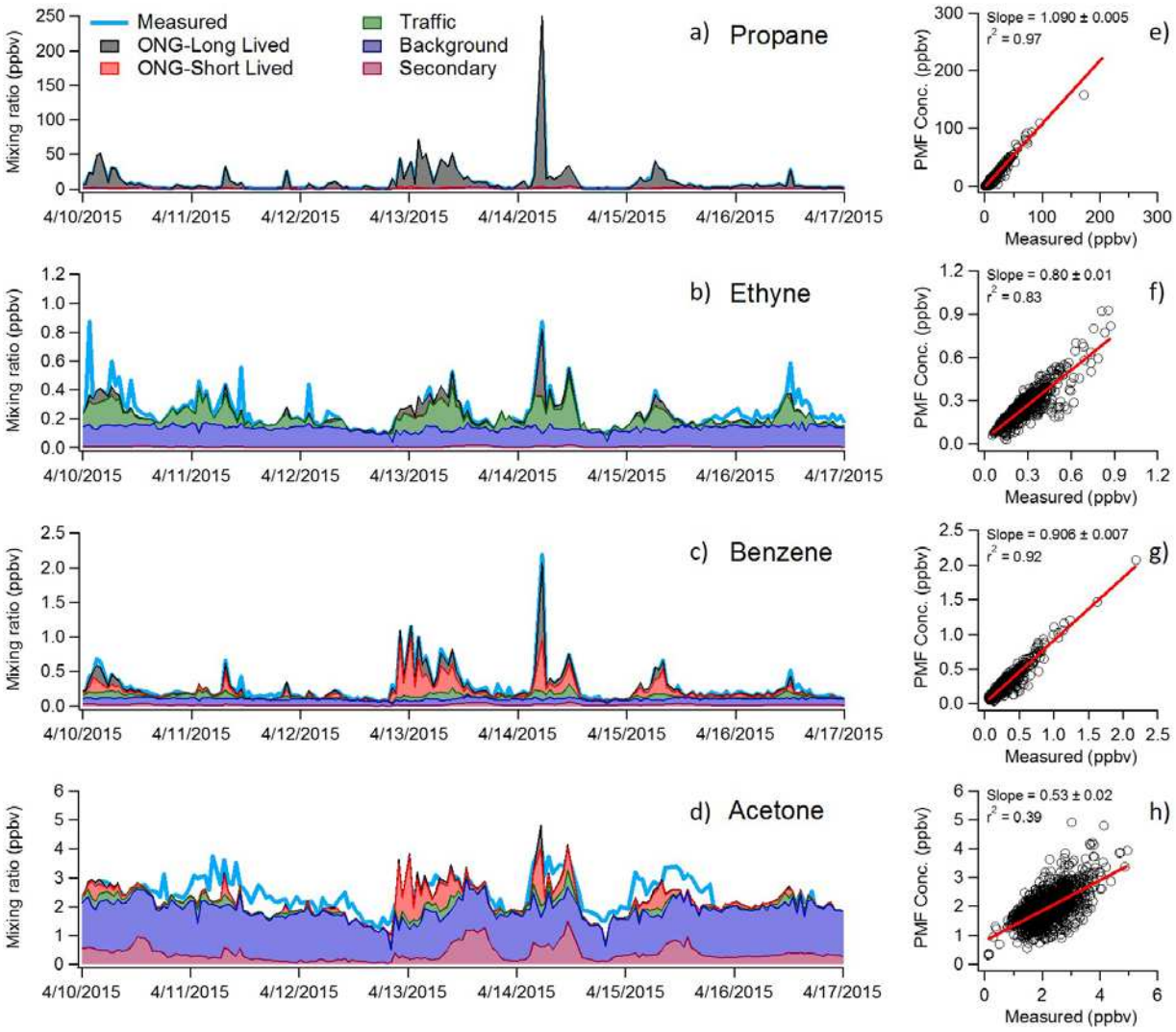

Figure 3.4. The observed mixing ratios (light blue line) and PMF reconstructions (shaded regions: ONG-Long Lived, grey; ONG-Short Lived, red; Traffic, dark green; Background, blue; Secondary, magenta) of four VOC species for one week (10 April – 17 April 2015) demonstrate the PMF-derived sources of each VOC. For example, the contribution of the ONG-Long Lived factor (a, black shading) to the observed propane concentration is calculated from the product of the ONG-Long Lived time-series (Figure S5-S6) and the ONG-Long Lived fractional contribution from propane (0.12 ± 0.03, Figure 2a). Each factor has a positive non-zero contribution to every species, and the full reconstruction of a given species is the sum of the reconstructions from each factor. The correlations between full reconstructions and the measured concentrations vary from species to species. Propane is fully reconstructed (e), and almost entirely attributed to the ONG-Long Lived factor (a). Ethyne is dominated by the Background and Traffic factors (b) but incompletely reconstructed (f), while benzene has contributions from ONG, traffic and background factors (c, g). Acetone has large contributions from both the Background and Secondary factors (d), but was only partially reconstructed (h), indicating sources that were not captured by the PMF analysis.

biogenic factor dominated VOC reactivity in the afternoon (up to 49% of the reactivity between 2 and 6 PM) when O_3 mixing ratios were at their peak.

The morning domination of VOC reactivity by ONG sources is consistent with previous results at the same site, 55 ± 18% [*Gilman et al.*, 2013] and 52% [*Swarthout et al.*, 2013] inFebruary 2011 and 50% in summer 2014 [*McDuffie et al.*, 2016]. However, the strong contribution of biogenic VOCs to VOC reactivity is in contrast to a previous study. *McDuffie et al.* [2016] reported that isoprene and monoterpenes contributed only ~8% to total VOC reactivity in the summer of 2012. We hypothesize that the discrepancy is the result of varying biogenic emissions from different drought conditions between the two summers. Temperature distributions for the identical time periods in each year are very similar (Fig. A1.13). Summer 2012 has a larger percentage of winds coming from the west, while summer 2015 has a higher percentage coming from the south (Fig. A1.14). In summer 2015 samples with wind directions from the west had slightly enhanced isoprene mixing ratios. Thus even with less favorable wind directions for enhanced isoprene, summer 2015 still had significantly elevated mixing ratios.

During the summer of 2012, 33% of the contiguous U.S. was in severe to extreme drought, and 55% of the U.S. was in moderate to extreme drought [*NOAA*, 2012]. In particular, Colorado was in a severe to exceptional drought through July and August 2012 [*NOAA*, 2015]. In contrast to the drought conditions experienced in 2012, the majority of Colorado was not in any drought classification during July and August 2015, and there was also excess soil moisture [*NOAA*, 2015]. Likely as a result of the drought conditions, average isoprene mixing ratios in summer 2012 were 0.06 ppbv versus 0.18 ppbv in summer 2015 for 25 July – 12 August for both years. A detailed review of the density of isoprene emitters in the NFRMA and the impact of drought on each species is beyond the scope of this study. However, we note that biogenic isoprene emissions from many

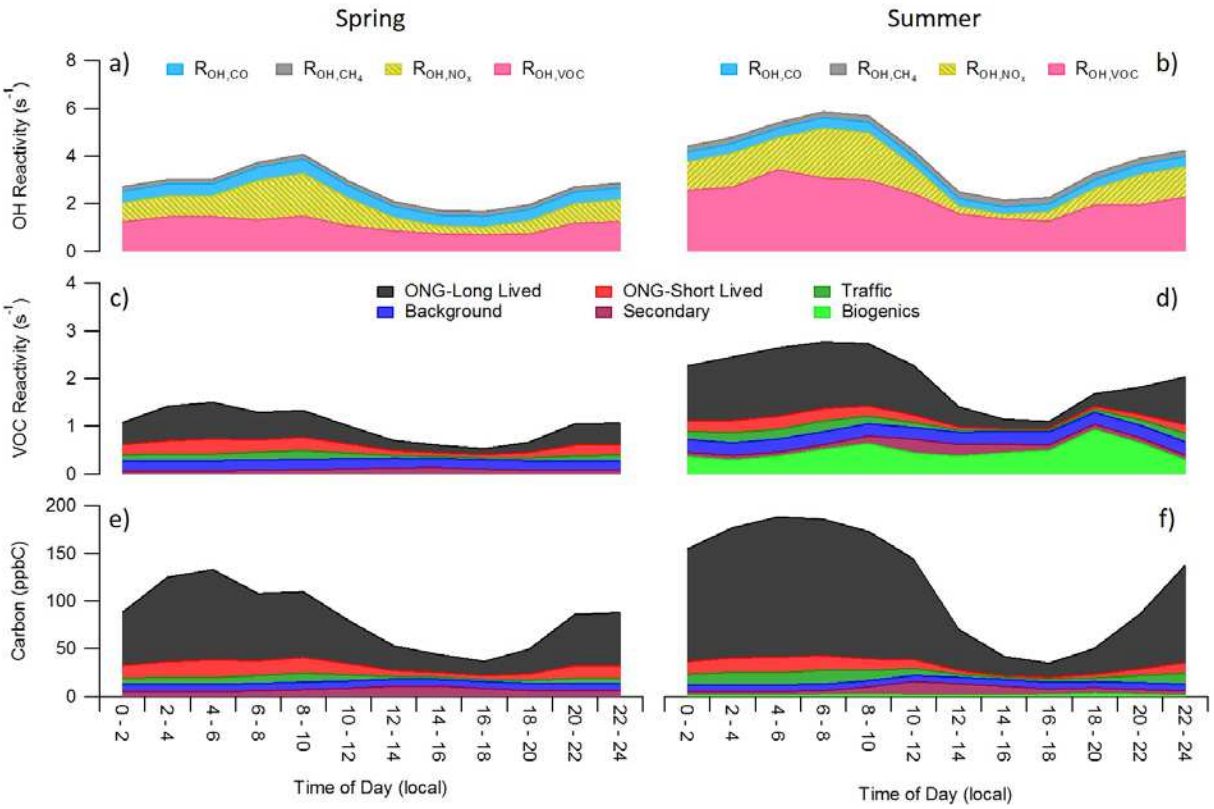

Figure 3.5. The top row shows diel cycles of calculated OH Reactivity from Equations (E1 – E3) for the spring (left column) and summer (right column). Each major contributor to total calculated OH reactivity (a,b) (VOCs, NO_x, CO, or CH_4) is shown stacked in a separate color. The middle and lower rows show the contributions from each PMF factor to the calculated (c,d) VOC reactivity and (e,f) calculated carbon mixing ratio as a diel cycle. The concentration of each species was reconstructed from PMF factors to determine the VOC reactivity contribution of each species for each factor and thus total VOC reactivity

plant species decrease with time and eventually cease under prolonged severe drought conditions [*Brilli et al.*, 2007; *Fortunati et al.*, 2008; *Guenther*, 2006], and that prolonged drought stress increases tree mortality rates [*Park et al.*, 2013].

Traffic is a minor source (<13%) of both organic carbon mixing ratio and VOC reactivity throughout the day in both seasons. While ethene and propene are known tail-pipe emissions [e.g. *Gentner et al.*, 2009; *Gentner et al.*, 2013], they were removed from the PMF analyses for both seasons as a result of spring measurement issues. However, their low summer mixing ratios and moderate OH reactivity accounts for < 4% of the calculated VOC reactivity. Acetaldehyde is the single largest VOC contributor to observed VOC reactivity, contributing 25% of the observed VOC reactivity in the spring, and 17% in the summer. To put this in perspective, the Background and Secondary factors, which accounted for the majority of the acetaldehyde, contributed a combined 28 - 48% and 21 - 33% of afternoon VOC reactivity in the spring and summer, respectively. In both factors acetone, acetaldehyde, and MEK are the dominant reactive species that contributed to VOC reactivity. These are clearly underestimates of total VOC reactivity; as most oxidized organic species were not measured in this study. In particular, formaldehyde, methyl vinyl ketone and methacrolein typically contribute substantially to VOC reactivity. For example, *Whalley et al.* [2016] reported that formaldehyde alone accounted for 23% of VOC reactivity in London during July – August 2012.

3.3.5. Comparison of VOC Reactivity to Other Regions

The magnitude of VOC reactivity and the relative contribution to that reactivity from different compounds or classes of compounds obviously varies across regions. Comparisons of VOC reactivity are difficult because of the varying number of VOCs measured across different campaigns and regions, as well as the reported VOC reactivity statistics (daytime versus full day

analyses; median versus average values). However, trends in reactivity have emerged from an array of urban areas, and qualitative comparisons of the similarities and differences between regions can be made and compared to the BAO site.

(1) Emissions of alkenes, aromatics, and alkynes from motor vehicle emissions or industrial/petrochemical processes tend to dominate anthropogenic VOC reactivity in urban regions. For example, *Borbon et al.* [2013] reported that aromatics and alkenes from motor vehicle emissions accounted for an average of 50% of calculated VOC reactivity during the CalNex campaign in Pasadena, CA. Similarly, *Gilman et al.* [2009] reported that C_2-C_6 alkenes and aromatics from motor vehicles and petrochemical refinery emissions were responsible for 42% (3.19 s^{-1}) of the 7.5 s^{-1} total calculated VOC reactivity in the Houston/Galveston Bay region.

In contrast, we observed little contribution of traffic-related VOCs to the overall VOC reactivity (3-13%), and instead find that ONG activity dominates the anthropogenic reactivity (17 - 66% of calculated VOC reactivity). However, the total observed VOC reactivity at the BAO site was substantially smaller in both the spring (1.2 s^{-1}) and summer (2.4 s^{-1}) relative to other urban sites.

(2) Urban areas in close proximity to forested regions (the eastern U.S. [e.g. *Chameides et al.*, 1988; *Millet et al.*, 2005; *Warneke et al.*, 2004]; and the San Joaquin Valley, CA [*Pusede et al.*, 2014]) can have significant contributions from biogenic VOCs and their oxidation products to total VOC reactivity. These biogenic sources can dominate VOC reactivity during the daytime. From VOC measurements made in Pittsburgh, PA in summer 2002, *Millet et al.* [2005] reported a median daytime VOC reactivity of 6.72 s^{-1} of which 70% (4.71 s^{-1}) was attributed to isoprene and isoprene oxidation products. Our observations suggest that biogenic VOCs were important contributors to VOC reactivity (up to 47%) in summer 2015, even though the absolute magnitude

of the biogenic contribution at BAO (0.29 - 0.93 s^{-1}) was far smaller than most other biogenic-influenced urban sites.

(3) OVOCs from primary urban emissions, oxidation of primary anthropogenic emissions, or oxidation of biogenic emissions can be major contributors to urban VOC reactivity ([e.g. *Borbon et al.*, 2013; *Gilman et al.*, 2009; *Millet et al.*, 2005; *Swarthout et al.*, 2015]) and can actually dominant VOC reactivity in some cities. Based on VOC measurements in London (July – August 2012), *Whalley et al.* [2016] reported that OVOCs excluding alcohols, but including formaldehyde, acetaldehyde, and isoprene oxidation products contributed 62% (3.45 s^{-1}) of the total calculated VOC reactivity of 5.54 s^{-1}. Unfortunately, our dataset is inadequate for extensively investigating the role of OVOCs to total VOC reactivity at BAO.

As noted by *McDuffie et al.* [2016], few studies have evaluated the impact of VOCs from ONG operations on regional summertime O_3 production, especially in urban regions. However, it is clear from the analysis above that VOC reactivity at BAO is quite different from other well-studied urban areas, and is more similar to semi-rural areas in close proximity to natural gas operations (*e.g.* Hickory site, Pennsylvania [*Swarthout et al.*, 2015]). The total calculated summer VOC reactivity of 2.4 s^{-1} in the NFRMA (excluding CH_4 and including biogenics) is much lower than urban areas detailed above, even when differences in VOC measurement suites are considered, but is similar to the value of 3.1 s^{-1} reported at the Hickory site [*Swarthout et al.*, 2015]. As discussed above, the NFRMA VOC composition in 2015 was predominantly ONG related C_2-C_6 alkanes and minimally impacted by traffic-related alkenes and aromatics. This contrasts with most other urban regions, in which traffic is typically the dominant anthropogenic VOC source. During summer 2015, biogenic VOCs (isoprene) impacted total VOC reactivity at BAO, accounting for an average of 20%, and up to 49%, of the total calculated VOC reactivity. These

fractional contributions of biogenic VOC reactivity to total reactivity were much higher than Pasadena (<2%) [*Borbon et al.*, 2013] and Houston (7%) [*Gilman et al.*, 2009], but lower than Pittsburgh (70%) [*Millet et al.*, 2005].

3.4. Conclusions

The spring and summer 2015 VOC dataset provides an updated long-term multi-season VOC measurement suite for the NFRMA that can be compared to previous measurements, and will be used to investigate O_3 production in the NFRMA. Using PMF source attribution we found that unlike most urban regions, traffic-related VOCs were minor contributors to reactivity. Instead, ONG sources contributed substantially to organic carbon mixing ratios and VOC reactivity, and remain obvious targets for VOC emissions control. Oxygenated VOCs from direct emissions or secondary production are a major OH radical sink. The enhanced isoprene contribution in the summer of 2015 relative to drought-stricken 2012 suggests that biogenic hydrocarbons from agriculture and urban trees have the potential to impact regional air quality, and may be strongly affected by drought stress [*Dai*, 2013]. Future drought-driven changes in biogenic VOCs have the potential to suppress VOC reactivity in the NFRMA [*Brilli et al.*, 2007; *Fortunati et al.*, 2008; *Guenther et al.*, 1996; *Park et al.*, 2013]. Despite their large contributions to VOC reactivity, the sources of OVOCs in the NFRMA (acetone, acetaldehyde, MEK) remain the least constrained of the measured VOC suite. PMF reconstructions of these species were poor, and future work characterizing the oxidized organic compounds and their chemistry are essential for constraining the OH reactivity and radical budget of the NFRMA region.

CHAPTER 3 REFERENCES

Altshuller, A. (1993), PANs in the atmosphere, *Air & Waste*, *43*(9), 1221-1230.

Baker, A. K., et al. (2008), Measurements of nonmethane hydrocarbons in 28 United States cities, *Atmospheric Environment*, *42*(1), 170-182.

Baudic, A., et al. (2016), Seasonal variability and source apportionment of volatile organic compounds (VOCs) in the Paris megacity (France), *Atmos. Chem. Phys.*, *16*(18), 11961-11989, doi:10.5194/acp-16-11961-2016.

Berger, B., and K. Anderson (1981), Modern petroleum: a basic primer of the industry.

Bon, D. M., et al. (2011), Measurements of volatile organic compounds at a suburban ground site (T1) in Mexico City during the MILAGRO 2006 campaign: measurement comparison, emission ratios, and source attribution, *Atmospheric Chemistry and Physics*, *11*(6), 2399-2421, doi:10.5194/acp-11-2399-2011.

Borbon, et al. (2013), Emission ratios of anthropogenic volatile organic compounds in northern mid-latitude megacities: Observations versus emission inventories in Los Angeles and Paris, *Journal of Geophysical Research: Atmospheres*, *118*(4), 2041-2057, doi:10.1002/jgrd.50059.

Brilli, F., et al. (2007), Response of isoprene emission and carbon metabolism to drought in white poplar (Populus alba) saplings, *New Phytologist*, *175*(2), 244-254.

Brown, S. S., et al. (2013), Nitrogen, Aerosol Composition, and Halogens on a Tall Tower (NACHTT): Overview of a wintertime air chemistry field study in the front range urban corridor of Colorado, *Journal of Geophysical Research: Atmospheres*, *118*(14), 8067-8085, doi:10.1002/jgrd.50537.

CDPHE (2014), Control of Ozone Via Ozone Precursors and Control of Hydocarbons Via Oil and Gas Emissions., edited, Denver, CO.

Chameides, W., R. Lindsay, J. Richardson, and C. Kiang (1988), The role of biogenic hydrocarbons in urban photochemical smog: Atlanta as a case study, *Science(Washington)*, *241*(4872), 1473-1475.

Chatani, S., et al. (2009), Sensitivity analyses of OH missing sinks over Tokyo metropolitan area in the summer of 2007, *Atmospheric Chemistry and Physics*, *9*(22), 8975-8986.

Chew, A. A., and R. Atkinson (1996), OH radical formation yields from the gas-phase reactions of O3 with alkenes and monoterpenes, *Journal of Geophysical Research: Atmospheres*, *101*(D22), 28649-28653.

Dai, A. (2013), Increasing drought under global warming in observations and models, *Nature Clim. Change*, *3*(1), 52-58, doi:http://www.nature.com/nclimate/journal/v3/n1/abs/nclimate1633.html#supplementary-information.

De Gouw, J., et al. (2005), Budget of organic carbon in a polluted atmosphere: Results from the New England Air Quality Study in 2002, *Journal of Geophysical Research: Atmospheres*, *110*(D16).

Di Carlo, P., et al. (2004), Missing OH reactivity in a forest: Evidence for unknown reactive biogenic VOCs, *Science*, *304*(5671), 722-725.

Dolgorouky, C., et al. (2012), Total OH reactivity measurements in Paris during the 2010 MEGAPOLI winter campaign, *Atmospheric Chemistry and Physics*, *12*(20), 9593-9612.

Dominutti, P. A., et al. (2016), One-year of NMHCs hourly observations in São Paulo megacity: meteorological and traffic emissions effects in a large ethanol burning context, *Atmospheric Environment*, *142*, 371-382.

Dusanter, S., et al. (2009), Measurements of OH and HO 2 concentrations during the MCMA-2006 field campaign–Part 2: Model comparison and radical budget, *Atmospheric Chemistry and Physics*, *9*(18), 6655-6675.

Edwards, P. M., et al. (2013), OH reactivity in a South East Asian tropical rainforest during the Oxidant and Particle Photochemical Processes (OP3) project, *Atmospheric Chemistry and Physics*, *13*(18), 9497-9514.

EIA (2016a), Crude Oil Production, edited.

EIA (2016b), Natural Gas Gross Withdrawals and Production, edited.

EIA (2016c), Number of Producing Gas Wells, edited.

EPA (2014), EPA Positive Matrix Factorization (PMF) 5.0 Fundamentals and User Guide, edited by O. o. R. a. Development, Washington, DC.

Fischer, E., et al. (2012), The role of the ocean in the global atmospheric budget of acetone, *Geophysical Research Letters*, *39*(1).

Fischer, E. V., et al. (2014), Atmospheric peroxyacetyl nitrate (PAN): a global budget and source attribution, *Atmos. Chem. Phys.*, *14*(5), 2679-2698, doi:10.5194/acp-14-2679-2014.

Flocke, et al. (2005), On the Measurement of PANs by Gas Chromatography and Electron Capture Detection, *Journal of Atmospheric Chemistry*, *52*(1), 19-43, doi:10.1007/s10874-005-6772-0.

Flocke, F., et al. (1998), Long-term measurements of alkyl nitrates in southern Germany: 1. General behavior and seasonal and diurnal variation, *Journal of Geophysical Research: Atmospheres*, *103*(D5), 5729-5746, doi:10.1029/97jd03461.

Fortunati, A., et al. (2008), Isoprene emission is not temperature-dependent during and after severe drought-stress: a physiological and biochemical analysis, *The Plant Journal*, *55*(4), 687-697.

Fraser, M. P., G. R. Cass, and B. R. Simoneit (1998), Gas-phase and particle-phase organic compounds emitted from motor vehicle traffic in a Los Angeles roadway tunnel, *Environmental science & technology*, *32*(14), 2051-2060.

Fuentes, J. D., et al. (2000), Biogenic hydrocarbons in the atmospheric boundary layer: a review, *Bulletin of the American Meteorological Society*, *81*(7).

Gentner, D. R., R. A. Harley, A. M. Miller, and A. H. Goldstein (2009), Diurnal and seasonal variability of gasoline-related volatile organic compound emissions in Riverside, California, *Environmental science & technology*, *43*(12), 4247-4252.

Gentner, D. R., et al. (2013), Chemical composition of gas-phase organic carbon emissions from motor vehicles and implications for ozone production, *Environ Sci Technol*, *47*(20), 11837-11848, doi:10.1021/es401470e.

Gilman, J. B., et al. (2009), Measurements of volatile organic compounds during the 2006 TexAQS/GoMACCS campaign: Industrial influences, regional characteristics, and diurnal dependencies of the OH reactivity, *Journal of Geophysical Research*, *114*, doi:10.1029/2008jd011525.

Gilman, J. B., B. M. Lerner, W. C. Kuster, and J. A. de Gouw (2013), Source signature of volatile organic compounds from oil and natural gas operations in northeastern Colorado, *Environ Sci Technol*, *47*(3), 1297-1305, doi:10.1021/es304119a.

Goldan, P. D., et al. (2004), Nonmethane hydrocarbon and oxy hydrocarbon measurements during the 2002 New England Air Quality Study, *Journal of Geophysical Research: Atmospheres*, *109*(D21), n/a-n/a, doi:10.1029/2003jd004455.

Goldstein, A. H. (2007), Known and unexplored organic constituents in the earth's atmosphere, *Environmental Science & Technology*, *41*(5), 1514-1521.

Guenther, A. (2006), Estimates of global terrestrial isoprene emissions using MEGAN (Model of Emissions of Gases and Aerosols from Nature), *Atmospheric Chemistry and Physics*, *6*.

Guenther, A., et al. (1996), Estimates of regional natural volatile organic compound fluxes from enclosure and ambient measurements, *Journal of Geophysical Research: Atmospheres*, *101*(D1), 1345-1359.

Guenther, A., P. Zimmerman, and M. Wildermuth (1994), Natural volatile organic compound emission rate estimates for US woodland landscapes, *Atmospheric Environment*, *28*(6), 1197-1210.

Guha, A., et al. (2015), Source apportionment of methane and nitrous oxide in California's San Joaquin Valley at CalNex 2010 via positive matrix factorization, *Atmospheric Chemistry and Physics*, *15*(20), 12043-12063.

Hansen, R., et al. (2014), Measurements of total hydroxyl radical reactivity during CABINEX 2009–Part 1: field measurements, *Atmospheric Chemistry and Physics*, *14*(6), 2923-2937.

Helmig, D., et al. (2016), Reversal of global atmospheric ethane and propane trends largely due to US oil and natural gas production, *Nature Geoscience*.

Hopke, P. K. (2000), A guide to positive matrix factorization, paper presented at Workshop on UNMIX and PMF as Applied to PM2.

Karl, T., et al. (2003), Seasonal variation of biogenic VOC emissions above a mixed hardwood forest in northern Michigan, *Geophysical Research Letters*, *30*(23).

Katzenstein, A. S., et al. (2003), Extensive regional atmospheric hydrocarbon pollution in the southwestern United States, *Proceedings of the National Academy of Sciences*, *100*(21), 11975-11979, doi:10.1073/pnas.1635258100.

Kesselmeier, J., and M. Staudt (1999), Biogenic Volatile Organic Compounds (VOC): An Overview on Emission, Physiology and Ecology, *Journal of Atmospheric Chemistry*, *33*(1), 23-88, doi:10.1023/a:1006127516791.

Lanz, V., et al. (2007), Source apportionment of submicron organic aerosols at an urban site by factor analytical modelling of aerosol mass spectra, *Atmospheric Chemistry and Physics*, *7*(6), 1503-1522.

Lee, E., C. K. Chan, and P. Paatero (1999), Application of positive matrix factorization in source apportionment of particulate pollutants in Hong Kong, *Atmospheric Environment*, *33*(19), 3201-3212.

Lindaas, J., et al. (2017), Changes in ozone and precursors during two aged wildfire smoke events in the Colorado Front Range in summer 2015, *Atmos. Chem. Phys.*, *17*(17), 10691-10707, doi:10.5194/acp-17-10691-2017.

Martinerie, P., et al. (2009), Long-lived halocarbon trends and budgets from atmospheric chemistry modelling constrained with measurements in polar firn, *Atmospheric Chemistry and Physics*, *9*(12), 3911-3934.

McCulloch, A. (2003), Chloroform in the environment: occurrence, sources, sinks and effects, *Chemosphere*, *50*(10), 1291-1308.

McCulloch, A., and P. M. Midgley (1996), The production and global distribution of emissions of trichloroethene, tetrachloroethene and dichloromethane over the period 1988–1992, *Atmospheric Environment*, *30*(4), 601-608.
McDuffie, E. E., et al. (2016), Influence of oil and gas emissions on summertime ozone in the Colorado Northern Front Range, *Journal of Geophysical Research: Atmospheres*, *121*(14), 8712-8729.
McHale, M. R., et al. (2009), Urban forest biomass estimates: is it important to use allometric relationships developed specifically for urban trees?, *Urban Ecosystems*, *12*(1), 95-113, doi:10.1007/s11252-009-0081-3.
Millet, D. B., et al. (2005), Atmospheric volatile organic compound measurements during the Pittsburgh Air Quality Study: Results, interpretation, and quantification of primary and secondary contributions, *Journal of Geophysical Research: Atmospheres*, *110*(D7).
NOAA (2012), State of the Climate: Drought for August 2012, edited, National Centers for Environmental Information.
NOAA (2015), State of the Climate: Drought for August 2015, edited, National Center for Environmental Information.
Paatero, P. (2000), User's guide for positive matrix factorization programs PMF2 and PMF3, *Helsinki: University of Helsinki*.
Paatero, P., and U. Tapper (1994), Positive matrix factorization: A non-negative factor model with optimal utilization of error estimates of data values, *Environmetrics*, *5*(2), 111-126.
Park, W., A., et al. (2013), Temperature as a potent driver of regional forest drought stress and tree mortality, *Nature Clim. Change*, *3*(3), 292-297, doi:http://www.nature.com/nclimate/journal/v3/n3/abs/nclimate1693.html#supplementary-information.
Pétron, G., et al. (2012), Hydrocarbon emissions characterization in the Colorado Front Range: A pilot study, *Journal of Geophysical Research: Atmospheres*, *117*(D4), n/a-n/a, doi:10.1029/2011jd016360.
Pétron, G., et al. (2014), A new look at methane and nonmethane hydrocarbon emissions from oil and natural gas operations in the Colorado Denver-Julesburg Basin, *Journal of Geophysical Research: Atmospheres*, *119*(11), 6836-6852.
Piccot, S. D., J. J. Watson, and J. W. Jones (1992), A global inventory of volatile organic compound emissions from anthropogenic sources, *Journal of Geophysical Research: Atmospheres*, *97*(D9), 9897-9912.
Pierson, W. R., A. W. Gertler, and R. L. Bradow (1990), Comparison of the SCAQS tunnel study with other on road vehicle emission data, *Journal of the Air & Waste management association*, *40*(11), 1495-1504.
Pusede, S., et al. (2014), On the temperature dependence of organic reactivity, nitrogen oxides, ozone production, and the impact of emission controls in San Joaquin Valley, California, *Atmospheric Chemistry and Physics*, *14*(7), 3373-3395.
Rigby, M., et al. (2013), Re-evaluation of the lifetimes of the major CFCs and CH₃CCl₃ using atmospheric trends, *Atmos. Chem. Phys.*, *13*(5), 2691-2702, doi:10.5194/acp-13-2691-2013.
Roberts, J. M. (1990), The atmospheric chemistry of organic nitrates, *Atmospheric Environment. Part A. General Topics*, *24*(2), 243-287.
Russo, R. S., et al. (2010a), Temporal variability, sources, and sinks of C 1-C 5 alkyl nitrates in coastal New England, *Atmospheric Chemistry and Physics*, *10*(4), 1865-1883.

Russo, R. S., et al. (2010b), Multi-year (2004–2008) record of nonmethane hydrocarbons and halocarbons in New England: seasonal variations and regional sources, *Atmospheric Chemistry and Physics*, *10*(10), 4909-4929, doi:10.5194/acp-10-4909-2010.
Seinfeld, J. H. (2016), *Atmospheric chemistry and physics: from air pollution to climate change*, John Wiley & Sons.
Simpson, I. J., et al. (2004), Long-term decrease in the global atmospheric burden of tetrachloroethene (C2Cl4), *Geophysical research letters*, *31*(8).
Simpson, I. J., et al. (2006), Long-term atmospheric measurements of C1–C5 alkyl nitrates in the Pearl River Delta region of southeast China, *Atmospheric Environment*, *40*(9), 1619-1632, doi:10.1016/j.atmosenv.2005.10.062.
Singh, H., et al. (2004), Analysis of the atmospheric distribution, sources, and sinks of oxygenated volatile organic chemicals based on measurements over the Pacific during TRACE-P, *Journal of Geophysical Research: Atmospheres*, *109*(D15).
Sive, B. C., et al. (2005), Development of a Cryogen-Free Concentration System for Measurements of Volatile Organic Compounds, *Analytical Chemistry*, *77*(21), 6989-6998, doi:10.1021/ac0506231.
Sommariva, R., et al. (2011), Emissions and photochemistry of oxygenated VOCs in urban plumes in the Northeastern United States, *Atmos. Chem. Phys.*, *11*(14), 7081-7096, doi:10.5194/acp-11-7081-2011.
Sommariva, R., et al. (2008), A study of organic nitrates formation in an urban plume using a Master Chemical Mechanism, *Atmospheric Environment*, *42*(23), 5771-5786.
Song, Y., et al. (2006), Source apportionment of PM2. 5 in Beijing by positive matrix factorization, *Atmospheric Environment*, *40*(8), 1526-1537.
Swarthout, R. F. (2014), Organic Compound Emissions from Unconventional Natural Gas Production: Source Signatures and Air Quality Impacts, Univ. of New Hampshire, Durham, NH, Univ. of New Hampshire, Durham, NH.
Swarthout, R. F., et al. (2013), Volatile organic compound distributions during the NACHTT campaign at the Boulder Atmospheric Observatory: Influence of urban and natural gas sources, *Journal of Geophysical Research: Atmospheres*, *118*(18), 10,614-610,637, doi:10.1002/jgrd.50722.
Swarthout, R. F., et al. (2015), Impact of Marcellus Shale natural gas development in southwest Pennsylvania on volatile organic compound emissions and regional air quality, *Environ Sci Technol*, *49*(5), 3175-3184, doi:10.1021/es504315f.
Thompson, C. R., J. Hueber, and D. Helmig (2014), Influence of oil and gas emissions on ambient atmospheric non-methane hydrocarbons in residential areas of Northeastern Colorado, *Elementa: Science of the Anthropocene*, *2*, 000035, doi:10.12952/journal.elementa.000035.
U.S.-Census (2016), Quick Facts - Colorado, edited.
Ulbrich, I., et al. (2009), Interpretation of organic components from Positive Matrix Factorization of aerosol mass spectrometric data, *Atmospheric Chemistry and Physics*, *9*(9), 2891-2918.
Warneke, C., et al. (2004), Comparison of daytime and nighttime oxidation of biogenic and anthropogenic VOCs along the New England coast in summer during New England Air Quality Study 2002, *Journal of Geophysical Research: Atmospheres*, *109*(D10).

Warneke, C., et al. (2014), Volatile organic compound emissions from the oil and natural gas industry in the Uinta Basin, Utah: point sources compared to ambient air composition, *Atmospheric Chemistry & Physics Discussions*, *14*, 11895-11927.

Watson, J. G., J. C. Chow, and E. M. Fujita (2001), Review of volatile organic compound source apportionment by chemical mass balance, *Atmospheric Environment*, *35*(9), 1567-1584.

Whalley, L., et al. (2016), Atmospheric OH reactivity in central London: observations, model predictions and estimates of in situ ozone production, *Atmospheric Chemistry and Physics*, *16*(4), 2109-2122.

Williams, B., et al. (2010), Major components of atmospheric organic aerosol in southern California as determined by hourly measurements of source marker compounds, *Atmospheric Chemistry and Physics*, *10*(23), 11577-11603.

Yañez-Serrano, A.-M., et al. (2016), Atmospheric mixing ratios of methyl ethyl ketone (2-butanone) in tropical, boreal, temperate and marine environments, *Atmospheric Chemistry and Physics Discussions*.

Yuan, B., et al. (2012), Volatile organic compounds (VOCs) in urban air: How chemistry affects the interpretation of positive matrix factorization (PMF) analysis, *Journal of Geophysical Research: Atmospheres*, *117*(D24), n/a-n/a, doi:10.1029/2012jd018236.

Zhou, Y., et al. (2008), Bromoform and dibromomethane measurements in the seacoast region of New Hampshire, 2002–2004, *Journal of Geophysical Research*, *113*(D8), doi:10.1029/2007jd009103.

Zhou, Y., et al. (2005), Coastal water source of short-lived halocarbons in New England, *Journal of Geophysical Research*, *110*(D21), doi:10.1029/2004jd005603.

CHAPTER 4 – ON THE USE OF THE ALKYL NITRATE PHOTOCHEMICAL CLOCK TO DERIVE AIRMASS AGING IN NORTHERN COLORADO[3]

4.1. Introduction

Short-chain alkyl nitrates (C_1–C_5 $RONO_2$) typically account for only a small fraction of both the organic nitrate ($RONO_2$) and NO_y budget (NO_y = NO + NO_2 + HNO_3 + HONO + $2N_2O_5$ + HO_2NO_2 + peroxyacyl nitrates and homologues + NO_3 + $RONO_2$ + $ROONO_2$). However, the production and loss of C_1-C_5 $RONO_2$ still impacts tropospheric ozone, HO_x (RO_2 + HO_2), and NO_x (NO + NO_2) budgets. Ozone and $RONO_2$ are produced simultaneously in the atmosphere (Figs. 1a,b), and the ratio of C_1-C_5 $RONO_2$ to their parent C_1-C_5 alkane can be used to determine the photochemical age of air masses [*S. B. Bertman et al.*, 1995]. However, uncertainties in the sources and sinks of $RONO_2$ are substantial, and can lead to uncertainties in photochemical clock analyses [*I. J. Simpson et al.*, 2003].

While direct emissions of C_1-C_2 $RONO_2$ have been observed from both the ocean [e.g. *E. Atlas et al.*, 1993; *N. J. Blake et al.*, 2003b; *N. J. Blake et al.*, 1999; *A. L. Chuck et al.*, 2002] and biomass burning [*I. J. Simpson et al.*, 2011; *I. J. Simpson et al.*, 2002], the dominant source of C_1–C_5 $RONO_2$ at continental mid-latitude sites is the photooxidation of anthropogenic precursors (R1-R3) [e.g. *S. B. Bertman et al.*, 1995; *F. Flocke et al.*, 1998; *J. M. Roberts*, 1990; *J. M. Roberts et al.*, 1998; *R. S. Russo et al.*, 2010a; *I. J. Simpson et al.*, 2003; *D. R. Worton et al.*, 2010] (Figs. 1a,b):

[3]The manuscript writing for this chapter has been prepared for publication by Andrew J. Abeleira, but has not yet been submitted for publication

$$RH + OH \xrightarrow{k_1, \alpha_1} R\cdot + H_2O \quad \text{(R1)}$$

$$R\cdot + O_2 \xrightarrow{k_2} RO_2\cdot \quad \text{(R2)}$$

$$RO_2\cdot + NO\cdot \xrightarrow{k_3, 1-\alpha_3} RO\cdot + NO_2\cdot \quad \text{(R3a)}$$

$$RO_2\cdot + NO\cdot \xrightarrow{k_3, \alpha_3} RONO_2 \quad \text{(R3b)}$$

The fraction of proton abstraction from the parent alkane (RH) at a particular carbon atom is α_1 (R1). The formation of the peroxy (RO_2) radical is fast. In the presence of NO_x, RO_2 reacts with NO (R3); the minor pathway forms monofunctional C_1–C_5 $RONO_2$ (R3b, α_3). Thus, the fraction of reactions between the parent alkane and OH in the presence of NO that lead to $RONO_2$ formation is the product of α_1 and α_3 ($\beta = \alpha_1\alpha_3$), the $RONO_2$ branching ratio. For the C_1–C_5 $RONO_2$, β ranges from 0.001 for methyl nitrate (CH_3ONO_2) to 0.074 for 2-butyl nitrate ($CH_3CH_2CH_2CH(ONO_2)CH_3$).

Reaction with OH (R4) and photolysis (R5) are the major sinks of C_1-C_5 $RONO_2$ [*S. B. Bertman et al.*, 1995; *A. Perring et al.*, 2013; *J. M. Roberts*, 1990; *R. Talukdar et al.*, 1997; *R. K. Talukdar et al.*, 1997], although deposition may also be important [*R. S. Russo et al.*, 2010a] (Fig. 4.1c). The products of $RONO_2$ + OH depend on the size and structure of the $RONO_2$. The major (>50%) products from proton abstraction of C_3–C_4 linear and branched $RONO_2$ by OH are NO_2 and either aldehydes or ketones via the decomposition of intermediate alkoxy radicals [*S. M. Aschmann et al.*, 2011]. For example, the reaction of OH with linear 2-hexyl and 3-hexyl $RONO_2$ produces a variety of aldehydes and ketones including 2-hexanone, 3-hexanone, propanal, and butanal. Interestingly, a fraction of those reactions retained the nitrate functionality to produce

multifunctional $RONO_2$, such as C_6-carbonyl nitrates, hydroxycarbonyl nitrates, and dinitrates [*S. M. Aschmann et al.*, 2012]

$$RONO_2 + OH \xrightarrow{k_4} products + NO_2 \cdot \quad \text{(R4)}$$

Photolysis of C_1-C_5 $RONO_2$ releases the corresponding alkoxy radical and NO_2 (R5) [*J. M. Roberts*, 1990; *J. M. Roberts and R. W. Fajer*, 1989; *R. K. Talukdar et al.*, 1997]:

$$RONO_2 \xrightarrow{J_5} RO \cdot + NO_2 \cdot \quad \text{(R5)}$$

$RONO_2$ photolysis rates vary with $RONO_2$ chemical structure, pressure (i.e. altitude), spectral radiance (intensity as a function of wavelength), and temperature. These photolysis rates are on the order of 10^{-7} - 10^{-6} s^{-1} for C_1–C_5 $RONO_2$ at mid-latitude surface sites through all seasons, corresponding to lifetimes against photolysis ranging from 6 – 125 days [*S. B. Bertman et al.*, 1995; *K. C. Clemitshaw et al.*, 1997; *J. M. Roberts*, 1990; *J. M. Roberts and R. W. Fajer*, 1989; *I. J. Simpson et al.*, 2003; *R. K. Talukdar et al.*, 1997; *M. Wang et al.*, 2013; *D. R. Worton et al.*, 2010].

Deposition and aerosol uptake are typically ignored as sinks of C_1-C_5 $RONO_2$ due to their low Henry's law constants (2.64 M atm^{-1} for $MeONO_2$; decreasing with increasing carbon number for monofunctional $RONO_2$ [*J. Kames and U. Schurath*, 1992]) and high vapor pressures (>3 torr [*R. G. Fischer and K. Ballschmiter*, 1998; *Y. B. Lim and P. J. Ziemann*, 2005; *J. M. Roberts*, 1990]). Solubility of monofunctional $RONO_2$ is low, and hydrolysis is slow (10^{-5} – 10^{-3} s^{-1}) [*R. E. Robertson et al.*, 1982]; water uptake is thus likely a small sink for C_1–C_5 $RONO_2$. However, the sum of all $RONO_2$ and peroxyacetyl nitrate deposition accounts for ~10% of annual global nitrogen deposition of 92.9 Tg [*J. C. Neff et al.*, 2002]. Speciated oxidized nitrogen deposition rates are essential for accurate modeling of oxidized nitrogen deposition [*J. C. Neff et al.*, 2002]. *R. S. Russo*

et al. [2010a] report dry deposition velocities of 0.13 cm s^{-1} for methyl nitrate ($MeONO_2$), which reduce the estimated summer lifetime of $MeONO_2$. The modeled global distribution of $MeONO_2$ is thus sensitive to the inclusion of dry deposition, which reduces the impact of long range transport of a $HO_x + NO_x$ source to remote regions of the globe [*J. Williams et al.*, 2014]. To the best of our knowledge, *R. S. Russo et al.* [2010a] provide the only observational estimate of speciated C_1–C_5 $RONO_2$ dry deposition, although eddy covariance flux measurements of speciated multifunctional nitrates and total organic nitrates (ΣANs) show substantial deposition [e.g. *D. K. Farmer and R. C. Cohen*, 2008; *T. B. Nguyen et al.*, 2015].

Using measurements of speciated C_1-C_5 $RONO_2$, hydrocarbons, ozone, and other trace gases, we explore seasonal trends in C_1–C_5 $RONO_2$ at the Boulder Atmospheric Observatory in the Front Range of Northern Colorado from winter, spring, and summer measurement campaigns. The Front Range is an interesting region to study C_1–C_5 $RONO_2$ because the abundances of C_2-C_5 alkanes are relatively high due to the high density of oil and natural gas operations [*A. Abeleira et al.*, 2017; *J. B. Gilman et al.*, 2013; *E. E. McDuffie et al.*, 2016; *G. Pétron et al.*, 2012; *G. Pétron et al.*, 2014; *R. F. Swarthout et al.*, 2013]. Specifically, C_2–C_5 alkane concentrations are 5 – 300x higher than most other ground sites with speciated C_1–C_5 $RONO_2$ measurements [e.g. *S. B. Bertman et al.*, 1995; *X. Lyu et al.*, 2015; *R. S. Russo et al.*, 2010a; *A. L. Swanson et al.*, 2003; *B. Wang et al.*, 2010; *M. Wang et al.*, 2013]. The Front Range includes densely populated urban areas and high traffic interstate highways, and the region violates the National Ambient Air Quality Standard for ozone. Outside of Denver, the Front Range appears to be transitioning from a NO_x-saturated ozone production regime to peak production [*A. J. Abeleira and D. K. Farmer*, 2017]. Here, we use a simple analytical model to explore the importance of – and uncertainties in – sources and sinks of C_1–C_5 $RONO_2$, and their impact on estimating the photochemical age of

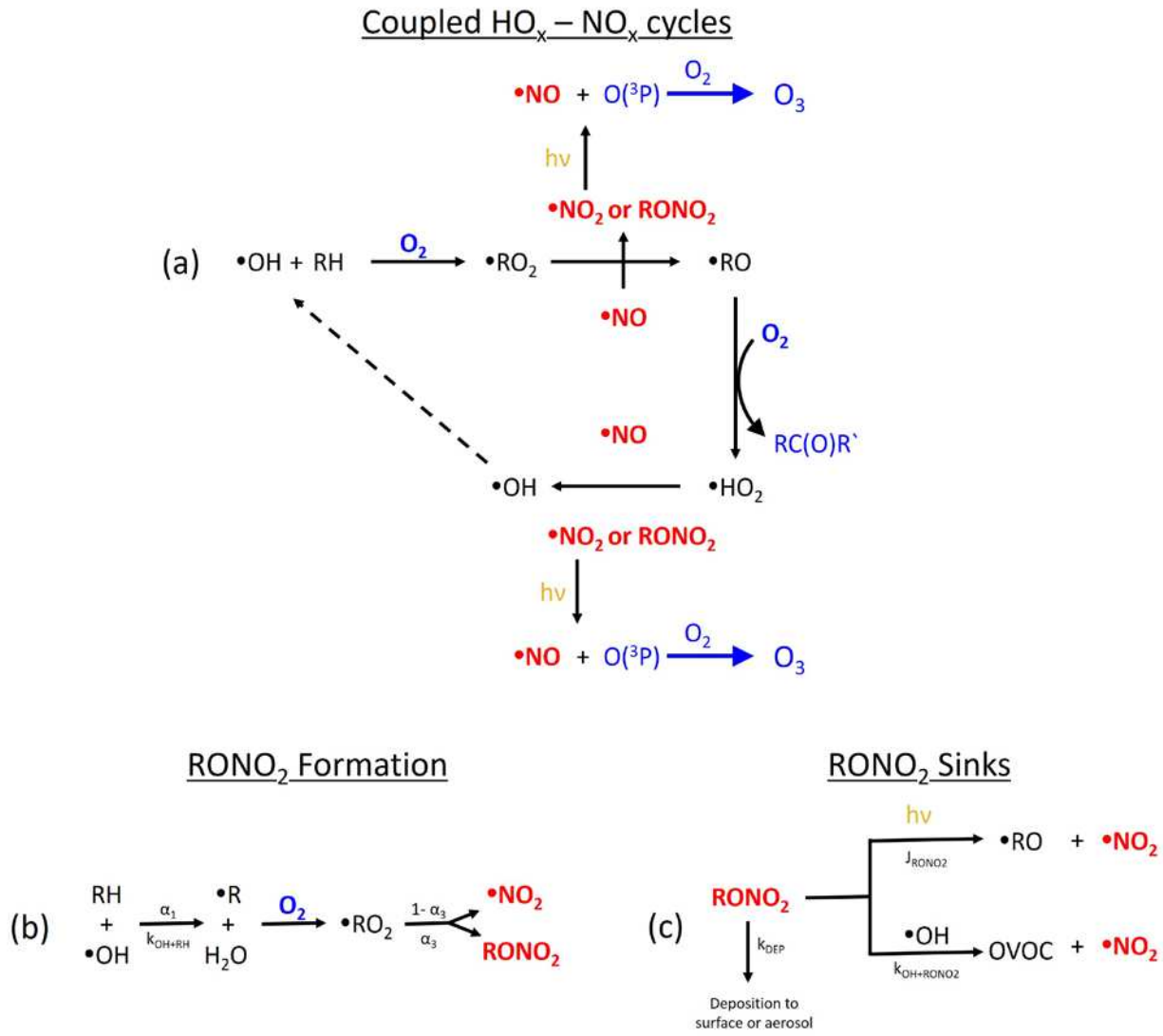

Figure 4.1. (a) Ozone production cycle. (b) $RONO_2$ formation reactions. (c) $RONO_2$ sinks.

sampled air masses. This analysis provides observational constraints on $RONO_2$ kinetics, includes estimates of dry deposition velocities of C_1–C_5 $RONO_2$, and allows us to investigate relationships between summer C_3–C_5 $RONO_2$, ozone, and photochemical age.

4.2. Methods

4.2.1 Campaigns and site description

C_1–C_5 alkyl nitrates, their parent alkane precursors, and other trace gases were measured at the NOAA Boulder Atmospheric Observatory (BAO) located in Northern Colorado during winter 2011, spring 2015, and summer 2015. The winter 2011 measurements were part of the Nitrogen, Aerosol Composition, and Halogens on a Tall Tower (NACHTT) study from 18 February 2011 to 13 March 2011 [*S. S. Brown et al.*, 2013; *R. F. Swarthout et al.*, 2013]. The spring 2015 measurements were associated with the Shale Oil and Gas Nexus (SONGNEX) study from 20 March 2015 to 17 May 2015 [*A. Abeleira et al.*, 2017; *NOAA*, 2014]. The summer 2015 measurements occurred from 24 July 2015 to 29 August 2015 [*A. Abeleira et al.*, 2017; *NOAA*, 2014]. The BAO site is described in detail elsewhere [i.e. *A. Abeleira et al.*, 2017; *S. S. Brown et al.*, 2013; *J. B. Gilman et al.*, 2013; *E. E. McDuffie et al.*, 2016; *R. F. Swarthout et al.*, 2013]; briefly, the BAO site is in a semirural region with major urban centers to the south (Denver, 35 km), west (Boulder, 30 km), north (Fort Collins, 65 km), and northeast (Greeley, 65 km). The site is located on the edge of the Wattenberg natural gas field in the Denver-Julesberg basin, and is in area of extensive oil and natural gas exploration and extraction.

4.2.2 Measurements

We measured methyl nitrate ($MeONO_2$), ethyl nitrate ($EtONO_2$), 1-propyl nitrate (1-$PrONO_2$), 2-propyl nitrate (2-$PrONO_2$), 2-butyl nitrate (2-$BuONO_2$), 2-pentyl nitrate (2-$PeONO_2$),

and 3-pentyl nitrate (3-$PeONO_2$) along with their parent alkanes (methane, ethane, propane, n-butane, and n-pentane) during all three campaigns, with the exception of methane, which was not measured during winter 2011. During winter 2011, the whole air samples were collected hourly by a canister sampling system, and analyzed off-line with a multi-channel gas chromatography system. Details of the measurements and calibration approaches are reported elsewhere [*R. F. Swarthout et al.*, 2013]. The analytical precision for the parent alkanes and alkyl nitrates were 1-8% and 3-8%, respectively. During spring and summer 2011, the alkyl nitrates and parent alkanes (except methane) were measured with a similar 4-channel online chromatography system as the canister samples, but instead utilized a cryogen-free concentration system to pre-concentrate ambient samples on 1 mm silica beads at -160°C for in situ measurement. The inlet was 22 m above ground level (agl) for the 2011 measurements, and 6 m agl for the 2015 measurements. Details of the measurements, calibrations, and 4-channel online chromatography system have been reported previously [*A. Abeleira et al.*, 2017]; the analytical precision for the parent alkanes and alkyl nitrates were 1-10%. During spring and summer 2015, methane was measured by a Picarro 6401 commercial Cavity Ring-Down Spectrometer with a precision of 6%, and O_3 was measured by a 2B Technologies O_3 monitor (Model 202) with a precision of 1 ppbv. NO was measured with a commercial chemiluminescence instrument (Teledyne Model 200EU).

Fixed-height temperature and wind-speed measurements are located on the 300 m BAO tower at 10, 100, and 300 m agl during all campaigns [*NOAA*, 2017]. Average daytime 10 m height temperatures were 5°C, 15°C, and 25°C for winter 2011, spring 2015, and summer 2015, respectively. Vertically resolved temperature and wind-speed measurements between 0 – 270 m agl were made during the winter 2011 study from an instrument enclosure mounted to a carriage on the 300 m BAO tower [*S. S. Brown et al.*, 2013].

4.2.3 Estimating photochemical age from $RONO_2$/RH with the Bertman model

The evolution of $RONO_2$ with air mass age can be described by a sequential reaction system in which the reaction of *A* to *B* represents the production of $RONO_2$, and *B* to *C* represents the loss pathways (R6).

$$A \xrightarrow{k_A} B \xrightarrow{k_B} C \tag{R6}$$

S. B. Bertman et al. [1995] described the evolution of $RONO_2$/RH as a function of air mass photochemical age (E1).

$$\frac{[RONO_2]}{[RH]} = \frac{\beta k_A}{(k_B - k_A)}\left(1 - e^{(k_A - k_B)t}\right) + \frac{[RONO_2]_0}{[RH]_0} e^{(k_A - k_B)t} \tag{E1}$$

The ratio of $RONO_2$/RH is calculated as a function of time (seconds) using kinetic parameters derived from laboratory studies. Because OH must be assumed, this time can be considered an 'OH equivalent' photochemical age – the age of the air mass required to reach a given $RONO_2$/RH ratio. The production term (k_A) is k_1[OH] and, in conjunction with β, represents the production of $RONO_2$. The destruction, or sinks, term (k_B) is k_4[OH] + J_5, and represents the loss of $RONO_2$ via oxidation and photolysis. The units of k_A and k_B are both s^{-1}. Modeling $RONO_2$/RH with E1 assumes the following: (1) The reaction between OH and RH is the rate limiting step in the production of $RONO_2$; (2) The evolution of $RONO_2$/RH is a result of gas phase hydrocarbon chemistry only [*S. B. Bertman et al.*, 1995]; (3) RO_2 only reacts with NO (*i.e.* no RO_2 self-reactions), which is expected in an urban/suburban 'high-NO_x' environment with NO > 0.1 ppbv [*F. Flocke et al.*, 1991; *J. M. Roberts et al.*, 1998]; and (4) The only sinks of $RONO_2$ are reaction with OH and photolysis [*S. B. Bertman et al.*, 1995; *J. M. Roberts*, 1990; *R. Talukdar et al.*, 1997; *R. K. Talukdar et al.*, 1997].

The photochemical age of a sampled air mass can be derived when two $RONO_2$/RH relationships are plotted against each other [*S. B. Bertman et al.*, 1995]. Typically, $RONO_2$/RH is plotted against 2-$BuONO_2$/n-butane because 2-$BuONO_2$ often exhibits the highest mixing ratios in polluted areas, is dominated by photochemical production [*S. B. Bertman et al.*, 1995; *X. Lyu et al.*, 2015; *M. Wang et al.*, 2013; *D. R. Worton et al.*, 2010], and has no reported primary sources [*E. Atlas et al.*, 1993; *I. J. Simpson et al.*, 2002]. Additionally, in the first 24 hours of photochemical aging, 95% of 2-$BuONO_2$ is produced via oxidation of n-butane [*R. Sommariva et al.*, 2008]. Plotting $RONO_2$/RH against 2-$BuONO_2$/n-butane enables comparison of ambient data to these models without *a priori* knowledge of the absolute aging timescale of the ambient data [*S. B. Bertman et al.*, 1995]. This approach provides not only a quantitative metric of photochemical age, but also useful context for exploring the sources and sinks of alkyl nitrates.

4.3. Results and discussion

4.3.1 C_1–C_5 $RONO_2$ mixing ratios

Table 4.1. Average alkyl nitrate mixing ratios (ppbv) at the BAO site for winter 2011, spring 2015, and summer 2015

Alkyl Nitrate	winter 2011	spring 2015	summer 2015
Average mixing ratios (standard deviation), ppbv			
$MeONO_2$	0.004 (0.001)	0.004 (0.001)	0.003 (0.001)
$EtONO_2$	0.004 (0.001)	0.004 (0.001)	0.003 (0.002)
1-$PrONO_2$	0.002 (0.001)	0.002 (0.001)	0.0013 (0.0009)
2-$PrONO_2$	0.016 (0.008)	0.013 (0.006)	0.011 (0.006)
2-$BuONO_2$	0.030 (0.020)	0.020 (0.014)	0.019 (0.015)
2-$PeONO_2$	0.012 (0.010)	0.006 (0.005)	0.008 (0.007)
3-$PeONO_2$	0.007 (0.006)	0.004 (0.004)	0.005 (0.005)

Despite the relatively high hydrocarbon mixing ratios observed at BAO, average $MeONO_2$, $EtONO_2$, and 1-$PrONO_2$ mixing ratios at BAO are similar to previous measurements from rural and remote sites [i.e. *J. M. Roberts et al.*, 1998; *R. S. Russo et al.*, 2010a; *A. L. Swanson et al.*, 2003], while 2-$PrONO_2$ and the C_4-C_5 $RONO_2$ were more representative of polluted urban sites [i.e. *X. Lyu et al.*, 2015; *M. Wang et al.*, 2013; *D. R. Worton et al.*, 2010] (Table 4.1).

4.3.2 Seasonal and diel trends in C_1–C_5 $RONO_2$ mixing ratios

Seasonal averages of 2-$PrONO_2$ and C_4–C_5 $RONO_2$ deviate little from winter 2011 to summer 2015 at BAO (Fig. 4.2). For example, 2-$BuONO_2$ decreases from 0.030 ppbv during winter 2011 to 0.019 during summer 2015, but remains within the average ± standard deviation for all seasons. Average mixing ratios of $MeONO_2$, $EtONO_2$, and 1-$PrONO_2$ do not change seasonally. Measurements at other ground sites and during flight campaigns show greater contrasts in seasonal variation for C_1–C_5 $RONO_2$, and attributed these differences to meteorology, transport, and OH abundances [*H. J. Beine et al.*, 1996; *N. J. Blake et al.*, 2003a; *X. Lyu et al.*, 2015; *R. S. Russo et al.*, 2010a; *I. J. Simpson et al.*, 2004; *A. L. Swanson et al.*, 2003; *M. Wang et al.*, 2013]. Remote sites typically observe maxima in C_1–C_5 $RONO_2$ in the winter and minima in the summer [*H. J. Beine et al.*, 1996; *N. J. Blake et al.*, 2003a; *A. L. Swanson et al.*, 2003] due to increased photochemical removal of $RONO_2$ during summertime without an increase in production due to low precursor abundances [*A. L. Swanson et al.*, 2003]. In contrast, summer maxima are observed in polluted air masses outside of Sacramento, California and Freiburg, Germany [*D. A. Day et al.*, 2003; *F. Flocke et al.*, 1998].

The diel cycles of 2-$PrONO_2$ and C_4–C_5 $RONO_2$ have more pronounced diurnal variability in summer 2015 compared to the winter or spring campaigns (Figs. 2b,c). During winter 2011, average 2-$BuONO_2$ increases by a factor of 1.3 from 0.024 to 0.031 ppbv between 04:00 and 14:00

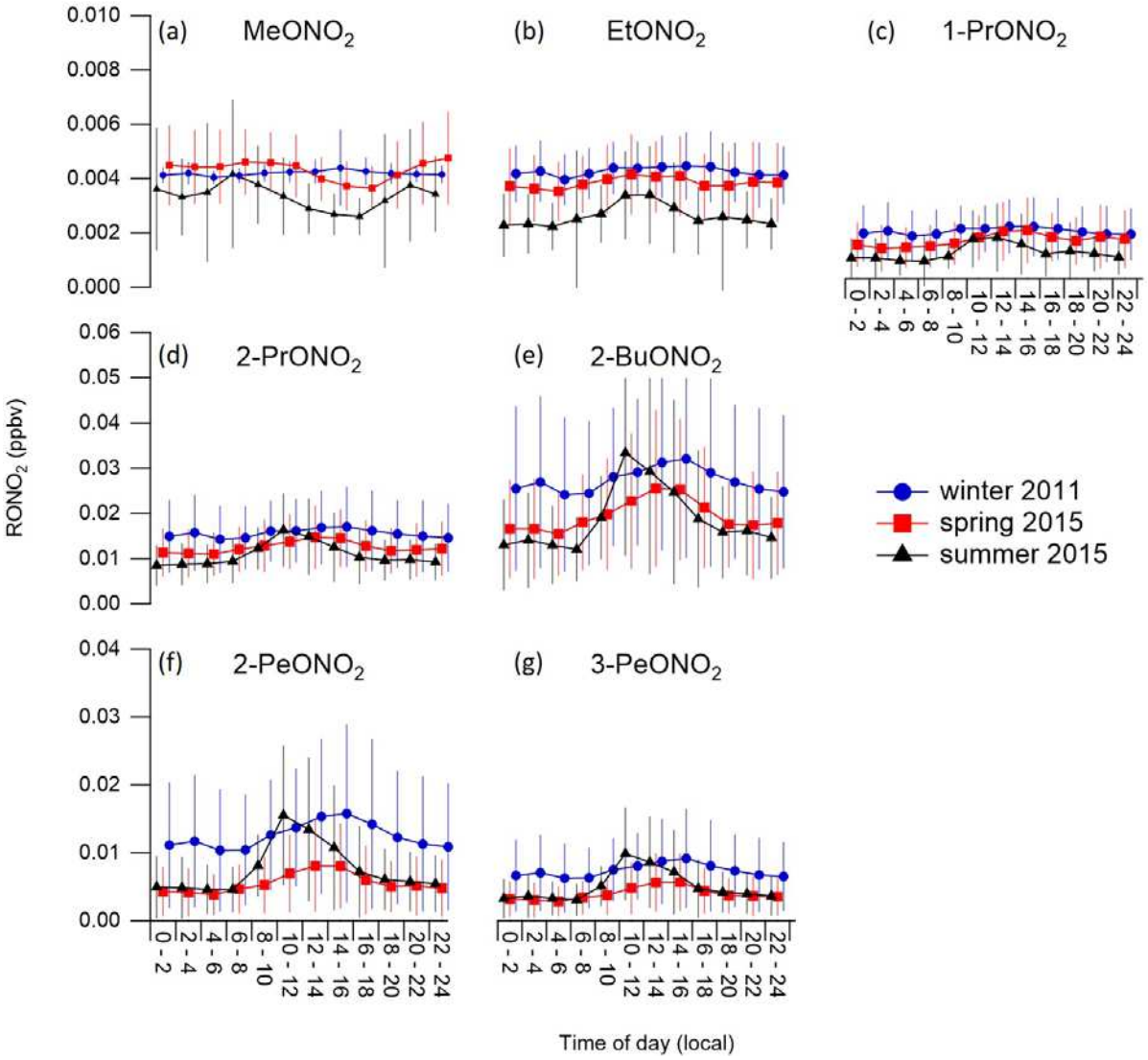

Figure 4.2. Average diel patterns for (a) $MeONO_2$, (b) $EtONO_2$, (c) $1\text{-}PrONO_2$, (d) $2\text{-}PrONO_2$, (e) $2\text{-}BuONO_2$, (f) $2\text{-}PeONO_2$ and (g) $3\text{-}PeONO_2$ for the winter 2011 (blue circles), spring 2015 (red squares), and summer 2015 (black triangles) measurement campaigns. Error bars represent ± 1 standard deviation from the mean of each 2-hour time bin.

(local time); during summer 2015, 2-$BuONO_2$ increases by a factor of 2.5 from 0.013 to 0.033 ppbv (Fig. 4.2b). A distinct summer maxima occurs earlier in the day between 10:00 – 12:00, unlike the broad afternoon maxima observed during winter and spring. In contrast, $MeONO_2$, $EtONO_2$, and 1-$PrONO_2$ exhibit little diel variability in all seasons (Fig. 4.2a). Although daytime winter 2011 and summer 2015 mixing ratios were similar for 2-$PrONO_2$ and C_4-C_5 $RONO_2$, the rapid decrease to lower background levels in the summer is consistent with increased removal of the more reactive $RONO_2$. The diel cycles of 2-$PrONO_2$ and C_4-C_5 $RONO_2$ are thus consistent with photochemical sources that increase with increased summertime OH, but also increased removal from greater OH and photolysis.

4.3.3 Uncertainties in the $RONO_2$/RH model

Uncertainties in reported $RONO_2$ formation branching ratios and the choice of OH concentration are the main sources of uncertainty that affect the agreement between modeled and measured $RONO_2$/RH and the estimation of the photochemical age from $RONO_2$/RH. The use of an initial $RONO_2$/RH value when modeling $RONO_2$/RH also impacts the agreement between modeled and measured $RONO_2$/RH, particularly at lower photochemical ages. We investigate these uncertainties by comparing modeled and observed $MeONO_2$/methane, $EtONO_2$/ethane, and 2-$BuONO_2$/n-butane ratios for the spring 2011 campaign. These uncertainties impact the interpretation of $RONO_2$ sources, $RONO_2$ sinks, and the photochemical age of sampled air masses.

4.3.3.1 Selection of OH concentration

Estimates of photochemical age of a sampled air mass using the Bertman model depend on the choice of OH concentration for E1. The chosen OH concentration should accurately represent the average OH encountered by an air mass. OH is responsible for not only initiating $RONO_2$

Table 4.2. Kinetic parameters for the production and sinks of C_1-C_5 $RONO_2$ during Winter 2011, Spring 2015, and Summer 15 at the BAO site. The listed values of k_1 and k_4 are for 298 K, although k_A and k_B were calculated with temperature-dependent parameters for the three seasons with average daytime (08:00 – 18:00) 10 m agl temperatures (5°C, 12°C, and 25°C for Winter 2011, Spring 2015, and Summer 2015). Production of $RONO_2$ (k_A) was calculated with temperature-adjusted k_1 and seasonal Northern Colorado OH concentration ranges (details in section 3.3.1). Selection and calculation of J_5 is detailed in the SI. Units of k_1 and k_4 are $x10^{-12}$ cm^3 $molecule^{-1}$ s^{-1}. Units of k_A,k_B, and J_5 are $x10^{-6}$ s^{-1}. Seasonal lifetimes of C_1-C_5 $RONO_2$ relative to OH oxidation and photolysis at the BAO site are in appendix 2 (Table A2.1).

Production					
AN	Parent	k_1[a]	α_1[b,c,d]	α_3	
				(lower)	(upper)
MeONO2	Methane	0.0064	1	0.005[e]	0.01[j]
EtONO2	Ethane	0.248	1	0.006[f]	0.03[k]
1-PrONO2	Propane	1.1	0.26	0.02[g]	0.034[l]
2-PrONO2	Propane	1.1	0.74	0.036[g]	0.042[b]
2-BuONO2	n-butane	2.36	0.87	0.079[h]	0.09[b]
2-PeONO2	n-pentane	3.8	0.57	0.096[i]	0.129[b]
3-PeONO2	n-pentane	3.8	0.35	0.116[i]	0.131[b]

Production					
AN	β		k_A		
	(lower)	(upper)	(Winter 2011)	(Spring 2015)	(Summer 2015)
MeONO2	0.005	0.01	0.004 - 0.014	0.010 - 0.024	0.026 - 0.051
EtONO2	0.006	0.03	0.189 - 0.566	0.420 - 1.05	0.99 - 1.98
1-PrONO2	0.005	0.009	0.93 - 2.80	1.98 - 4.94	4.98 - 8.75
2-PrONO2	0.027	0.031	0.93 - 2.80	1.98 - 4.94	4.98 - 8.75
2-BuONO2	0.069	0.078	2.11 - 6.32	4.37 - 10.97	9.43 - 18.89
2-PeONO2	0.055	0.074	3.44 - 10.31	7.13 - 17.82	15.21 - 30.42
3-PeONO2	0.041	0.046	3.44 - 10.31	7.13 - 17.82	15.21 - 30.42
Sinks					
AN	k_4		J_5		
			(Winter 2011)	(Spring 2015)	(Summer 2015)
MeONO2	0.04[m]		0.07 - 0.50	0.19 - 0.79	0.30 - 0.94
EtONO2	0.218[n]		0.11 - 0.82	0.32 - 1.32	0.49 - 1.52
1-PrONO2	0.597[n]		0.17 - 1.10	0.47 - 1.75	0.70 - 1.99
2-PrONO2	0.302[o]		0.15 - 1.00	0.42 - 1.56	0.63 - 1.78
2-BuONO2	0.86[n]		0.12 - 0.98	0.31 - 1.55	0.48 - 1.99
2-PeONO2	1.84[p]		0.10 - 0.82	0.27 - 1.33	0.47 - 1.93
3-PeONO2	1.13[p]		0.08 - 0.80	0.27 - 1.34	0.47 - 1.94

Sinks			
AN	k_B		
	(Winter 2011)	(Spring 2015)	(Summer 2015)
MeONO2	0.11 - 0.62	0.27 - 0.99	0.46 - 1.26
EtONO2	0.33 - 1.47	0.76 - 2.41	1.36 - 3.26
1-PrONO2	0.77 - 2.89	1.66 - 4.74	3.09 - 6.68
2-PrONO2	0.45 - 1.91	1.02 - 3.07	1.84 - 4.2
2-BuONO2	0.98 - 3.56	2.03 - 5.85	3.92 - 8.87
2-PeONO2	1.98 - 6.34	3.95 - 10.53	7.83 - 16.63
3-PeONO2	1.21 - 4.19	2.53 - 6.99	4.99 - 10.98

(a) [*R. Atkinson*, 2003], (b) [*R. Atkinson et al.*, 1987], (c) [*E. S. Kwok and R. Atkinson*, 1995], (d) [*D. Mackay and R. S. Boethling*, 2000], (e) [*G. Tyndall et al.*, 2001], (f) [*D. L. Ranschaert et al.*, 2000], (g) [*R. Atkinson et al.*, 1982], (h) [*C. Espada et al.*, 2005], (i) [*S. M. Aschmann et al.*, 2006], *(j) [N. Butkovskaya et al., 2012],* (k) [*N. Butkovskaya et al.*, 2010], (l) [*N. I. Butkovskaya et al.*, 2010], (m) Preferred values from the Master Chemical Mechanism, MCM v3.3 ([*M. E. Jenkin et al.*, 1997; *S. M. Saunders et al.*, 2003]) via *http://mcm.leeds.ac.uk/MCM,* (n) [*J. Morin et al.*, 2016], (o) [*M. N. Romanias et al.*, 2015], (p) [*R. Atkinson*, 1990]

production via oxidation of the parent alkanes (i.e. the source, k_A), but also removing $RONO_2$ (i.e. a key sink, k_B). This interplay between source and sink dictates the rate at which $RONO_2$ increases and RH decreases, and subsequently controls the rate of increase of $RONO_2$/RH in Fig. 4.3.

In Table 4.2 we use an OH range of $(1 – 3)x10^6$ molecule cm^{-3} to calculate k_A and k_B for winter 2011, based on co-located, simultaneous OH measurements [*S. Kim et al.*, 2014]. An average daytime range of $(4 – 8)x10^6$ molecule cm^{-3} for the summer 2015 campaign is derived from OH measurements made during summer 2014 in the Northern Colorado Front Range [*C. J. Ebben et al.*, 2017]. We estimate an OH range of $(2 – 5)x10^6$ molecule cm^{-3} for the spring 2015 campaign. We select an OH concentration of $3.5x10^6$ molecule cm^{-3} for the base case $RONO_2$/RH ratios (Figs. 3a,b). To illustrate the impact of OH concentration on $RONO_2$/RH from E2, we calculate a high OH case (OH = $5 x10^6$ molecule cm^{-3}) and a low OH case (OH = $2 x10^6$ molecule cm^{-3}) for spring 2015 (Fig. 43).

Overestimating OH causes an under-estimation of photochemical age. The rate of $RONO_2$ formation and RH consumption clearly increases with increasing OH concentration for 2-$BuONO_2$ and $EtONO_2$ (Figs. 3a, b). At a photochemical age of 1 second, the ratios of 2-$BuONO_2$ and $EtONO_2$ are 2.5x larger in the high OH case than the low OH case, directly corresponding to the difference in OH between cases. The reactivity of n-butane to OH is greater than 2-$BuONO_2$ to OH, which causes a higher rate of increase in $RONO_2$/RH in the 'high OH' case versus 'low OH' by factors of 30 and 500 at a photochemical age of 10 days. The opposite is true for $EtONO_2$ and ethane where the reactivity of $EtONO_2$ with OH is greater than that of ethane. Thus the enhancement of $EtONO_2$/ethane for the high OH versus low OH case decreases from 2.5 to 2.2 after 10 days. The ratio of $RONO_2$ destruction to production (k_B/k_A) is a useful metric for predicting how $RONO_2$/RH will increase or decrease over time. For example, in the low OH case

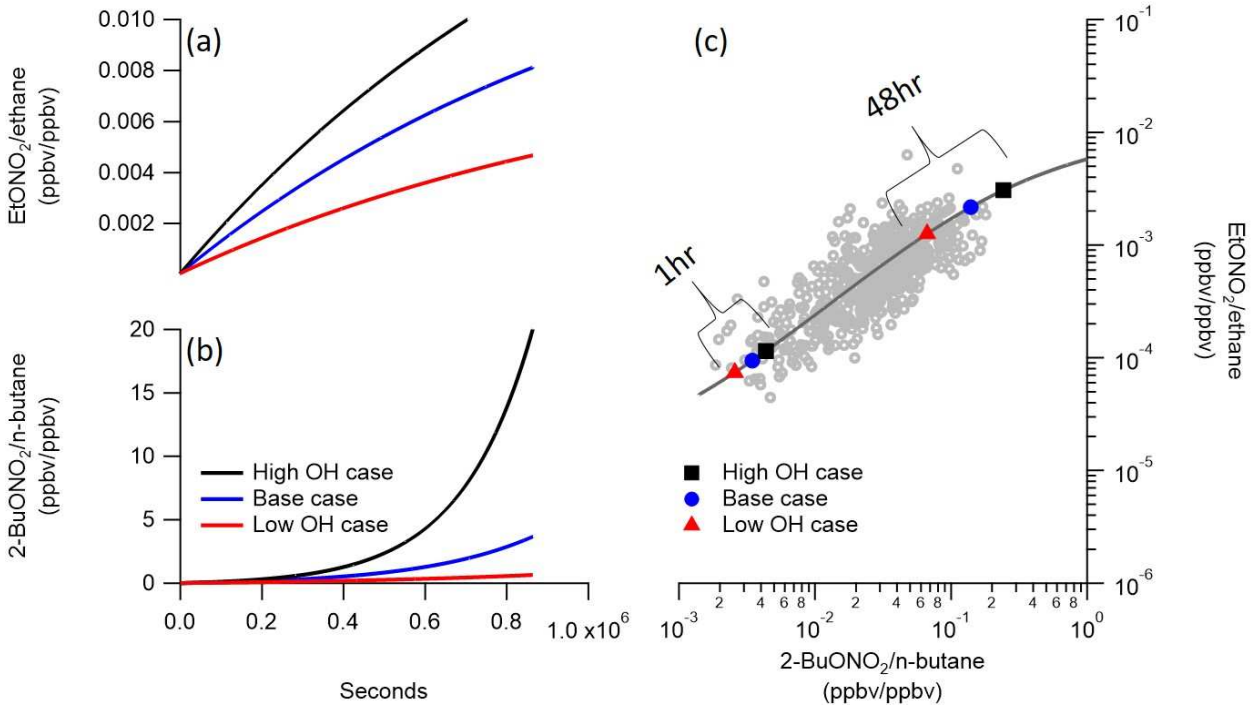

Figure 4.3. $RONO_2/RH$ models for (a) $EtONO_2$/ethane and (b) 2-$BuONO_2$/n-butane vary with OH. The rate of production from OH + RH (k_A) and rate of destruction from OH and photolysis (k_B) are calculated for each OH case. Photolysis rates are spring averages (Table 4.2). Branching ratios are 0.018 ($EtONO_2$) and 0.074 (2-$BuONO_2$). (c) Observed (grey circles) and modeled (line, for each OH case) $EtONO_2$/ethane ratios are plotted against 2-$BuONO_2$/n-butane for the daytime (08:00 – 18:00) spring data (grey circles, c). Markers for 1 hour and 48 hours of photochemical aging for the three OH cases are overlaid on the modeled curves.

the ratio of the destruction rate to production rate for 2-$BuONO_2$ is 0.70, and decreases to 0.49 in the high OH case. This corresponds to a faster rate of consumption of the parent alkane and production of $RONO_2$, which is balanced by a smaller increase in the rate of removal of $RONO_2$ in the 'high OH' case because 2-$BuONO_2$ has a lower reactivity than n-butane. Increasing OH causes higher $RONO_2$/RH ratio values to occur with less aging. For example, the $EtONO_2$/ethane versus 2-$BuONO_2$/n-butane value at 2 days of aging in the high OH case is not reached until 5 days of aging in the low OH case.

4.3.3.2 Selection of $RONO_2$ branching ratio (β_{RONO2})

Branching ratios for the formation of $RONO_2$ from RO_2 + NO (R3a,b) are poorly constrained, and the uncertainties propagate to the $RONO_2$ branching ratio (β). The ranges of reported branching ratios for the C_1-C_5 $RONO_2$ measured herein are summarized in Table 4.2. Experimentally-derived branching ratios range from 0.006 to 0.030 for $EtONO_2$ [*N. Butkovskaya et al.*, 2010; *D. L. Ranschaert et al.*, 2000], 0.001 to 0.01 for $MeONO_2$ [*N. Butkovskaya et al.*, 2012; *E. S. Kwok and R. Atkinson*, 1995; *M. Wang et al.*, 2013], and 0.055 to 0.074 for 2-$PeONO_2$ [*S. M. Aschmann et al.*, 2006; *R. Atkinson et al.*, 1987] (Table 4.2).

In Fig. 4.4a, we calculate $EtONO_2$/ethane with a branching ratio of 0.006 (lower limit, low β case), 0.018 (average, base case), and 0.030 (upper limit, high β case). The branching ratio for 2-$BuONO_2$ has a smaller reported range with values between 0.069 [*C. Espada et al.*, 2005] and 0.078 [*R. Atkinson et al.*, 1982; *R. Atkinson et al.*, 1987]; we use an average n-butane to 2-$BuONO_2$ branching ratio of 0.074 for every scenario in Fig. 4.5c. The base case model with an $EtONO_2$ branching ratio of 0.018 agrees well with the observed values (Figs. 4.4b,c). Higher branching ratios (β_{EtONO2} = 0.030) overpredict $EtONO_2$/ethane by 32-95%, with an increasing discrepancy with photochemical age. Lower branching ratios underpredict $EtONO_2$/ethane by 61-74%.

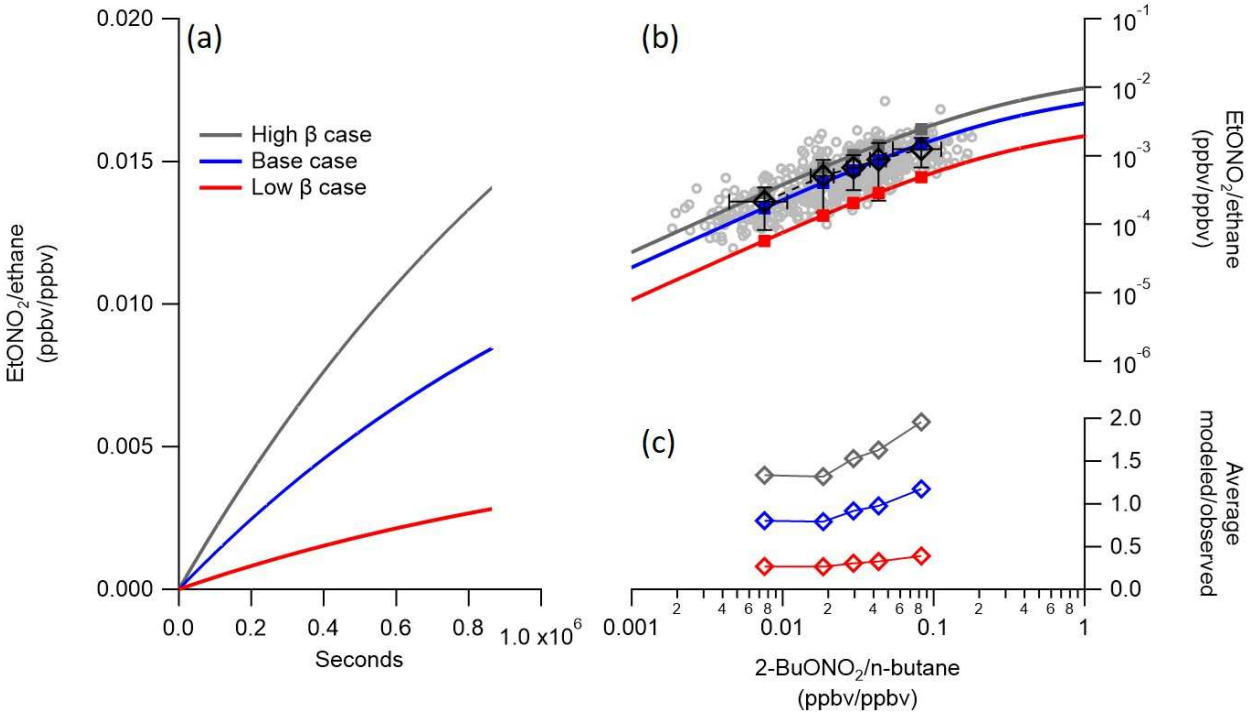

Figure 4.4. (a) $RONO_2/RH$ is modeled using E2 for $EtONO_2$/ethane with three different branching ratio values (β_{RONO2}) that span the reported range. Branching ratios of 0.006, 0.018 and 0.03 are used for the Low β, Base, and High β cases, respectively. Temperature follows spring values, and OH = 3.5×10^6 molecule cm^{-3}. (b) Observed (grey circles) and modeled (lines, for each β) $EtONO_2$/ethane are plotted against 2-$BuONO_2$/n-butane for the daytime (08:00 – 18:00) spring 2015 campaign. We use a branching ratio for 2-$BuONO_2$ of 0.074. (c) Ratios of modeled to average observed bins for each branching ratio case.

Previous studies often use lower branching values for $EtONO_2$ of 0.006 to 0.014, and report model under-prediction for $EtONO_2$/ethane by factors of 2-10 [*S. B. Bertman et al.*, 1995; *R. S. Russo et al.*, 2010a; *I. J. Simpson et al.*, 2003; *M. Wang et al.*, 2013; *D. R. Worton et al.*, 2010]. This underprediction was attributed to additional sources of ethyl radicals from the decomposition of larger alkoxy radicals [*S. B. Bertman et al.*, 1995; *J. M. Roberts et al.*, 1998; *D. R. Worton et al.*, 2010]. For example, *R. Sommariva et al.* [2008] suggest that OH+ethane reactions only account for 15% of $EtONO_2$ in the first 24 hours of processing, while decomposition of peroxy radicals from larger alkanes account for the rest. This is one interpretation of the need for higher branching ratio values for $EtONO_2$ in the BAO data. Alternately, the model-measurement agreement with $\beta_{EtONO2} = 0.030$ could be consistent with the original branching ratios (*i.e.* $\beta_{EtONO2} = 0.006 - 0.014$) being too low, thereby underestimating the efficiency of $EtONO_2$ production from ethane.

In contrast to $EtONO_2$, the base case branching ratio ($\beta_{3PeONO2} = 0.044$) overpredicts 3-$PeONO_2$/n-pentane ratios by 2-3x, despite the narrow range in literature branching ratios (0.041 – 0.046) [*S. M. Aschmann et al.*, 2006; *R. Atkinson et al.*, 1987]. Overpredictions of 3-$PeONO_2$/n-pentane ratios have been previously reported [*S. B. Bertman et al.*, 1995; *R. S. Russo et al.*, 2010a; *I. J. Simpson et al.*, 2003; *C. A. Stroud et al.*, 2001; *D. R. Worton et al.*, 2010]. The model overpredictions were attributed to the decomposition of pentyl peroxy radicals to smaller C_1-C_3 peroxy radicals, thus reducing the available pool of pentyl peroxy radicals for $RONO_2$ production [*C. E. Reeves et al.*, 2007], or to an overestimate of 3-PeONO2 branching ratios. Our data are consistent with both scenarios.

4.3.3.3 Selection of initial $RONO_2$/RH ratios

$RONO_2$ is often assumed to be absent if no photochemistry has occurred in an airmass (*e.g.* [*S. B. Bertman et al.*, 1995; *J. M. Roberts et al.*, 1998], although observations suggest this is not

always the case. A non-zero initial $RONO_2$/RH ratio accounts for non-zero $RONO_2$/RH ratios during periods with no photochemistry in air masses impacted by marine and biomass burning $RONO_2$ emissions [*E. Atlas et al.*, 1993; *N. J. Blake et al.*, 1999; *I. J. Simpson et al.*, 2002]. Non-zero $RONO_2$/RH ratios in the absence of photochemistry are also common for the less reactive C_1-C_2 $RONO_2$ [*S. B. Bertman et al.*, 1995; *R. S. Russo et al.*, 2010a]. Continental ground sites removed from oceanic sources and biomass burning plumes, including the BAO site, exhibit non-zero $RONO_2$/RH in the morning prior to sunrise, likely due to carryover from the previous day's photochemical $RONO_2$ production. It has become common practice to use a non-zero initial $RONO_2$/RH ratio when applying the Bertman model [*R. S. Russo et al.*, 2010a; *M. Wang et al.*, 2013].

Figure 4.5 shows the evolution of $RONO_2$/RH for $MeONO_2$ and 2-$BuONO_2$ with initial $RONO_2$/RH ratios of zero (blue line) versus an initial ratio calculated from the 5th percentile of those $RONO_2$/RH pairs between 00:00 and 06:00 (black line). Accounting for initial $RONO_2$ concentrations (*i.e.* carry-over from the previous day, or non-photochemical sources) yields better model-measurement agreement, particularly at photochemical ages <6 hours (Fig. 4.5c). $MeONO_2$/methane is the most extreme case in which a pure photochemistry model (initial $RONO_2$/RH = 0) fails to capture trends in the observed values, regardless of photochemical age (Fig. 4.5c). The initial ratio is small, due to the low concentration of $MeONO_2$ relative to methane at BAO, and consistent, due to the low reactivity of both $MeONO_2$ ($k_{OH+MeONO2}$ = $4x10^{-14}$ cm^3 $molecule^{-1}$ s^{-1}) and methane ($k_{OH+methane}$ = $6.4x10^{-15}$ cm^3 $molecule^{-1}$ s^{-1}). However, despite including the initial $MeONO_2$/methane ratio, the model overpredicts observations >6 hours of photochemical aging. This indicates the need for a larger sink term in E2.

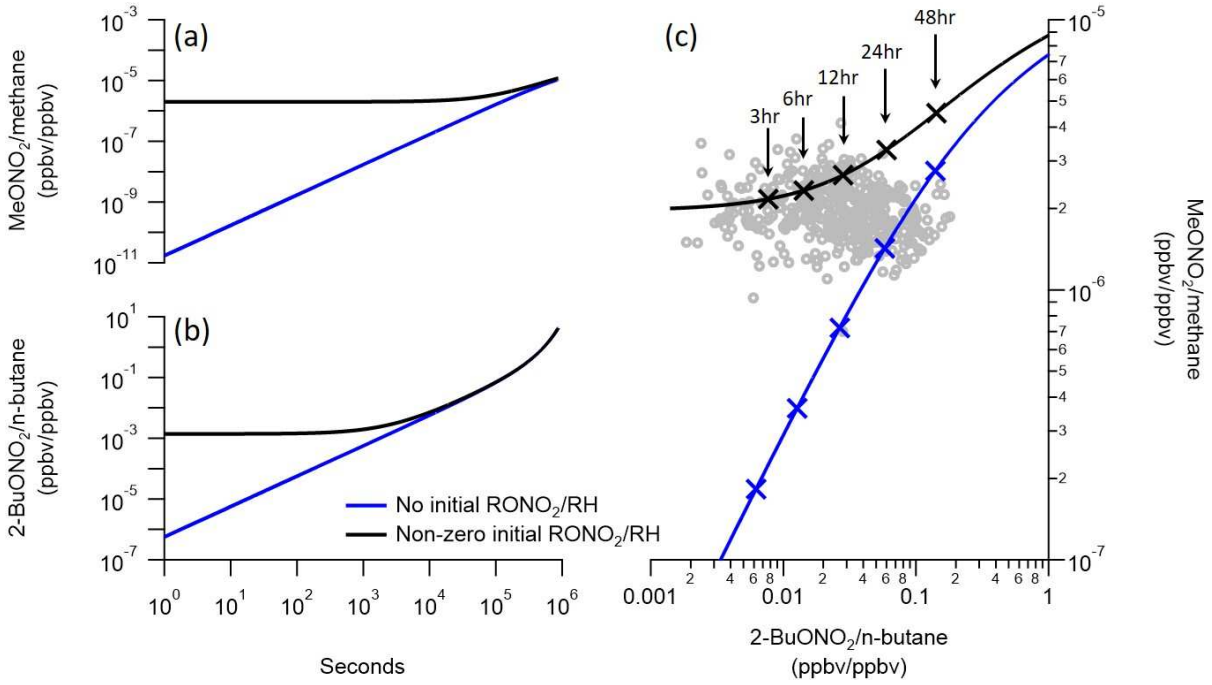

Figure 4.5. $RONO_2/RH$ is modeled using E2 for (a) $MeONO_2$/methane and (b) 2-$BuONO_2$/n-butane using initial $RONO_2/RH$ ratios of zero and non-zero values for spring 2015 conditions and branching ratios of 0.074 for 2-$BuONO_2$ and 0.001 for $MeONO_2$. Non-zero $RONO_2/RH$ initial ratios are defined as the 5th percentile of $RONO_2/RH$ during morning (00:00 – 06:00) hours for spring 2015. (c) $MeONO_2$/methane is plotted against 2-$BuONO_2$/n-butane for the daytime (08:00 – 18:00) spring 2015 data. Observations are in grey circles, while model results are in lines with markers indicating photochemical age.

4.3.4 Dry deposition

Deposition is one loss process that is rarely considered for the alkyl nitrates. *R. S. Russo et al.* [2010a] report dry deposition velocities (V_d) for $MeONO_2$ from summer observations in rural New Hampshire of 0.13 ± 0.07 cm s^{-1}. Following the approach developed by *R. S. Russo et al.* [2010a], we estimate a similar average winter and spring $MeONO_2$ dry deposition velocity of 0.17 ± 0.09 cm s^{-1}. Briefly the *R. S. Russo et al.* [2010a] approach calculates dry deposition fluxes from the nighttime decay rate of alkyl nitrates (change in concentration over a given time, ppbv/s) multiplied by the nocturnal boundary layer height (H). Dividing the flux by the average concentration and multiplying by negative 1 gives a deposition velocity (V_d, converted to cm/s). A negative flux and positive deposition velocity indicate a flux from the atmosphere to a surface. The loss rate due to dry deposition (k_{dep}) is calculated as V_d/H, where H is the boundary layer height. This method is limited to nights with low wind-speed (<4 m/s), and characteristics of a stable nocturnal boundary layer (See SI for detailed description of calculation and selection criteria – Fig. A2.6). We did not calculate dry deposition velocities for summer 2015 because of the challenge in identifying stable nocturnal boundary layer heights (see SI for discussion); we instead apply an average summer boundary layer height of 1500 m [*H. S. Halliday et al.*, 2016; *J. M. Schneider and D. K. Lilly*, 1999] and use the winter/spring V_d to calculate dry deposition rates. The dry deposition loss rate is calculated as the dry deposition velocity divided by the estimated boundary layer height.

Dry deposition velocities increase with carbon number, from 0.15 – 0.18 cm s^{--1} for C_1-C_3 $RONO_2$ to 0.34 cm/s for 3-$PeONO_2$ (Table 4.3). This is consistent with observed increasing V_d of oxygenated volatile organic compounds with molecular weight [*T. B. Nguyen et al.*, 2015]. The C_1-C_5 $RONO_2$ V_d reported herein are in the range of dry deposition velocities for peroxy acetyl

Table 4.3. Calculated flux, dry deposition velocity (V_d), nocturnal lifetimes against dry deposition (τ_d; calculated for boundary layer heights of 100-1500 m), and the number of data points contributing to the flux calculation (n).

$RONO_2$	Flux	V_d	τ_d	n
	(nmol m^{-2} hr^{-1})	(cm s^{-1})	(days)	
$MeONO_2$	-1.0 (0.6)	0.17 (0.09)	0.7 - 10	5
$EtONO_2$	-0.9 (0.3)	0.15 (0.07)	0.8 - 12	5
1-$PrONO_2$	-0.5 (0.2)	0.18 (0.07)	0.7 - 10	5
2-$PrONO_2$	-3 (1)	0.16 (0.06)	0.6 – 10	9
2-$BuONO_2$	-7 (2)	0.21 (0.07)	0.5 – 8	9
2-$PeONO_2$	-3 (1)	0.3 (0.1)	0.4 – 6	9
3-$PeONO_2$	-2.2 (0.7)	0.34 (0.08)	0.3 – 6	6

nitrate (PAN) (0.09 – 0.25 cm s^{-1})[*G. Dollard et al.*, 1990; *J. A. Garland and S. A. Penkett*, 1976; *L. Zhang et al.*, 2002] and isoprene nitrate (0.30 cm s^{-1}) [*T. B. Nguyen et al.*, 2015]. Our estimates suggest that dry deposition may be an important sink of C_1-C_5 $RONO_2$ at the BAO site in winter and spring, with dry deposition lifetimes of 0.3 – 12 days for boundary layer heights of 100-1500 m (Table 4.3). These lifetimes against dry deposition are shorter than daytime lifetimes against photolysis plus reaction with OH for $MeONO_2$ for winter and spring (τ_{OH+hv} = 12 – 105 days, Table A2.1) and have some overlap with summer $MeONO_2$ photolysis + OH lifetimes (τ_{OH+hv} = 9 – 25 days, Table A2.1). Lifetimes against dry deposition are comparable with photolysis + OH lifetimes for 2-$BuONO_2$, 2-$PeONO_2$, and 3-$PeONO_2$ for winter, spring and summer (τ_{OH+hv} = 0.7 – 12 days, Table A2.1), and for 2-$PrONO_2$ during spring and summer (τ_{OH+hv} = 3 – 11 days, Table A2.1). The importance of dry deposition for $RONO_2$ loss varies throughout the day, and typically decreases with increase carbon number. For instance, loss by dry deposition accounts for 100% of $MeONO_2$ loss at night, but decreases to 46% between 12:00 and 14:00 as photolysis rates and loss to OH increase to 42% and 12% respectively (Fig. A2.1a). Alternatively, between 12:00 and 14:00 dry deposition only accounts for 12% of 2-$PeONO_2$ loss while photolysis and OH account for 8% and 79% respectively (Fig. A2.1b).

As 2-$BuONO_2$ and 2-$PrONO_2$ are often used to determine photochemical age using the Bertman model, we investigate the impact of dry deposition on derived aging (Fig. A2.2). Accounting for dry deposition offsets the estimated photochemical age derived from observations by <5% for photochemical ages <24 hours (Fig. A2.2). Including dry deposition does not affect model-measurement agreement for any $RONO_2$/RH pairs for summer 2015 data (Fig. A2.3). The dry deposition rate coefficient in summer 2015 is half that of spring 2015 because the estimated summer boundary layer height is twice as high than spring. In addition, removal of $RONO_2$ in the

summer is subject to increased removal by OH and photolysis. Thus including dry deposition improves the model-measurement agreement, but is inadequate for fully explaining the observations.

4.3.5 $MeONO_2$

$MeONO_2$/methane exhibits the largest model-measurement discrepancy of all the measured $RONO_2$/RH pairs (Fig. A2.4). Estimating an average spring boundary layer height of 750 m (See SI for boundary layer height estimations), we determine dry deposition rate coefficients (k_{dep}) of 2.3×10^{-6} s^{-1} and 2.8×10^{-6} s^{-1} for $MeONO_2$ and 2-$BuONO_2$, respectively. Including dry deposition improves model-measurement agreement slightly (by 10-25% for spring 2011), but fails to resolve the overall model-measurement discrepancy for $MeONO_2$ (after 6 hours of aging, models still overpredict $MeONO_2$/methane by 50-100%). Despite including dry deposition, the model still fails to predict the observed constant $MeONO_2$/methane for any of the seasons. Large model-observation discrepancies for $MeONO_2$ have been observed elsewhere [*M. Wang et al.*, 2013; *D. R. Worton et al.*, 2010].

Equation 2 predicts that $MeONO_2$/methane increases with both photochemical age and increasing 2-$BuONO_2$/n-butane (Fig. 4.5). However, observed $MeONO_2$/methane does not increase with increasing 2-$BuONO_2$/n-butane during either spring or summer 2015, and instead exhibits a constant ratio with averages of $(2.0 \pm 0.4) \times 10^{-6}$ and $(1.6 \pm 0.6) \times 10^{-6}$ ppbv/pbbv during spring and summer 2015, respectively (Figs. S4). Branching ratios, kinetics and photolysis rates for $MeONO_2$ are at least as well-constrained as other $RONO_2$ species (see Supplemental for detailed discussion). We thus hypothesize that the large local source of methane in Northern Colorado, coupled to the slow reaction of methane with OH means that the formation of $MeONO_2$ is not balanced by an obvious decrease in methane. This causes a small dynamic range in

$MeONO_2/CH_4$ ratios, and a failure to meet a key assumption of the Bertman model (that the parent hydrocarbon decreases proportionally to the increase in $RONO_2$).

4.3.6 C_{2+} $RONO_2$

$EtONO_2$/ethane is well-described by the Bertman model ($\beta_{EtONO2} = 0.018$) (Fig. 4.6). Small under-predictions (32-48% for winter 2011, 6-14% for spring 2015 and 16-30% for summer 2015; <24 hours aging) are within the standard deviations of the binned data. This is in contrast to previous studies, in which the model underpredicts observed $EtONO_2$/ethane by factors of 2 or more [*S. B. Bertman et al.*, 1995; *R. S. Russo et al.*, 2010a; *I. J. Simpson et al.*, 2003; *M. Wang et al.*, 2013; *D. R. Worton et al.*, 2010]. However, these previous studies used lower branching ratios ($\beta_{EtONO2} \leq 0.014$) [*S. B. Bertman et al.*, 1995; *R. S. Russo et al.*, 2010a; *I. J. Simpson et al.*, 2003; *M. Wang et al.*, 2013; *D. R. Worton et al.*, 2010]. In section 3.3.2, we show that lower branching ratios underestimate $EtONO_2$ produced from reaction of EtO_2 radicals + NO. Additionally, the BAO site is heavily impacted by emissions from oil and natural gas extraction, and has high ambient ethane [*A. Abeleira et al.*, 2017; *J. B. Gilman et al.*, 2013; *E. E. McDuffie et al.*, 2016; *G. Pétron et al.*, 2012; *G. Pétron et al.*, 2014; *R. F. Swarthout et al.*, 2013]. This high ethane may be the dominant source of EtO_2 radicals at BAO, as opposed to the substantial secondary sources from fragmentation of larger alkoxy radicals invoked at other sites with fewer local ethane sources. Average ethane mixing ratios ranged from 16 to 35 ppbv for the NACHTT and SONGNEX field campaigns respectively [*A. Abeleira et al.*, 2017; *J. B. Gilman et al.*, 2013; *R. F. Swarthout et al.*, 2013]. These values were 5 – 30x greater than ethane observed at other ground sites [*S. B. Bertman et al.*, 1995; *R. S. Russo et al.*, 2010b; *B. Wang et al.*, 2010] and flight plumes [*I. J. Simpson et al.*, 2003; *R. Sommariva et al.*, 2008].

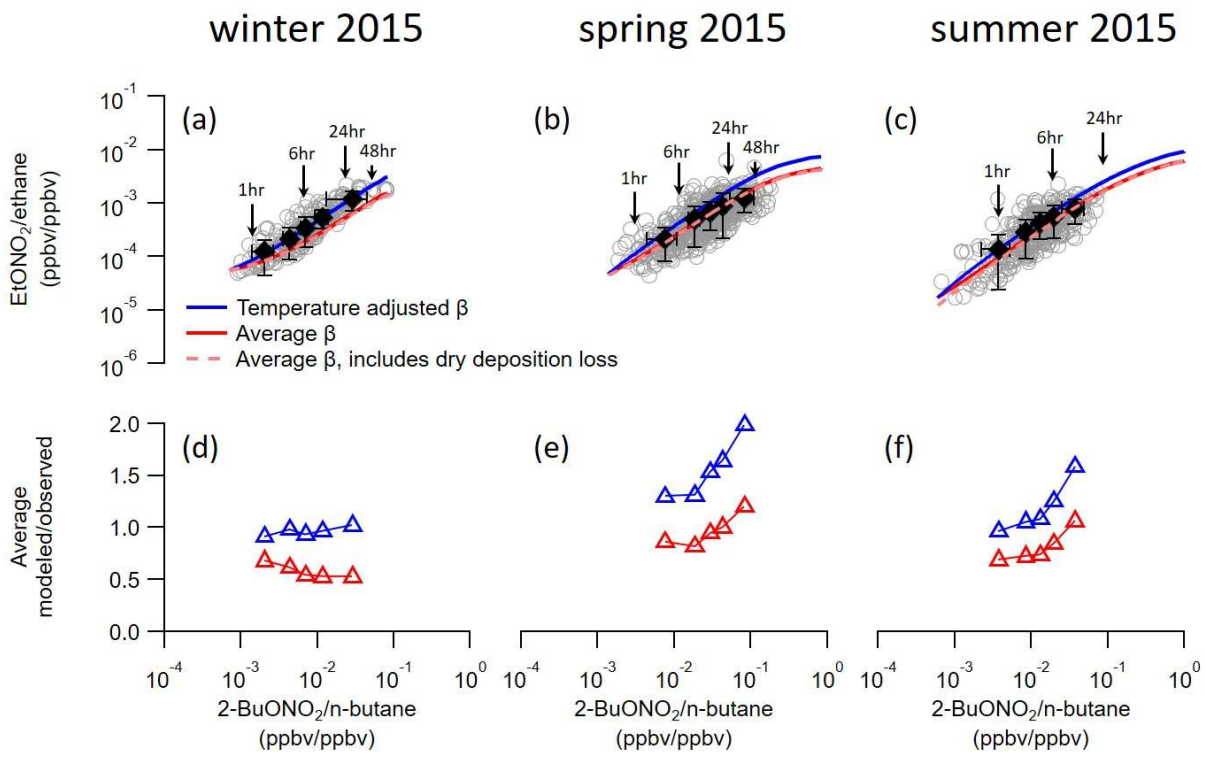

Figure 4.6. Daytime (08:00 – 18:00) $EtONO_2$/ethane ratios are plotted against 2-$BuONO_2$/n-butane (grey circles) for (a) winter 2011, (b) spring 2015 and (c) summer 2015. Modeled ratios are calculated using branching ratios adjusted for average daytime temperature (solid blue line; see text for description), an average branching ratio (β_{EtONO2} = 0.018; solid red line), and an average branching ratio plus dry deposition (dashed red line). Error bars represent one standard deviation around the bin averages. Modeled/observed ratios are shown for (d) winter 2011, spring 2015 (e) and summer 2015 (f) for the temperature-adjusted branching ratio versus average branching ratio scenarios. Photochemical ages derived from E2 for the model scenarios are listed above the models.

The branching ratio for ethane to $EtONO_2$ is temperature dependent [*N. Butkovskaya et al.*, 2010]. Average daytime temperatures at BAO vary from 5°C during winter 2011 to 15°C during spring 2015 to 25°C during summer 2015. Accounting for temperature-dependence in β_{ErONO2} results in branching ratios of 0.036 for winter 2011, 0.032 for spring 2015, and 0.027 for summer 2015. The increase in the winter 2011 branching ratio brought the model and averaged measurements into near-perfect agreement (Fig. 4.6b). However, the temperature-adjusted branching ratios overpredict average measurements by 30-100% for spring 2015, and 25-60% for summer 2015 (>6 hours aging) (Fig. 4.6b). The spring and summer observations are consistent with $EtONO_2$ branching ratios between 0.018 and 0.032.

Modeled and observed 2-$PrONO_2$/propane are in good agreement for the three campaigns (±36%, within the standard deviation of averaged observations). Winter 2011 model-measurement comparisons are within the standard deviation of observed values for 2-$PeONO_2$ and 3-$PeONO_2$. In contrast, the model overpredicts ratios for the spring and summer campaigns (67-280%). Accounting for the temperature dependence of C_5-$RONO_2$ branching ratios [*R. Atkinson et al.*, 1987], we decrease the branching ratio by 20% (spring 2015) and 30% (summer 2015). This decrease in branching ratio improves the model/measurement agreement for the pentyl nitrates (19-61% over-prediction, <20 hours aging).

The remaining lack of model-measurement agreement is consistent with previous studies. For example, *C. E. Reeves et al.* [2007] attributed comparable model over-prediction to decomposition of C_5 peroxy radicals before reacting with NO. The spring and summer 2015 2-$PeONO_2$ and 3-$PeONO_2$ model overpredictions are consistent with the proposed decomposition of C_5 peroxy radicals.

4.3.7 Photochemical age at BAO

We use the 2-$PrONO_2$/propane and 2-BuONO2/n-butane ratios to derive photochemical ages during summer 2015 at BAO (OH = $6x10^6$ molecules cm^{-3}, $\beta_{2\text{-}PrONO2}$ = 0.029, $\beta_{2\text{-}BuONO2}$= 0.074, and average summer k_A and k_B values from Table 4.2). The alkyl nitrate photochemical clock appears to capture daily photochemistry: i.*e.,* 70% of daytime data at BAO exhibit photochemical ages <12 hours, which aligns with hours since sunrise during summer months (Fig. A2.8a). The mechanistic connection between O_3 and $RONO_2$ formation suggests that in an environment dominated by photochemical O_3 production (as opposed to transport events), O_3 should correlate to photochemical age. However, the summer BAO data shows that high daytime O_3 does not consistently correlate with older photochemical ages (*i.e.* high $RONO_2$/RH ratios) (Fig. 4.7). A key assumption of the $RONO_2$/RH photochemical clock is that $RONO_2$/RH increases because $RONO_2$ is produced at the expense of RH (*i.e.* $RONO_2$ increases proportionally to the decrease in RH). The production of O_3 and $RONO_2$ are coincident (Fig. 4.1a): as $RONO_2$ increases, so should ozone. Thus, we expect $RONO_2$ and O_3 to increase and the parent alkane to decrease as $RONO_2$/RH increases with increasing photochemical age. However, this assumption is not always met at BAO: Figure A2.8 shows that propane mixing ratios decrease with photochemical age, but that while 2-$PrONO_2$ should increase proportionally, there are days in which 2-$PrONO_2$ actually decreases with decreasing propane. Thus the assumption behind the Bertman model is not always met.

There are three possible reasons for this discrepancy between propane and 2-$PrONO_2$ trends: (1) very low NO pushes the system to a very NO_x-limited regime in which little $RONO_2$ is produced and HO_x self-reactions dominate; (2) there is a missing sink of 2-$PrONO_2$ that is not accounted for in the updated Bertman model; and (3) substantial contributions of an airmass with

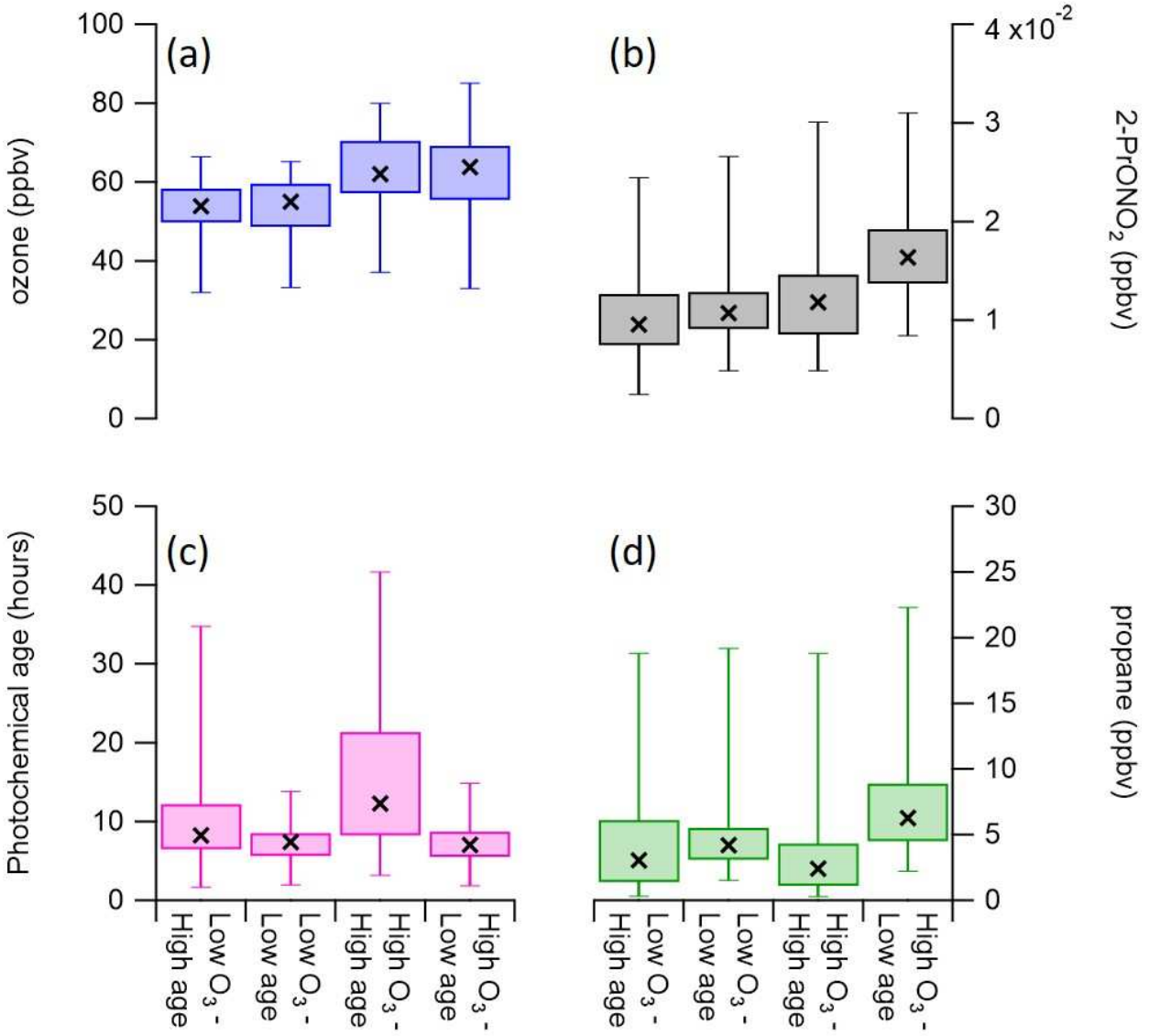

Figure 4.7. Box and whisker plots (5^{th}, 33^{rd}, 50^{th}, 67^{th}, and 95^{th} percentiles) for summer 2015 daytime (08:00-18:00) for (a) O_3 concentrations, (b) 2-$PrONO_2$ concentrations, (c) photochemical age, and (d) propane concentrations. Photochemical age is calculated by rearranging E1 to solve for time using the measured 2-$PrONO_2$/propane values. Days during the summer 2015 campaign were split into groups depending on daytime O_3 concentrations and 2-$PrONO_2$/propane. The Low O_3 designation is for days with O_3 < 70ppbv, and high O_3 is days with O_3 > 70 ppbv. Low age is days with photochemical aging <24 hours. High age is days with photochemical aging >24 hours. The number of days in each group is 11, 9, 8, and 8 for Low O_3 – High age, Low O_3 – Low age, High O_3 – High age, and High O_3 – Low age respectively.

low propane and low 2-$PrONO_2$ that mix with the high propane Front Range airmass and fail the assumption of a homogeneous airmass. The first hypothesis – that NO is low (<0.1 ppbv), causing RO_2 self-reactions to compete with R3 [*F. Flocke et al.*, 1991; *J. M. Roberts et al.*, 1998], thereby decreasing the parent alkane without increasing $RONO_2$ or O_3 – requires low NO. However, daytime (08:00 – 18:00) NO mixing ratios during summer 2015 at the BAO site are between 0.1 – 3 ppbv [*A. Abeleira et al.*, 2017], which should be adequate for RO_2+NO reactions to dominate over RO_2+RO_2. The second hypothesis (missing sink) is unlikely: we include OH reactions, photolysis and dry deposition of $RONO_2$. The vapor pressure of 2-$PrONO_2$ is (>3 torr [*R. G. Fischer and K. Ballschmiter*, 1998; *Y. B. Lim and P. J. Ziemann*, 2005; *J. M. Roberts*, 1990]) and unlikely to cause substantial partitioning to the aerosol phase. Wet deposition may occur, reducing mixing ratios of hydrocarbons and alkyl nitrates unevenly. However, the solubility of 2-$PrONO_2$ is low, and little precipitation occurred during summer 2015 in the Front Range. The third hypothesis – inhomogeneous mixing of airmasses – is thus the simplest explanation for our observations. Specifically, smoke impacted days around 20 August 2015 – 22 August 2015 exhibit high photochemical ages before 11:00.[*J. Lindaas et al.*, 2017]

To further investigate the relationship between O_3 and photochemical age, we classify all summer 2015 days as having either high or low O_3 maxima (> or < 70 ppbv), and either high or low photochemical age maxima (> or < 24 hours). We find equal numbers of high O_3 days that occur with high or low photochemical ages. Consistent with that observation, daily maximum O_3 is better correlated with daily maximum 2-$PrONO_2$ (r^2 = 0.50, Fig. A2.7b) than with daily maximum 2-$PrONO_2$/propane, a proxy for photochemical aging (r^2 = 0.05, Fig. A2.7a). We attribute this lack of correlation to a breakdown in the assumptions of the Bertman model as a photochemical clock – specifically, the need for sampling of a homogeneous airmass.

4.4. Conclusions

Uncertainties in OH concentration selection, $RONO_2$ branching ratios, and the rates of $RONO_2$ photolysis and oxidation all impact modeled $RONO_2$/RH and thus photochemical age. However, OH concentration is the most sensitive factor when estimating photochemical age of a sampled air mass using the Bertman model, although incorporation of temperature-dependent branching ratios are useful for reducing model-measurement discrepancies of $EtONO_2$/ethane ratios. However, the application of the Bertman model to derive photochemical ages of air masses is clearly limited at BAO not only by these uncertainties, but also by the balance between photochemical removal of parent alkanes, photochemical production of alkyl nitrates, and the impact of mixing of non-homogenous airmasses. Despite these discrepancies, we find that 70% of sample airmasses during summer 2015 have a photochemical age <12 hours, which aligns with daily photochemistry – *i.e.* hours since sunrise for summer days. Days with much higher calculated photochemical ages is likely due to the mixing of airmasses with low propane.

Dry deposition is a sink for C_1–C_5 $RONO_2$ at BAO, with dry deposition velocities for C_1-C_5 $RONO_2$ that are estimated to be between 0.15-0.17 cm s^{-1} during winter and spring at BAO, which results in dry deposition lifetimes of 0.3 – 12 days for boundary layer heights of 100-1500m. Thus, dry deposition accounts for similar $RONO_2$ losses as photolysis and OH reaction in winter, spring, and summer for 2-$PrONO_2$, 2-$BuONO_2$, 2-$PeONO_2$, and 3-$PeONO_2$. Lifetimes to dry deposition for $MeONO_2$ are shorter than photolysis and OH reaction during winter and spring. Despite this role as a sink, inclusion of dry deposition in the Bertman model has little impact on derived photochemical ages, particularly in the summer months when photolysis and reaction with OH dominant the $RONO_2$ sink. *J. Williams et al.* [2014] find that the distribution of $MeONO_2$ mixing ratios in a 3-D chemical transport model are highly sensitive to the inclusion of loss to dry

deposition, and that direct oceanic emissions of $MeONO_2$ are lost near source regions. Because $RONO_2$ species are thought to react with OH to release NO_2 and RO_2 radicals, their production and export can contribute to downwind production of ozone, and potentially HNO_3 or aerosol nitrate. However, deposition mitigates the impact on ozone of long-range transport of $MeONO_2$ out of the source region [*J. Williams et al.*, 2014]. Our work suggests C_2–C_5 $RONO_2$ can also be deposited near source regions, thus reducing their impact on downwind ozone. This could be particularly relevant for estimating the impact of emissions from oil and gas influenced regions (e.g. Northern Colorado) that have large alkane sources.

CHAPTER 5 REFERENCES

Abeleira, A., I. Pollack, B. Sive, Y. Zhou, E. Fischer, and D. Farmer (2017), Source characterization of volatile organic compounds in the Colorado Northern Front Range Metropolitan Area during spring and summer 2015, *Journal of Geophysical Research: Atmospheres*, *122*(6), 3595-3613.

Abeleira, A. J., and D. K. Farmer (2017), Summer ozone in the northern Front Range metropolitan area: weekend–weekday effects, temperature dependences, and the impact of drought, *Atmos. Chem. Phys.*, *17*(11), 6517-6529, doi:10.5194/acp-17-6517-2017.

Aschmann, S. M., J. Arey, and R. Atkinson (2012), Products of the OH radical-initiated reactions of 2-and 3-hexyl nitrate, *Atmospheric environment*, *46*, 264-270.

Aschmann, S. M., W. D. Long, and R. Atkinson (2006), Pressure dependence of pentyl nitrate formation from the OH radical-initiated reaction of n-pentane in the presence of NO, *The Journal of Physical Chemistry A*, *110*(21), 6617-6622.

Aschmann, S. M., E. C. Tuazon, J. Arey, and R. Atkinson (2011), Products of the OH radical-initiated reactions of 2-propyl nitrate, 3-methyl-2-butyl nitrate and 3-methyl-2-pentyl nitrate, *Atmospheric environment*, *45*(9), 1695-1701.

Atkinson, R. (1990), Gas-phase tropospheric chemistry of organic compounds: a review, *Atmospheric Environment. Part A. General Topics*, *24*(1), 1-41.

Atkinson, R. (2003), Kinetics of the gas-phase reactions of OH radicals with alkanes and cycloalkanes, *Atmospheric Chemistry and Physics*, *3*(6), 2233-2307.

Atkinson, R., S. M. Aschmann, W. P. Carter, A. M. Winer, and J. N. Pitts Jr (1982), Alkyl nitrate formation from the nitrogen oxide (NOx)-air photooxidations of C2-C8 n-alkanes, *The Journal of Physical Chemistry*, *86*(23), 4563-4569.

Atkinson, R., S. M. Aschmann, and A. M. Winer (1987), Alkyl nitrate formation from the reaction of a series of branched RO 2 radicals with NO as a function of temperature and pressure, *Journal of atmospheric chemistry*, *5*(1), 91-102.

Atlas, E., W. Pollock, J. Greenberg, L. Heidt, and A. Thompson (1993), Alkyl nitrates, nonmethane hydrocarbons, and halocarbon gases over the equatorial Pacific Ocean during SAGA 3, *Journal of Geophysical Research: Atmospheres*, *98*(D9), 16933-16947.

Beine, H. J., D. A. Jaffe, D. R. Blake, E. Atlas, and J. Harris (1996), Measurements of PAN, alkyl nitrates, ozone, and hydrocarbons during spring in interior Alaska, *Journal of Geophysical Research: Atmospheres*, *101*(D7), 12613-12619, doi:10.1029/96JD00342.

Bertman, S. B., J. M. Roberts, D. D. Parrish, M. P. Buhr, P. D. Goldan, W. C. Kuster, F. C. Fehsenfeld, S. A. Montzka, and H. Westberg (1995), Evolution of alkyl nitrates with air mass age, *Journal of Geophysical Research: Atmospheres*, *100*(D11), 22805-22813.

Blake, N. J., D. R. Blake, B. C. Sive, A. S. Katzenstein, S. Meinardi, O. W. Wingenter, E. L. Atlas, F. Flocke, B. A. Ridley, and F. S. Rowland (2003a), The seasonal evolution of NMHCs and light alkyl nitrates at middle to high northern latitudes during TOPSE, *Journal of Geophysical Research: Atmospheres*, *108*(D4), n/a-n/a, doi:10.1029/2001JD001467.

Blake, N. J., D. R. Blake, A. L. Swanson, E. Atlas, F. Flocke, and F. S. Rowland (2003b), Latitudinal, vertical, and seasonal variations of C1-C4 alkyl nitrates in the troposphere

over the Pacific Ocean during PEM-Tropics A and B: Oceanic and continental sources, *Journal of Geophysical Research: Atmospheres*, *108*(D2).

Blake, N. J., D. R. Blake, O. W. Wingenter, B. C. Sive, C. H. Kang, D. C. Thornton, A. R. Bandy, E. Atlas, F. Flocke, and J. M. Harris (1999), Aircraft measurements of the latitudinal, vertical, and seasonal variations of NMHCs, methyl nitrate, methyl halides, and DMS during the First Aerosol Characterization Experiment (ACE 1), *Journal of Geophysical Research: Atmospheres*, *104*(D17), 21803-21817.

Brown, S. S., et al. (2013), Nitrogen, Aerosol Composition, and Halogens on a Tall Tower (NACHTT): Overview of a wintertime air chemistry field study in the front range urban corridor of Colorado, *Journal of Geophysical Research: Atmospheres*, *118*(14), 8067-8085, doi:10.1002/jgrd.50537.

Butkovskaya, N., A. Kukui, and G. Le Bras (2010), Pressure and Temperature Dependence of Ethyl Nitrate Formation in the C2H5O2 + NO Reaction, *The Journal of Physical Chemistry A*, *114*(2), 956-964, doi:10.1021/jp910003a.

Butkovskaya, N., A. Kukui, and G. Le Bras (2012), Pressure and Temperature Dependence of Methyl Nitrate Formation in the CH3O2 + NO Reaction, *The Journal of Physical Chemistry A*, *116*(24), 5972-5980, doi:10.1021/jp210710d.

Butkovskaya, N. I., A. Kukui, and G. Le Bras (2010), Pressure Dependence of Iso-Propyl Nitrate Formation in the i-C3H7O2+ NO Reaction, *Zeitschrift für Physikalische Chemie*, *224*(7-8), 1025-1038.

Chuck, A. L., S. M. Turner, and P. S. Liss (2002), Direct evidence for a marine source of C1 and C2 alkyl nitrates, *Science*, *297*(5584), 1151-1154.

Clemitshaw, K. C., J. Williams, O. V. Rattigan, D. E. Shallcross, K. S. Law, and R. A. Cox (1997), Gas-phase ultraviolet absorption cross-sections and atmospheric lifetimes of several C2□C5 alkyl nitrates, *Journal of Photochemistry and Photobiology A: Chemistry*, *102*(2-3), 117-126.

Day, D. A., M. B. Dillon, P. J. Wooldridge, J. A. Thornton, R. S. Rosen, E. C. Wood, and R. C. Cohen (2003), On alkyl nitrates, O3, and the "missing NOy", *Journal of Geophysical Research: Atmospheres*, *108*(D16).

Dollard, G., B. Jones, and T. Davies (1990), Dry deposition of HNO3 and PAN, *AERE Report*, *13780*.

Ebben, C. J., T. L. Sparks, P. J. Wooldridge, T. L. Campos, C. A. Cantrell, R. L. Mauldin, A. J. Weinheimer, and R. C. Cohen (2017), Evolution of NOx in the Denver Urban Plume during the Front Range Air Pollution and Photochemistry Experiment, *Atmos. Chem. Phys. Discuss.*, *2017*, 1-13, doi:10.5194/acp-2017-671.

Espada, C., J. Grossenbacher, K. Ford, T. Couch, and P. B. Shepson (2005), The production of organic nitrates from various anthropogenic volatile organic compounds, *International journal of chemical kinetics*, *37*(11), 675-685.

Farmer, D. K., and R. C. Cohen (2008), Observations of HNO₃, ΣAN, ΣPN and NO₂ fluxes: evidence for rapid HO_x chemistry within a pine forest canopy, *Atmos. Chem. Phys.*, *8*(14), 3899-3917, doi:10.5194/acp-8-3899-2008.

Fischer, R. G., and K. Ballschmiter (1998), Determination of vapor pressure, water solubility, gas-water partition coefficient P GW, Henry's law constant, and octanol-water partition coefficient P OW OF 26 alkyl dinitrates, *Chemosphere*, *36*(14), 2891-2901.

Flocke, F., A. Volz-Thomas, H.-J. Buers, W. Pätz, H.-J. Garthe, and D. Kley (1998), Long-term measurements of alkyl nitrates in southern Germany: 1. General behavior and seasonal and diurnal variation, *Journal of Geophysical Research: Atmospheres*, *103*(D5), 5729-5746, doi:10.1029/97jd03461.

Flocke, F., A. Volz-Thomas, and D. Kley (1991), Measurements of alkyl nitrates in rural and polluted air masses, *Atmospheric Environment. Part A. General Topics*, *25*(9), 1951-1960.

Garland, J. A., and S. A. Penkett (1976), Absorption of peroxy acetyl nitrate and ozone by natural surfaces, *Atmospheric Environment (1967)*, *10*(12), 1127-1131, doi:http://dx.doi.org/10.1016/0004-6981(76)90122-0.

Gilman, J. B., B. M. Lerner, W. C. Kuster, and J. A. de Gouw (2013), Source signature of volatile organic compounds from oil and natural gas operations in northeastern Colorado, *Environ Sci Technol*, *47*(3), 1297-1305, doi:10.1021/es304119a.

Halliday, H. S., A. M. Thompson, A. Wisthaler, D. R. Blake, R. S. Hornbrook, T. Mikoviny, M. Müller, P. Eichler, E. C. Apel, and A. J. Hills (2016), Atmospheric benzene observations from oil and gas production in the Denver-Julesburg Basin in July and August 2014, *Journal of Geophysical Research: Atmospheres*, *121*(18), 11,055-011,074, doi:10.1002/2016JD025327.

Jenkin, M. E., S. M. Saunders, and M. J. Pilling (1997), The tropospheric degradation of volatile organic compounds: a protocol for mechanism development, *Atmospheric Environment*, *31*(1), 81-104.

Kames, J., and U. Schurath (1992), Alkyl nitrates and bifunctional nitrates of atmospheric interest: Henry's law constants and their temperature dependencies, *Journal of Atmospheric Chemistry*, *15*(1), 79-95.

Kim, S., T. C. VandenBoer, C. J. Young, T. P. Riedel, J. A. Thornton, B. Swarthout, B. Sive, B. Lerner, J. B. Gilman, and C. Warneke (2014), The primary and recycling sources of OH during the NACHTT-2011 campaign: HONO as an important OH primary source in the wintertime, *Journal of Geophysical Research: Atmospheres*, *119*(11), 6886-6896.

Kwok, E. S., and R. Atkinson (1995), Estimation of hydroxyl radical reaction rate constants for gas-phase organic compounds using a structure-reactivity relationship: an update, *Atmospheric Environment*, *29*(14), 1685-1695.

Lim, Y. B., and P. J. Ziemann (2005), Products and mechanism of secondary organic aerosol formation from reactions of n-alkanes with OH radicals in the presence of NO x, *Environmental science & technology*, *39*(23), 9229-9236.

Lindaas, J., D. K. Farmer, I. B. Pollack, A. Abeleira, F. Flocke, R. Roscioli, S. Herndon, and E. V. Fischer (2017), Changes in ozone and precursors during two aged wildfire smoke events in the Colorado Front Range in summer 2015, *Atmos. Chem. Phys.*, *17*(17), 10691-10707, doi:10.5194/acp-17-10691-2017.

Lyu, X., Z. Ling, H. Guo, S. Saunders, S. Lam, N. Wang, Y. Wang, M. Liu, and T. Wang (2015), Re-examination of C 1–C 5 alkyl nitrates in Hong Kong using an observation-based model, *Atmospheric environment*, *120*, 28-37.

Mackay, D., and R. S. Boethling (2000), *Handbook of property estimation methods for chemicals: environmental health sciences*, CRC press.

McDuffie, E. E., P. M. Edwards, J. B. Gilman, B. M. Lerner, W. P. Dubé, M. Trainer, D. E. Wolfe, W. M. Angevine, J. deGouw, and E. J. Williams (2016), Influence of oil and gas

emissions on summertime ozone in the Colorado Northern Front Range, *Journal of Geophysical Research: Atmospheres*, *121*(14), 8712-8729.
Morin, J., Y. Bedjanian, and M. N. Romanias (2016), Kinetics and Products of the Reactions of Ethyl and n-Propyl Nitrates with OH Radicals, *International Journal of Chemical Kinetics*, *48*(12), 822-829.
Neff, J. C., E. A. Holland, F. J. Dentener, W. H. McDowell, and K. M. Russell (2002), The origin, composition and rates of organic nitrogen deposition: A missing piece of the nitrogen cycle?, *Biogeochemistry*, *57*(1), 99-136, doi:10.1023/a:1015791622742.
Nguyen, T. B., J. D. Crounse, A. P. Teng, J. M. S. Clair, F. Paulot, G. M. Wolfe, and P. O. Wennberg (2015), Rapid deposition of oxidized biogenic compounds to a temperate forest, *Proceedings of the National Academy of Sciences*, *112*(5), E392-E401.
NOAA (2014), Shale Oil and Natural Gas Nexus White Paper, edited by N. O. a. A. Administration.
NOAA (2017), BAO site information, edited.
Perring, A., S. Pusede, and R. Cohen (2013), An observational perspective on the atmospheric impacts of alkyl and multifunctional nitrates on ozone and secondary organic aerosol, *Chemical reviews*, *113*(8), 5848-5870.
Pétron, G., et al. (2012), Hydrocarbon emissions characterization in the Colorado Front Range: A pilot study, *Journal of Geophysical Research: Atmospheres*, *117*(D4), n/a-n/a, doi:10.1029/2011jd016360.
Pétron, G., A. Karion, C. Sweeney, B. R. Miller, S. A. Montzka, G. J. Frost, M. Trainer, P. Tans, A. Andrews, and J. Kofler (2014), A new look at methane and nonmethane hydrocarbon emissions from oil and natural gas operations in the Colorado Denver-Julesburg Basin, *Journal of Geophysical Research: Atmospheres*, *119*(11), 6836-6852.
Ranschaert, D. L., N. J. Schneider, and M. J. Elrod (2000), Kinetics of the C2H5O2+ NO x Reactions: Temperature Dependence of the Overall Rate Constant and the C2H5ONO2 Branching Channel of C2H5O2+ NO, *The Journal of Physical Chemistry A*, *104*(24), 5758-5765.
Reeves, C. E., J. Slemr, D. E. Oram, D. Worton, S. A. Penkett, D. J. Stewart, R. Purvis, N. Watson, J. Hopkins, and A. Lewis (2007), Alkyl nitrates in outflow from North America over the North Atlantic during Intercontinental Transport of Ozone and Precursors 2004, *Journal of Geophysical Research: Atmospheres*, *112*(D10).
Roberts, J. M. (1990), The atmospheric chemistry of organic nitrates, *Atmospheric Environment. Part A. General Topics*, *24*(2), 243-287.
Roberts, J. M., S. B. Bertman, D. D. Parrish, F. C. Fehsenfeld, B. T. Jobson, and H. Niki (1998), Measurement of alkyl nitrates at Chebogue Point, Nova Scotia during the 1993 North Atlantic Regional Experiment (NARE) intensive, *Journal of Geophysical Research: Atmospheres*, *103*(D11), 13569-13580, doi:10.1029/98jd00266.
Roberts, J. M., and R. W. Fajer (1989), UV absorption cross sections of organic nitrates of potential atmospheric importance and estimation of atmospheric lifetimes, *Environmental science & technology*, *23*(8), 945-951.
Robertson, R. E., K. M. Koshy, A. Annessa, J. N. Ong, J. M. W. Scott, and M. J. Blandamer (1982), Kinetics of solvolysis in water of four secondary alkyl nitrates, *Canadian Journal of Chemistry*, *60*(13), 1780-1785.

Romanias, M. N., J. Morin, and Y. Bedjanian (2015), Experimental Study of the Reaction of Isopropyl Nitrate with OH Radicals: Kinetics and Products, *International Journal of Chemical Kinetics*, *47*(1), 42-49.

Russo, R. S., Y. Zhou, K. Haase, O. Wingenter, E. Frinak, H. Mao, R. Talbot, and B. Sive (2010a), Temporal variability, sources, and sinks of C 1-C 5 alkyl nitrates in coastal New England, *Atmospheric Chemistry and Physics*, *10*(4), 1865-1883.

Russo, R. S., Y. Zhou, M. L. White, H. Mao, R. Talbot, and B. C. Sive (2010b), Multi-year (2004–2008) record of nonmethane hydrocarbons and halocarbons in New England: seasonal variations and regional sources, *Atmospheric Chemistry and Physics*, *10*(10), 4909-4929, doi:10.5194/acp-10-4909-2010.

Saunders, S. M., M. E. Jenkin, R. Derwent, and M. Pilling (2003), Protocol for the development of the Master Chemical Mechanism, MCM v3 (Part A): tropospheric degradation of non-aromatic volatile organic compounds, *Atmospheric Chemistry and Physics*, *3*(1), 161-180.

Schneider, J. M., and D. K. Lilly (1999), An observational and numerical study of a sheared, convective boundary layer. Part I: Phoenix II observations, statistical description, and visualization, *Journal of the atmospheric sciences*, *56*(17), 3059-3078.

Simpson, I. J., S. Akagi, B. Barletta, N. Blake, Y. Choi, G. Diskin, A. Fried, H. Fuelberg, S. Meinardi, and F. Rowland (2011), Boreal forest fire emissions in fresh Canadian smoke plumes: C 1-C 10 volatile organic compounds (VOCs), CO 2, CO, NO 2, NO, HCN and CH 3 CN, *Atmospheric Chemistry and Physics*, *11*(13), 6445-6463.

Simpson, I. J., N. J. Blake, D. R. Blake, E. Atlas, F. Flocke, J. H. Crawford, H. E. Fuelberg, C. M. Kiley, S. Meinardi, and F. S. Rowland (2003), Photochemical production and evolution of selected C2–C5 alkyl nitrates in tropospheric air influenced by Asian outflow, *Journal of Geophysical Research: Atmospheres*, *108*(D20).

Simpson, I. J., S. Meinardi, D. R. Blake, N. J. Blake, F. S. Rowland, E. Atlas, and F. Flocke (2002), A biomass burning source of C1–C4 alkyl nitrates, *Geophysical Research Letters*, *29*(24).

Simpson, I. J., S. Meinardi, N. J. Blake, F. S. Rowland, and D. R. Blake (2004), Long-term decrease in the global atmospheric burden of tetrachloroethene (C2Cl4), *Geophysical research letters*, *31*(8).

Sommariva, R., M. Trainer, J. A. de Gouw, J. M. Roberts, C. Warneke, E. Atlas, F. Flocke, P. D. Goldan, W. C. Kuster, and A. L. Swanson (2008), A study of organic nitrates formation in an urban plume using a Master Chemical Mechanism, *Atmospheric Environment*, *42*(23), 5771-5786.

Stroud, C. A., J. M. Roberts, J. Williams, P. D. Goldan, W. C. Kuster, T. B. Ryerson, D. Sueper, D. D. Parrish, M. Trainer, and F. C. Fehsenfeld (2001), Alkyl nitrate measurements during STERAO 1996 and NARE 1997: Intercomparison and survey of results, *Journal of Geophysical Research: Atmospheres*, *106*(D19), 23043-23053.

Swanson, A. L., N. J. Blake, E. Atlas, F. Flocke, D. R. Blake, and F. S. Rowland (2003), Seasonal variations of C2–C4 nonmethane hydrocarbons and C1–C4 alkyl nitrates at the Summit research station in Greenland, *Journal of Geophysical Research: Atmospheres*, *108*(D2), n/a-n/a, doi:10.1029/2001JD001445.

Swarthout, R. F., R. S. Russo, Y. Zhou, A. H. Hart, and B. C. Sive (2013), Volatile organic compound distributions during the NACHTT campaign at the Boulder Atmospheric

Observatory: Influence of urban and natural gas sources, *Journal of Geophysical Research: Atmospheres*, *118*(18), 10,614-610,637, doi:10.1002/jgrd.50722.
Talukdar, R., J. Burkholder, M. Gilles, and J. Roberts (1997), Atmospheric fate of several alkyl nitrates Part 2UV absorption cross-sections and photodissociation quantum yields, *Journal of the Chemical Society, Faraday Transactions*, *93*(16), 2797-2805.
Talukdar, R. K., S. C. Herndon, J. B. Burkholder, J. M. Roberts, and A. Ravishankara (1997), Atmospheric fate of several alkyl nitrates Part 1Rate coefficients of the reactions of alkyl nitrates with isotopically labelled hydroxyl radicals, *Journal of the Chemical Society, Faraday Transactions*, *93*(16), 2787-2796.
Tyndall, G., R. Cox, C. Granier, R. Lesclaux, G. Moortgat, M. Pilling, A. Ravishankara, and T. Wallington (2001), Atmospheric chemistry of small organic peroxy radicals, *Journal of Geophysical Research: Atmospheres*, *106*(D11), 12157-12182.
Wang, B., M. Shao, S. Lu, B. Yuan, Y. Zhao, M. Wang, S. Zhang, and D. Wu (2010), Variation of ambient non-methane hydrocarbons in Beijing city in summer 2008, *Atmospheric Chemistry and Physics*, *10*(13), 5911.
Wang, M., M. Shao, W. Chen, S. Lu, C. Wang, D. Huang, B. Yuan, L. Zeng, and Y. Zhao (2013), Measurements of C1–C4 alkyl nitrates and their relationships with carbonyl compounds and O 3 in Chinese cities, *Atmospheric environment*, *81*, 389-398.
Williams, J., G. Le Bras, A. Kukui, H. Ziereis, and C. Brenninkmeijer (2014), The impact of the chemical production of methyl nitrate from the NO+ CH 3 O 2 reaction on the global distributions of alkyl nitrates, nitrogen oxides and tropospheric ozone: a global modelling study, *Atmospheric Chemistry and Physics*, *14*(5), 2363-2382.
Worton, D. R., C. E. Reeves, S. A. Penkett, W. T. Sturges, J. Slemr, D. E. Oram, B. J. Bandy, W. J. Bloss, N. Carslaw, and J. Davey (2010), Alkyl nitrate photochemistry during the tropospheric organic chemistry experiment, *Atmospheric Environment*, *44*(6), 773-785.
Zhang, L., M. D. Moran, P. A. Makar, J. R. Brook, and S. Gong (2002), Modelling gaseous dry deposition in AURAMS: a unified regional air-quality modelling system, *Atmospheric Environment*, *36*(3), 537-560, doi:http://dx.doi.org/10.1016/S1352-2310(01)00447-2.

CHAPTER 5 – UNDERSTANDING CURRENT AND FUTURE O_3 TRENDS IN NORTHERN COLORADO

The direction for regulatory action to reduce O_3 in Northern Colorado remains unclear despite recent studies in the NFR of;

- Long-term O_3 and NO_2 trends [*Abeleira et al.*, 2017b]
- Volatile organic compound (VOC) abundances and sources [*Abeleira et al.*, 2017a; *Gilman et al.*, 2013; *Lindaas et al.*, 2017; *McDuffie et al.*, 2016; *Swarthout et al.*, 2013]
- O_3 precursor sinks and distributions ([*Ebben et al.*, 2017], Abeleira et. al 2017 in prep),
- Local O_3 production [*Baier et al.*, 2017; *McDuffie et al.*, 2016; *Schroeder et al.*, 2017]
- Meteorological drivers of interannual variability of summertime O_3 over Colorado [*Reddy et al.*, 2016]

Three major open questions regarding O_3 production in the NFR are;

1) How diverse is the spatial distribution of O_3 precursors (VOCs and NO_x) in the region?
2) How does the mixing of VOC and NO_x emissions affect O_3 production in the urban, rural, and transitionary areas of the region?
3) How will an increasing population change the magnitude and distribution of O_3 precursor emissions in the region?

Long-term collocated VOC, NO_x, and O_3 measurements throughout the Front Range would provide valuable information for answering these questions.

Ozone and precursors in the NFR are not homogenous across the region, which causes differences in the O_3 production regime, and summertime O_3 exposure in the region. Median daytime O_3 is higher in the foothills outside of Boulder at the rural Rocky Flats site relative to downtown Denver or Platteville (Fig 5.1a). Median daytime NO_2 concentrations in summer 2015

differed by a factor of 4 (5 – 22 ppbv) at the four NO_2 monitoring sites within 15 miles of each other in Denver (Fig. 5.1b).[*Abeleira et al.*, 2017b] The median daytime NO_2 at the BAO site in summer 2015, 20-30 miles from the Denver sites, was only 1 ppbv. As NO_x is transported away from urban centers it undergoes photochemical oxidation, and is converted to a variety of oxidized nitrogen species with varying lifetimes. Most of the NO_x emitted into the Denver urban plume is deposited as HNO_3 within 100 km of Denver or converted to peroxy nitrates, suggesting a large NO_x gradient across NFR with most of the region being NO_x-limited outside of Denver [*Abeleira et al.*, 2017b; *Ebben et al.*, 2017; *McDuffie et al.*, 2016]. However, the magnitude and impact of NO_x emissions from the more densely populated Fort Collins and Greeley areas is unknown. *Thompson et al.* [2014] report significant heterogeneity in VOC levels in the NFR with enhanced concentrations of C_2-C_5 alkanes, benzene, and toluene in a residential area within the Greater Wattenberg Field relative to Denver and Boulder. Additionally, residences in Erie, CO near the BAO site exhibited VOC levels 18-77x greater than the regional background [*Thompson et al.*, 2014]. The abundances of different VOCs throughout the region can have large impacts on the availability of reactive carbon, which will impact the NO_x cross-over point between NO_x-limited and NO_x-saturated O_3 chemistry locally.

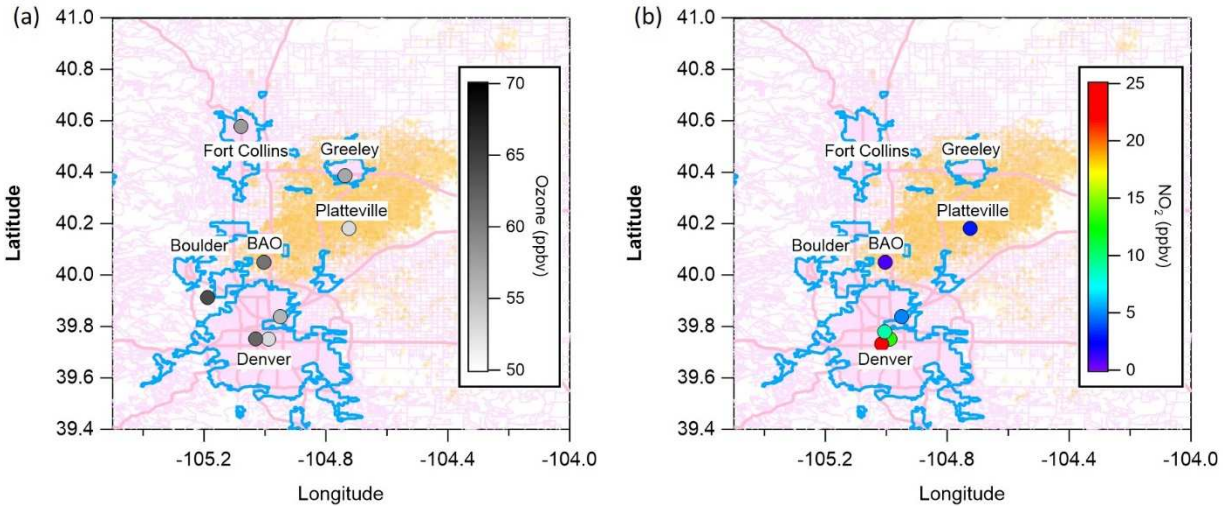

Figure 5.1. Median daytime (10:00 – 16:00 local) O_3 (a) and NO_2 (b) at measurement sites in the NFR. BAO median O_3 and NO_2 were calculated from data collected during summer 2015 [*Abeleira et al.*, 2017a]. Platteville O_3 and NO_2 data were collected as a part of the summer 2014 Front Range Air Pollution and Photochemistry Experiment [*Kaser et al.*, 2017]. The remaining sites are CDPHE monitoring sites [*Abeleira et al.*, 2017b].

O_3 and air quality in the NFR is largely impacted by transport and mixing of O_3 precursors throughout the region [*Haagenson*, 1979; *Vu et al.*, 2016]. Summertime air mass transport in the NFR is complex. Northern Colorado experiences complicated regional mixing due to a mountain-valley diel pattern and the regional vortex circulation pattern [*Crook et al.*, 1990; *Toth et al.*, 1985]. These different regional transport patterns affect the mixing and distribution of precursor emissions throughout the NFR, which alters the local O_3 production regimes. Complex transport patterns can lead to increased or decreased O_3 mixing ratios throughout the region. Despite the importance of these mixing and transport mechanisms, a thorough understanding of the impact of these mechanisms on the transport and mixing of O_3 precursors, and the subsequent impact on the O_3 production gradient in the region is lacking.

Emissions and spatial distribution of O_3 precursors and ambient O_3 mixing ratios in NFR have, and will continue to change with changes in **(1) population**, **(2) traffic**, **(3) energy production**, **(4) oil and gas extraction and processing activities**, and **(5) drought and wildfires**. Future changes in precursor concentrations through increased sources or improved controls can alter the spatial distribution of precursors in the NFR, which will alter the O_3 production regime (i.e. NO_x-limited versus NO_x-saturated) in the region. Furthermore, drought and wildfires in the western United States are predicted to increase with a changing climate [*IPCC*, 2014; *Westerling*, 2016]. Wildfires have the potential to increase O_3 in the region [*Jaffe et al.*, 2008; *Lindas et al.*, 2017], while drought may reduce O_3 in the region [*Abeleira et al.*, 2017b]. Understanding the O_3 exposure of the growing NFR population with changes in regional O_3 and precursor emissions will require a greater focus on regional O_3 and precursor monitoring. The potential changes in precursor emissions, distribution, and the subsequent impact on O_3 production and ambient O_3 in the NFR are addressed below.

The population in the eight NFR counties that are currently out of the National Ambient Air Quality Standard O_3 attainment have experienced an average population growth rate of 11% (3.3 million to 3.7 million) from 2010 to 2016 [*U.S.-Census*, 2016], with a projected population of 5.7 million by 2050 (Fig. 5.2) [*CDPHE*, 2017]. This rapid population growth increases the number of people exposed to enhanced summertime O_3 in the NFR annually, but it only partially drives the emissions of O_3 precursors. As the population grows in the NFR, so should the average number of automobiles on the road without substantial improvements in the public transportation systems in the region. The metropolitan area surrounding Denver, Fort Collins, Boulder, and Greeley continues to undergo 'suburbanization' and 'ex-urban' expansion [*Goetz*, 2013; *Pendall et al.*, 2013]. Continued 'suburbanization' suggests that personal automobiles will remain a dominant source of personal transportation in the region, while the I-25 corridor will likely remain a major commercial trucking throughway. From traffic counting stations in and around downtown Denver, the Colorado Department of Transportation predicts a 30-40% increase in passenger automobiles and commercial trucks in Denver between 2017 and 2050 [*CDOT*, 2017]. During the same time period, traffic projections for Weld and Larimer counties predict an 80-100% increases in passenger automobiles and commercial trucks [*CDOT*, 2017]. Estimated NO_x and VOC emissions trends in Colorado suggest that even with increased emission control efforts, vehicles are still the dominant source of NO_x (45%) and a large source of VOCs (21%) in the region in 2016 (Fig. 5.3) [*EPA*, 2001; 2016].

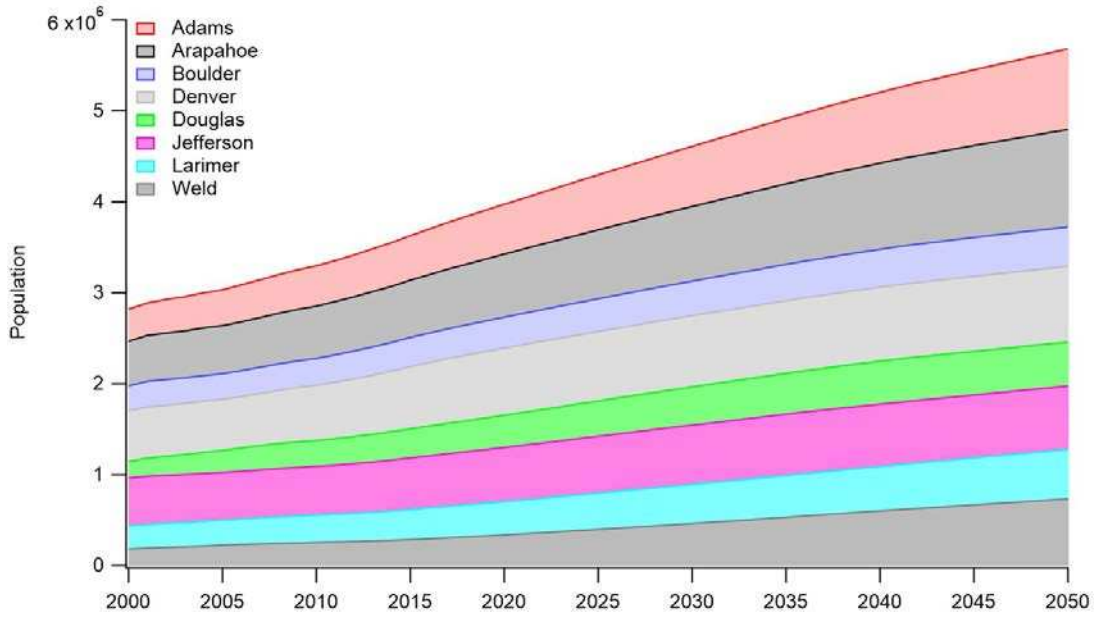

Figure 5.2. Population estimates (2000-2017) and projections (2018-2050) for the eight counties in Northern Colorado that are out of attainment for the 2015 O_3 NAAQS [*Colorado*, 2017a].

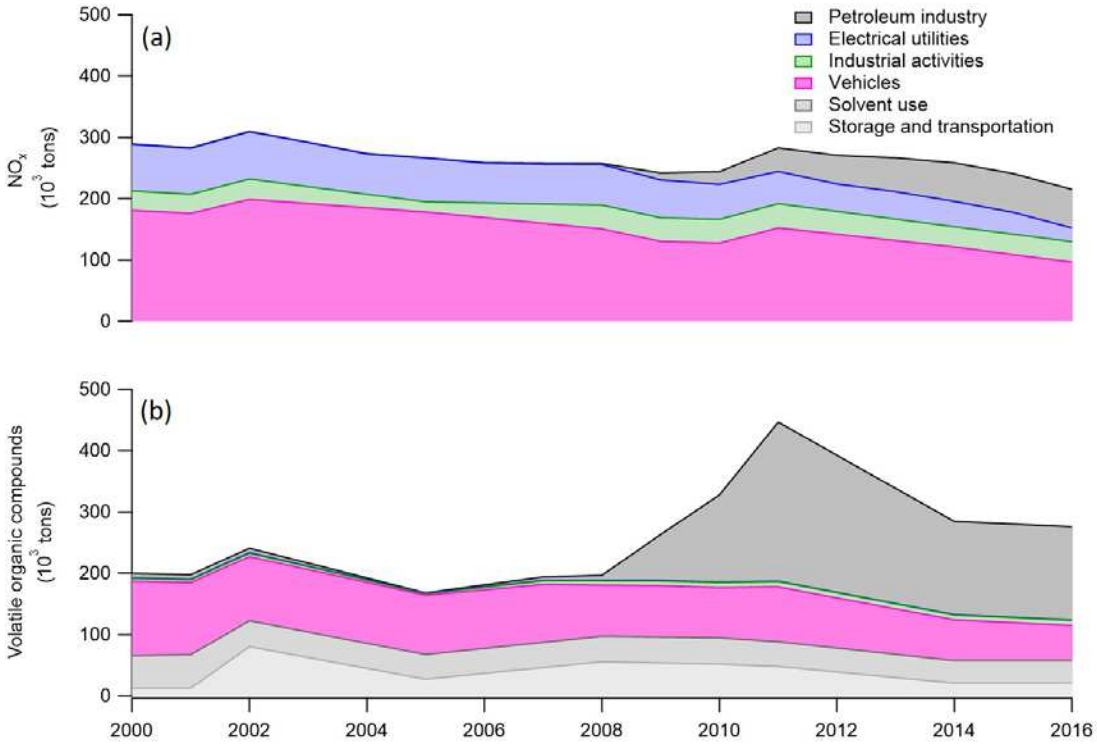

Figure 5.3. VOC (a) and NO_x (b) emission estimates from the EPA Air Emissions Inventories for Tier 1 source categories in Colorado [*EPA*, 2016].

Without substantial improvements in emission reduction technology, increases in the number of personal and commercial automobiles in the NFR will likely increase net NO_x and VOC emissions. This will shift the O_3 production regime towards peak production at a higher VOC reactivity in areas of Northern Colorado that are currently NO_x-limited (Fig. 5.4, scenario A). Areas in and around Denver that are currently transitioning to peak O_3 production from a NO_x-saturated regime could reverse that trend, but O_3 production would increase at a higher VOC reactivity (Fig. 5.4, scenario B). These scenarios suggest that more rural areas with less NO_x outside of Denver may experience greater increases in O_3 than the Denver area with increases in traffic.

In 2015, coal, natural gas, and gasoline dominated total energy consumption in Colorado (Fig. 5.5a), while coal, renewables, and natural gas dominated grid energy production (Fig. 5.5b). Coal and natural gas provided 60% and 20% of net electricity generation in Colorado during 2015, while renewables such as wind generation accounted for an additional 17% [*EIA*, 2017b]. Coal-fired electricity generating power plants are a major source of NO_x emissions in the United States [*Frost et al.*, 2006]. However, emissions in the United States have been decreasing even with increased energy production from the combination of natural-gas firing and emission mitigation technologies [*Abel et al.*, 2017; *De Gouw et al.*, 2014; *Kim et al.*, 2006]. The percentage of NO_x emissions attributed to electrical utilities in Northern Colorado has decreased from 25% in the 2000s to 10% in 2015 (Fig. 5.3a). NO_x emissions should continue to decrease even with an increasing energy demand as the Colorado Renewable Portfolio Standard requires 30% of domestic electricity to be produced by renewable technologies by 2020 [*Colorado*, 2017b]. Decreases in NO_x emissions from energy production without coincident decreases in VOCs would

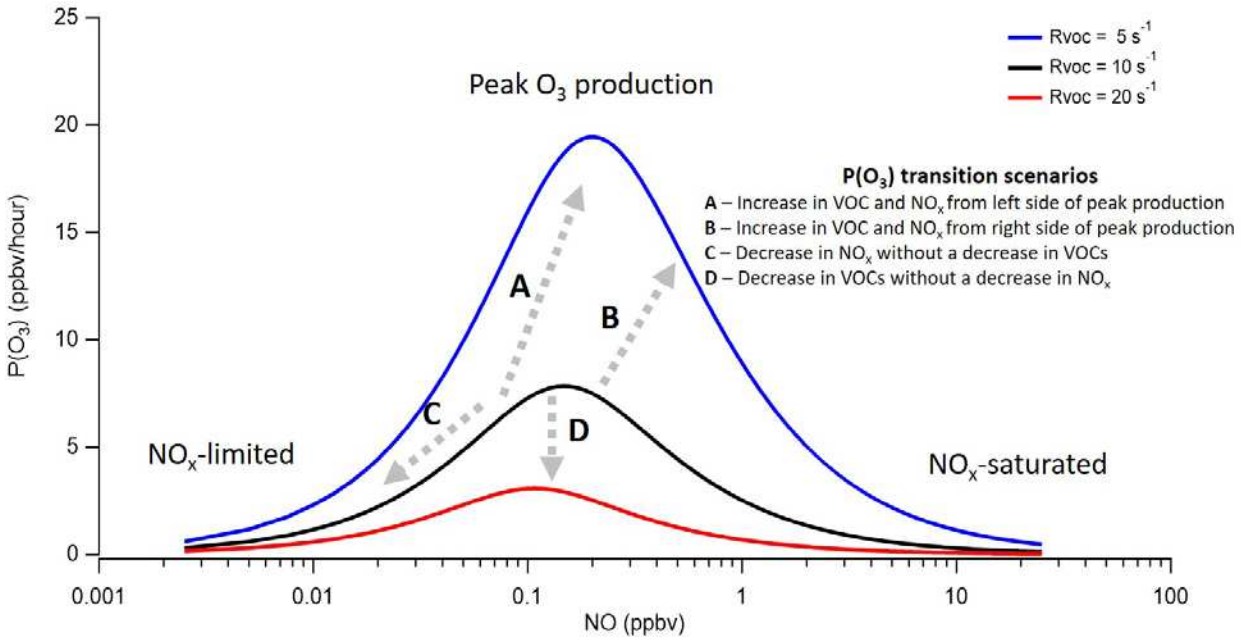

Figure 5.4. O_3 production calculated with an analytical model (details in chapter 1) for three different VOC reactivity values, and varying NO concentrations. Dashed grey lines and letters represent different scenarios for future changes in O_3 precursors. **A** is the transition to maximum O_3 production at a higher VOC reactivity curve from increases in both NO_x and VOCs. **B** is the transition to a higher VOC reactivity curve past the maximum $P(O_3)$ region from increases in both NO_x and VOCs. **C** is the transition to NO_x-limited O_3 production from a reduction in NO_x. **D** is the transition to a lower peak O_3 production from a reduction in VOCs without a reduction in NO_x.

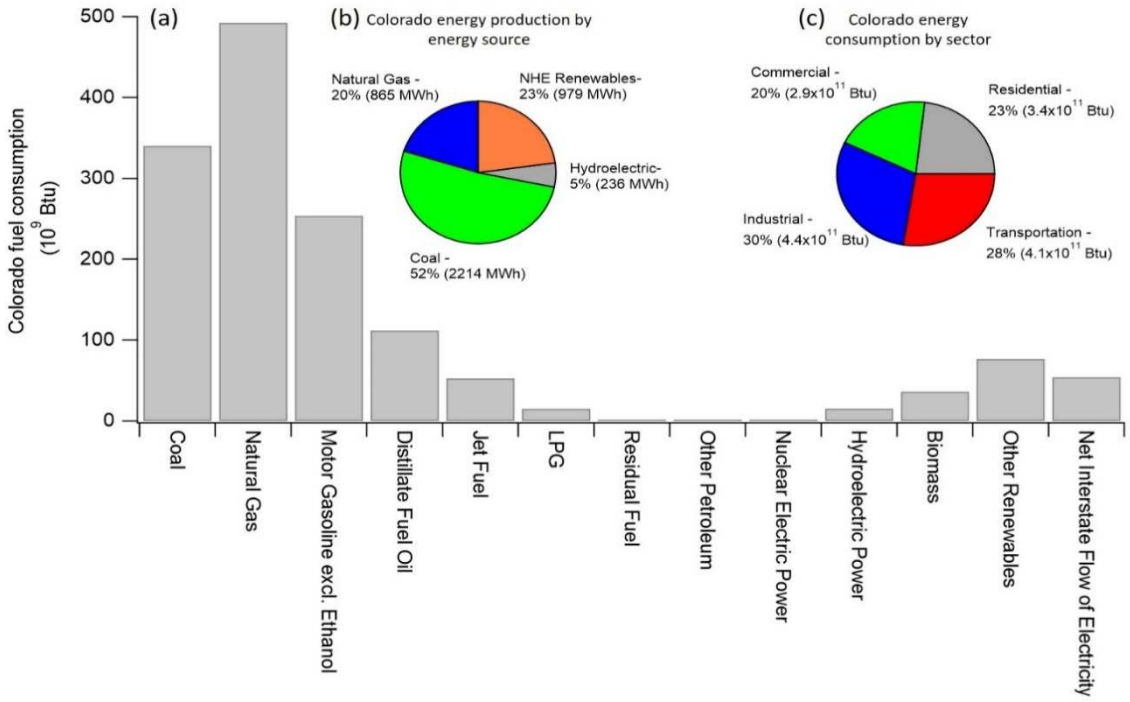

Figure 5.5. Colorado energy consumption and production estimates for 2015. (a) Colorado energy consumption by fuel type. (b) Colorado energy production by fuel type (NHE = Nonhydroelectric renewables). (c) Colorado energy consumption by sector.[*EIA*, 2017b]

push the O_3 production regime towards a NO_x-limited regime in areas of the region with lower NO_x to (Fig. 5.4, scenario C), but could contribute to the shift towards peak production in higher NO_x areas around Denver.

As evident in Fig. 5.3, between 2008 and 2016 VOC and NO_x emissions from the petroleum industry in Colorado increased 22x and 88x respectively. The number of active oil and natural gas extraction wells in the NFR doubled to 27,000+ between 2008 and 2015 [*McDuffie et al.*, 2016]. Crude oil production increased 5-fold in Weld County between 2010 and 2015, with 9 of 10 barrels of Colorado crude being produced in Weld County [*EIA*, 2016; 2017b]. The two Colorado crude oil refineries are located in Commerce City outside of Denver, and produce motor gasoline, diesel fuel, and asphalt, of which 90% is used by the transportation sector in Colorado [*EIA*, 2017b; c]. Natural gas withdrawals in Colorado have increased 2-fold since 2001 primarily due to withdrawals in the Denver-Julesberg Basin, with the residential sector being the dominant natural gas consumer via home heating [*EIA*, 2017b]. The impact of oil and natural gas operations on VOC abundances and distribution, and the subsequent impact on O_3 in Northern Colorado has been the focus of a number of studies [*Abeleira et al.*, 2017a; *Gilman et al.*, 2013; *McDuffie et al.*, 2016; *Pétron et al.*, 2012; *Pétron et al.*, 2014; *Swarthout et al.*, 2013; *Thompson et al.*, 2014]. Trace gas measurement studies at the Boulder Atmospheric Observatory (BAO) in Erie, CO found that 50-66% of VOC reactivity in air masses intercepted at the site in winter, spring, and summer was due to emissions from oil and natural gas operations [*Abeleira et al.*, 2017a; *Gilman et al.*, 2013; *McDuffie et al.*, 2016; *Swarthout et al.*, 2013]. *McDuffie et al.* [2016] used a chemical box model constrained with trace gas measurements from two summers at BAO, and found that VOCs from oil and gas operations contribute 17.4% (2.9 ppbv) of the photochemical O_3 at the site, which scaled non-linearly with changes in VOCs due to the site being NO_x-limited. Projections of future

oil and gas extraction volumes are sensitive to technology developments, energy demand, and economic forces, but the U.S. Energy Information Administration predicts up to an 80% increase in domestic oil and gas extractions in the United States [*EIA*, 2017a]. Increases in VOCs and NO_x from increased oil and gas extraction in the NFR would impact O_3 production similar to increased traffic emissions. NO_x-limited areas in NFR would potentially experience higher O_3 as those areas move towards peak production, or to a higher VOC reactivity O_3 production curve (Fig 5.4. scenarios A and B). However, those changes will depend on the amount of VOCs emitted relative to NO_x.

The frequency, duration, and scale of drought and wildfires in the Western United States are predicted to increase in the future with a changing climate [*IPCC*, 2014; *Spracklen et al.*, 2009; *Westerling*, 2016]. Wildfires can emit substantial amounts of VOCs and NO_x, and lead to enhanced O_3 at sites thousands of kilometers away from the source region [e.g. *Akagi et al.*, 2011; *Andreae et al.*, 2001; *Burling et al.*, 2010; *Cook et al.*, 2007; *Jaffe et al.*, 2012; *Lindaas et al.*, 2017]. *Spracklen et al.* [2009] predict a 54% increase in mean annual burn area in the Western United States by 2050, and a larger increase of 175% in the Rocky Mountains. Enhanced O_3 precursors and O_3 abundances in the NFR have been linked to the transport of wildfire emissions through the Western United States [*Jaffe et al.*, 2008; *Lindas et al.*, 2017]. Increased VOC and NO_x emissions from wildfires would affect the regional O_3 production regimes similar to increased traffic and oil and gas emissions (Fig 5.4. scenarios A and B). Alternatively, severe and sustained drought is associated with reductions in biogenic VOC emissions [*Brilli et al.*, 2007; *Fortunati et al.*, 2008; *Guenther*, 2006]. Drought is linked to reduced isoprene emissions in the NFR, which suppresses the O_3-temperature relationship [*Abeleira et al.*, 2017a; *Abeleira et al.*, 2017b]. Increased drought in the Western United States may offset O_3 enhancement from increases in precursor emission

from other sources by reducing the availability of highly reactive biogenic VOCs. Reducing VOCs without coincident reductions in NO_x reduces O_3 production by reducing the propensity for initiating the O_3 production cycle through OH initiated VOC oxidation (Fig. 5.4 scenario D).

In Fig. 5.6 a 3 by 3 grid of measurement sites with collocated VOC, NO_x, and O_3 is proposed to cover a large portion of the Northern Front Range including the metropolitan areas of Fort Collins, Greeley, Boulder, and Denver along with the rural and suburban areas between those metropolitan sites. The sources of VOCs have been well studied in the NFR area [*Abeleira et al.*, 2017a; *Gilman et al.*, 2013; *Swarthout et al.*, 2013]. Oil and natural gas and traffic related VOCs are major contributors to the reactive carbon budget in the region [*Abeleira et al.*, 2017a; *Gilman et al.*, 2013; *Swarthout et al.*, 2013]. Oxygenated VOCs including acetone, acetaldehyde, and methyl ethyl ketone also contribute to VOC reactivity [*Abeleira et al.*, 2017a]. Although isoprene concentrations are lower in the NFR than other areas in the country, biogenic emissions can account for a large fraction of VOC reactivity during summer afternoons [*Abeleira et al.*, 2017a]. VOC measurements at the proposed sites should include;

- major oil and gas related VOCs (C_2 – C_6 alkanes, benzene, toluene)
- traffic related VOCs (ethyne, benzene, toluene, potentially other aromatics)
- oxygenated VOCs from various primary and secondary sources (acetone, acetaldehyde, methyl ethyl ketone, methyl vinyl ketone, methacrolein, formaldehyde, methanol, and ethanol)
- biogenic VOCs (isoprene, α-pinene, and β-pinene)
- wildfire markers (acetonitrile, hydrogen cyanide)

Collocated VOC, NO_x, and O_3 measurements at these sites will provide a better understanding of where these precursors are emitted, how they are transported and mixed in the region, and how

O_3 production chemistry changes throughout the region. Long-term, multi-year, measurements will provide useful insight into how different regional synoptic meteorological patterns affect the mixing of these precursors with better statistics than typical 4-8-week ground site or flight campaigns can provide. Additionally, long-term measurements will allow for the monitoring of changing precursor emissions and the impact on O_3 in the region with changes in population, traffic, energy production, oil and gas extraction and processing activities, and drought and wildfires. Long-term measurements will also provide a means to investigate the impact of current and future anthropogenic emission controls on regional O_3.

A variety of analysis approaches can be utilized with such spatially and temporally robust datasets. The 'weekend-weekday' effect is a simple analysis that takes advantage of changes in VOC and NO_x emissions on different days of the week to understand changes in O_3 and O_3 production [*Abeleira et al.*, 2017b]. Typically, in urban and downwind areas NO_x emissions decrease on weekends from a reduction in commercial trucking and a lack of a defined morning rush-hour, while VOC emissions remain relatively constant. Reductions in NO_x without concurrent reductions in VOCs can increase or decrease O_3 relative to weekdays, which provides information about the O_3 production regime in an area. Chemical box models constrained with VOC and NO_x observations provide a means to probe how different VOCs and VOC sources impact O_3 production. This allows for more targeted emission regulations on important VOCs regarding O_3 production. Additionally, chemical box models allow the user to increase or decrease input concentrations to mimic potential future emission scenarios, and predict the impact of those changing emissions. The use of source apportionment techniques such as positive matrix factorization can provide a means to monitor how different sources contribute to useful metrics such as VOC reactivity. The impact of different VOC sources likely changes spatially in the region,

and those contributions are also likely to change in the future. The combination of these analysis techniques with data collected at the proposed measurement sites will provide researchers with the necessary information to better understand the important drivers of O_3 production throughout the region.

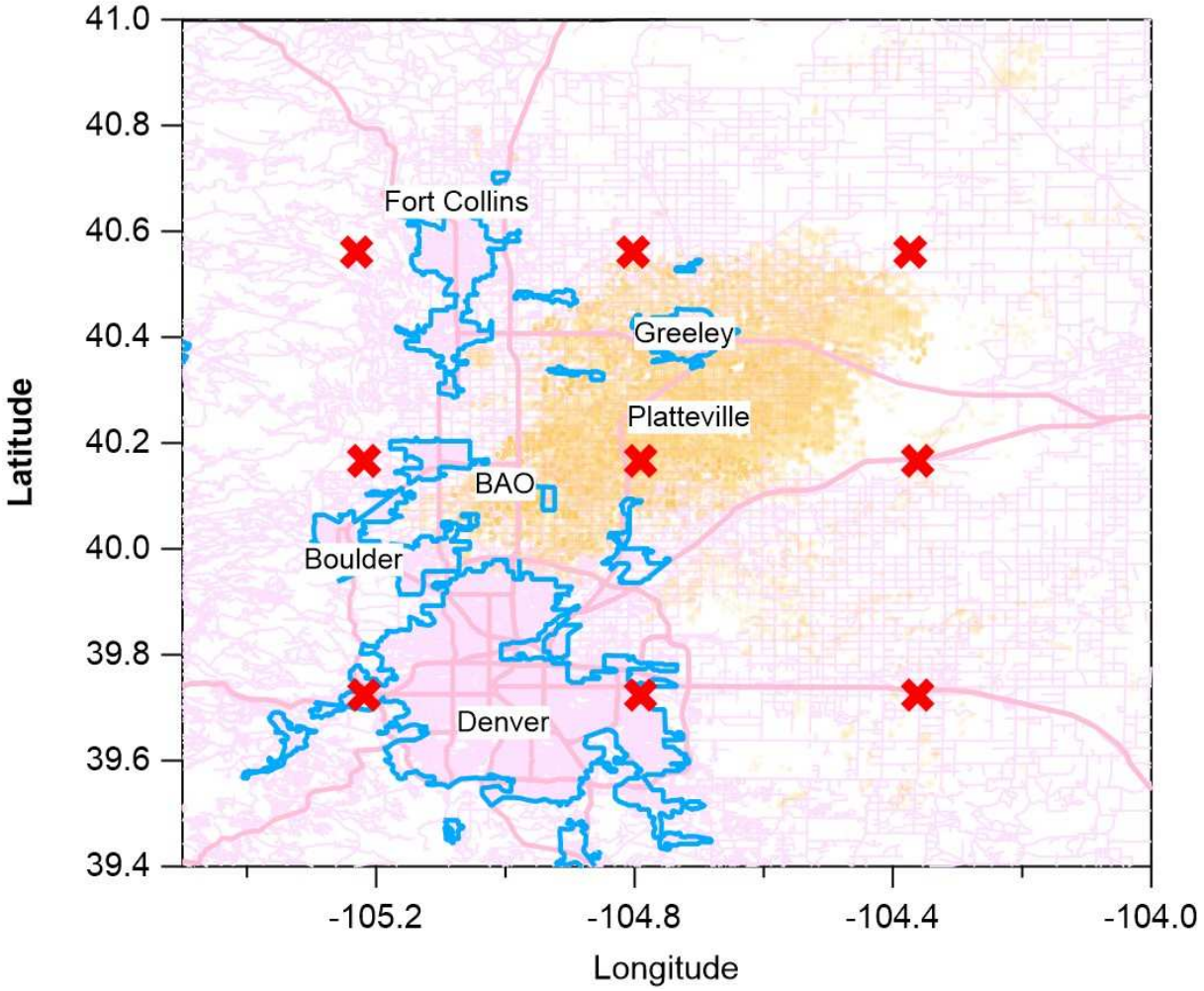

Figure 5.6. Proposed locations of long-term measurement sites with collocated VOC, NO_x, and O_3 measurements.

CHAPTER 5 REFERENCES

Abel, D., et al. (2017), Response of Power Plant Emissions to Ambient Temperature in the Eastern United States, *Environmental Science & Technology*, *51*(10), 5838-5846, doi:10.1021/acs.est.6b06201.

Abeleira, A., et al. (2017a), Source characterization of volatile organic compounds in the Colorado Northern Front Range Metropolitan Area during spring and summer 2015, *Journal of Geophysical Research: Atmospheres*, *122*(6), 3595-3613.

Abeleira, A. A., and D. K. Farmer (2017b), Summer ozone in the Northern Front Range Metropolitan Area: Weekend-weekday effects, temperature dependences and the impact of drought, *Atmos. Chem. Phys. Discuss.*, *2017*, 1-21, doi:10.5194/acp-2017-160.

Akagi, S., et al. (2011), Emission factors for open and domestic biomass burning for use in atmospheric models, *Atmospheric Chemistry and Physics*, *11*(9), 4039-4072.

Andreae, M. O., and P. Merlet (2001), Emission of trace gases and aerosols from biomass burning, *Global biogeochemical cycles*, *15*(4), 955-966.

Baier, B., et al. (2017), Higher measured than modeled ozone production at increased NOx levels in the Colorado Front Range, *Atmos. Chem. Phys. Discuss.*, *2017*, 1-29, doi:10.5194/acp-2016-1089.

Brilli, F., et al. (2007), Response of isoprene emission and carbon metabolism to drought in white poplar (Populus alba) saplings, *New Phytologist*, *175*(2), 244-254.

Burling, I., et al. (2010), Laboratory measurements of trace gas emissions from biomass burning of fuel types from the southeastern and southwestern United States, *Atmospheric Chemistry and Physics*, *10*(22), 11115-11130.

CDOT (2017), Colorado Traffic Data Explorer, edited, Colorado Department of Transportation.

CDPHE (2017), Population Totals For Colorado Counties, edited.

Colorado, S. o. (2017a), Population Projections in Colorado, edited, Colorado Information Marketplace.

Colorado, S. o. (2017b), Renewable Energy Standard, edited, Colorado Energy Office.

Cook, P. A., et al. (2007), Forest fire plumes over the North Atlantic: p-TOMCAT model simulations with aircraft and satellite measurements from the ITOP/ICARTT Campaign, *Journal of Geophysical Research: Atmospheres*, *112*(D10).

Crook, N. A., T. L. Clark, and M. W. Moncrieff (1990), The Denver cyclone. Part I: Generation in low Froude number flow, *Journal of the atmospheric sciences*, *47*(23), 2725-2742.

De Gouw, J., D. Parrish, G. Frost, and M. Trainer (2014), Reduced emissions of CO2, NOx, and SO2 from US power plants owing to switch from coal to natural gas with combined cycle technology, *Earth's Future*, *2*(2), 75-82.

Ebben, C. J., et al. (2017), Evolution of NOx in the Denver Urban Plume during the Front Range Air Pollution and Photochemistry Experiment, *Atmos. Chem. Phys. Discuss.*, *2017*, 1-13, doi:10.5194/acp-2017-671.

EIA (2016), Crude Oil Production, edited.

EIA (2017a), Annual Energy Outlook 2017 with Projections to 2050, edited by U. S. E. I. Administration.

EIA (2017b), Colorado State Profile and Energy Estimates, edited, EIA.

EIA (2017c), Number and capacity of petroleum refineries, in *Petroleum & Other Liquids*, edited.
EPA (2001), Procedures Document for National Emission Inventory, Criteria Air Pollutants 1985-1999, edited by O. o. A. Q. P. a. Standards, Researcg Triangle Park, NC.
EPA (2016), Air Pollutants Emission Trends, edited.
Fortunati, A., et al. (2008), Isoprene emission is not temperature-dependent during and after severe drought-stress: a physiological and biochemical analysis, *The Plant Journal*, *55*(4), 687-697.
Frost, G. J., et al. (2006), Effects of changing power plant NOx emissions on ozone in the eastern United States: Proof of concept, *Journal of Geophysical Research: Atmospheres*, *111*(D12), n/a-n/a, doi:10.1029/2005JD006354.
Gilman, J. B., B. M. Lerner, W. C. Kuster, and J. A. de Gouw (2013), Source signature of volatile organic compounds from oil and natural gas operations in northeastern Colorado, *Environ Sci Technol*, *47*(3), 1297-1305, doi:10.1021/es304119a.
Goetz, A. (2013), Suburban sprawl or urban centres: Tensions and contradictions of smart growth approaches in Denver, Colorado, *Urban Studies*, *50*(11), 2178-2195.
Guenther, A. (2006), Estimates of global terrestrial isoprene emissions using MEGAN (Model of Emissions of Gases and Aerosols from Nature), *Atmospheric Chemistry and Physics*, *6*.
Haagenson, P. L. (1979), Meteorological and climatological factors affecting Denver air quality, *Atmospheric Environment (1967)*, *13*(1), 79-85.
IPCC (2014), Climate Change 2014–Impacts, Adaptation and Vulnerability: Regional Aspects, edited by I. P. o. C. Change, Cambridge University Press.
Jaffe, D., et al. (2008), Influence of fires on O3 concentrations in the western US, *Environmental science & technology*, *42*(16), 5885-5891.
Jaffe, D. A., and N. L. Wigder (2012), Ozone production from wildfires: A critical review, *Atmospheric Environment*, *51*, 1-10.
Kaser, L., et al. (2017), The effect of entrainment through atmospheric boundary layer growth on observed and modeled surface ozone in the Colorado Front Range, *Journal of Geophysical Research: Atmospheres*, *122*(11), 6075-6093, doi:10.1002/2016JD026245.
Kim, S. W., et al. (2006), Satellite-observed U.S. power plant NOx emission reductions and their impact on air quality, *Geophysical Research Letters*, *33*(22), n/a-n/a, doi:10.1029/2006GL027749.
Lindaas, J., et al. (2017), Changes in ozone and precursors during two aged wildfire smoke events in the Colorado Front Range in summer 2015, *Atmos. Chem. Phys.*, *17*(17), 10691-10707, doi:10.5194/acp-17-10691-2017.
Lindas, J., et al. (2017), The impact of aged wildfire smoke on atmospheric composition and ozone in the Colorado Front Range in summer 2015, *Atmospheric Chemistry and Physics*, *in preparation*.
McDuffie, E. E., et al. (2016), Influence of oil and gas emissions on summertime ozone in the Colorado Northern Front Range, *Journal of Geophysical Research: Atmospheres*, *121*(14), 8712-8729.
Pendall, R., M. Weir, and C. Narducci (2013), Governance and the geography of poverty: Why does suburbanization matter, *MacArthur Foundation Network on Building Resilient Regions*, 5.

Pétron, G., et al. (2012), Hydrocarbon emissions characterization in the Colorado Front Range: A pilot study, *Journal of Geophysical Research: Atmospheres*, *117*(D4), n/a-n/a, doi:10.1029/2011jd016360.

Pétron, G., et al. (2014), A new look at methane and nonmethane hydrocarbon emissions from oil and natural gas operations in the Colorado Denver-Julesburg Basin, *Journal of Geophysical Research: Atmospheres*, *119*(11), 6836-6852.

Reddy, P. J., and G. G. Pfister (2016), Meteorological factors contributing to the interannual variability of mid-summer surface ozone in Colorado, Utah, and other western US states, *Journal of Geophysical Research: Atmospheres*.

Schroeder, J. R., et al. (2017), New insights into the column CH2O/NO2 ratio as an indicator of near-surface ozone sensitivity, *Journal of Geophysical Research: Atmospheres*, *122*(16), 8885-8907, doi:10.1002/2017JD026781.

Spracklen, D. V., et al. (2009), Impacts of climate change from 2000 to 2050 on wildfire activity and carbonaceous aerosol concentrations in the western United States, *Journal of Geophysical Research: Atmospheres*, *114*(D20), n/a-n/a, doi:10.1029/2008JD010966.

Swarthout, R. F., et al. (2013), Volatile organic compound distributions during the NACHTT campaign at the Boulder Atmospheric Observatory: Influence of urban and natural gas sources, *Journal of Geophysical Research: Atmospheres*, *118*(18), 10,614-610,637, doi:10.1002/jgrd.50722.

Thompson, C. R., J. Hueber, and D. Helmig (2014), Influence of oil and gas emissions on ambient atmospheric non-methane hydrocarbons in residential areas of Northeastern Colorado, *Elementa: Science of the Anthropocene*, *2*, 000035, doi:10.12952/journal.elementa.000035.

Toth, J. J., and R. H. Johnson (1985), Summer surface flow characteristics over northeast Colorado, *Monthly weather review*, *113*(9), 1458-1469.

U.S.-Census (2016), Quick Facts - Colorado, edited.

Vu, K. T., et al. (2016), Impacts of the Denver Cyclone on regional air quality and aerosol formation in the Colorado Front Range during FRAPPÉ 2014, *Atmos. Chem. Phys.*, *16*(18), 12039-12058, doi:10.5194/acp-16-12039-2016.

Westerling, A. L. (2016), Increasing western US forest wildfire activity: sensitivity to changes in the timing of spring, *Philosophical Transactions of the Royal Society B: Biological Sciences*, *371*(1696), doi:10.1098/rstb.2015.0178.

APPENDIX 1 – CHAPTER 3 SUPPLEMENTAL INFORMATION (A1)

Text A1.1. Q/Q_{exp}, FPEAK, and Bootstrapping Investigation.

Although a global minimum solution is usually reached with the PMF least-squares fitting process, it is not necessarily a unique solution. Varying the FPEAK parameter allows one to investigate the rotational ambiguity of a particular PMF solution, which is inherent to this type of factor analysis. We explored an FPEAK range of ±3 for both datasets. In the spring PMF analysis, Q/Q_{exp} was very stable (range of 2.47 to 2.51, RSD < 1%) across an FPEAK range of ± 1. A sharp rise in Q/Q_{exp} occurred at FPEAK > 1, and a gradual rise in Q/Q_{exp} occurred at FPEAK < -1 (sharp increase at FPEAK <-2). The summer PMF analysis resulted in similar FPEAK dependencies. Within an FPEAK range of ± 1, Q/Q_{exp} was stable (5.85 to 5.88, RSD < 1%). At FPEAK <-1.6, the PMF algorithm fails to converge. As FPEAK is increased above 1.4, Q/Q_{exp} increases slowly. We chose PMF solutions for both seasons at FPEAK = 1 based on previous studies, in which the largest positive FPEAK value prior to a large increase in Q/Q_{exp} generally represents the most realistic solution.

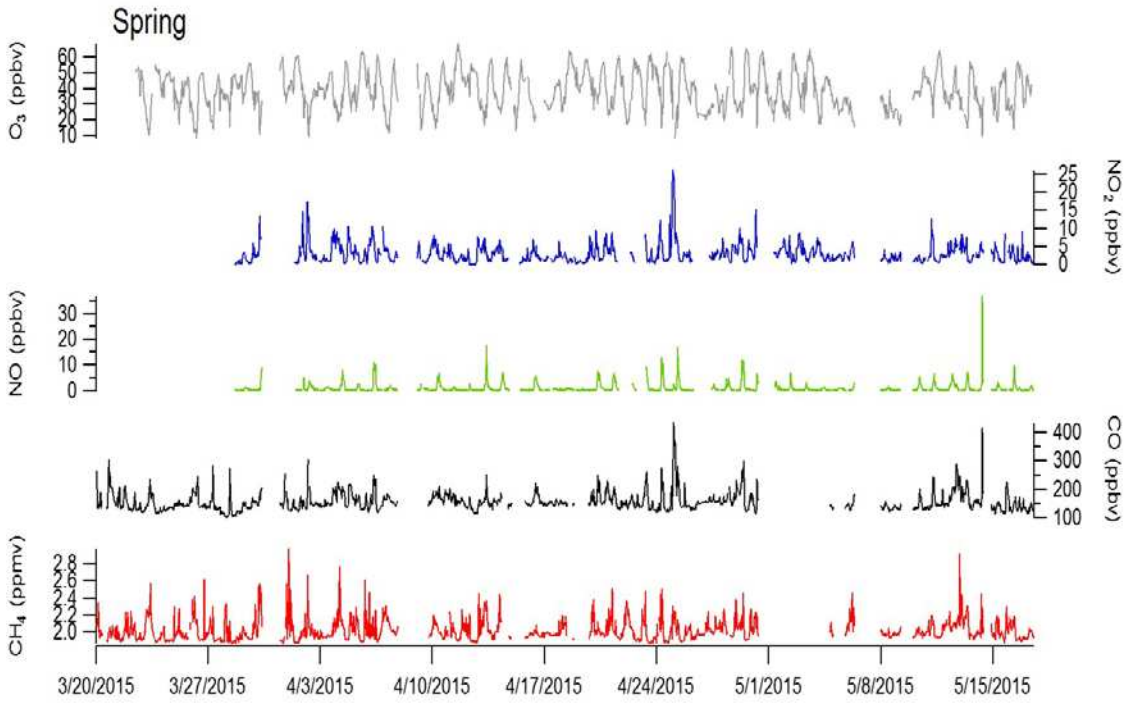

Figure A1.1. Spring (20 March 2015 – 17 May 2015) time-series for CH_4 (red), CO (black), NO (green), NO_2 (blue) and O_3 (grey) averaged to ± 2 minutes around each VOC sampling point timestamp.

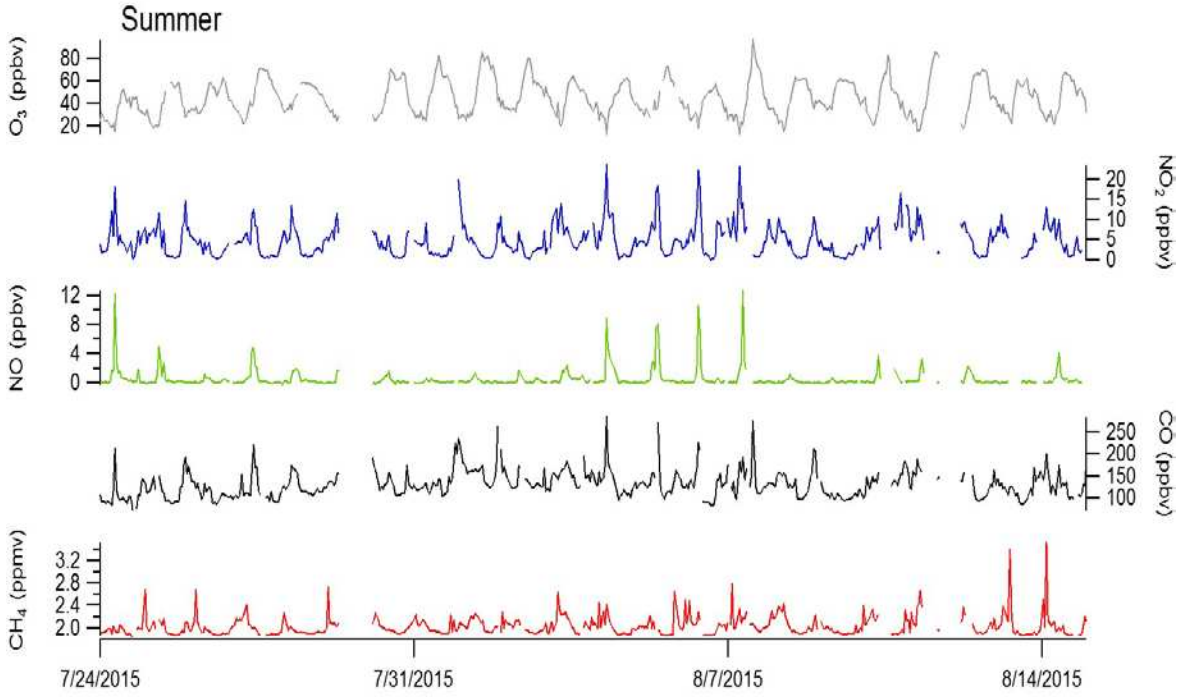

Figure A1.2. Summer (24 July 2015 – 14 August 2015) time-series for CH_4 (red), CO (black), NO (green), NO_2 (blue) and O_3 (grey) averaged to ± 2 minutes around each VOC sampling point timestamp.

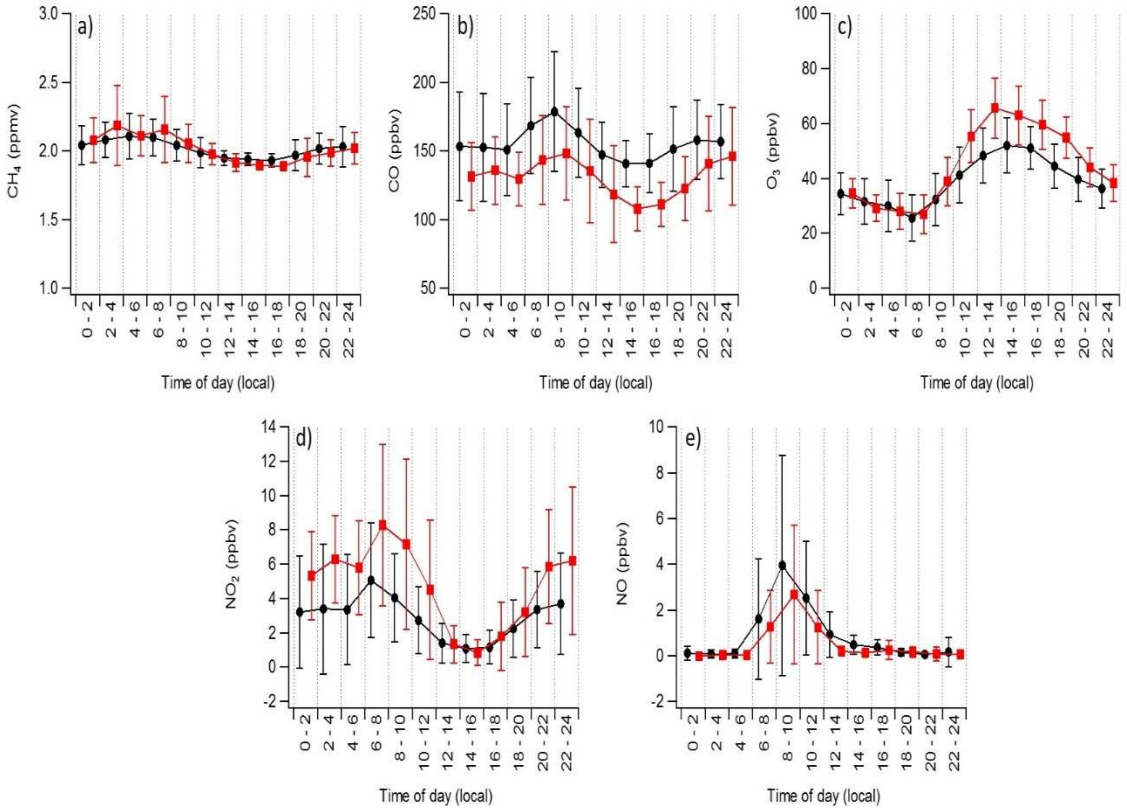

Figure A1.3. Diel cycles of (a) CH_4, (b) CO, (c) O_3, (d) NO_2, and (e) NO_2 for spring (black circles, 20 March 2015 – 17 May 2015) and summer (red squares, 24 July 2015 – 14 August 2015) binned by two hours. Stacked plots are slightly offset on the x-axis for viewing purposes. Error bars represent ± 1 standard deviation of bin means.

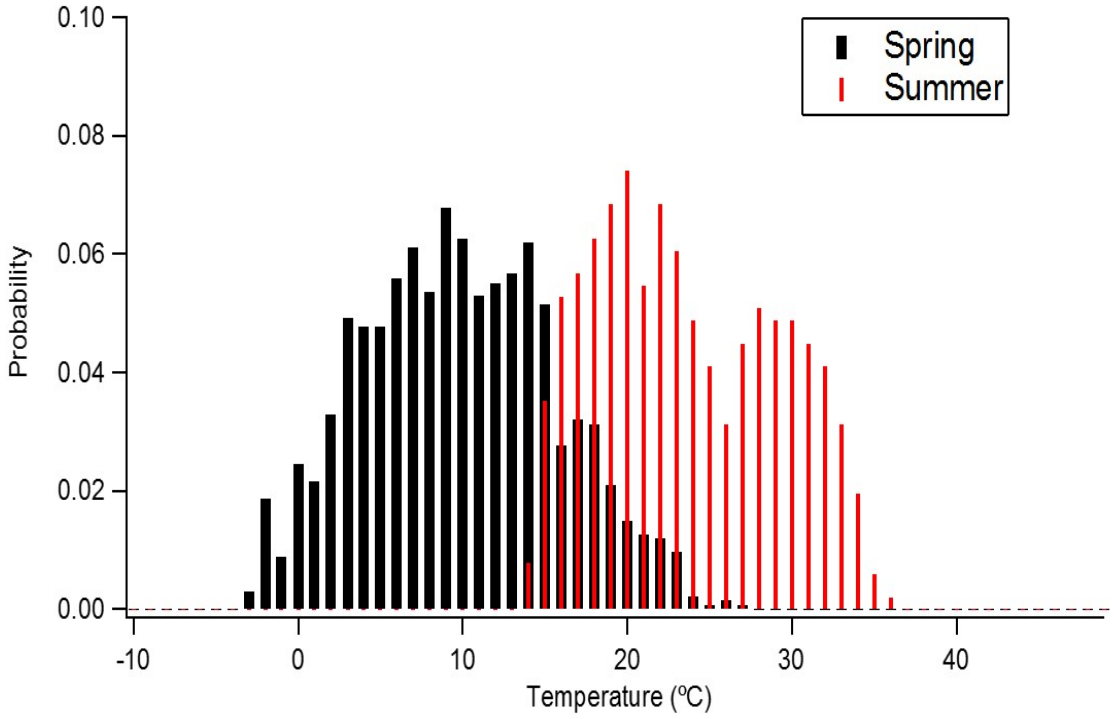

Figure A1.4. Histogram of spring (black, 20 March - 17 May 2015) and summer (red, 24 July 2015 – 14 August 2015) ambient air temperatures (10 m a.g.l) at the BAO site.

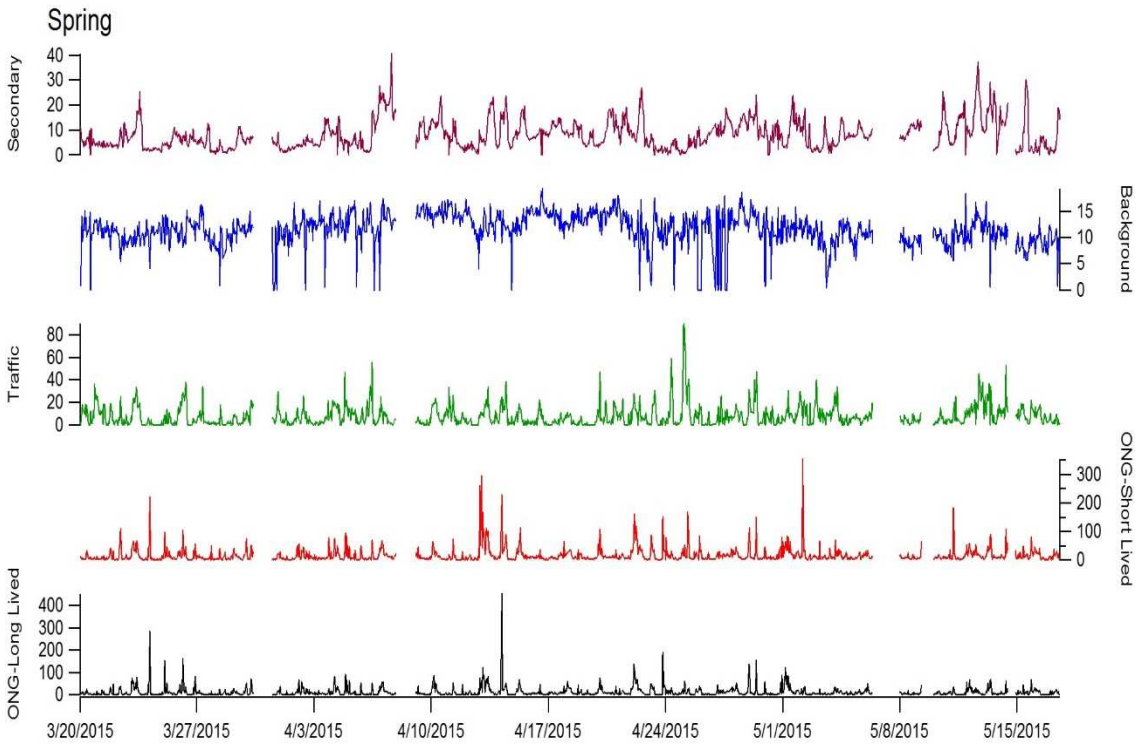

Figure A1.5. Spring (20 March 2015 – 17 May 2015) time-series for PMF factors: ONG-Short Lived (black), ONG-Long Lived (red), Traffic (green), Background (blue), and Secondary (purple).

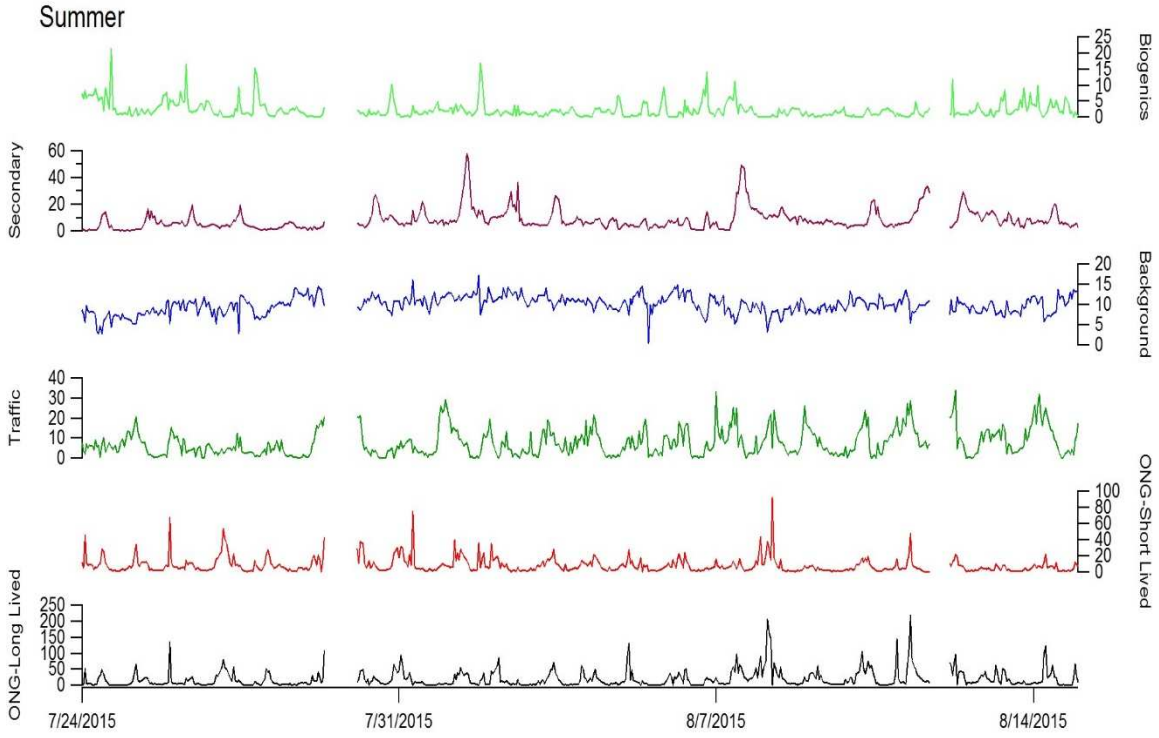

Figure A1.6. Summer (24 July 2015 – 14 August 2015) time-series for PMF factors: ONG-Short Lived (black), ONG-Long Lived (red), Traffic (green), Background (blue), Secondary (purple), and Biogenics (lime green).

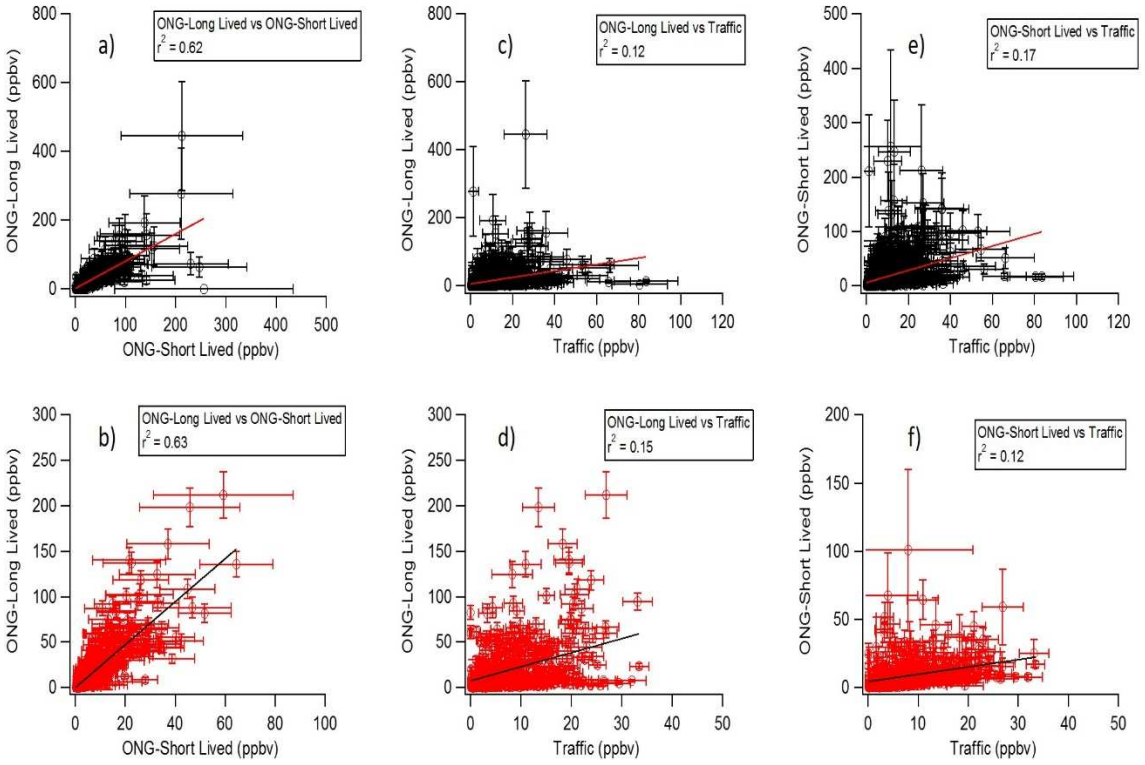

Figure A1.7. Correlations of ONG-Short-Lived Vs ONG-Long-Lived factors for (a) spring (black, 20 March 2015 – 17 May 2015) and (b) summer (red, 24 July 2015 – 14 August 2015), ONG-Short Lived Vs Traffic (c) spring and (d) summer, and ONG-Long Lived vs Traffic (e) spring and (f) summer. Error bars represent ± 1 standard deviation from mean of bootstrapping analysis.

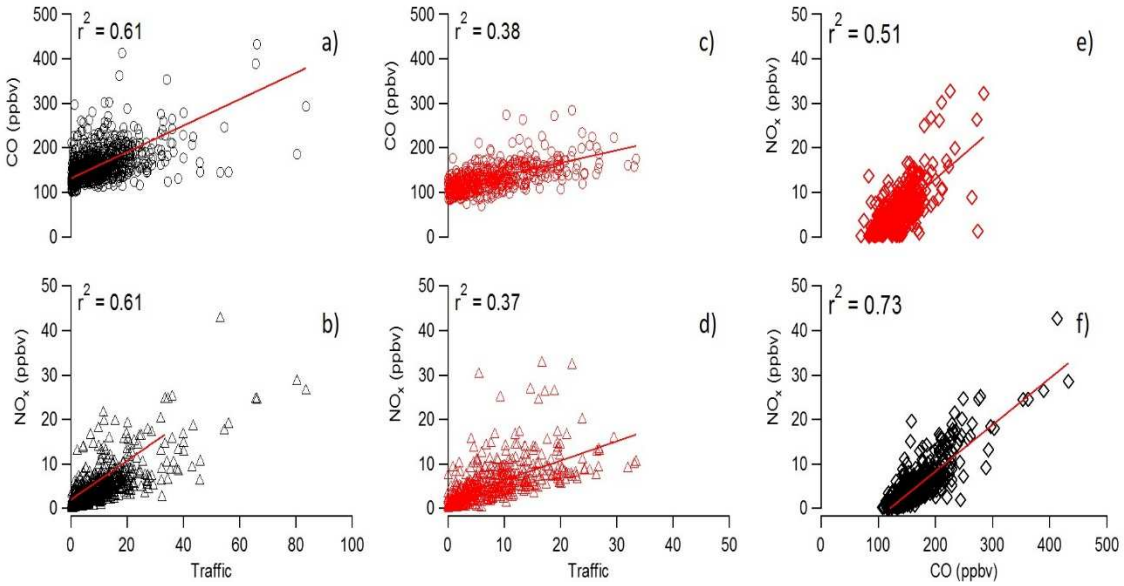

Figure A1.8. a) Correlations between (a) CO and (b) NO_x and the Traffic factor for spring (20 March 2015 – 17 May 2015). Correlations between (c) CO and (d) NO_x and the Traffic factor for summer (24 July 2015 – 14 August 2015). Correlations between NO_x and CO for (e) summer and (f) spring.

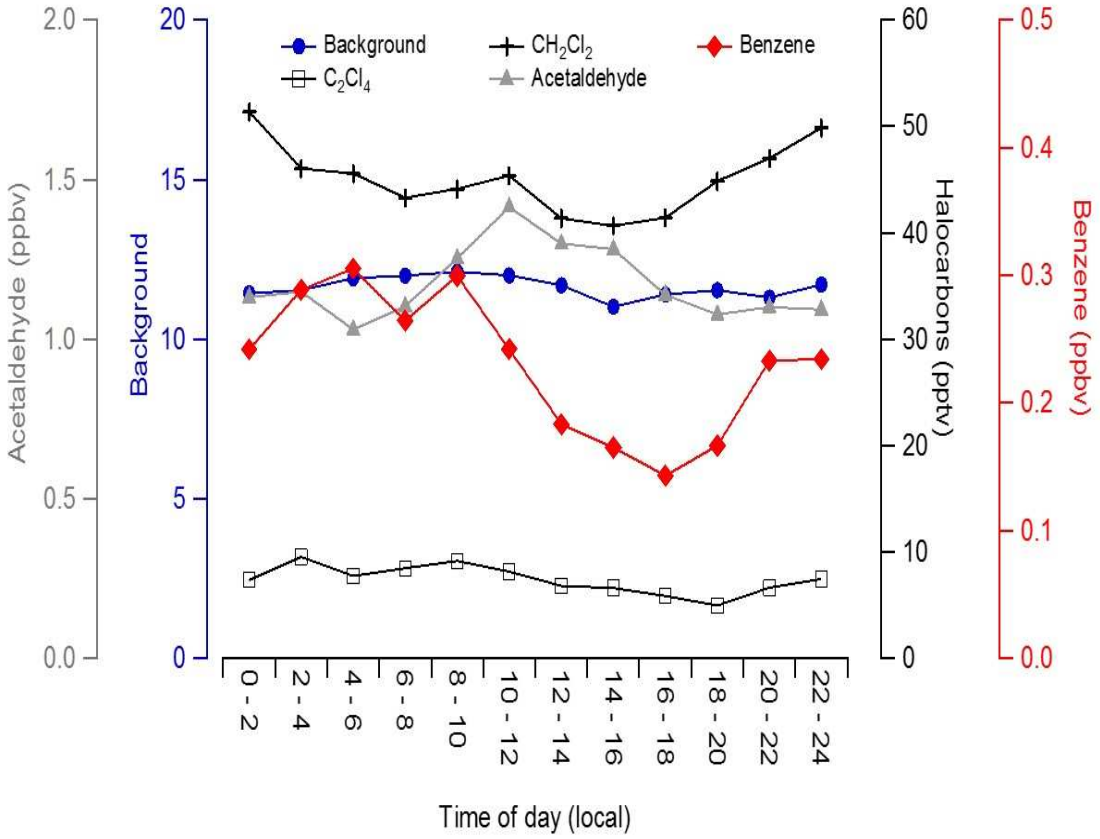

Figure A1.9. Diel cycles with 2-hour time bins of the spring Background factor with major contributors to the Background factor (Acetaldehyde, CH_2Cl_2, $C2_2Cl_4$, and Benzene).

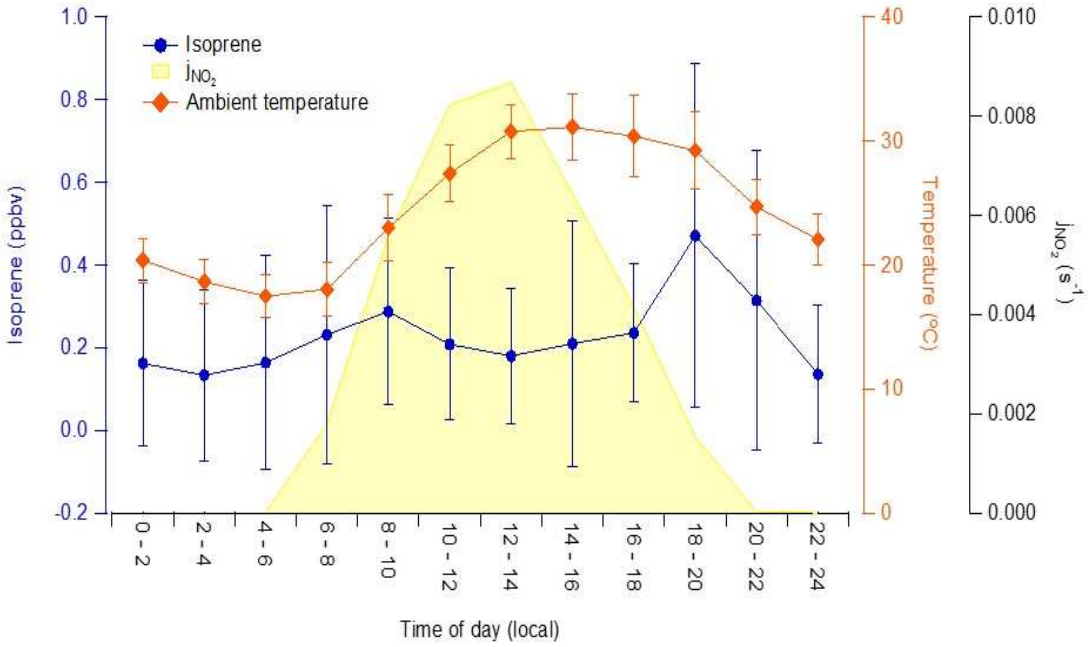

Figure A1.10. Average diel cycles of isoprene (blue circles) and temperature (red diamonds) for summer (24 July 2015 – 14 August 2015). Isoprene was measured hourly with an online GC system. Error bars represent plus/minus one standard deviation for each two-hour time bin. NO_2 photolysis rates (j_{NO2}) was measured during the previous summer (2014) at the BAO site by the National Center for Atmospheric Research using a CCD Actinic Flux Spectroradiometer. These photolysis rates provide a proxy for diel profiles in photon flux at the site.

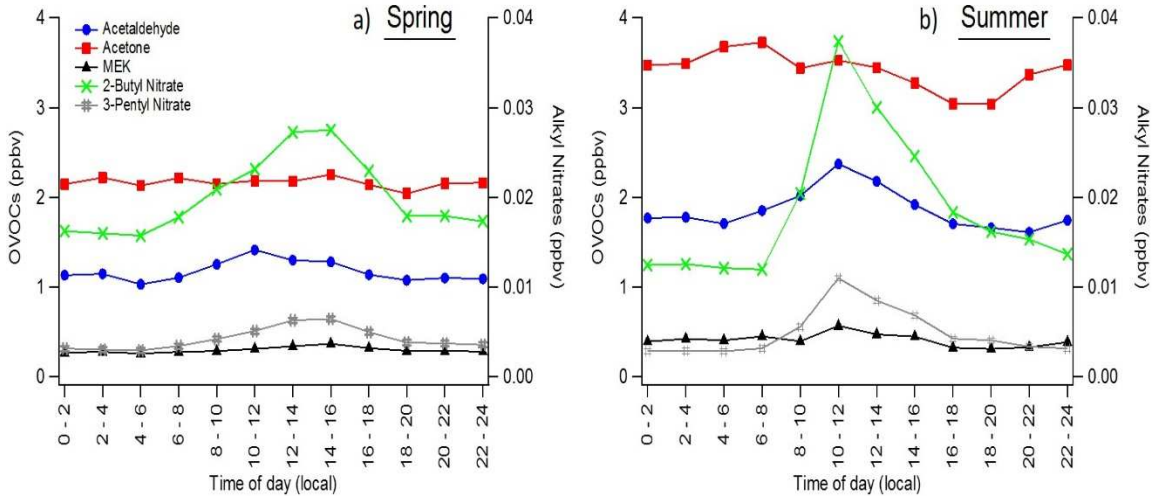

Figure A1.11. Diel cycles of measured OVOCs, 2-butyl nitrate, and 3-pentyl nitrate for (a) spring (20 March 2015 – 17 May 2015) and (b) summer (24 July 2015 – 14 August 2015) with two-hour binning.

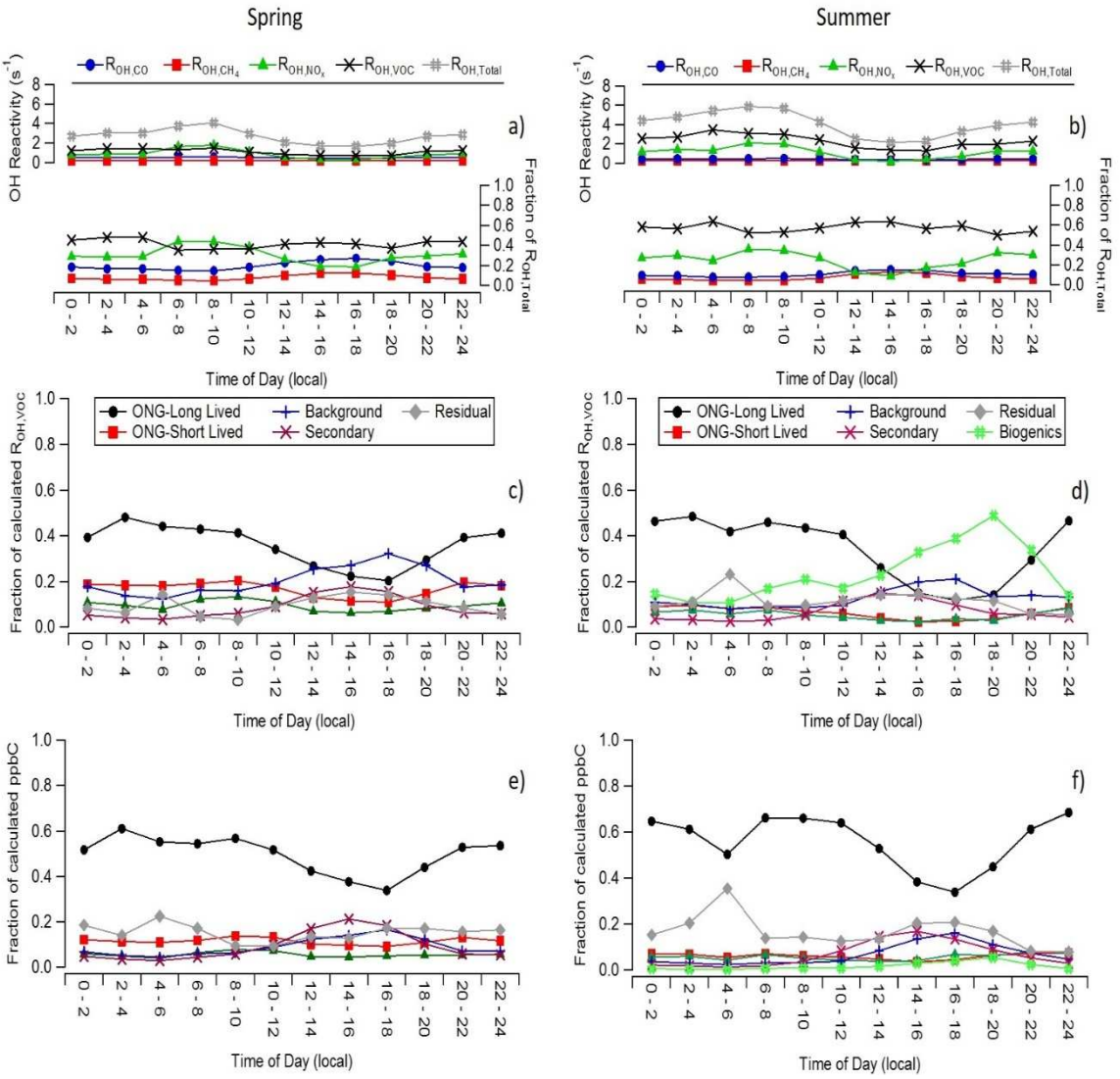

Figure A1.12. The top row shows diel cycles of calculated OH Reactivity ($R_{OH,Total}$, s^{-1}) for the (a) spring (20 March 2015 – 17 May 2015) and (b) summer (24 July 2015 – 14 August 2015). Each major contributor to total calculated OH reactivity ($R_{OH,X}$: X = VOCs, NO_x, CO, or CH_4) is shown stacked in a separate color. Figures c – f show the contributions from each PMF factor to the calculated VOC reactivity ($R_{OH,VOC}$, s^{-1}) and calculated carbon mixing ratio as a diel cycles. $R_{OH,Total}$ and $R_{OH,X}$ were calculated using E1, E2, and E3 described in the introduction. The rate constants ($k_{OH,X}$) of trace gases and VOCs were adjusted for ambient temperature and pressure (see references in Table 1). For each factor the mixing ratio of each measured compound was reconstructed. The VOC reactivity contribution of each compound for each factor was determined from the PMF factor mixing ratio reconstructions and the temperature and pressure adjusted rate constant with OH. The contribution of each PMF factor to organic carbon mixing ratio (ppbC) is summarized in as diel cycles (e, f).

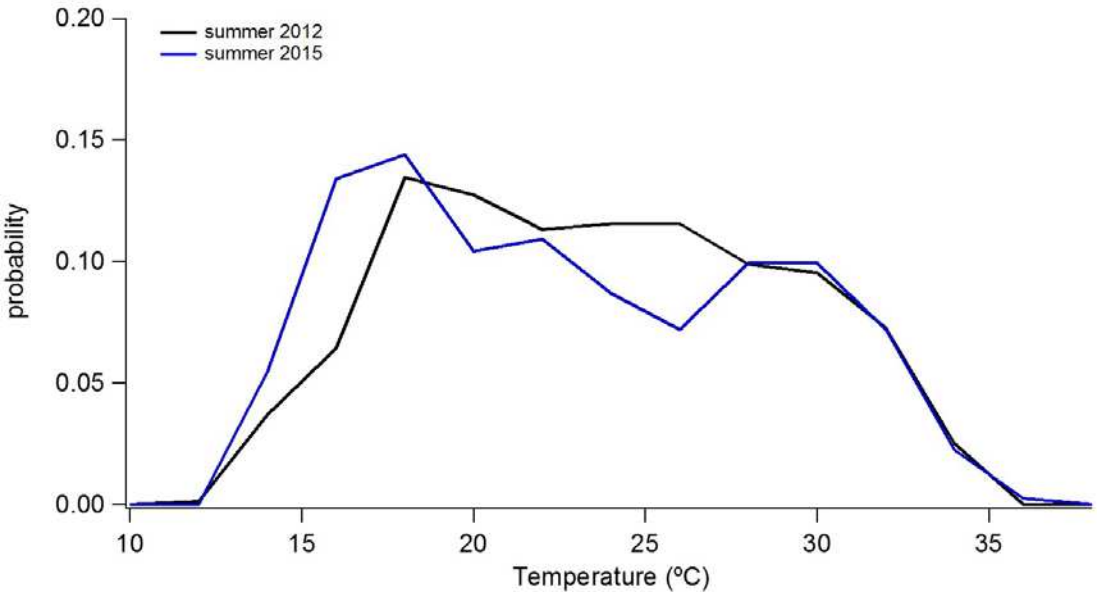

Figure A1.13. Histogram of ambient sampling temperatures for 7/26 – 8/12 for summer 2012 (black) and summer 2015 (blue).

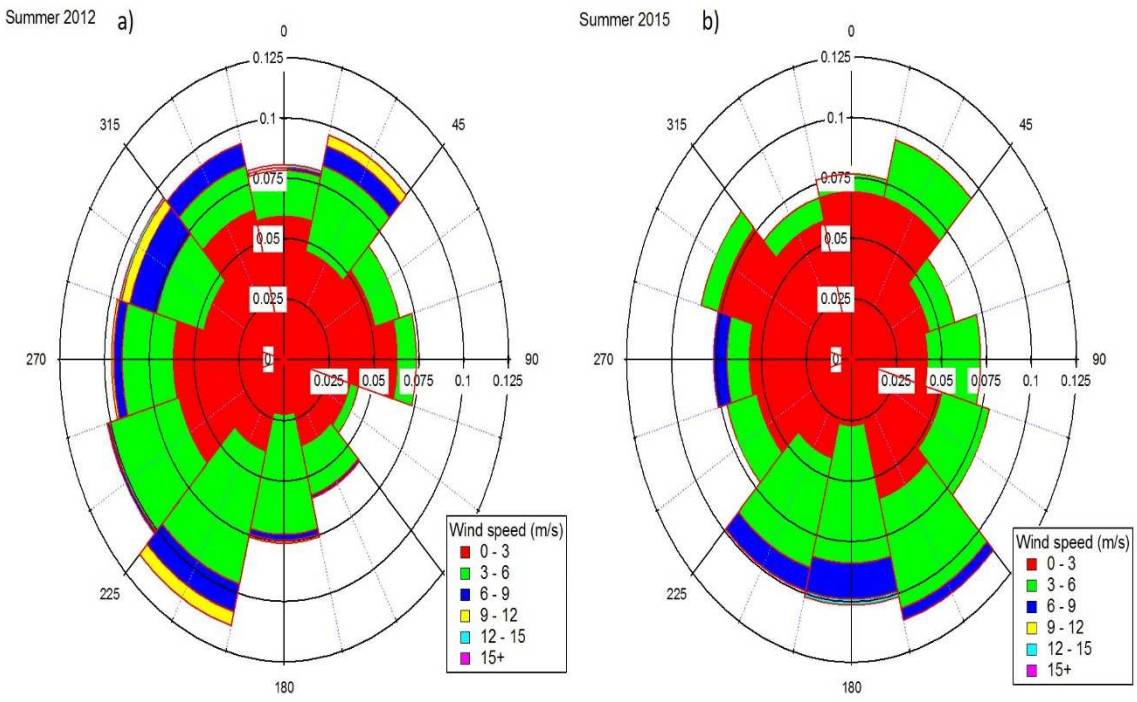

Figure A1.14. Histogram of ambient sampling temperatures for 7/26 – 8/12 for summer 2012 (black) and summer 2015 (blue).

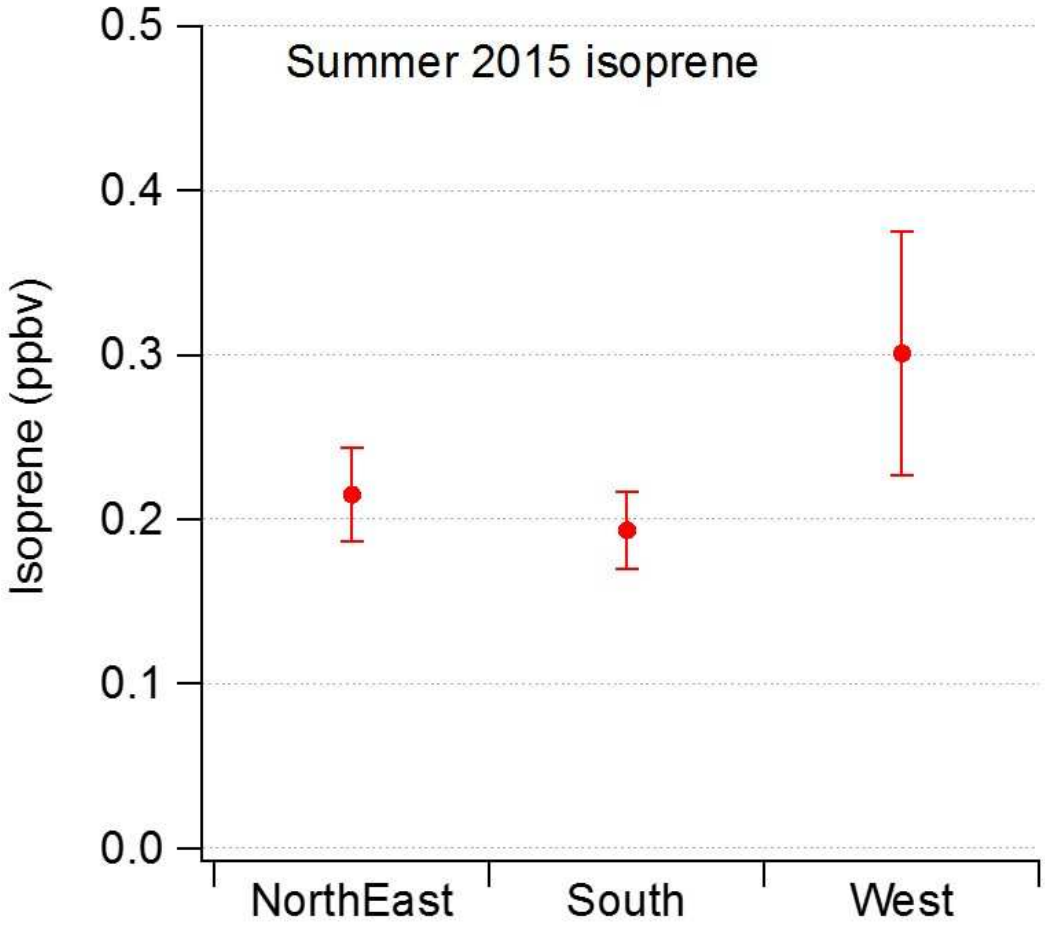

Figure A1.15. Wind enhancement plot for isoprene summer 2015.

Table A1.1. - Continued. Summary of statistics for spring and summer 2015 mixing ratios and OH reactivity at the BAO site

Spring							
	Mixing Ratios (ppb_v)[a]		$R_{OH,VOC}$ (s^{-1})[a]				
Compound	Max	Average	Max	Average	$k_{OH,VOC}$[b]	Ref[c]	LOD (ppb_v)
Ethane	443	16 (22)	1.95	0.07 (0.10)	0.25	a	0.008
Propane	205	9 (13)	4.3	0.2 (0.3)	1.09	a	0.01
i-Butane	28	1 (1)	1.37	0.04 (0.07)	2.1	a	0.007
n-Butane	59	2 (3)	2.8	0.1 (0.2)	2.4	a	0.005
i-Pentane	62	1 (3)	5.1	0.1 (0.2)	3.6	a	0.003
n-Pentane	49	1 (2)	3.7	0.1 (0.2)	3.8	a	0.003
n-Hexane	6.5	0.2 (0.3)	0.68	0.02 (0.03)	5.2	a	0.004
Cyclohexane	4.2	0.2 (0.3)	0.6	0.03 (0.04)	7	a	0.02
2,3-dimethylpentane	2	0.1 (0.1)	0.3	0.02 (0.02)	7	c	0.02
2-methylhexane	0.61	0.04 (0.05)	0.092	0.006 (0.008)	7	c	0.02
3-methylhexane	2.5	0.1 (0.2)	0.38	0.02 (0.03)	7	c	0.02
n-Heptane	2.3	0.1 (0.2)	0.32	0.02 (0.03)	6.76	a	0.01
Methylcyclohexane	4	0.2 (0.3)	0.81	0.05 (0.07)	9.6	a	0.02
2,2,4-trimethylpentane	0.63	0.05 (0.07)	0.042	0.004 (0.004)	3.34	a	0.02
2,2,3-trimethylpentane	0.34	0.02 (0.03)	0.048	0.003 (0.005)	6.6	a	0.02
2-Methylheptane	1.02	0.07 (0.09)	0.19	0.01 (0.02)	9	c	0.02
3-Methylheptane	0.58	0.04 (0.05)	0.109	0.007 (0.010)	9	c	0.01
n-Octane	1.06	0.06 (0.08)	0.18	0.01 (0.01)	8.11	a	0.02
Ethene	2.11	0.04 (0.01)	0.45	0.01 (0.02)	8.5	a	0.003
Propene	0.49	0.01 (0.02)	0.33	0.005 (0.009)	26.3	a	0.01
cis-2-Butene	0.19	0.01 (0.01)	0.25	0.01 (0.02)	56.4	a	0.004
Isoprene					100	a	0.01
Benzene	2.3	0.2 (0.2)	0.059	0.006 (0.005)	1.22	a	0.03
Toluene	2.5	0.3 (0.3)	0.21	0.02 (0.02)	5.63	a	0.02
Ethylbenzene	0.58	0.03 (0.05)	0.085	0.005 (0.007)	7	a	0.01
ortho-Xylene	0.35	0.03 (0.04)	0.1	0.01 (0.01)	13.6	a	0.01
Ethyne	2.3	0.2 (0.1)	0.044	0.004 (0.003)	0.87	d	0.006
Acetaldehyde	4.9	1.2 (0.5)	1.2	0.3 (0.1)	15	a	0.08
Acetone	5.9	2.2 (0.7)	0.021	0.008 (0.002)	0.17	a	0.1
Methyl ethyl ketone	1.6	0.3 (0.2)	0.04	0.008 (0.004)	1.22	a	0.06

(a) Standard deviation of averages reported in parentheses

(b) Units of $k_{OH,VOC}$: 10^{-12} cm^3 $molec^{-1}$ s^{-1}

(c) References for $k_{OH,VOC}$: (a) Atkinson et al. [2003], (b) Rosen et al. [2004], (c) Farmer et al. [2011], (d) Atkinson [1986], (e) Sander et al. [2015], (f) Atkinson et al. [2001]

Table A1.1. - Continued. Summary of statistics for spring and summer 2015 mixing ratios and OH reactivity at the BAO site.

	Spring						
	Mixing Ratios (ppb_v)[a]		$R_{OH,VOC}$ (s^{-1})[a]				
Compound	Max	Average	Max	Average	$k_{OH,VOC}$[b]	Ref[c]	LOD (ppb_v)
$CFCl_3$	0.41	0.25 (0.03)	$5.5x10^{-16}$	$9x10^{-17}$ ($7x10^{-17}$)	$1x10^{-13}$	e	$7x10^{-5}$
CCl_2FCClF_2	0.102	0.076 (0.006)	$6.6x10^{-7}$	$4.9x10^{-7}$ ($4x10^{-8}$)	0.0003	e	$2x10^{-4}$
CH_2Cl_2	0.25	0.05 (0.02)	$5.1x10^{-4}$	9x10-5 (4x10-5)	0.1	e	0.006
$CHCl_3$	0.031	0.010 (0.002)	$6.1x10^{-5}$	$1.6x10^{-5}$ ($5x10^{-6}$)	0.001	f	$2x10^{-4}$
CH_2Br_2	0.008	0.002 (0.001)	$1.9x10^{-5}$	$4.3x10^{-5}$ ($2x10^{-6}$)	0.12	e	$6x10^{-5}$
$CHBrCl_2$	0.0043	$5x10^{-4}$ ($3x10^{-4}$)	$1.5x10^{-5}$	$2x10^{-6}$ ($1x10^{-6}$)	0.17	e	$2x10^{-5}$
C_2Cl_4	0.093	0.007 (0.006)	$3.5x10^{-4}$	$3x10^{-5}$ ($2x10^{-5}$)	0.17	f	$7x10^{-5}$
Methylnitrate	0.012	0.004 (0.001)	$5x10^{-6}$	$2x10^{-6}$ ($1x10^{-6}$)	0.023	a	$2x10^{-4}$
Ethylnitrate	0.011	0.004 (0.001)	$4x10^{-5}$	$1x10^{-5}$ ($1x10^{-5}$)	0.018	a	$4x10^{-4}$
2-Propylnitrate	0.048	0.013 (0.006)	$2.9x10^{-4}$	$8x10^{-5}$ ($4x10^{-5}$)	0.029	a	$2x10^{-4}$
1-Propylnitrate	0.008	0.002 (0.001)	$9x10^{-5}$	$2x10^{-5}$ (1x10-5)	0.58	a	$8x10^{-4}$
2-Butylnitrate	0.11	0.02 (0.01)	0.002	$4x10^{-4}$ ($3x10^{-4}$)	0.86	a	$5x10^{-4}$
3-Pentylnitrate	0.032	0.004 (0.004)	$6.9x10^{-4}$	$9x10^{-5}$ ($8x10^{-5}$)	1	a	$2x10^{-4}$
2-Pentylnitrate	0.04	0.006 (0.005)	0.0015	$2x10^{-4}$ ($2x10^{-4}$)	1.7	a	2x10-4

(a) Standard deviation of averages reported in parentheses

(b) Units of $k_{OH,VOC}$: 10^{-12} cm^3 $molec^{-1}$ s^{-1}

(c) References for $k_{OH,VOC}$: (a) Atkinson et al. [2003], (b) Rosen et al. [2004], (c) Farmer et al. [2011], (d) Atkinson [1986], (e) Sander et al. [2015], (f) Atkinson et al. [2001]

Table A1.1. - Continued. Summary of statistics for spring and summer 2015 mixing ratios and OH reactivity at the BAO site.

Summer							
	Mixing Ratios (ppb_v)[a]		$R_{OH,VOC}$ (s^{-1})[a]				
Compound	Max	Average	Max	Average	$k_{OH,VOC}$[b]	Ref[c]	LOD (ppb_v)
Ethane	338	23 (33)	1.6	0.1 (0.2)	0.25	a	0.008
Propane	149	8 (11)	3.2	0.2 (0.2)	1.09	a	0.01
i-Butane	14	2 (2)	0.68	0.07 (0.09)	2.1	a	0.007
n-Butane	78	4 (6)	3.7	0.2 (0.3)	2.4	a	0.005
i-Pentane	82	3 (5)	6.8	0.2 (0.4)	3.6	a	0.003
n-Pentane	82	3 (5)	6.3	0.2 (0.4)	3.8	a	0.003
n-Hexane	6.8	0.4 (0.5)	0.72	0.04 (0.05)	5.2	a	0.004
Cyclohexane	2.2	0.2 (0.2)	0.31	0.03 (0.03)	7	a	0.02
2,3-dimethylpentane	0.76	0.09 (0.09)	0.11	0.01 (0.01)	7	c	0.02
2-methylhexane	0.72	0.09 (0.09)	0.11	0.01 (0.01)	7	c	0.02
3-methylhexane	1.3	0.1 (0.1)	0.19	0.01 (0.02)	7	c	0.02
n-Heptane	1.5	0.1 (0.2)	0.21	0.02 (0.02)	6.76	a	0.01
Methylcyclohexane	2.3	0.2 (0.2)	0.47	0.04 (0.05)	9.6	a	0.02
2,2,4-trimethylpentane	0.66	0.06 (0.06)	0.044	0.004 (0.004)	3.34	a	0.02
2,2,3-trimethylpentane	0.55	0.03 (0.04)	0.075	0.004 (0.006)	6.6	a	0.02
2-Methylheptane	0.54	0.04 (0.05)	0.097	0.008 (0.009)	9	c	0.02
3-Methylheptane	0.56	0.06 (0.07)	0.11	0.01 (0.01)	9	c	0.01
n-Octane	0.54	0.06 (0.07)	0.09	0.01 (0.01)	8.11	a	0.02
Ethene	1.9	0.3 (0.2)	0.36	0.05 (0.04)	8.5	a	0.003
Propene	0.41	0.05 (0.04)	0.23	0.03 (0.02)	26.3	a	0.01
cis-2-Butene	0.35	0.02 (0.03)	0.42	0.03 (0.04)	56.4	a	0.004
Isoprene	2	0.2 (0.3)	4	0.5 (0.5)	100	a	0.01
Benzene	1.1	0.2 (0.1)	0.028	0.004 (0.003)	1.22	a	0.03
Toluene	1.5	0.3 (0.2)	0.12	0.02 (0.02)	5.63	a	0.02
Ethylbenzene	0.95	0.04 (0.05)	0.132	0.005 (0.008)	7	a	0.01
ortho-Xylene	0.47	0.05 (0.05)	0.13	0.01 (0.01)	13.6	a	0.01
Ethyne	2.1	0.2 (0.2)	0.036	0.004 (0.003)	0.87	d	0.006
Acetaldehyde	5.7	1.9 (0.6)	1.3	0.4 (0.1)	15	a	0.08
Acetone	8	3 (1)	0.026	0.001 (0.004)	0.17	a	0.1
Methyl ethyl ketone	2.5	0.4 (0.3)	0.063	0.010 (0.006)	1.22	a	0.06

(a) Standard deviation of averages reported in parentheses

(b) Units of $k_{OH,VOC}$: 10^{-12} cm^3 $molec^{-1}$ s^{-1}

(c) References for $k_{OH,VOC}$: (a) Atkinson et al. [2003], (b) Rosen et al. [2004], (c) Farmer et al. [2011], (d) Atkinson [1986], (e) Sander et al. [2015], (f) Atkinson et al. [2001]

Table A1.1. - Continued. Summary of statistics for spring and summer 2015 mixing ratios and OH reactivity at the BAO site.

Summer							
	Mixing Ratios (ppb_v)[a]		$R_{OH,VOC}$ (s^{-1})[a]				
Compound	Max	Average	Max	Average	$k_{OH,VOC}$[b]	Ref[c]	LOD (ppb_v)
$CFCl_3$	0.36	0.20 (0.02)	$1.0x10^{-15}$	$3x10^{-16}$ ($2x10^{-16}$)	$1x10^{-13}$	e	$7x10^{-5}$
CCl_2FCClF_2	0.111	0.061 (0.007)	$6.8x10^{-7}$	$3.7x10^{-7}$ ($4x10^{-8}$)	0.0003	e	$2x10^{-4}$
CH_2Cl_2	1.84	0.04 (0.09)	0.0039	$1x10^{-4}$ ($2x10^{-4}$)	0.1	e	0.006
$CHCl_3$	0.022	0.009 (0.003)	$4.2x10^{-5}$	$1.8x10^{-5}$ ($6x10^{-6}$)	0.001	f	$2x10^{-4}$
CH_2Br_2	0.0028	0.0010 ($4x10^{-4}$)	$6x10^{-6}$	$2x10^{-6}$ ($1x10^{-6}$)	0.12	e	$6x10^{-5}$
$CHBrCl_2$	0.0059	$8x10^{-4}$ ($8x10^{-4}$)	$2.0x10^{-5}$	$3x10^{-6}$ ($3x10^{-6}$)	0.17	e	$2x10^{-5}$
C_2Cl_4	0.025	0.006 (0.003)	$8x10^{-5}$	$2x10^{-5}$ ($1x10^{-5}$)	0.17	f	$7x10^{-5}$
Methylnitrate	0.021	0.003 (0.002)	$1.00x10^{-5}$	$1.4x10^{-6}$ ($8x10^{-7}$)	0.023	a	$2x10^{-4}$
Ethylnitrate	0.023	0.002 (0.002)	$8.4x10^{-5}$	$9x10^{-6}$ ($6x10^{-6}$)	0.018	a	$4x10^{-4}$
2-Propylnitrate	0.045	0.011 (0.006)	$2.6x10^{-4}$	$6x10^{-5}$ ($4x10^{-5}$)	0.029	a	$2x10^{-4}$
1-Propylnitrate	0.0082	0.0012 ($9x10^{-4}$)	$1.0x10^{-4}$	$1x10^{-5}$ ($1x10^{-5}$)	0.58	a	$8x10^{-4}$
2-Butylnitrate	0.12	0.02 (0.02)	0.0021	$3x10^{-4}$ ($3x10^{-4}$)	0.86	a	$5x10^{-4}$
3-Pentylnitrate	0.035	0.005 (0.005)	$7.0x10^{-4}$	$1.0x10^{-4}$ ($9x10^{-5}$)	1	a	$2x10^{-4}$
2-Pentylnitrate	0.055	0.007 (0.007)	0.0019	$3x10^{-4}$ ($3x10^{-4}$)	1.7	a	2x10-4

(a) Standard deviation of averages reported in parentheses

(b) Units of $k_{OH,VOC}$: 10^{-12} cm^3 $molec^{-1}$ s^{-1}

(c) References for $k_{OH,VOC}$: (a) Atkinson et al. [2003], (b) Rosen et al. [2004], (c) Farmer et al. [2011], (d) Atkinson [1986], (e) Sander et al. [2015], (f) Atkinson et al. [2001]

Table A1.2. Statistics of PMF Reconstructions for select VOCs for spring and summer. Reconstructions are calculated from PMF factor time-series and PMF factor profile output. 1-sided linear regression of species mixing ratio reconstructions versus measured mixing ratios were used to generate slope values with errors in parentheses.

	Spring		Summer	
Compound	slope	r^2	Slope	r^2
Ethane	0.43 (0.1)	0.57	0.51 (0.02)	0.65
i-Butane	0.952 (0.003)	0.98	0.984 (0.007)	0.98
n-Butane	0.934 (0.002)	0.99	0.958 (0.005)	0.98
i-Pentane	0.640 (0.007)	0.87	0.81	0.9
n-Pentane	0.713 (0.006)	0.91	0.738 (0.010)	0.92
n-Hexane	0.821 (0.004)	0.97	0.878 (0.008)	0.96
n-Heptane	0.834 (0.005)	0.95	0.939 (0.008)	0.97
n-Octane	0.590 (0.10)	0.73	0.80 (0.01)	0.9
Cyclohexane	0.931 (0.005)	0.97	0.954 (0.008)	0.97
2-Methylheptane	0.794 (0.007)	0.88	0.77 (0.02)	0.81
Toluene	0.825 (0.008)	0.89	0.91 (0.02)	0.88
Ortho-xylene	0.42 (0.01)	0.5	0.49 (0.02)	0.54
Ethylbenzene	0.49 (0.01)	0.63	0.44 (0.01)	0.57
isoprene			0.967 (0.004)	0.99
Acetaldehyde	0.34 (0.02)	0.26	0.54 (0.02)	0.52
Methyl ethyl ketone	0.46 (0.01)	0.55	0.46 (0.02)	0.5
CH_2Cl_2	0.12 (0.01)	0.06	0.08 (0.01)	0.07
C_2Cl_4	0.330 (0.009)	0.49	0.57 (0.2)	0.65
$CHCl_3$	0.28 (0.02)	0.09	0.39 (0.02)	0.38
Methylnitrate	0.34 (0.01)	0.24	0.31 (0.02)	0.39
Ethylnitrate	0.83 (0.01)	0.68	0.90 (0.02)	0.87
1-propylnitrate	0.65 (0.01)	0.6	0.78 (0.02)	0.76
2-propylnitrate	0.984 (0.009)	0.89	1.05 (0.02)	0.9
2-butylnitrate	0.950 (0.006)	0.94	0.961 (0.010)	0.95
2-pentylnitrate	0.859 (0.005)	0.95	0.80 (0.01)	0.93
3-pentylnitrate	0.878 (0.006)	0.94	0.81 (0.01)	0.93
$R_{OH,VOC}$	0.909 (0.004)	0.97	0.900 (0.007)	0.97
ppbC	0.905 (0.006)	0.95	0.84 (0.01)	0.93

APPENDIX 1 REFERENCES

Atkinson, R. (1986), Kinetics and mechanisms of the gas-phase reactions of the hydroxyl radical with organic compounds under atmospheric conditions, *Chemical Reviews*, *86*(1), 69-201.

Atkinson, R., and J. Arey (2003), Atmospheric degradation of volatile organic compounds, *Chemical reviews*, *103*(12), 4605-4638.

Atkinson, R., et al. (2001), Summary of evaluated kinetic and photochemical data for atmospheric chemistry, *Not in System*, 1-56.

Farmer, D., et al. (2011), Impact of organic nitrates on urban ozone production, *Atmospheric Chemistry and Physics*, *11*(9), 4085-4094.

Rosen, R., et al. (2004), Observations of total alkyl nitrates during Texas Air Quality Study 2000: Implications for O3 and alkyl nitrate photochemistry, *Journal of Geophysical Research: Atmospheres (1984–2012)*, *109*(D7).

Sander, S. P., et al. (2015), Chemical kinetics and photochemical data for use in atmospheric studies evaluation number 18.

APPENDIX 2 – CHAPTER 4 SUPPLEMENTAL INFORMATION (A2)

Text A2.1. J_{RONO2} value determinations

Seasonal photolysis rates (J_{RONO2}) for $MeONO_2$, $EtONO_2$, 1-$PrONO_2$, and 2-$BuONO_2$ were calculated with the National Center for Atmospheric Research Quick TUV calculator (http://cprm.acom.ucar.edu/Models/TUV/Interactive_TUV/_).[*Madronich et al.*, 1998] The model was initiated with the longitude and latitude of the Boulder Atmospheric Observatory (BAO) in Erie, CO (40, -105), and an elevation of 1.56 km asl. Seasonal J_{RONO2} values were calculated every 2 hours from 08:00 – 18:00. For the NACHTT Winter 2011 campaign J_{RONO2} values were generated for March 1, 2011. For the SONGNEX Spring 2015 campaign J_{RONO2} values were generated for April 1, 2015 and May 1, 2015. For the Summer 2015 campaign J_{RONO2} values were generated for July 1, 2015 and August 1, 2015. Two dates, one near the beginning and end of the campaign, were chosen for a better representation of the longer SONGNEX field campaigns. Average and standard deviation J_{RONO2} values were calculated from the 08:00 – 18:00 J_{RONO2} values for the single day for NACHTT, and both days for the SONGNEX campaigns. The range of J_{RONO2} values reported in Table 2 were generated as the Average ± Standard Deviation for each campaign.

The TUV calculator does not report J_{RONO2} values for 2-$PrONO_2$, 2-$PeONO_2$, and 3-$PeONO_2$. However, the TUV calculator outputs the actinic flux for an atmospherically relevant wavelength range. The photolysis rates for 2-$PrONO_2$, 2-$PeONO_2$, and 3-$PeONO_2$ were calculated with the following expression;

$$J_{RONO_2} = \int_{\lambda_{min}}^{\lambda_{max}} I(\lambda)\sigma(\lambda)\Phi(\lambda)d\lambda \quad \text{(E1)}$$

where I(λ) is the actinic flux at wavelength λ, σ(λ) is the absorption cross-section at wavelength λ, and Φ(λ) is the photodissociation quantum yield at wavelength λ. Absorption cross-sections for 2-$PrONO_2$ were taken from *R Talukdar et al.* [1997a]. Absorption cross-sections for 2-$PeONO_2$ were taken from *Roberts and Fajer* [1989]. Due to the lack of 3-$PeONO_2$ absorption cross-sections in literature for 3-$PeONO_2$, the absorption cross-sections for 2-$PeONO_2$ were used for 3-$PeONO_2$. The photodissociation quantum yields were assumed to be unity [*Roberts and Fajer*, 1989; *R Talukdar et al.*, 1997a].

Uncertainties are not reported from the TUV calculator. We took the uncertainty to be the RSD of each seasonal daytime (08:00 – 18:00) J_{RONO2} average. The uncertainty is reported as the range of J_{RONO2} for each campaign in Table 2.

Text A2.2. Deposition calculations

Flux and dry deposition velocities (V_d) were estimated from a simplification of the following mass balance equation (SI E2) [*Russo et al.*, 2010; *Swarthout et al.*, 2013].

$$\frac{d[X_{BL}]}{dt} = \frac{ER}{H} + P - k_{OH}[OH][X_{BL}] - \frac{V_e}{H}(X_{BL} - X) - J_X + Advection \qquad \text{(E2)}$$

where $d[X_{BL}]/dt$ is the change in concentration of X in the boundary layer during time (t), ER/H is the emissions rate of X in a boundary layer depth of H, P is the production rate of X, $k_{OH}[OH][X_{BL}]$ is the loss of X to oxidation by OH, V_e/H is the vertical transfer coefficient of X in a boundary layer depth of H, which is scaled by the difference in X_{BL} and X in the mixed layer aloft, and J_x is the photolysis rate of X at the surface. By choosing a nighttime period for these calculations the chemical production, loss to OH, and photolysis terms go to zero. Loss to nighttime oxidants such as O_3 and NO_3 is negligible [*Roberts*, 1990; *R Talukdar et al.*, 1997a; *R K Talukdar et al.*, 1997b].

Advection and vertical mixing is assumed to be negligible when a stable nocturnal boundary layer forms and wind speeds are low. Under such cases the mass balance equation reduces to E3.

$$\frac{d[X_{BL}]}{dt} = \frac{ER}{H} \quad \text{(E3)}$$

Outside of sites impacted by oceanic emissions or fresh biomass burning plumes the direct emissions of $RONO_2$ do not contribute to ambient $RONO_2$ mixing ratios. The emission ratio can be replaced with flux by rearranging to E4;

$$\frac{d[X_{BL}]}{dt} \cdot H = Flux \quad \text{(E4)}$$

Flux of $RONO_2$ were estimated from the nighttime decay rate of alkyl nitrates (change in concentration over given time, ppb/s) multiplied by the nocturnal boundary layer height for nights with surface wind speeds under 4 m/s, and when $RONO_2$ exhibited decreasing mixing ratios between 22:00 and 06:00 with an r^2 of >0.70 between mixing ratio and time (Fig. A2.1a). Dry deposition velocity is then calculated with E5 [*Russo et al.*, 2010];

$$V_d = \frac{Flux}{-C} \quad \text{(E5)}$$

where C is the mean $RONO_2$ mixing ratio during the flux period.

Fixed-height meteorological measurements of temperature and wind speed were continuously made at the BAO site at 10, 100, and 300 meter heights for all campaigns (Fig. S1c). During the NACHTT campaign, additional time-resolved vertical profiles of potential temperature and wind speed were made on a moveable carriage on the 300 m tower (Fig. S1b). These higher resolution temperature measurements allowed us to determine nights with a stable nocturnal boundary layer (*i.e.* potential temperature inversions and stratified wind speeds). The fixed-height meteorological measurements in conjunction with the meteorological vertical profiles during

NACHTT allowed us to identify characteristics in the fixed-height measurements that coincided with the formation of a stable nocturnal boundary layer. Namely, stable nocturnal boundary layers were characterized by rapid decreases in temperature, 100m-300m temperature inversions, and 10-100m wind speed convergence observed with the fixed-height measurements. We used these characteristics to identify nights during which a stable nocturnal boundary layer likely formed during the Spring 2015 campaign. From vertical profiles of potential temperature and wind speed, we estimated an average nocturnal boundary layer height of 100 m for the selected nights during both campaigns (Fig. S1b). This agrees with previous estimates of stable nocturnal boundary layer heights of 120 ± 50 m during NACHTT [*VandenBoer et al.*, 2013]. Consistent stable nocturnal boundary layer heights could not be identified for the Summer 2015 data, so this deposition analysis was limited to Winter 2011 and Spring 2015 datasets. Flux and dry deposition velocities scale with boundary layer height [*Russo et al.*, 2010], so the values in Table 3 should be considered estimates.

Seasonal dry deposition rate coefficients (k_{dep}, s^{-1}) were calculated with E6;

$$k_{dep} = \frac{V_d}{H} \quad \text{(E6)}$$

where H is the average boundary layer height for each season. Average boundary layer heights of 375, 750, and 1500 m were used for winter, spring, and summer respectively. Winter and summer heights were estimated from previous studies in the region.[*Haagenson*, 1979; *Halliday et al.*, 2016; *Neff*, 1997; *Schneider and Lilly*, 1999]

Text A2.3. $MeONO_2$ loss uncertainties

The preferred rate coefficient for CH_4+OH from the IUPAC Task Group On Atmospheric Chemical Kinetic Data has an error of 1% for the ambient temperature range during the spring 2015 and summer 2015 campaigns [*IUPAC*, 2017]. We use the lowest reported branching ratio of 0.001 to model $MeONO_2$/methane.[*Ranschaert et al.*, 2000; *Wang et al.*, 2010] The preferred $MeONO_2$+OH rate coefficient has an uncertainty of 22% at 298 K [*IUPAC*, 2017]. Uncertainties for the average spring 2015 daytime J_{RONO2} for $MeONO_2$ and 2-$BuONO_2$ are 61 and 67%, respectively. The uncertainties in J_{RONO2} selection have a negligible impact on the agreement between modeled and measured $RONO_2$/RH (Fig. A2.3).

Table A2.1. Seasonal lifetime ranges in days of C_1-C_5 $RONO_2$ at the BAO site in respect to OH oxidation ($\tau_{OH} = 1/k_4$), photolysis ($\tau_{hv} = 1/J_5$), and OH + photolysis ($\tau_{OH+hv} = 1/k_B$)**.**

	Lifetimes								
AN	τ_{OH} - Winter 2011	τ_{OH} - Spring 2015	τ_{OH} - Summer 2015	τ_{hv} - Winter 2011	τ_{hv} - Spring 2015	τ_{hv}- Summer 2015	$\tau_{OH + hv}$ - Winter 2011	$\tau_{OH + hv}$ - Spring 2015	$\tau_{OH + hv}$ - Summer 2015
MeONO2	174-524	98-243	54-108	23-165	15-61	12-39	18-105	12-43	9-25
EtONO2	20-60	12-29	7-13	14-105	9-36	8-24	8-35	5-15	4-9
1-PrONO2	7-22	4-11	2-5	10-68	6-25	6-17	4-15	2-7	2-4
2-PrONO2	14-41	8-20	5-10	12-77	7-28	7-18	6-26	4-11	3-6
2-BuONO2	4-13	3-6	2-3	12-98	7-38	6-24	3-12	2-6	1-3
2-PeNONO2	2-6	1-3	0.8-1.5	14-115	9-43	6-24	2-6	1-3	0.7-1.5
3-PeONO2	3-10	2-5	1-3	15-145	9-43	6-24	3-10	2-5	1-2

Table A2.2. Groupings of days according to days exhibiting low O_3 with high 2-$PrONO_2$/propane (Group 1), low O_3 with low 2-$PrONO_2$/propane (Group 2), high O_3 with high 2-$PrONO_2$/propane (Group 3), and high O_3 with low 2-$PrONO_2$/propane (Group 4). High O_3 days are defined as days with a measured daytime O_3 concentration that exceeds 70 ppbv. High 2-$PrONO_2$/propane days are defined as days with 2-$PrONO_2$/propane that exceed 0.01 ppbv/ppbv. Low O_3 and 2-$PrONO_2$/propane days are defined as days with all measurements below the high thresholds.

Group 1	Group 2	Group 3	Group 4
Dates			
7/24/2015	8/4/2015	7/27/2015	7/30/2015
7/25/2015	8/8/2015	7/31/2015	8/7/2015
7/26/2015	8/9/2015	8/1/2015	8/11/2015
7/28/2015	8/13/2015	8/2/2015	8/15/2015
8/3/2015	8/17/2015	8/5/2015	8/20/2015
8/6/2015	8/18/2015	8/21/2015	8/23/2015
8/14/2016	8/19/2015	8/26/2015	8/24/2015
8/15/2015	8/27/2015	8/29/2015	8/25/2015
8/16/2017	8/28/2015		
8/17/2015			
8/22/2015			

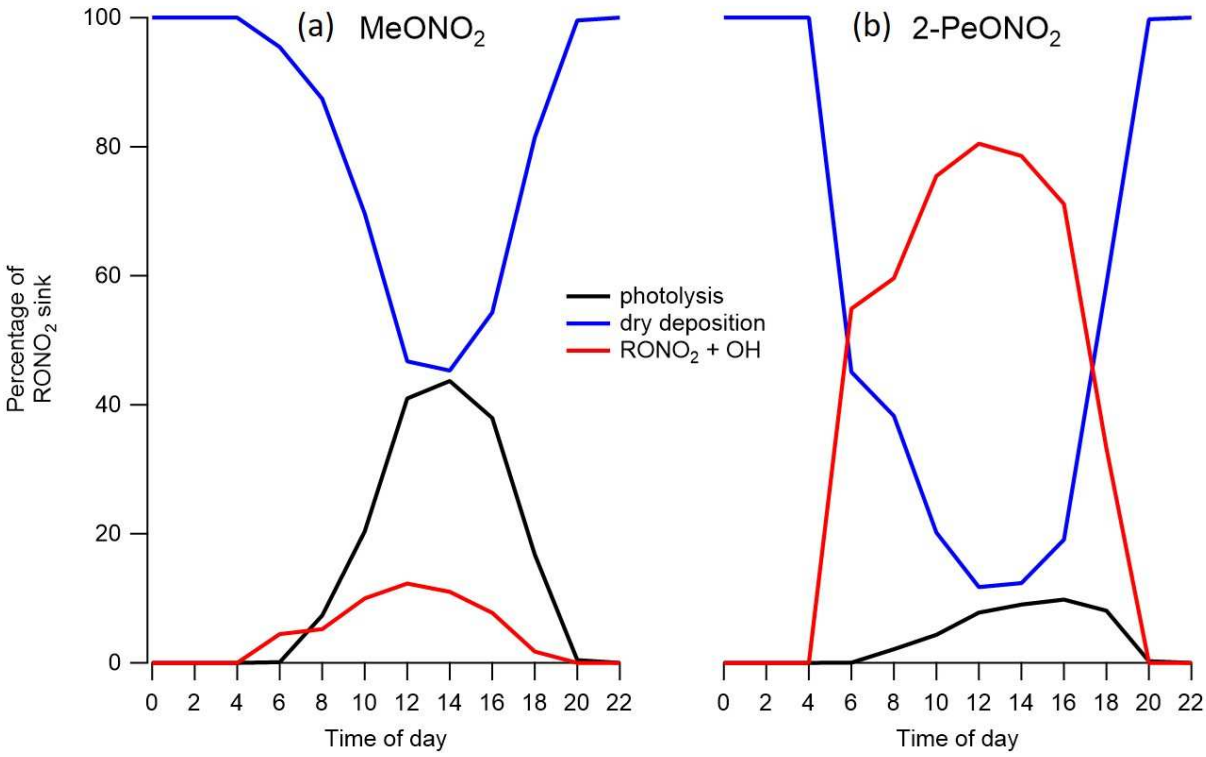

Figure A2.1. Diel cycle of the percentage of total $RONO_2$ sink for loss by photolysis, dry deposition, and $RONO_2$ + OH for (a) $MeONO_2$ and (b) 2-$PeONO_2$ for summer. Photolysis rates were generated every 2 hours for $MeONO_2$ and 2-$PeONO_2$ as described above in the J values determination section. Dry deposition loss rates were calculated as described above in the Deposition calculations section. Diel cycle boundary layer heights were calculated from NASA's Vaisala ceilometer measurements during summer 2014 at the BAO site. The loss rate to OH was calculated as $k_{RONO2+OH}$[OH]. Diel cycle OH concentrations were calculated from aircraft OH measurements over the Front Range of Northern Colorado during summer 2014.[*Ebben et al.*, 2017]

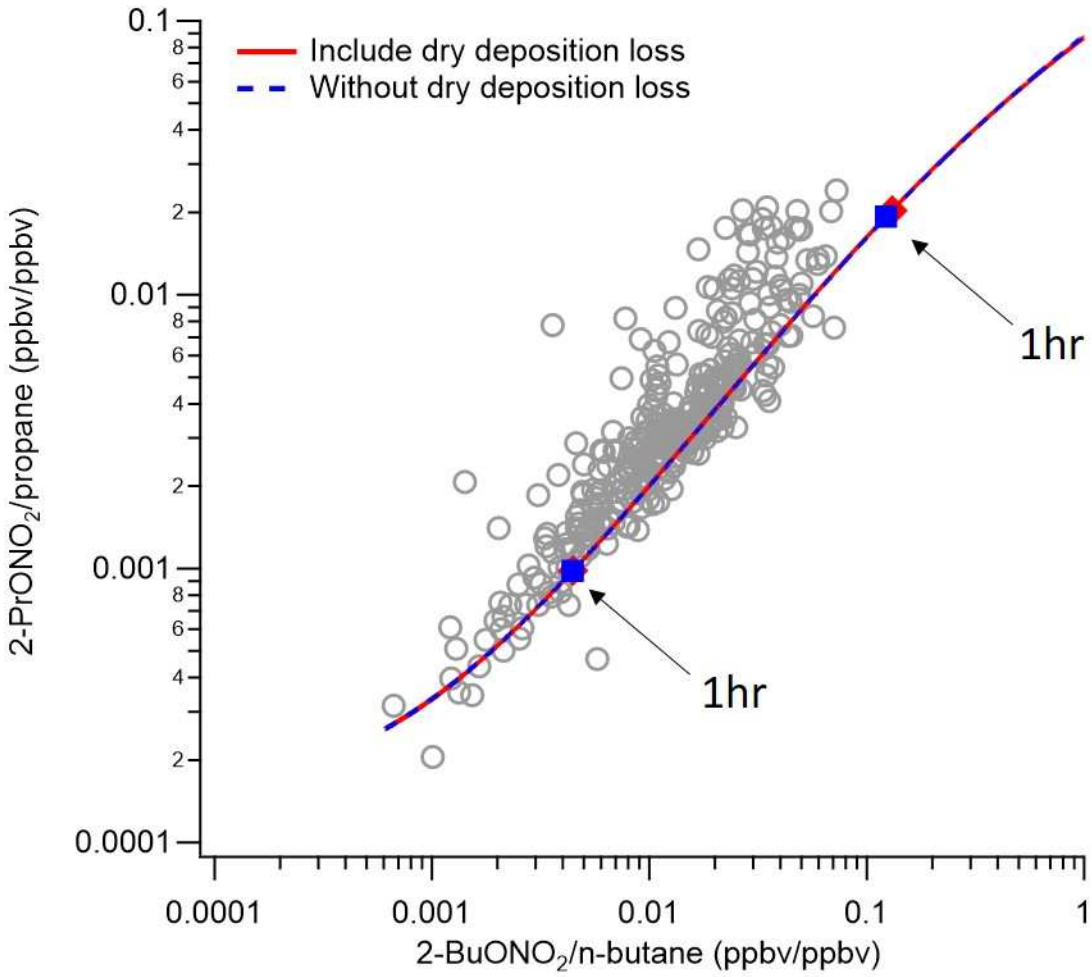

Figure A2.2. $RONO_2/RH$ is modeled using E2 for 2-$PrONO_2$/propane and 2-$BuONO_2$/n-butane including loss by dry deposition, and without loss by dry deposition. Branching ratios are averages from Table 2 ($\beta_{2\text{-PrONO2}} = 0.029$; $\beta_{2\text{BuONO2}} = 0.074$). With an estimated summer average daytime boundary layer height the dry deposition loss rates are calculated to be 1.1×10^{-6} s^{-1} and 1.4×10^{-6} s^{-1} for 2-$PrONO_2$ and 2-$BuONO_2$ respectively. Observed (grey circles) and modeled (line, with and without dry deposition) 2-$PrONO_2$/propane are plotted against 2-$BuONO_2$/n-butane for the daytime (08:00 – 18:00) SONGNEX-summer data (grey circles). Markers for 1 hour and 24 hours of photochemical aging for the two models are overlaid on the modeled curves.

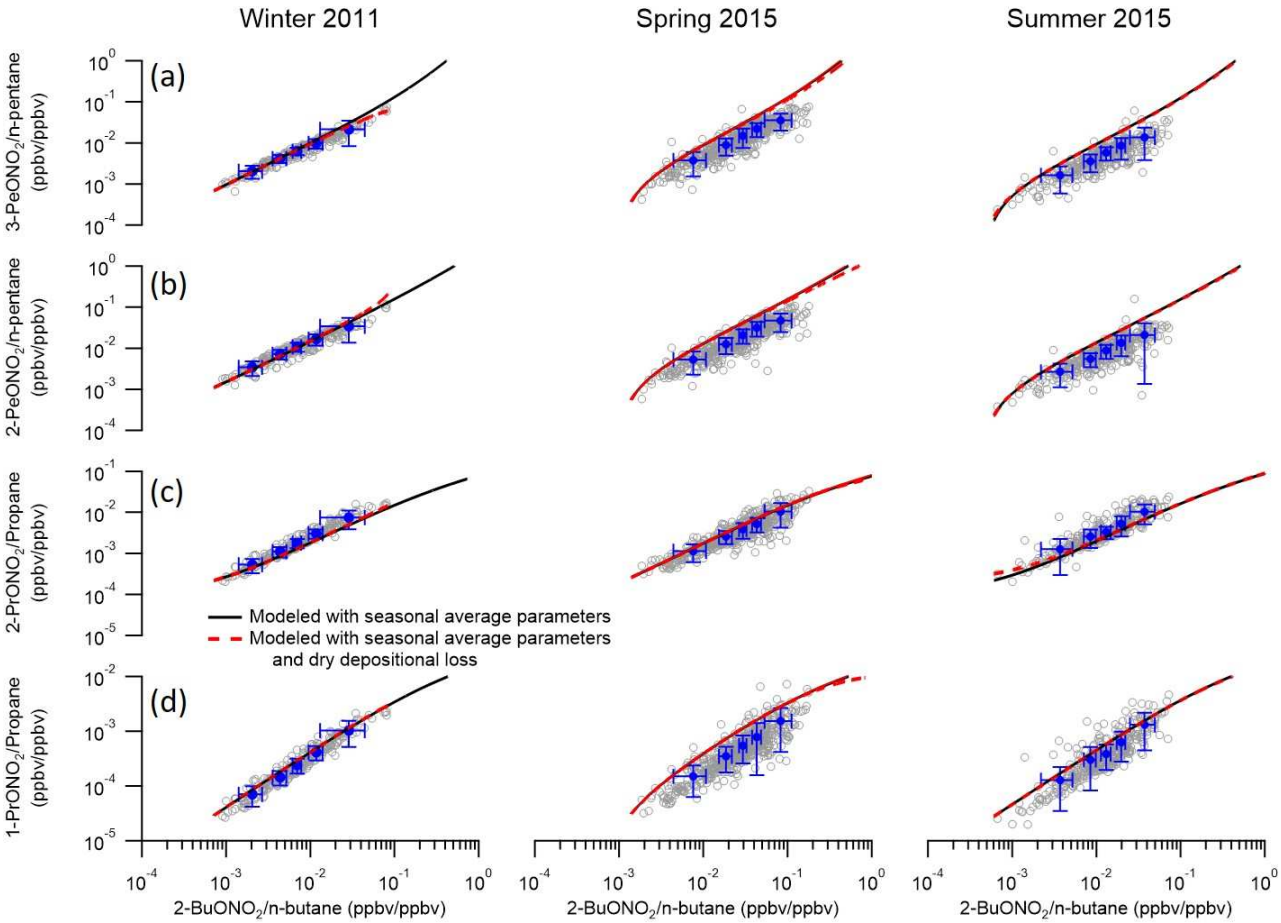

Figure A2.3. Observed daytime (08:00 – 18:00) $RONO_2/RH$ was plotted against 2-$BuONO_2$/n-butane (grey circles) for Winter 2011 (left), Spring 2015 (middle) and Summer 2015 (right). Modeled $RONO_2/RH$ were generated with E2 using average campaign β, k_A, and k_B values reported in Table 2. Models were generated with non-zero initial ratios (black solid lines) defined as the 5th percentile value of $RONO_2/RH$ between 00:00 – 06:00 for all days during each respective campaigns. Dashed red lines are modeled $RONO_2/RH$ including loss by dry deposition (k_{dep}, Table 3). Solid blue circles are average $RONO_2/RH$ versus 2-$BuONO_2$/n-butane values with an equal number of points per averaging bin (n = 46 for NACHTT, 110 for SONGNEX-spring, and 69 for SONGNEX-summer). Error bars are one standard deviation of the $EtONO_2$/ethane and 2-$BuONO_2$/n-butane averages.

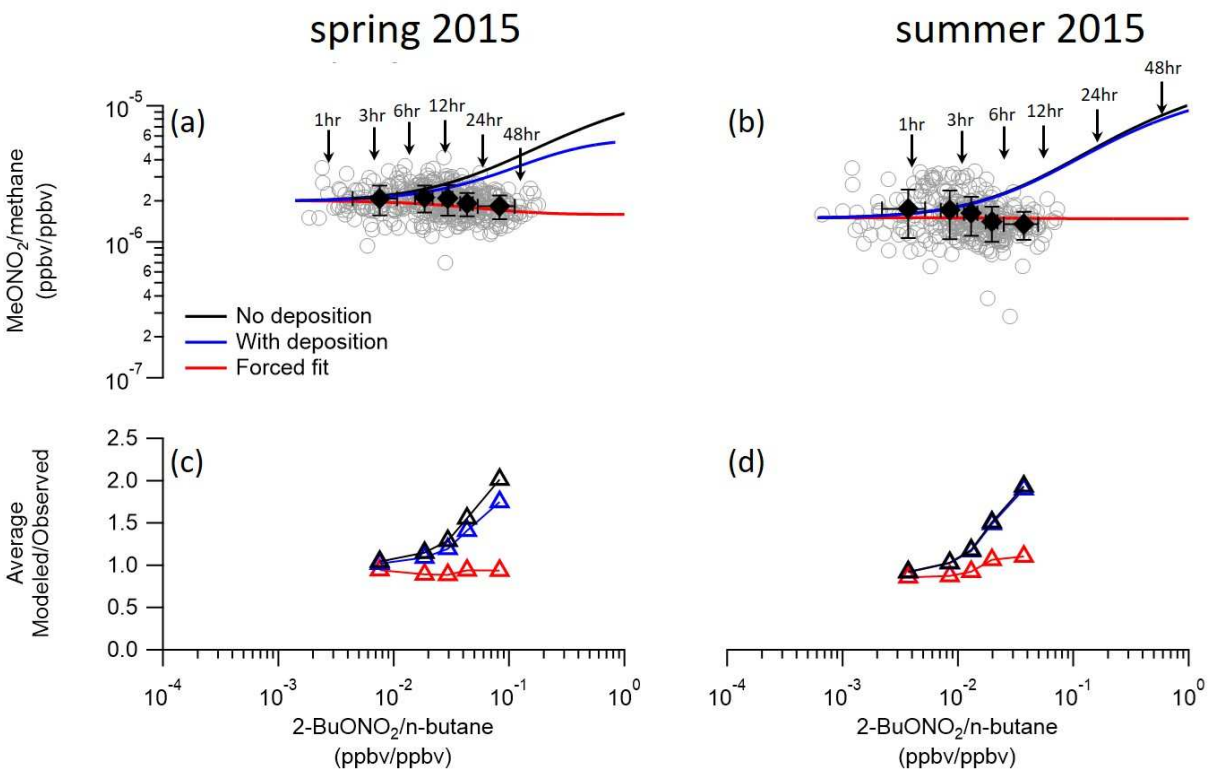

Figure A2.4. Observed $MeONO_2$/methane was plotted against 2-$BuONO_2$/n-butane for spring 2015 (grey circles, a) and summer 2015 (grey circles, b). Model ratios are shown that exclude loss by dry deposition (black), include dry deposition determined from nighttime data (blue), and include enhanced non-photochemical losses. All models use upper J_{RONO2} values for each $RONO_2$ (Table 2). Black diamonds are average $MeONO_2$/methane versus 2-$BuONO_2$/n-butane averaged into five bins of equal number of points (n = 110/bin for spring 2015 and n = 69 for summer 2015). Error bars represent one standard deviation around the bin averages. Modeled/observed ratios are plotted for spring 2015 (c) and summer 2015 (d) for each scenario. Photochemical ages derived from the model scenarios are indicated.

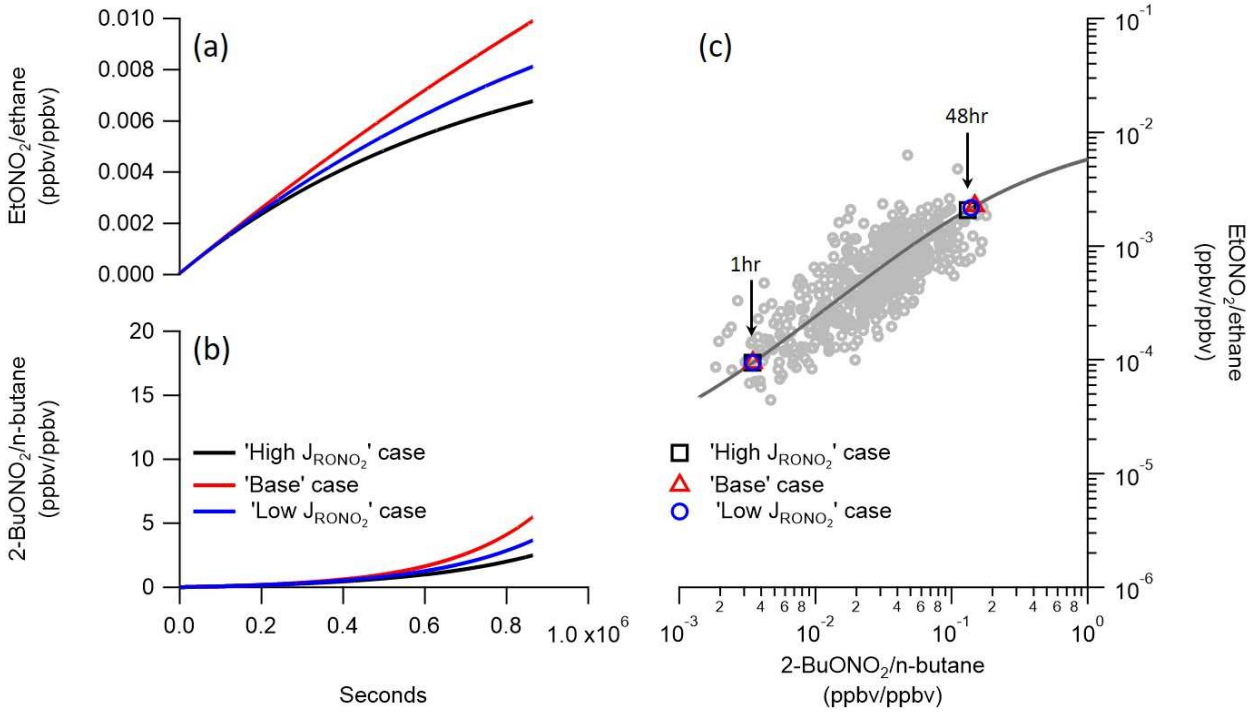

Figure A2.5. $RONO_2/RH$ is modeled using E2 for (a) $EtONO_2$/ethane and (b) 2-$BuONO_2$/n-butane. Three cases are modeled using different J_{RONO2} values (see text and SI for details). k_B ($k_{OH+RONO2}$ + J_{RONO2}) were calculated for each J_{RONO2} case. OH and temperature are taken for spring 2015 conditions. Branching ratios are averages from Table 2 (β_{EtONO2} = 0.018; $\beta_{2BuONO2}$ = 0.074). (c) Observed (grey circles) and modeled (line, each J_{RONO2} case) $EtONO_2$/ethane are plotted against 2-$BuONO_2$/n-butane for the daytime (08:00 – 18:00) SONGNEX-spring data (grey circles, c). Markers for 1 hour and 48 hours of photochemical aging for the three OH cases are overlaid on the modeled curves.

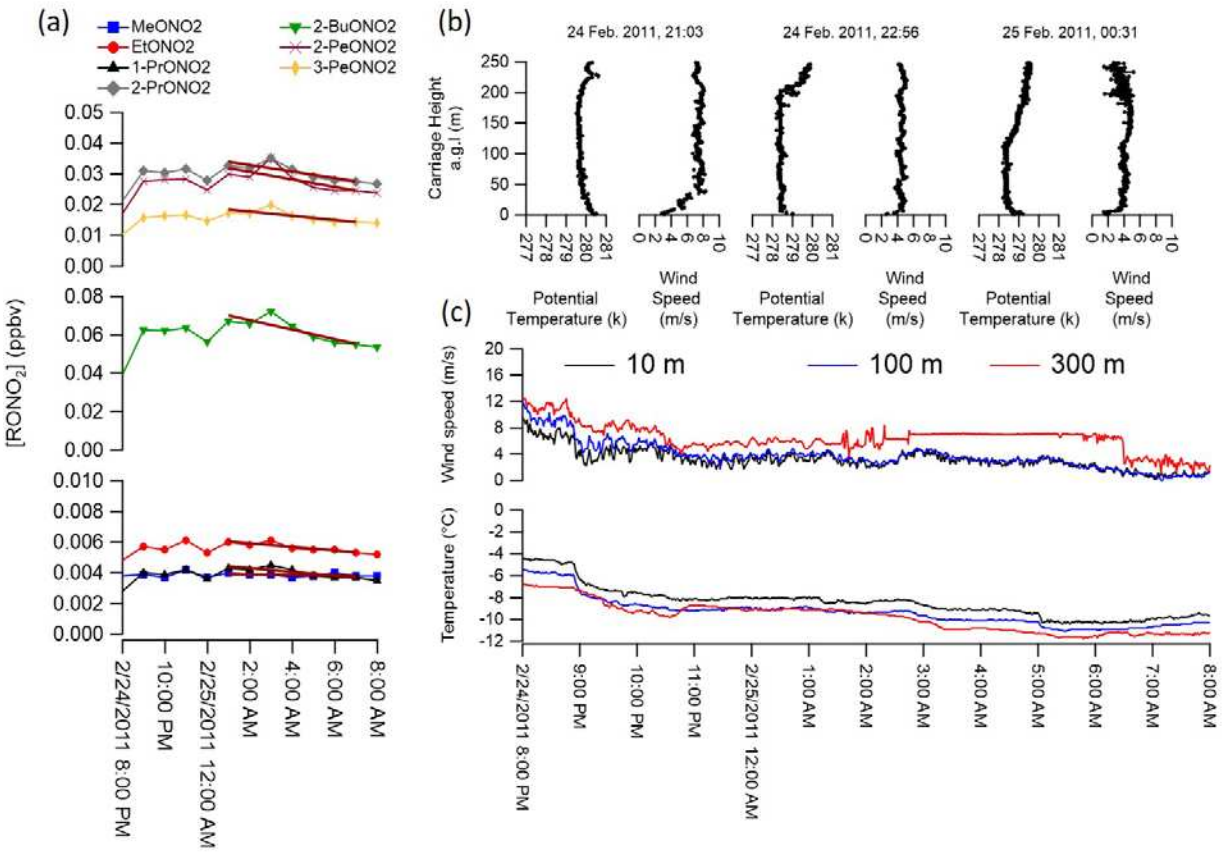

Figure A2.6. $RONO_2$ and meteorological data for dry deposition velocity calculations from the NACHTT campaign for 24 February 2011 – 25 February 2011. (a) $RONO_2$ versus time for C_1 – C_5 $RONO_2$. (b) Individual vertical profiles of potential temperature and wind speed that show the formation of a stable nocturnal boundary layer. (c) Temperature and wind speed measurements made at 10 m (black), 100 m (blue), and 300 m (red) on the tower at the BAO site.

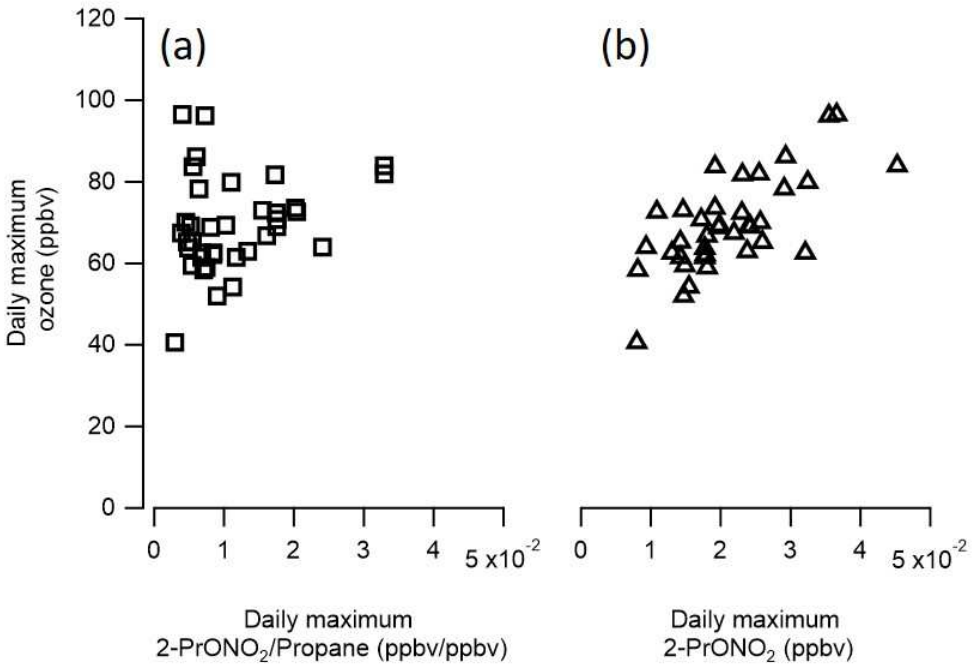

Figure A2.7. Daily maximum ozone versus (a) daily maximum 2-$PrONO_2$/propane and (b) daily maximum 2-$PrONO_2$ for the SONGNEX-summer campaign. Maximum values were determined for each day of the SONGNEX-summer campaign.

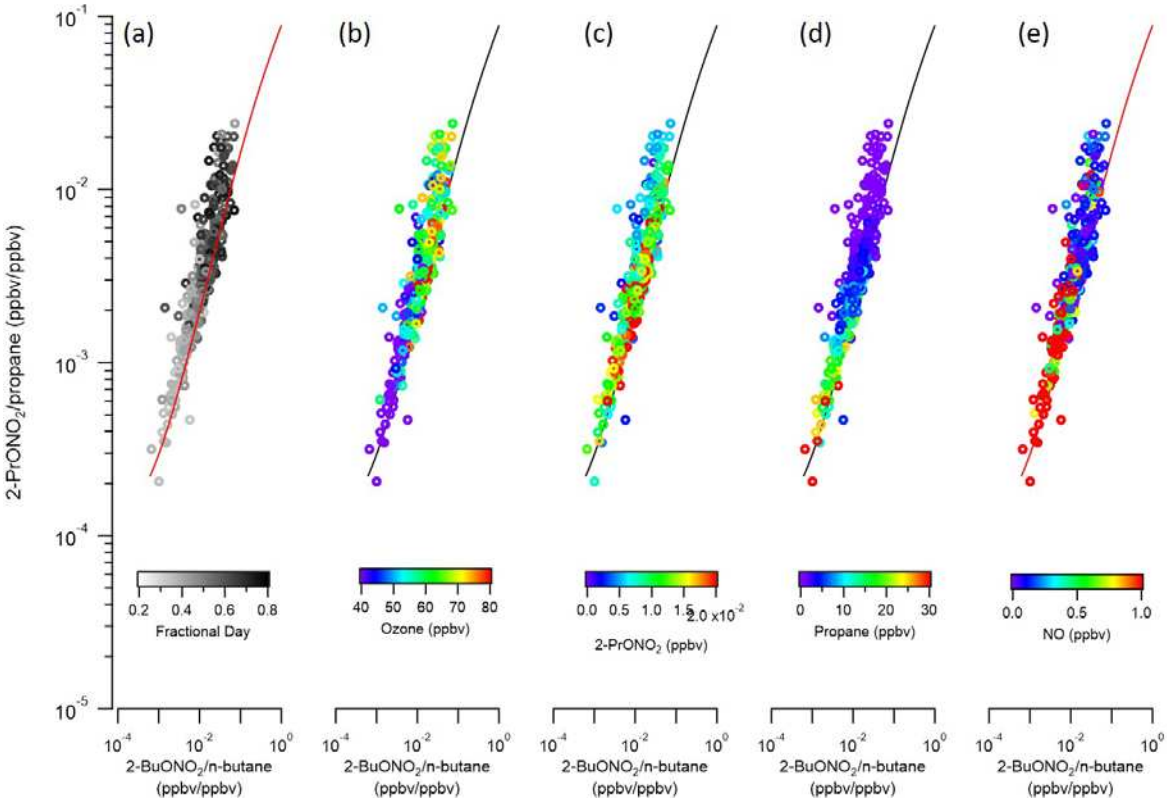

Figure A2.8. Daytime (08:00 – 18:00) 2-$PrONO_2$/propane versus 2-$BuONO_2$/n-butane was plotted for the summer 2015 campaign and colored by (a) fraction of the day for each data point (i.e. 0.33 = 08:00 and 0.75 = 18:00); (b) ambient ozone mixing ratio averaged to the VOC measurements time resolution; (c) 2-$PrONO_2$ ambient mixing ratio; (d) ambient NO mixing ratio averaged to the VOC measurements time resolution; and (e) ambient propane mixing ratio.

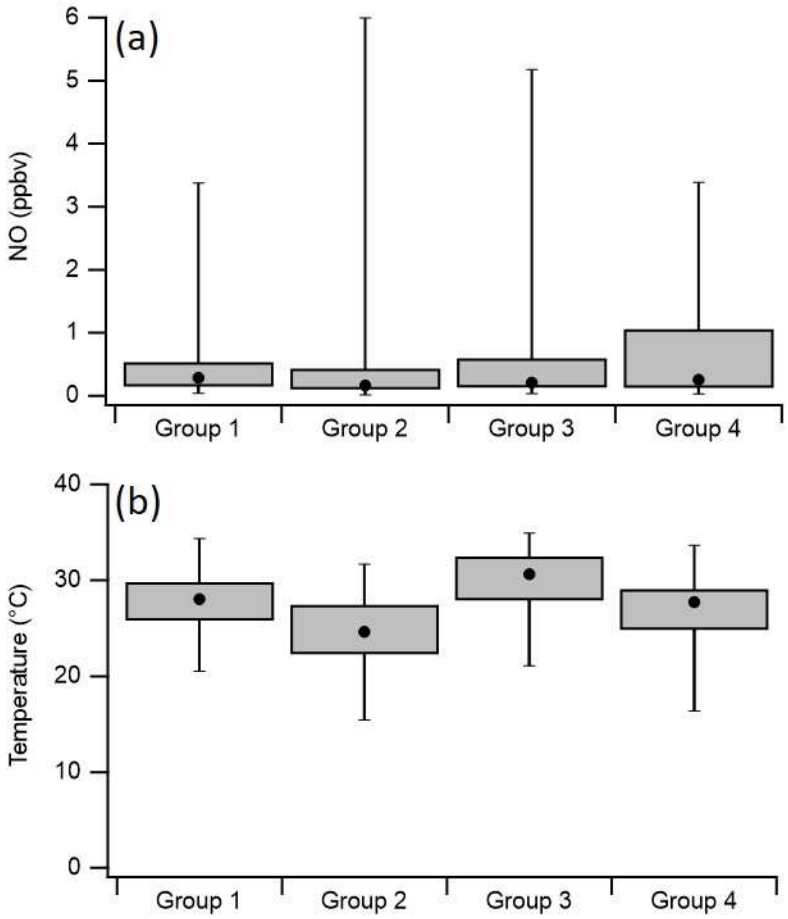

Figure A2.9. Box and whisker plots (5^{th}, 33^{rd}, 50^{th}, 67^{th}, and 95^{th} percentiles) for summer 2015 daytime (08:00-18:00) for (a) NO concentration and (b) site temperature (10 m a.g.l). Days during the summer 2015 campaign were split into groups depending on daytime O_3 concentrations and 2-$PrONO_2$/propane. The groupings correspond to days that exhibit low O_3 with high 2-$PrONO_2$/propane (Group 1), low O_3 with low 2-$PrONO_2$/propane (Group 2), high O_3 with high 2-$PrONO_2$/propane (Group 3), and high O_3 with low 2-$PrONO_2$/propane (Group 4). High O_3 days are defined as days with a measured daytime O_3 concentration that exceeds 70 ppbv. High 2-$PrONO_2$/propane days are defined as days with 2-$PrONO_2$/propane ratios that exceed 0.01 ppbv/ppbv. The number of days in each group is 11, 9, 8, and 8 for Group 1, Group 2, Group 3, and Group 4 respectively.

APPENDIX 2 REFERENCES

Ebben, C. J., T. L. Sparks, P. J. Wooldridge, T. L. Campos, C. A. Cantrell, R. L. Mauldin, A. J. Weinheimer, and R. C. Cohen (2017), Evolution of NOx in the Denver Urban Plume during the Front Range Air Pollution and Photochemistry Experiment, *Atmos. Chem. Phys. Discuss.*, *2017*, 1-13, doi:10.5194/acp-2017-671.

Haagenson, P. L. (1979), Meteorological and climatological factors affecting Denver air quality, *Atmospheric Environment (1967)*, *13*(1), 79-85.

Halliday, H. S., A. M. Thompson, A. Wisthaler, D. R. Blake, R. S. Hornbrook, T. Mikoviny, M. Müller, P. Eichler, E. C. Apel, and A. J. Hills (2016), Atmospheric benzene observations from oil and gas production in the Denver-Julesburg Basin in July and August 2014, *Journal of Geophysical Research: Atmospheres*, *121*(18), 11,055-011,074, doi:10.1002/2016JD025327.

IUPAC (2017), Task Group on Atmospheric Chemical Kinetic Data Evaluation, edited.

Madronich, S., R. L. McKenzie, L. O. Björn, and M. M. Caldwell (1998), Changes in biologically active ultraviolet radiation reaching the Earth's surface, *Journal of Photochemistry and Photobiology B: Biology*, *46*(1), 5-19, doi:https://doi.org/10.1016/S1011-1344(98)00182-1.

Neff, W. D. (1997), The Denver Brown Cloud studies from the perspective of model assessment needs and the role of meteorology, *Journal of the Air & Waste Management Association*, *47*(3), 269-285.

Ranschaert, D. L., N. J. Schneider, and M. J. Elrod (2000), Kinetics of the C2H5O2+ NO x Reactions: Temperature Dependence of the Overall Rate Constant and the C2H5ONO2 Branching Channel of C2H5O2+ NO, *The Journal of Physical Chemistry A*, *104*(24), 5758-5765.

Roberts, J. M. (1990), The atmospheric chemistry of organic nitrates, *Atmospheric Environment. Part A. General Topics*, *24*(2), 243-287.

Roberts, J. M., and R. W. Fajer (1989), UV absorption cross sections of organic nitrates of potential atmospheric importance and estimation of atmospheric lifetimes, *Environmental science & technology*, *23*(8), 945-951.

Russo, R. S., Y. Zhou, K. Haase, O. Wingenter, E. Frinak, H. Mao, R. Talbot, and B. Sive (2010), Temporal variability, sources, and sinks of C 1-C 5 alkyl nitrates in coastal New England, *Atmospheric Chemistry and Physics*, *10*(4), 1865-1883.

Schneider, J. M., and D. K. Lilly (1999), An observational and numerical study of a sheared, convective boundary layer. Part I: Phoenix II observations, statistical description, and visualization, *Journal of the atmospheric sciences*, *56*(17), 3059-3078.

Swarthout, R. F., R. S. Russo, Y. Zhou, A. H. Hart, and B. C. Sive (2013), Volatile organic compound distributions during the NACHTT campaign at the Boulder Atmospheric Observatory: Influence of urban and natural gas sources, *Journal of Geophysical Research: Atmospheres*, *118*(18), 10,614-610,637, doi:10.1002/jgrd.50722.

Talukdar, R., J. Burkholder, M. Gilles, and J. Roberts (1997a), Atmospheric fate of several alkyl nitrates Part 2UV absorption cross-sections and photodissociation quantum yields, *Journal of the Chemical Society, Faraday Transactions*, *93*(16), 2797-2805.

Talukdar, R. K., S. C. Herndon, J. B. Burkholder, J. M. Roberts, and A. Ravishankara (1997b), Atmospheric fate of several alkyl nitrates Part 1Rate coefficients of the reactions of alkyl nitrates with isotopically labelled hydroxyl radicals, *Journal of the Chemical Society, Faraday Transactions*, *93*(16), 2787-2796.

VandenBoer, T. C., et al. (2013), Understanding the role of the ground surface in HONO vertical structure: High resolution vertical profiles during NACHTT-11, *Journal of Geophysical Research: Atmospheres*, *118*(17), 10,155-110,171, doi:10.1002/jgrd.50721.

Wang, B., M. Shao, S. Lu, B. Yuan, Y. Zhao, M. Wang, S. Zhang, and D. Wu (2010), Variation of ambient non-methane hydrocarbons in Beijing city in summer 2008, *Atmospheric Chemistry and Physics*, *10*(13), 5911.